Punching Shear Retrofit Method Using Shear Bolts for Reinforced Concrete Slabs under Seismic Loading

by

Wensheng Bu

A thesis
presented to the University of Waterloo
in fulfillment of the
thesis requirement for the degree of
Doctor of Philosophy
in
Civil Engineering

Waterloo, Ontario, Canada, 2008

AUTHOR'S DECLARATION

I hereby declare that I am the sole author of this thesis. This is a true copy of the thesis, including any required final revisions, as accepted by my examiners.

I understand that my thesis may be made electronically available to the public.

Abstract

Reinforced concrete slab-column structures are widely used because of their practicality. However, this type of structures can be subject to punching-shear failure in the slab-column connections. Without shear reinforcement, the slab-column connection can undergo brittle punching failure, especially when the structure is subject to lateral loading in seismic zones.

The shear bolts are a new type of transverse reinforcement developed for retrofit of existing structures against punching. This research focuses on how the shear bolts can improve the punching-shear capacity and ductility of the existing slab-column connections under vertical service and lateral seismic loads.

A set of nine full-scale reinforced concrete slab-column connection specimens were tested under vertical service and cyclic loads. The vertical (gravity) load for each specimen was kept at a constant value throughout the testing. The cyclic lateral drift with increasing intensity was applied to the columns. The specimens were different in number of bolts, concrete strength, number of openings, and level of gravity punching load. Strains in flexural rebars in the slabs, crack widths, lateral loads, and displacements were obtained.

The peak lateral load (moment) and its corresponding drift ratio, connection stiffness, crack width, and ductility were compared among different specimens. The testing results show that shear bolts can increase lateral peak load resisting capacity, lateral drift capacity at peak load, and ductility of the slab-column connections. Shear bolts also change the failure mode of the slab-column connections and increase the energy dissipation capacity.

The thesis includes also research on the development of guidelines for shear bolt design for concrete slab retrofitting, including the punching shear design method of concrete slab (with shear bolts), dimensions of bolts, spacing, and influence of bolt layout patterns. Suggestions are given for construction of retrofitting method using shear bolts. Recommendations are also presented for future research.

Acknowledgements

This research was undertaken under the supervision of Professor Maria Anna Polak. Without Professor Polak's direction, help, and encouragement, this thesis could hardly be accomplished so well as presented. Thus, I would like to express my greatest gratitude to her.

The presented research was funded by a grant from the Natural Sciences and Engineering Council (NSERC) of Canada. The shear bolts were manufactured and donated by Decon Inc. The ready mixed concrete was donated by Hogg Fuel and Supply Ltd. in Kitchener, Ontario. Ric Sherping and Sika Canada graciously donated Sikadur 30 for repairing drilling holes on concrete slabs.

This research involved experimental work in the Structural Laboratory of Civil and Environmental Engineering, University of Waterloo. I would like to thank Professor Timothy H. Topper for his help and instructions. I also appreciate the great help from Richard Morrison, Doug Hirst, Ken Bowman, Dick Powers, Terry Ridgway, Mark Sobon, Bruce Stickney, and the staff in the Machine Shop; without their help, my experiments could not be done.

For helping me in the laboratory, I need to thank Nick Lawler, José Andrés Alvarado, Mike Kuebler , Jeff West, Hongtao Liu, Yanjun Yang, Xianxun Yuan, Qinghua Huang, Jinyu Zhu, Hongli Huang, Xiaohong Huang, Xiaoguang Chen, Yuxin Liu, Ying An, Dan Mao and Tianjin Chen.

Professor Mahesh Pandey and Professor Wei-Chau Xie offered me help during my research and study; I also benefited from the discussion and teaching of Professor Donald E. Grierson and Gregory Glinka.

Finally, I would like to express special thanks to my wife and daughter. I appreciate their understanding, support and patience.

To My Parents

Table of Contents

List of Figures

List of Tables

Chapter 1
Introduction

1.1 Reinforced Concrete Flat Slab Column Structures and Punching Shear Failure

Among many types of reinforced concrete buildings, reinforced concrete flat slab structure is very popular. It consists of flat plate and columns, with no beams between the columns to support the slab. Figure 1.1 (a) shows a flat plate floor, and Figure 1.1 (b) shows a flat slab with drop panels and column capitals. Figure 1.1 (c) shows a beam slab floor. In this thesis, the flat slab column structures are such as represented in Figure 1.1 (a). Figure 1.2 shows an example of a system that consists of flat plates supported on columns. The research addresses the behaviour, design, and retrofit of this type of structures. Emphasis is on the punching shear retrofit of slab-column connections in seismic zones.

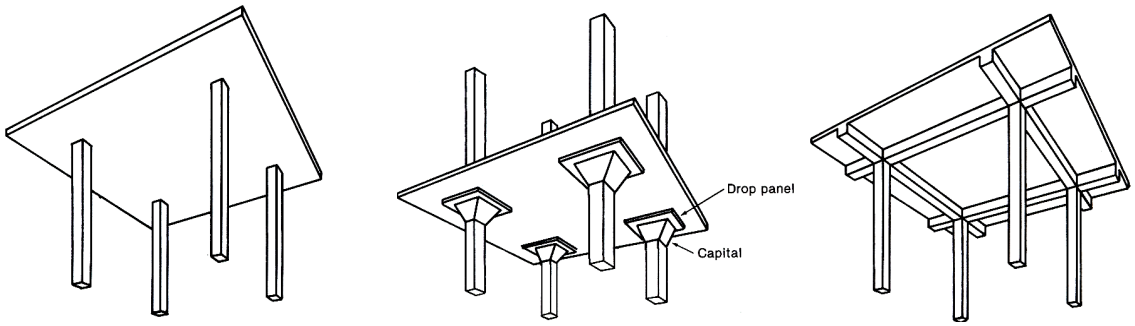

(a) Flat plate (slab) floor (b) Flat slab floor (c) Beam-slab floor

Figure 1.1 Flat slab (plate) floor and beam-slab floor (adapted from MacGregor and Bartlett, 2000)

Flat slab-column structural systems are popular due to reduction of building storey height, easy setting up of formwork, convenience for HVAC utilities layout, and good slab's appearance. However, this type of structure can easily be subject to brittle punching shear failure. When the flat-slab-column connections are subjected to heavy vertical loading, cracks will occur inside the slab in the vicinity of the column. These cracks then propagate through the slab thickness at an angle of 20 to 45 degree to the bottom of the slab. This can lead to punching shear failure of the slab along the cracks (Fig.1.3). When subjected to seismic lateral load, shear stresses in the slab increase due to an

unbalanced moment (from horizontal loading), and the slab-column connection is more likely to fail by punching shear.

Figure 1.2 Reinforced concrete flat slab building (Cope and Clark, 1984, courtesy of British Lift Slab Ltd.)

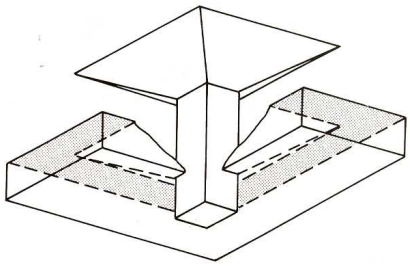

Figure 1.3 Failure surface of punching shear (adapted from MacGregor, 2000)

There have been several cases of punching shear failure in the last few decades. Punching shear failure can happen during the utilization of buildings. For example, in 1962, in New York City, a three year old concrete deck of a plaza, which was part of a roof of a car garage, collapsed suddenly (Feld and Carper, 1997). The roof was supporting 1.2 m deep earth cover with vegetation on it. It was found that the slab punched through a column and there was little damage in other places of the slab.

The reason was that the earth on the slab top was saturated and frozen, which increased the load. Moreover, the slab was constructed with insufficient punching shear capacity.

Figure 1.4 Collapse of Skyline Plaza (adapted from Building Science Series 179, 2003, by Building and Fire Research Laboratory of the National Institute of Standards and Technology, USA)

Punching shear failure can also occur during construction, when the weight of the fresh concrete and shoring are transferred to the adjacent lower stories. These construction loads are sometimes larger than the designed live loads. If the shoring is removed too early, the concrete strength of the lower story may not be sufficient, resulting in lower punching shear capacity. In 1973, the Skyline Plaza (high-rise apartment building in construction) suffered a progressive collapse from the 23rd floor to the basement which caused fourteen workers' death (Fig. 1.4). The investigation revealed that the failure started from 23rd floor by failure of the slab near one or more columns due to premature removal of shoring and the low punching shear strength of concrete (Carino, et al., 1983).

Openings in slabs are often necessary and are often located near columns. This makes the slab column connections weaker in punching shear. Feld and Carper (1997) reported punching shear failures of concrete slabs due to construction of openings beside columns (Feld and Carper, 1997).

1.2 Reinforced Concrete Flat Slab Column Structures under Earthquakes

There are more than 10,000 earthquakes recorded each year and approximately 60 of them are significant and potentially destructive (Bertero, 1994). Earthquakes occur in Canada mainly in the east and west coast areas and in the Arctic.

During an earthquake, the horizontal movement of the ground induces large horizontal inertia forces and lateral drifts in the buildings. The inter-story drift makes the flat slab-column connection rotate and produce moments in the connection. The moments increase punching shear stress in a concrete slab around the column area. Therefore, the flat slab structures are easy to be damaged in earthquakes.

In 1985 Mexico City earthquake, 91 waffle slab structures collapsed and 44 were severely damaged (Rosenblueth et al., 1986). This type of structure was the most vulnerable to collapse in that earthquake. Waffle slabs have solid slabs at the column connections, thus they have similar behaviour to flat slab structures. Some of them were damaged by punching shear failure of the slabs. Others were damaged by column failures.

In the 1994 Northridge earthquake, a four-story reinforced concrete slab-column building was severely damaged. Its typical plan view is shown in Figure1.5. The outside perimeter consisted of ductile moment frames. Slabs (with drop panels) were post tensioned. Each of the first floor and the second floor was damaged in six slab-column connections (Figure 1.5). Also, there was cracking and spalling of concrete on the perimeter frame (Sabol 1994, Wallace et al., 2000)

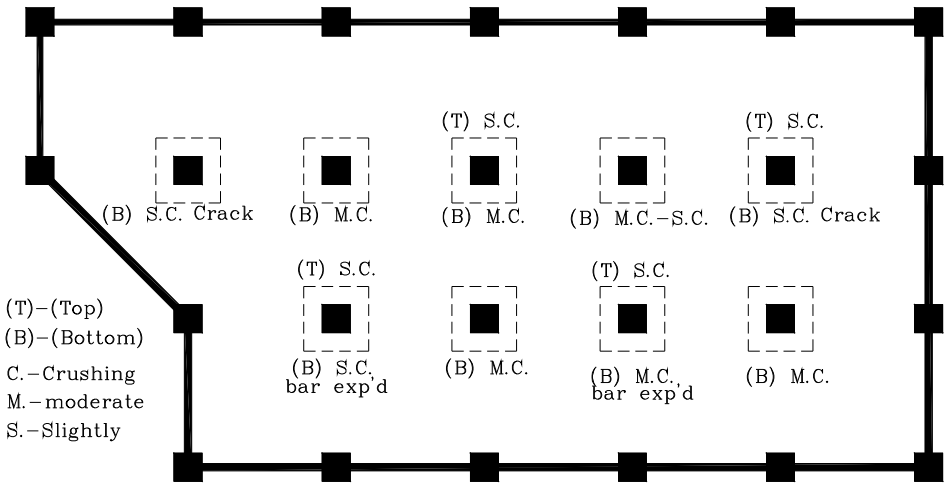

Figure 1.5 Damage of the slab due to punching shear (Sabol, 1994)

1.3 Objective of This Research

Strength and ductility are both important for structures designed for seismic zones. It would not economical to make all buildings to deform elastically under earthquakes. Most structural members are allowed to have plastic hinges and deform plastically. An important philosophy is that these members must be able to sustain load under large deformations to let people be evacuated during an earthquake. Thus, these structures must possess ductility. A general definition of ductility can be stated as: the ductility is the ratio of the ultimate displacement (drift, or rotation) over displacement (drift or rotation) at the onset of yielding.

It was not until in 1976 that the United Building Code specified ductility requirements for structures. A large number of buildings, including flat slab column structures, constructed before that are therefore lacking ductility. Recent earthquakes show that buildings designed using newer structural codes behave much better than the older ones. Therefore, it is desirable to find effective method to strengthen the existing reinforced concrete flat slab column structures. It is important to increase the punching shear capacity, ductility, and lateral drift capacity of the slab column connections.

Adding shear reinforcement is one way to meet these requirements. Among many kinds of shear reinforcements, steel shear bolt, was developed for existing concrete slabs. Figure 1.6 shows one shear bolt and its washer and nut. This type of shear bolt set was used in this research. The bolt stems were of 3/8” (9.5mm) diameter. Figure 1.7 gives the dimensions of the bolt. The washer at the threaded end was machined to be 9mm thick and 44mm diameter with 14mm diameter holes centered. The washer at the other end was of 44mm diameter, thickness 3mm and a hole of diameter 18mm. This washer was provided to increase the bearing area under the head which had a diameter 30mm (typical for shear studs).

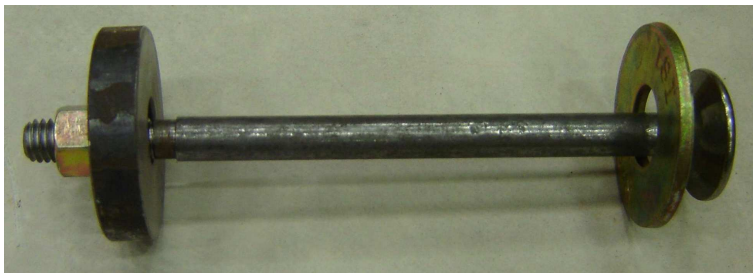

Figure 1.6 Picture of shear bolt

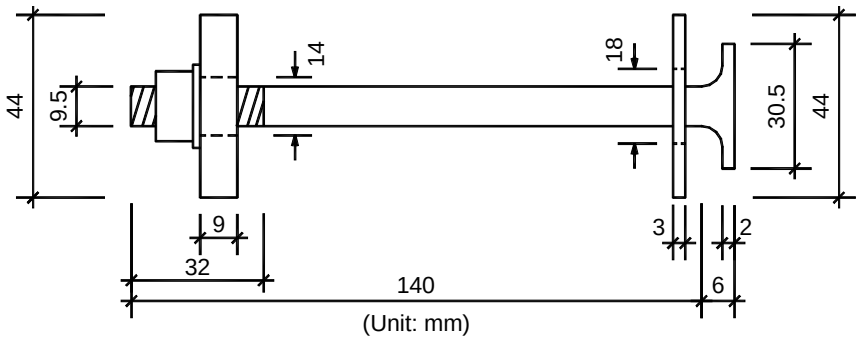

Figure 1.7 Dimensions of boll, washer and nut

The shear bolts were installed vertically through the holes drilled in the concrete slabs around the columns. Figure 1.8 shows the shear bolts installed in a slab. The bolts intersected with the potential punching shear crack, holding the outer part of concrete slab from punching. Figure 1.9 shows the possible pattern: orthogonal and radial layout of bolts in the concrete slab. Figure 1.10 and Figure 1.11 show the top and bottom view of the concrete slab with shear bolts, respectively.

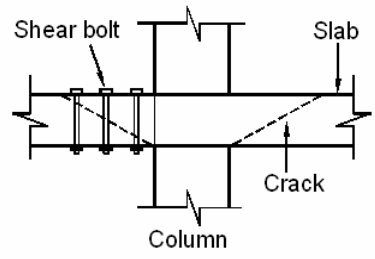

Figure 1.8 Shear bolts installation in the concrete flat slab

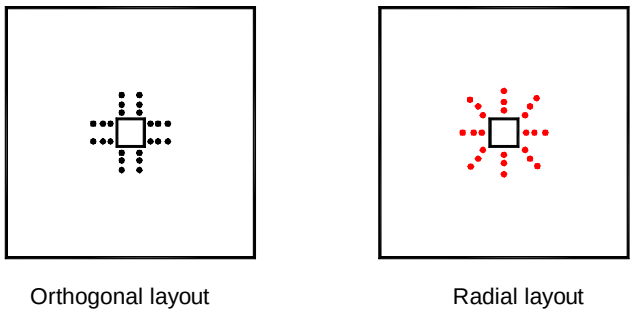

Figure 1.9 Layout pattern of shear bolts in the concrete slab

Figure 1.10 Top view of the slab with steel shear bolts

Figure 1.11 bottom view of the slab with shear bolts

Since 1996, research has been carried out on flat slab column structures strengthened by shear bolts. First, El-Salakawy et al. (2003) published test results on edge slab column connections strengthened with shear bolts subjected to a constant ratio of gravity load and lateral loads. Then, Adetifa and Polak (2005) tested six interior flat slab column connections. Those experiments showed that under

static loads shear bolts can improve the punching shear capacity and ductility of the slab column connections.

Since punching shear strength and ductility of flat slab-column connections is especially important in seismic zones, the behaviour of slabs strengthened with shear bolts became the primary objective of this research. This behaviour was investigated in the experimental program designed to study the load-displacement responses. Nine full scale specimens were tested. Comparisons were done with slabs without shear reinforcements. In addition, the effect of openings in slabs, intensity of gravity loads and bolts patterns in the slabs were varied in the tests. The thesis is concluded by a detailed investigation of the design recommendations regarding shear bolt size, anchorage head size and spacing of bolts in slabs.

1.4 Contribution of This Research

This research involved experimental investigation on the behaviour of interior slab column connections with shear bolts subjected to gravity load and pseudo seismic loading. Nine slab column specimens, in two series, were cast. Three of them were designed with 150x150mm openings next to column faces. Three of the specimens had applied constant vertical load of 110kN and the others were subjected to 160kN.

This research is the first to present test results of slab column specimens strengthen with shear bolts under pseudo seismic loading. It involved design and testing of nine specimens (six of them with shear bolts) under gravity load and cyclic lateral displacement loading. The obtained results were analyzed regarding lateral load capacity, lateral drift ratios, cracking, strains, deflections, and ductilities of the specimens. Series I, which was an initial test series, was designed to study the effect of shear bolts in slabs, number of shear bolt rows, and gravity load intensity under cyclic displacements. Series II was designed to study effect of openings and bolt pattern on the overall behaviour of connections.

In order to conduct this research, a detailed testing setup was defined. An existing steel test frame in the laboratory was first modified and an additional steel supporting frame was designed and constructed. An independent steel rack was designed and installed for displacement transducers to record the specimen deformation.

In addition to testing, a theoretical investigation was completed on the design aspects of shear bolts and slabs reinforced with shear bolts. To provide a design and construction guide for strengthening of

flat slab column structures, bolt heads were analyzed using elastic thin plate theory and finite element analysis. Equation for head area was derived based on concrete bearing strength. Relation among head thickness, bolt diameter and diameter of holes was provided.

Bolt spacing in slabs was analyzed and appropriate design procedures were provided. These included strength requirements for concrete slabs retrofitted with shear bolts and requirements related to inclined crack propagation. Seismic design requirements regarding to slabs with shear bolts were given. Finally, some suggestions were provided for the retrofitting construction, fire and corrosion protection of steel shear bolts, and maintenance.

1.5 Organization of the Thesis

Chapter 1 of this thesis introduces the background, explains the objective of the research, and presents the contributions.

Chapter 2 describes a literature review on: 1) punching shear research; 2) seismic behaviour and research on flat slab column structures; 3) previous research work carried out at the University of Waterloo.

In Chapter 3, the experimental setup is introduced, including the design and setting up of steel test frame, steel supporting frame, instrumentation, and design and fabrication of the concrete flat slab column connections.

Chapter 4 presents the experimental results. Comparisons are made which show the advantages of the steel shear bolts. Analysis of the results is done which shows the performance of slabs with shear bolts. Loads, drift ratios, strains, and cracks are presented.

In Chapter 5, the design of steel shear bolt is introduced. Also the design of the existing concrete slabs strengthened with shear bolts is explained in terms of number of bolts, the spacing and layout of the bolts in the slab. Some suggestions are also given on the operation of retrofitting, protection and maintenance of the shear bolts.

Chapter 6 presents the conclusions and provides suggestions for future research.

Chapter 2
Literature Review

2.1 Introduction

This chapter describes literature on punching shear research work that has been done by previous researchers. First, in section 2.2, it introduces the research completed on reinforced concrete flat slab column connections under vertical (gravity) load or a combination of vertical load and static moments only. Second, in section 2.3, it addresses previous research on punching shear behaviour of flat slab-column structures subjected to seismic loads and gravity load. Then in section 2.4, some typical mechanics models for punching shear of slab-column connections are reviewed. In section 2.5, the code design methods for punching shear of flat slab column structures are introduced. Finally, section 2.6 presents research on shear bolt strengthening method that has been done at the University of Waterloo, which includes work on edge slab-column connections under gravity loads and static moments, and behavior of interior flat slab-column connections subjected to monotonically increasing gravity loading.

2.2 Punching Shear Behaviour in Reinforced Concrete Slabs under Vertical Load or Vertical Load Combined with Static Moments

When a reinforced concrete flat slab column structure is subjected to heavy gravity (vertical) load, punching shear cracks occur inside the slab at the column vicinity. They propagate at 20 ~ 50 degree angles through the slab thickness. A truncated conical or pyramid failure surface around the column forms. In addition to vertical loads, the slab-column connections may be subjected to unbalanced moments, which are caused by unequal spans on both sides of the column or by lateral loading such as wind or earthquakes. The unbalanced moment is resisted by a combination of stresses in slab flexural reinforcements, shear strength of concrete, and shear reinforcement in the vicinity of column. Effect of unbalanced moments from earthquakes (reversed cyclic loading) will be discussed in Section 2.3. Punching shear transfer mechanisms (internal forces equilibrating punching force) include: aggregate interlock at the crack, compression and tension in concrete, dowel force from flexural steel, and tension in transverse reinforcements if present.

2.2.1 Parameters Influencing Punching Shear Strength of Slab-Column Connections

Many factors affect the punching shear capacity of flat slab-column connections under static loads. Slab thickness, column dimensions, concrete strength, flexural reinforcing ratio and pattern, and shear reinforcement are all the parameters influencing punching shear capacity. In experiments, the testing methods and conditions, such as the loading rate and scale of specimens, also influence the results, and supporting conditions. The discussion below is based on some selected references related to the above factors.

2.2.1.1 Concrete Strength

Research has been done to find the relation between the concrete compressive strength, f_c' and the shear strength. Moe (1961) was the first to conclude that the shear strength relates not to f_c' but to $\sqrt{f_c'}$. Based on the testing results, he obtained the following equation for ultimate nominal punching shear capacity V_n:

$$V_n = [15(1-0.075\frac{c}{d}) - 5.25\phi_0]\sqrt{f_c'} \tag{2.1}$$

where c is the column dimension, d is the effective slab depth, $\phi_0 = \frac{V_n}{V_{flex}}$, V_{flex} is the vertical punching shear force at the calculated ultimate flexural capacity of the slab. Moe explained that shear strength is primarily affected by concrete tensile splitting strength which is often assumed proportional to $\sqrt{f_c'}$. Current research also suggests that high strength concrete can increase 20% of the shear strength of the slab-column connection (Emam, Marzouk, and Hilal, 1997).

2.2.1.2 Column Size and Slab Thickness

As shown in equation (2.1), Moe (1961) proposed that shear strength depends on the ratio of concentric load area (column) dimension c to slab effective thickness d . In equation (2.1), if let $\phi_0 = 1$, the value of $\frac{V_n}{\sqrt{f_c'}}$ would be in linear relation with $\frac{c}{d}$. This means when dimensions of

concentrated load area increase, or when the slab effective thickness decrease, $\frac{V_n}{\sqrt{f_c^{'}}}$ decreases as well.

2.2.1.3 Flexural Reinforcement

The strength of flexural reinforcement, reinforcement pattern and layout, and the amount of compression reinforcements have effects on punching shear capacity. These are explained as follows.

(1) Strength and Ratio of Flexural Reinforcement

Research indicates that shear strength can be related to flexural effects. Yitzhaki (1966) tested 14 slab-column specimens and proposed that the shear strength depends proportionally on the flexural reinforcement strength and the column size.

Dowel forces develop in the flexural reinforcements when they cut across the inclined shear crack. Vertical forces also develop due to the membrane effect in the flexural reinforcement mat when the rigid parts of a slab (outside of shear cracks) rotate around the column. Kinnunen (1963) concluded that dowel forces and vertical forces from membrane effect account for 35 percent of the punching shear capacity. Therefore, according to Kinnenun's conclusion, slab punching shear capacity increases if the ratio and strength of flexural reinforcements increases.

Moe (1961) proposed the relation between $\frac{V_n}{V_0^{'}}$ and $\frac{V_n}{V_{flex}}$, as in equation 2-2,

$$\frac{V_n}{V_0^{'}} + C^{'}\frac{V_n}{V_{flex}} = 1.0 \qquad (2\text{-}2)$$

where V_n is the nominal punching shear strength (vertical punching shear force of the column), V_{flex} is the vertical punching shear force at the calculated ultimate flexural capacity of the slab, $C^{'}$ is a constant between 0 and 1, and $V_0^{'}$ is a fictitious reference value of shear, $V_0^{'} = A^{'}bd\sqrt{f_c^{'}}$, $A^{'}$ is a constant, b is the perimeter length of the critical section, d is the effective thickness of a slab. From Figure 2.1, it is found that if $\frac{V_n}{V_{flex}} = 1$, $\frac{V_n}{V_0^{'}}$ approaches a constant. This means if we design a slab

governed by flexural failure ($V_n = V_{flex}$, which is a preferred mode of failure), V_n can be calculated using $V_0^{'} = A^{'}bd\sqrt{f_c^{'}}$, which is independent of the flexural reinforcing ratio.

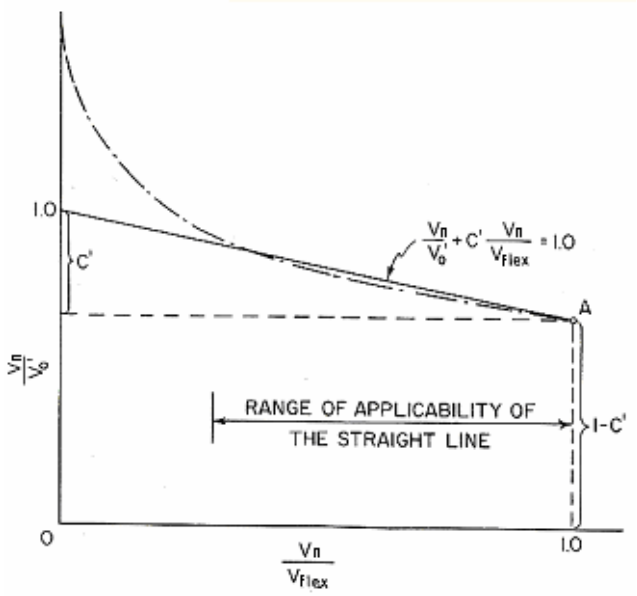

Figure 2.1 Interaction between Shearing and Flexural Strength (Moe, 1961)

(2) Pattern of Flexural Reinforcement

Tests by Kinnunen and Nylander (1960) showed that the failure loads can be about 20%-50% higher in circular slabs reinforced with two-way bars than that in slabs with ring reinforcements.

(3) Concentration of Tensile Reinforcement

Hawkins et al. (1974) summarized that concentration of tensile reinforcement over a column is preferable because it increases slab stiffness, delay the first yielding of tension reinforcement, and decrease the crack width under the same loading condition.

(4) Compression Reinforcements

Elstner and Hognestad (1956) reported that, for $\phi_0 = \frac{V_n}{V_{flex}} < 1$, there is little effect on shear strength with the variation of the compression reinforcement, where V_n, V_{flex} are defined as in equation (2-1). However, when $\phi_0 \geq 1$, the shear strength increases if the ratio of the compression reinforcement increases. Compression reinforcements also increase the dowel force after punching failure, which can prevent progressive collapse of a structure.

2.2.1.4 Shear Reinforcements

Conical punching shear cracks form if the slab is subjected to a vertical load or a vertical load with an unbalanced moment. To prevent punching shear crack from propagating, shear reinforcements can be used. Shear reinforcement is, in general, a bar (or other shape) crossing the inclined cracks to prevent punching shear failure. The bar should have adequate tension strength, ductility and good anchorage to develop its strength if punching shear occurs. There are many types of shear reinforcements for new or existing reinforced concrete slabs.

(1) Shear Reinforcements for New Construction

For new construction, shear reinforcements are embedded with the flexural reinforcements before the concrete is cast. They can be divided into three groups: 1) Structural steel sections such as I shape steel, or channels; 2) Bent bars and stirrups; 3) Headed reinforcements including shear studs and headed bars

Hawkins and Coley (1974) investigated the effect of I-shape steel in edge slab-column connections (Figure 2.2). They found that I-shape steel increase shear capacity and rotation capacity of the slab-column connections. However, I-shape steel sections need to pass through the slab-column connection, and therefore sections in one direction need to be welded or bolted onto the I-steel sections in the other direction. This congests the slab column connections. In addition, the I-shapes can only be embedded between the top and bottom rebar mats, otherwise holes have to be drilled to let the rebars go through. Thus this kind of punching shear reinforcement is not a favorable one in construction, with the exception of thick slabs and large columns where they may work.

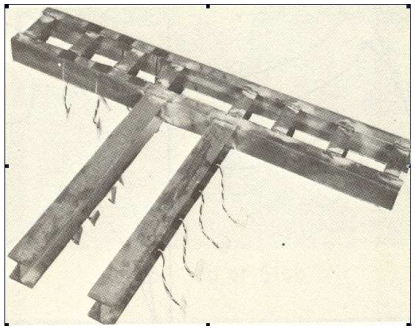

Figure 2.2 I-shape shear reinforcement (Hawkins and Coley, 1974)

Headed shear studs welded to a bottom steel strip were first tested at the University of Calgary by Dilger and Ghali (1981) (Figure 2.3). The area of a head on the top of the bar is usually at least ten times of the bar sectional area. Tests using this shear reinforcement show that the shear capacity and ductility are increased.

Figure 2.3 Headed shear studs welded to a bottom steel plate

Megally and Ghali (2000) compare five 150mm thick interior slab-column connections under vertical loading. Four of them were strengthened by shear capital, drop panel, stirrups, and shear studs, respectively. It is shown that the shear capital and drop panel increase punching shear capacity, but the strengthened slabs show no better ductility than non-strengthened slab (Figure2.4). Stirrups

increase strength, but not ductility for 150mm thick slab (due to poor anchorage). Shear studs substantially increase strength and ductility of the connections.

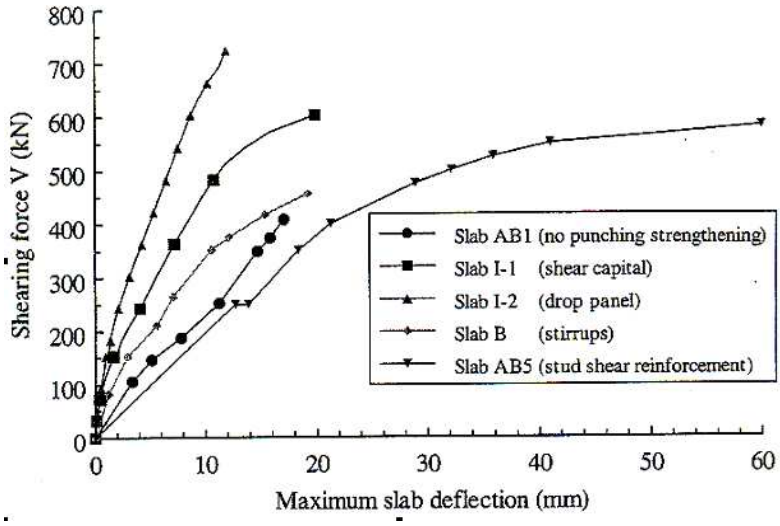

Figure 2.4 Load-deflection curves of slabs with different punching strengthening methods (adapted from Magally and Ghali, 2000)

(2) Shear Reinforcement for Retrofit of Existing Reinforced Concrete Slab-Column Structures

Existing concrete slabs may need to be strengthened due to insufficient punching shear capacity. This may be caused by change of the building use, new openings in a slab, design and constructions errors. There have been several methods proposed for punching shear retrofit of existing slab column connections. A steel support can be installed around the column on the bottom of the slab. Also reinforced concrete capital or a drop panel can be added to the bottom of a slab.

Ghali et al. (1974) tested 10 specimens with prestressed shear bolts in three groups (Figure 2.5). The twelve bolts for each specimen were 3/4 inch diameter high tensile strength steel bolts with a 4x4x3/4 inch steel plate at each end. The unbonded bolts were tensioned to 75.3kN before testing. One group of specimens (Group B) were subjected to monotonically increased moments, and another group (Group C) were subjected to monotonically increasing vertical load. The results showed that the prestressed slab had much higher deflection capacity and failure load than unreinforced slabs. In Group C, specimen # 10 (no bolts) obtained an ultimate load of 413 kN, but specimen #9 (prestressed bolts) obtained 690 kN ultimate vertical load, an increase of 67% compared with specimens #10. In

group C, specimens #5 (without bolts) reached 196 kNm ultimate moment, and specimen #4 (with prestressed bolts) reached 241 kNm moment, a 23% increase.

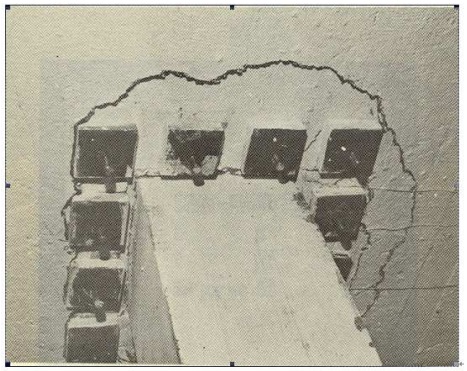

Figure 2.5 Prestressed shear bolts for slab under vertical load (Ghali et al. 1974)

A new shear strengthening technique using steel shear bolts for existing slab was proposed by El-Salakaway et al. (2003), and Adetifa and Polak (2005). Results of the tests show that the maximum deflections measured at ultimate loads are between 54-162% larger for slabs with shear bolts than those of non-shear-reinforced slabs. The ultimate punching shear capacity can also be increased by using shear bolts. These will be introduced in Section 2.6.

2.3 Previous Research on Seismic Behaviour of Reinforced Concrete Slabs

2.3.1 Flat Slab Column Structures in Seismic Zones

In seismic zones, flat slab column structures must deform without damage together with the primary lateral load resisting system such as shear walls or braced moment frames. If the slabs do not have adequate ductility and strength, punching shear failure of slab-column connection can occur. When the concrete slab column structures experience cyclic loading during an earthquake, the behaviour of the structure is different from those in non seismic zones. The punching shear strength and stiffness of concrete decrease under cyclic load, hence the slab-column connections need to possess certain strength and ductility to undergo inelastic deformations. Lateral deforming capability and ductility are two main necessary properties of slab-column structure in seismic zones. Furthermore, this type of structures needs to have post-failure resistance after an earthquake to support service loads.

Substantial research work has been done on punching shear behaviour of slab-column structures in seismic zones. Most of the previous experiments were done using interior or edge connection subassemblies isolated from prototype structures consisting of a slab with columns extending from the top and bottom of the slab. These subassemblies are subjected to vertical loading from either the top of columns or slab surface, and cyclic loading on the column ends or slab edges. This method is easy to carry out and the test results have been utilized in design codes. There is also some research was done using continuous slab column specimens. Other experimental methods include testing model structures on shaking tables.

Many factors influence seismic punching shear capacity and ductility of slab-column connection in seismic zones. In addition to the ones described in section 2.2, the following are also important in seismic zones: biaxial loading or uniaxial loading and the magnitude of the gravity load shear.

2.3.2 Behaviour of Slab-Column Connections under Cyclic Loading

2.3.2.1 Effect of Gravity Load

Robertson and Durrani (1992) tested three specimens each with two exterior and one interior slab-column connections as shown in Figure 2.6. The three specimens were subjected to different vertical and lateral cyclic loadings. The specimen A, B and C were subjected to vertical load of 140, 285, 420 lb/ft^2 (6.7kPa, 13.6kPa, 20.1kPa) respectively. Specimen A reached a peak lateral load of 19.8 kips (88.0 kN) at 3.5% drift, while peak load on specimens B and C were 13.1 kip (58.3kN) and 9.6 kip(42.7kN) respectively (Table 2.1). Specimen A reached maximum drift of 5% at failure, while specimen B and C reached 1.5% and 1%, respectively.

This work demonstrates that when the gravity load level (gravity shear level) increases, the capacity for moment transfer and ductility of the connection decrease. The hysteresis curves of unbalanced moment versus drift for three specimens A, B and C (with increasing gravity loading) show that the capacity of lateral drift, stiffness, and energy dissipation decrease as the gravity loading increase. Robertson and Durrani (1992) suggested a design limit, $\frac{V_u}{V_0} \leq 0.35$, where V_u is the direct shear force at peak lateral load, and V_0 is the nominal shear capacity of slab in the absence of moment transfer.

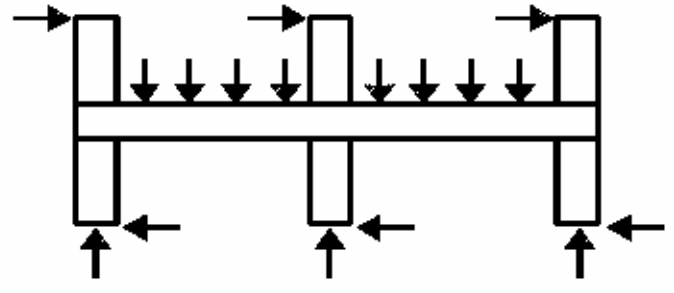

Figure 2.6 Specimens including exterior and interior slab –column connection

Table 2.1 Vertical load influence on peak load and drift (from Robertson and Durrani, 1992)

Specimen	Superimpose slab load (lb/ft^2)	Peak load and corresponding drift	Drift of first failure
A	140	19.8 kip at 3.5% drift	5% at one exterior connection
B	285	13.1 kip at 1.5%	1.5 % at interior connection
C	420	9.6 kip at 1%	1% at interior connection

1kip=4.448kN, lb/ft^2 =47.88Pa

2.3.2.2 Effect of Biaxial Lateral Cyclic Loading

Pan and Moehle (1992) investigated the effect of biaxial lateral loading and gravity loading on the behaviour of slab-column connections. Their test set-up is schematically showed in Figure 2.7. Some of the specimens were subjected to uniaxial cyclic drift, while the others were subjected to biaxial loading. It was found that lateral cyclic loading reduces the lateral stiffness, strength, and drift capacity of the slab-column connections. Figure 2.8 shows the lateral force versus drift envelopes for Specimens 1 to 4. Specimen 1 and specimen 2 have the same average gravity nominal shear stress on the critical section, $1.4\sqrt{f_c'}$ psi ($0.12\sqrt{f_c'}$ MPa), specimen 3 and 4 are with the same gravity shear stress of $0.88\sqrt{f_c'}$ psi ($0.07\sqrt{f_c'}$ MPa). Specimens 2 and 4 were subjected to biaxial loading. It is concluded that the biaxial cyclic loading results in decrease in stiffness, strength, and available drift

capacity as compared to uniaxial cyclic loading situation. Figure 2.8 also demonstrates that higher gravity level loads lead to decrease in stiffness, strength, and available drift capacity.

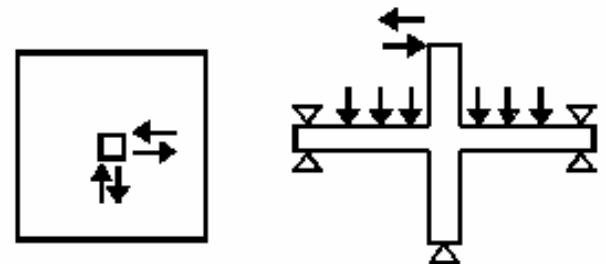

Figure 2.7 Test set up of biaxial loading

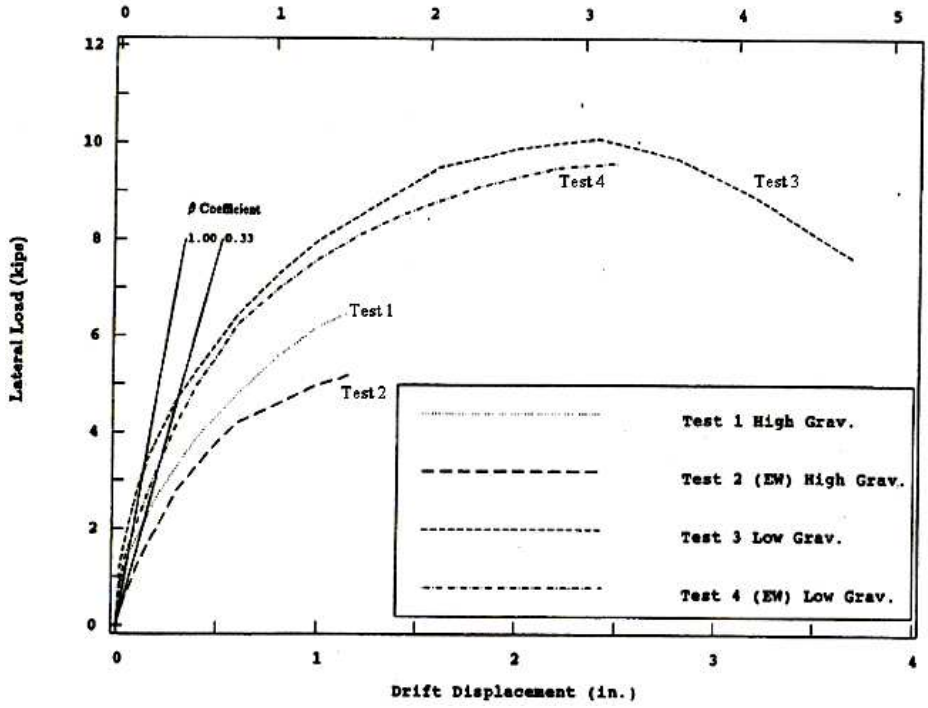

Figure 2.8 Experimental envelopes

2.3.2.3 Shear Capitals and Drop Panels

Since shear capitals increase the thickness of a slab near the column, they are helpful for increasing punching shear capacity. This was confirmed by Wey and Durrani's tests (1992). They tested three

specimens with shear capitals under vertical load and cyclic moment. It was concluded that when the shear capital is too small, and the connection is under high moment reversals, the net positive moment at the connection may result in an inverted punching failure and the thickness of the shear capital is not effective in increasing the shear capacity.

As mentioned in section 2.2.1, Megally and Ghali (2000) concluded that shear capitals can only increase shear capacity, but not enhance ductility of the slab-column connections.

2.3.2.4 Effect of Concrete Strength on Seismic Punching Shear

Emam, Marzouk and Hilal (1997) researched seismic characteristics of slab-column structures constructed with high-strength concrete. According to their tests on four interior slab-column connections: two with high-strength concrete column and slab: H.H.H.C.0.5(1) and H.H.H.C.1.0(2), two with high-strength column and normal strength slab: N.H.H.C.0.5(3) and N.H.H.C.1.0(4). By using high strength concrete, the ductility of displacement and rotation increased by 100 and 125 percent, respectively, as the concrete strength increased from 35 to 75 MPa. Shear strength, moment capacity, drift percent, and rotation capacity increased by 20, 31, 37 and 50 percent, respectively.

However, Megally and Ghali (2000) concluded that although high strength concrete increase punching strength, the ultimate drift ratio and displacement ductility factor, it can hardly prevent brittle failure in severe earthquakes.

2.3.2.5 Shear Reinforcement for New Slabs

Several tests on slab-column structures under cyclic loading were conducted using stirrups, shear studs, bent-bars, or shearhead reinforcements. The summary of the findings is presented below.

(1) Stirrups, bent bars, and steel shearheads

Four slab-column connections (three with vertical closed stirrups and one without shear reinforcement) were tested under cyclic loading by Islam and Park (1976). Meanwhile they also tested other two specimens under monotonic lateral loading, one with bent-bars, the other with shearhead reinforcement (channel sections). The experimental results led to the conclusion that the closed stirrups increase the shear strength and significantly increase ductility of the connection under

cyclic unbalanced moment. The closed stirrups result in more ductile behaviour at large deflections than a structural steel shearheads. Bent bars and channel sections also increase shear strength, however, bent bars do not increase ductility and only resist punching shear in one direction; and channels only slightly increase ductility.

Hawkins et al. (1975) investigated the effectiveness of integral beam type stirrup reinforcement in slabs under cyclic loading. They concluded that the closed stirrups can increase the shear strength, ductility and change the 'hysteretic behaviour of the connections with low reinforcement ratios from a shear to a moment type of energy dissipation mechanism.' In order to make stirrups work efficiently, they should be closed and with 135 degree hooks, well anchored and extend far enough from the column.

(2) Shear studs

Shear studs were developed at the University of Calgary as mentioned in section 2.2. Cao and Dilger (1993) tested four specimens with shear studs. They found that the shear studs improve significantly the connection ductility and shear strength. Since shear studs are easy to install and do not interfere with flexural steel bars and with concrete casting, this type of reinforcement is preferred in construction. One other conclusion from Cao and Dilger (1993) is that under cyclic loading the concrete nominal shear strength of the connection is reduced. This should be included in punching shear design formulas for slabs in seismic zones.

Megally and Ghali (2000) published their test results of eight single edge slab-column connections with and without shear studs under cyclic loading. The conclusion was that shear studs increase the punching shear resistance and prevent brittle failure even in a severe earthquake. The connections can undergo ductile deformations up to 5% inter-storey drift ratio without punching shear failure.

2.3.2.6 Seismic Retrofit of Reinforced Concrete Slab Column Connections

Ebead and Marzouk (2002) tested two slabs, 1900x1900x150mm slab with 240x240 columns, which were strengthened by eight ASTM A325 bolts (19mm diameter) and 6 mm thick steel plates on top and bottom slab surface around the column. (Figure2.9). The bolts were bonded with concrete using epoxy. The specimens were subjected to constant vertical load and cyclic lateral load. They found that

the moment capacity increased about 15% and the strengthened connection could undergo 75% more lateral drift than those without bolts and steel plates. The strengthened connection could reach 8% drift before failure, whereas the non-strengthened slab could only reach about 4-5%.

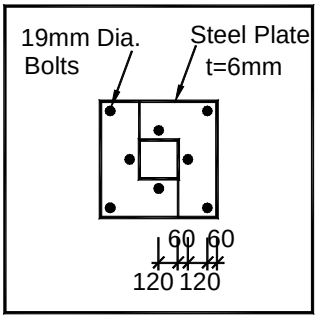

Figure 2.9 Slab strengthened by steel bolts and plates (Ebead and Marzouk, 2002)

Carbon fibre-reinforced polymer (CFRP) were also used to strengthen the existing concrete slabs. Stark et al. (2005) tested two slab specimens strengthened with CFRP. As shown in Figure 2.10, CFRP straps were wrapped with epoxy through the holes in the slabs. These CFRPs acted as stirrups. The slabs were detailed according to the old version of ACI 319-63. The columns were made from steel and were attached to the slab using steel bolts. A vertical constant load and reversed cyclic lateral load were applied to the specimens. Punching shear failure was found at about 2% for the non-strengthened specimen, while the strengthened specimens could undergo about 8% drift without significant strength losses. The moment capacity also increased. The retrofitted connections had two times displacement ductility and 3.5 times joint rotation ductility as compared to the non-strengthened ones.

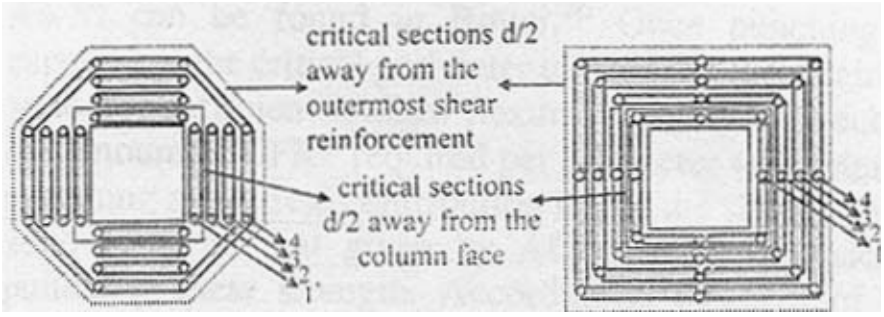

Figure 2.10 Slab strengthened by CFRP stirrups (Stark et al., 2005)

2.4 Analytical Models for Punching Shear

In the last few decades, intensive research work was done related to punching shear. Based on the experiments and analysis of the slab behaviour, several analytical models have been proposed. Some of them formed the basis of the design formulae employed in various structural codes and specifications. This section examines the background of the important models for punching shear.

(1) Punching Shear Model by Kinnunen and Nylander

Kinnunen and Nylander (1960) proposed a punching shear model based on static gravity-type test results of circular slab-column connections, with circular column and circular and radial reinforcements. Kinnunen (1963) developed the model suitable for circular slabs with two way orthogonal reinforcement mats on the tension side and considered dowel forces of the reinforcement. As shown in Figure 2.11, the part outside the inclined crack is divided into sectors bounded by the inclined crack, radial cracks and the perimeter of the slab specimen. The sectors as shown in Figure 2.12b, which are assumed to be rigid and supported by the imaginary conical concrete shell, rotate around the root of the inclined cracks. The conical shell, which supports all the sectors, is shown in Figure 2.12 and the shaded area in Figure 2.12 c.

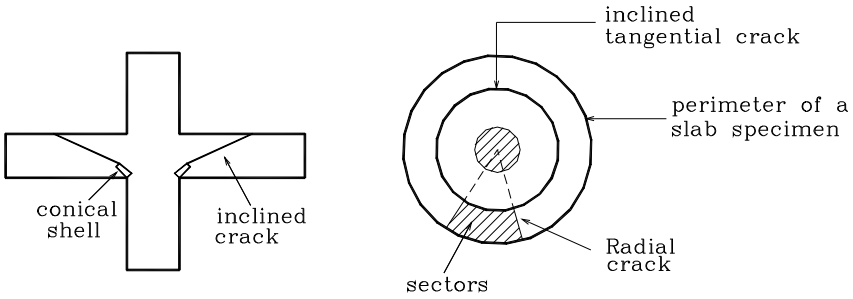

Figure 2.11 Assumption of conical shell and rigid sectors by Kinnunen and Nylander model

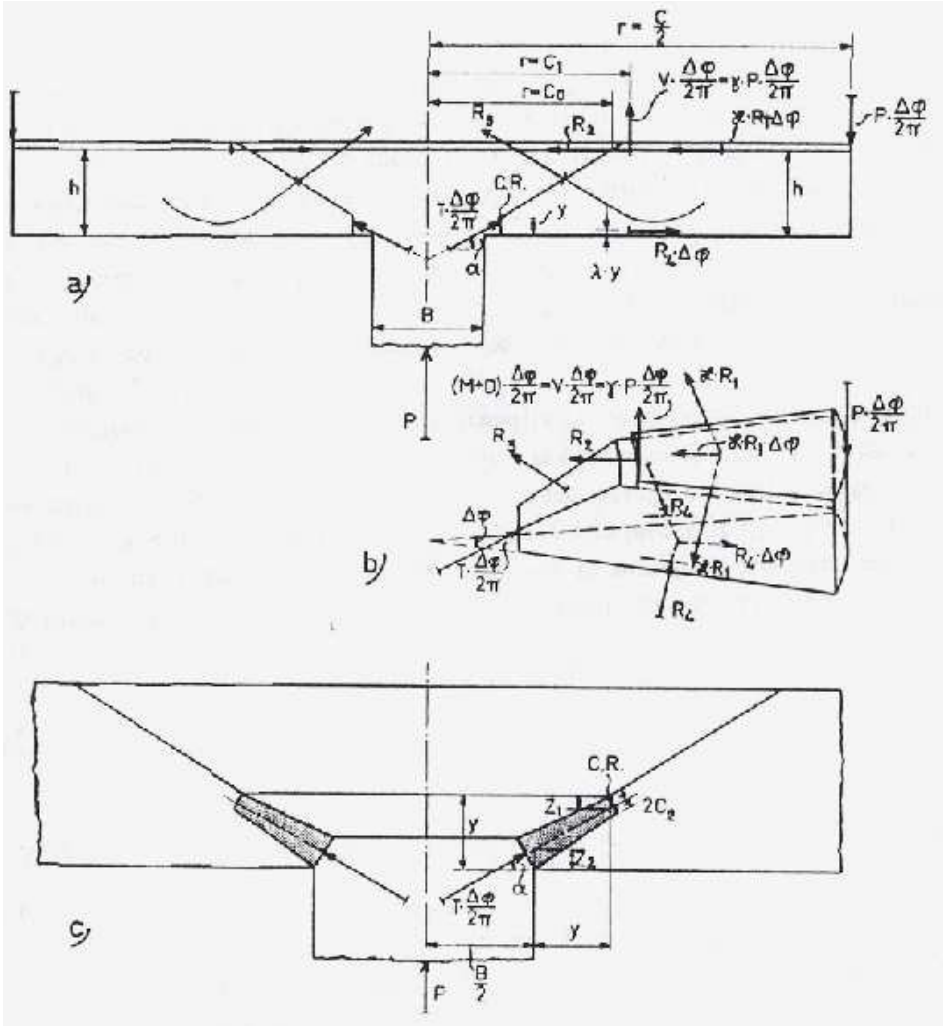

Figure 2.12 Punching shear model of Kinnunen, 1963

Through the equilibrium of the sectors, Kinnunen derived three equations as follows: equation (2-2) was set up by satisfying moment equilibrium; equation (2-3) and (2-4) were set up to satisfy force equilibrium in radial and vertical directions, respectively.

$$\gamma \cdot P \cdot (\frac{c}{2} - c_1) + T \cdot \sin\alpha \cdot (\frac{c}{2} - \frac{B}{2}) - T \cdot \cos\alpha \cdot (h - z_2) - 2\pi \cdot R_4 \cdot (h - \lambda \cdot y) = 0 \tag{2-2}$$

$$T \cdot \cos\alpha + 2\pi \cdot R_4 - 2\pi \cdot \kappa \cdot R_1 - 2\pi \cdot R_2 \cdot \frac{1}{\Delta\varphi} = 0 \tag{2-3}$$

$$P \cdot (1 - \gamma) = T \cdot \sin\alpha \tag{2-4}$$

where P is the punching shear load on the connection (the applied load at the slab periphery or at the column), T is the inclined compression force in the conical shell, κR_1 is the force component in the tangential direction of reinforcement cutting across the shear crack, R_2 is the force in radial direction of the reinforcement cutting across the shear crack, R_3 is the force of shear reinforcement (not included in this model), R_4 is the tangential resultant of concrete compression stress at the bottom of the section, M is the vertical component of membrane force in reinforcement mat caused by the rotation of the section, D is the dowel force in the reinforcement intersecting with the conical shear crack, $V = M + D = \gamma P$, γ is the ratio of V over P, $\Delta\varphi$ is the slice angle of the rigid section, α is the incline angle of the imaginary compression concrete conical shell, y is the vertical height of the conical shell from the slab bottom surface, λy is the vertical height of the resultant force R_4 from the slab bottom, B is column diameter, z_1 and z_2 see Figure 2.12 c.

Kinunnen also assumed that the failure criterion is: "The tangential compressive concrete strain on the bottom surface of the slab under the root of the shear crack reaches a characteristic value at which favorable embedment of the conical shell is impaired".

Using the compression stress in the slab bottom concrete, we obtain punching load P_1. Then using the forces in the reinforcements, a punching load P_2 can be calculated. The ultimate punching load P is obtained by an iterative process: assume an initial value of $\frac{y}{h}$ to calculate α, calculate P_1, and P_2; if P_1 is not close to P_2, assume another $\frac{y}{h}$, and repeat till $P_1 = P_2$, which is then equal to the ultimate punching load P.

(2) Truss Model by Alexander and Simmonds

Alexander and Simmonds (1987) proposed a truss model to simulate the punching shear mechanism of slab-column connections. The model assumes the top steel bars as horizontal chords and the concrete from the bottom of slab to the top reinforcement as inclined struts (gravity struts). As shown in Figure 2.13, the gravity concrete struts resist the downward movement, while the uplift struts resist upward movement. (Uplift struts consist of bottom rebar and concrete from top slab to bottom rebar.) When the punching load or the moment is large, the

stress in the struts would be large enough to push the reinforcement mat apart from the concrete. To determine the inclination angle α of the struts, Alexander et al. (1987) gave the following equation based on experimental results:

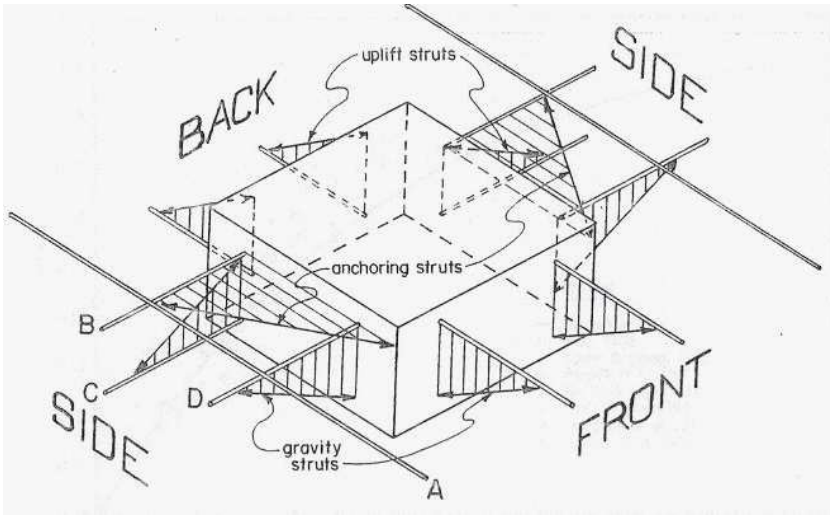

Figure 2.13 Truss model of slab punching shear (Alexander and Simmonds, 1987)

$$\tan\alpha = 1.0 - e^{-2.35K} \tag{2-5}$$

$$K = \frac{s_{eff} \cdot d' \cdot \sqrt{f_c'}}{A_{bar} \cdot f_y \cdot (c/d_s)^{0.25}}$$

where s_{eff} is the effective tributary width of reinforcing bar, d' is the cover of reinforcing mat measuring from center of the mat to the near slab surface, A_{bar} is the area of a single reinforcing bar, c is the dimension of column face perpendicular to the bar being considered, d_s is the effective depth of the slab, f_y is the yield strength of the reinforcement, and f_c' is the concrete compression strength. For interior slab-column connections under vertical load only, once the strut angle α is determined, the ultimate punching shear load P can be calculated using the following equation:

$$P = A_{st}^{T} \cdot f_y \cdot \tan\alpha \tag{2-6}$$

where A_{st}^{T} is the section area of flexural reinforcements that are close enough to the column to participate as a shear strut.

(3) Bond model by Alexander and Simmonds

On the basis of their truss model, Alexander and Simmonds (1992) proposed a bond model for concentric punching shear. In the truss model, the shear is resisted by vertical component of the force of the straight-line compression struts. However, tests show that a curved arch is more consistent with strain measurements than the straight-line strut (Figure 2.14). The shear is transferred to the column by the curved, radial compression arch. Let T be the tension force in the reinforcing bar as shown in Figure 2.14. The shear force V can be expressed as

$$V = \frac{d(T \cdot jd)}{dx} = \frac{d(T)}{dx} jd + \frac{d(jd)}{dx} T$$

where jd is the moment arm, $\frac{d(T)}{dx} jd$ is the beam action part in which tension force in the rebar varies with location x (stress gradient in the rebar), whereas $\frac{d(jd)}{dx} T$ is the arching action part in which the arm jd changes with x.

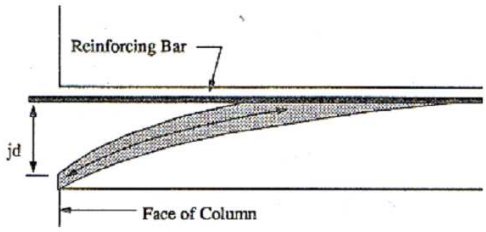

Figure 2.14 Curved compression strut (adapted from Alexander et al., 1992)

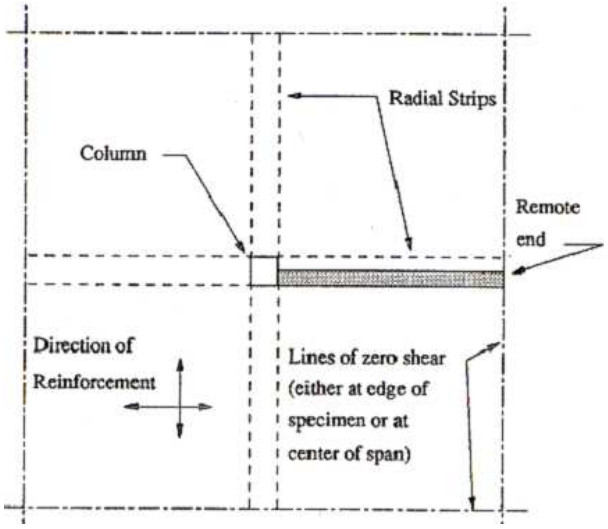

Figure 2.15 Layout of radial strip (adapted from Alexander et al., 1992)

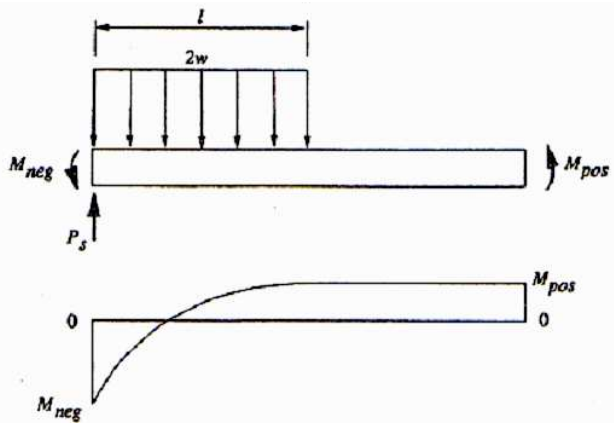

Figure 2.16 Equilibrium of Radial Strip (adapted from Alexander et al., 1992)

It is assumed the loads on the slab are transferred to four radial strips intersecting with the column (Figure 2.15). Each radial strip can be assumed to be a cantilever beam (Figure 2.16) when the far end is free of moment, as in many punching shear tests for slab-column connections, ie $M_{pos} = 0$ in Figure 2.16. w is the maximum shear load that may be delivered to one side of a radial strip by the adjacent quadrant of the two-way slab. Alternatively, w is calculated from the maximum force

gradient in the reinforcement perpendicular to the radial strip. The punching capacity of the slab-column connection P is

$$P = 8w^{*}l = 8\sqrt{M_{neg}w} \tag{2-7}$$

where $M_{neg} = \frac{2wl^2}{2}$

M_{neg} is the flexural capacity of the strip, which can be calculated by the following equation:

$$M_{neg} = \rho \cdot f_y \cdot c \cdot jd^2 \tag{2-8}$$

where ρ is the effective reinforcing ratio (tension reinforcement on the slab top) within the radial strip, c is the width of the strip, f_y is the yield stress of the reinforcement, jd is the internal moment arm within the slab.

In order to calculate the ultimate punching shear load P as in equation (2-7), the distributed load w is estimated using either the maximum stress gradient in the rebar perpendicular to the strip or the nominal maximum one-way shear stress v_c which is specified by the ACI code 318. Alexander and Simmonds applied bond stress to calculate stress gradient in the reinforcements, which is then used to calculate w:

$$w = jd \cdot (\frac{\pi \cdot d_b}{s} \cdot \tau_{co}) \tag{2-9}$$

$$\tau_{co} = \sqrt{f_c^{'}} \cdot (0.09614 b_i + 0.1337) \tag{2-10}$$

$$b_i = \min \begin{Bmatrix} b_{si} = \frac{s}{d_b} - 1 \\ b_{vi} = \sqrt{3} \cdot \frac{2d'}{d_b} \end{Bmatrix} \tag{2-11}$$

where s is the spacing of rebar perpendicular to the strip, d_b is the diameter of the rebar, d' is the concrete cover thickness (from rebar center to top slab surface).

The second alternative to estimate the distributed load w is using the nominal maximum concrete shear stress v_c for a beam subjected to shear and flexure only, which is specified in ACI 318-05 clause 11.3.1 as:

$$v_c = 2\sqrt{f_c^{'}(psi)} = 0.166\sqrt{f_c^{'}(MPa)} \tag{2-12}$$

It is assumed that the maximum shear stress of the strip (beam) section is transferred to the strip. Therefore, the value of w is:

$$w = d * v_c = d(0.166)\sqrt{f_c^{'}} \quad \text{(MPa)} \tag{2-13}$$

where d is the effective thickness of the slab.

(4) Plasticity Model of Braestrup (1976)

Braestrup et al. (1976) proposed an upper bound plasticity punching model for axisymmetric slabs Figure 2.17 shows the section of an axisymmetric slab, which is simply supported by a circle ring with diameter D on the bottom. As shown in Figure 2.18, a vertical load P is applied on the top center area with diameter d; the diameter of the punched opening on the bottom surface is d_1; curve A-B-E is the inclined punching shear crack. It is assumed that the generatrix of the failure surface is $r = r(x)$ and the displacement vector is at an angle $\alpha = \alpha(x)$ to the failure surface. The energy (W_I) dissipated at the failure surface should be equal to the work (W_P) done by the punching load P.

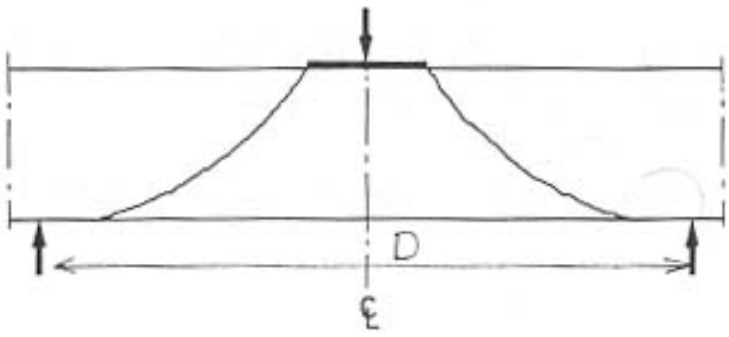

Figure 2.17 Axisymmetric punching (Braestrup et al., 1976)

$$W_I = \int_0^h \frac{1}{2}\delta f_c(\lambda - \mu \sin\alpha) \cdot 2\pi r \frac{dx}{\cos\alpha} \tag{2-14}$$

$$W_P = P \cdot \delta \tag{2-15}$$

where δ is the relative velocity (displacement), f_c is the uniaxial concrete strength, f_t is the tensile strength of concrete, $\rho = \frac{f_t}{f_c}$, $\lambda = 1-\rho(k-1)$, $\mu = 1-\rho(k+1)$, $k = \frac{1+\sin\varphi}{1-\sin\varphi}$, φ is the friction angle of concrete.

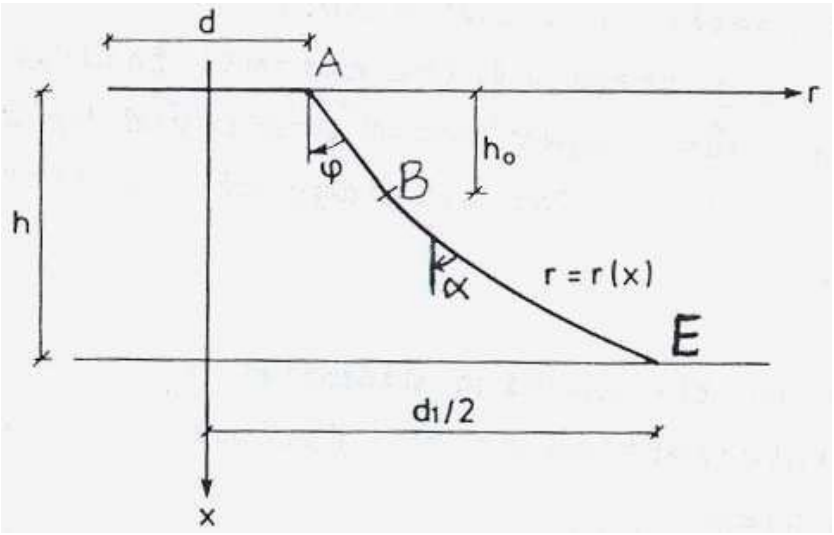

Figure 2.18 Predicted failure surface (Braestrup et al., 1976)

By equating (2-14) and (2-15), the upper bound ultimate punching load P can be obtained. Braestrup et al. (1976) optimized the failure surface and they found that it includes a conical part and a catenary part. In the failure surface A-B-E in Figure 2.18, AE is an inclined straight line; BE is a catenary curve. Thus the ultimate punching load P includes two parts: P_1 from the upper cone and P_2 from the lower catenary part.

$$P = P_1 + P_2 \tag{2-16}$$

$$P_1 = \pi f_c \frac{h_0}{2} \frac{(d\cos\varphi + h_0 \sin\varphi)(1-\sin\varphi)}{\cos^2\varphi} \tag{2-17}$$

$$P_2 = \frac{1}{2}\pi f_c [\lambda c(h-h_0) + \lambda(\frac{d_1}{2}\sqrt{(\frac{d_1}{2})^2 - c^2} - ab) - \mu((\frac{d_1}{2})^2 - a^2)] \tag{2-18}$$

where h is the slab depth and h_0 is the height of the top cone part of the failure crack, $a = \frac{d}{2} + h_0 \tan\varphi$, $b = c\tan\varphi$, $c = \sqrt{a^2 - b^2}$.

This model assumes the concrete as a perfectly plastic material. It gives good qualitative explanation to punching shear failure. The variation of the calculated ultimate punching loads was about 16% as mentioned in their conclusion.

(5) Shear Friction Model by Dilger (2000) and Dechka (2001)

Based on the shear-friction criterion (Loov, 1978) for beam shear, Dilger (2000) and Dechka (2001) developed the shear-friction model for punching shear of reinforced concrete slabs with or without shear reinforcements, under concentric load. According to shear-friction criterion, the shear stress v on a concrete failure surface is related to the normal stress σ on that surface and the compressive strength $f_c^{'}$, which can be expressed as equation (2-19):

$$v = k\sqrt{\sigma \cdot f_c^{'}} \tag{2-19}$$

where v is the average shear stress on the shear failure plane, σ is the normal stress on that plane, $f_c^{'}$ is the 28-day compressive cylinder strength, k is the correlation coefficient determined from experiment data. In order to obtain reasonable results, they modified equation (2-19) by adding the concrete tension strength f_t to σ**:**

$$v = k\sqrt{(\sigma + f_t) \cdot f_c^{'}} \tag{2-20}$$

Two forms of the shear-friction model were developed: general model and the simplified model. The general model is suitable for computer programming while the simplified model can be used for hand calculation. Figure 2.19 shows the free body diagram of the slab-column connection for general model. The failure surface includes eight facets. The ultimate punching shear capacity $V_{sf,gen}$, as in equation (2-21), is the summation of the shear capacity of each facet which is obtained by incorporating equilibrium equations of the facet into equation (2-20).

$$V_{sf,gen} = \sum \left\{ \frac{K}{2}\left[1 + \cot^2\theta\right] \left[\sqrt{4\left(\frac{T}{K} + \frac{r_t}{k^2}\right) + \cot^2\theta} - \cot\theta \right] - T\cot\theta + T_v \right\} \tag{2-21}$$

$$K = 0.5k^2 f_c^{'}(b_{bot} + b_{top})h$$

$$r_1 = \frac{f_t}{f_c^{'}}$$

$T =$ tension force in the flexural reinforcements

T_v =tension force in each shear stud

$\theta =$ angle of the failure facet

$h =$ slab thickness

$b_{bot} =$ bottom edge length of the facet

$b_{top} =$ top edge length of the facet

x_{bot} =the distance between column face and the bottom of the failure facet

By assuming a suitable range of x_{bot} and angle θ, a series of $V_{sf,gen}$ can be obtained using computer program. The minimum $V_{sf,gen}$ and its corresponding θ are the ultimate punching shear capacity. The simple form of shear-friction model, as in equation (2-22), was derived from the general model:

$$V_{sf,simple} = \frac{k^2 f_c' h}{4}\left(\frac{h}{x} + \frac{4r_t}{k^2}\right)(l_o + \pi x) + A_{vs} f_{yv}\left(\frac{x\, h_{s,eff}}{s\, h}\right) \quad (2\text{-}22)$$

$$l_0 = 2(c_x + c_y) + 4\sqrt{2}(s_0 + (n-1)s),$$

$$x = \frac{k}{2}\sqrt{\frac{hl_o}{\pi r_t + \frac{A_{vs} f_{yv} h_{s,eff}}{f_c' h^2 s}}}$$

where $V_{sf,simple}$ is the nominal shear force resisted by the connection as given by shear friction, $h_{s,eff} =$ average effective length of the stud, c_x, c_y are column dimensions, s, s_0 are spacing of bolts, n is the number of shear studs, A_{vs} is the section area of the stud stem, f_{yv} is the yield strength of the shear studs.

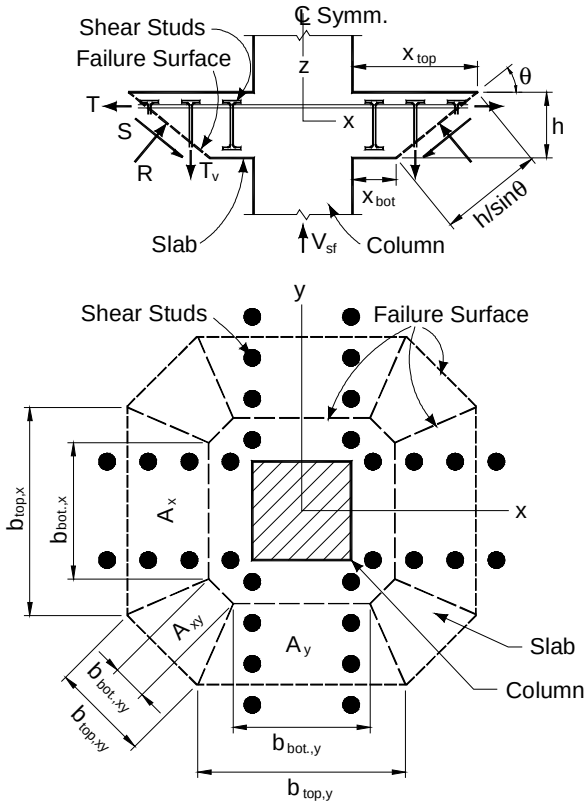

Figure 2.19 Free body diagram of slab-column connection for shear friction model (Dilger, 2000, and Dechka, 2001)

(6) Yield Line Model (Ranking and Long, 1987)

When a reinforced concrete slab is subjected to a heavy vertical load, the flexural reinforcement in the slab may yield at the maximum moment locations and concrete would crack there. Finally, some crack patterns, i.e. yield line patterns, would occur in the slab, which divide the slab into several elastic plates connected by plastic hinges. The ultimate load that the slab can sustain is calculated by considering the equilibrium of all these divided plates or by equating the external work of the slab loads and the internal work of the divided plates.

Rankin and Long (1987) developed the following equation (2-23) to calculate the ultimate vertical load P_{flex} when the flexural steel bars in the concrete slab yield, by assuming the yield line pattern as shown in Figure 2.20.

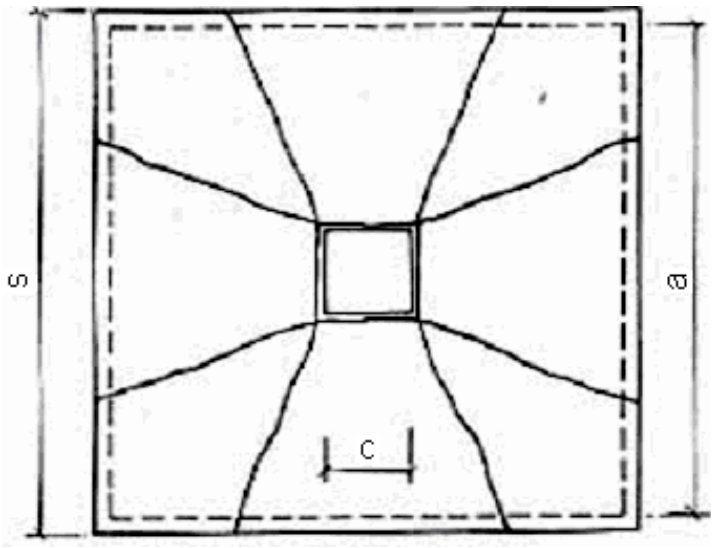

Figure 2.20 Yield line pattern in the slab (Rankin and Long, 1987)

$$P_{flex} = 8(\frac{s}{a-c} - 0.172)M_b \tag{2-23}$$

where s is the square slab edge length, a is the support length on four sides, c is the dimension of the square column section, M_b is nominal capacity of the slab section using tension reinforcements.

Ranking and Long also proposed an empirical formula to calculate the shear punching strength P_{vs} of the slab when the concrete subjected to punching shear failure.

$$P_{vs} = 1.66\sqrt{f_c'}(c+d)d(100\rho)^{0.25} \tag{2-24}$$

where d is the effective slab thickness, ρ is the flexural reinforcement ratio.

For the slab-column connections subjected to gravity load and moment, Cao (1993) proposed equation (2-25) to estimated the unbalanced moment capacity M assuming the yield line crack

pattern in Figure 2.21 (ring cracks belong to compression surface; other cracks are on the negative surface).

$$M = 2(1+\pi)(1+k)mc - 0.5cV \tag{2-25}$$

where k is the ratio of positive to negative moment capacity per unit length, m is the negative moment per unit length which is equal in the two orthogonal directions x and y, c is the column dimension, V is the shear force applied on the slab-column connection.

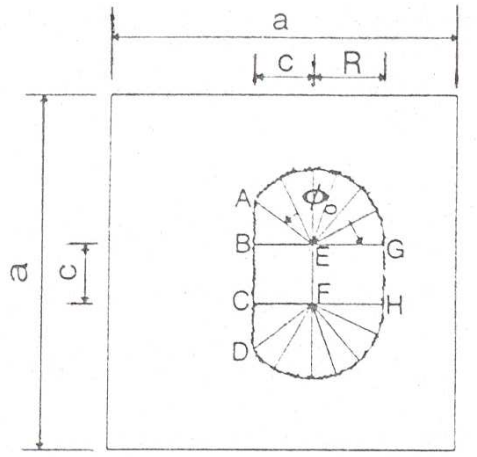

Figure 2.21 Yield line pattern of interior slab-column connection subjected to shear and unbalanced moment (Cao, 1993)

(7) Critical Section Models

Talbot (1913) first proposed the shearing stress formula (Moe referred to it in his report, 1957) for reinforced concrete footing slabs based on the assumption that the failure occurs on a so called critical section:

$$v = \frac{V}{4(r+2d)\,jd} \tag{2-26}$$

where r is the side length of the loaded area, d is the effective depth of the slab, jd is the distance between tension and compression resultants $(\approx 0.9d)$, and V is the shear force. The critical section in this case is at column faces and it is is a hypothetical failure plane, perpendicular to the surface of the slab.

Forsell and Holmberg assumed (1946) that the shearing stresses are parabolically distributed across the depth of slab. They proposed the shear stress formula:

$$v = \frac{1.5V}{bh} \tag{2-27}$$

where b is the perimeter length of the critical section which is at $h/2$ from the column faces, h is the slab thickness.

Moe (1961) suggested that the critical section should be at a column face. Based on his testing results of 42 slab-column specimens and others' testing results, Moe proposed the ultimate shear strength v_u (psi) as

$$v_u = \frac{V_u}{bd} = \frac{15(1-0.075\frac{r}{d})\sqrt{f_c'}}{1+5.25bd\sqrt{f_c'}/V_{flex}} \tag{2-28}$$

where V_u is ultimate shear force (lb), V_{flex} is a shear force at ultimate flexural (yield line) capacity of the slab (lb) , r is the column size (in.), b is the column perimeter length (in.), and d is the effective slab thickness (in.).

Based mainly on Moe's work, the ACI-ASCE Committee 326 (1962) specified the critical section at $d/2$ from the column face to simplify the equation (2-28). They proposed the following equation to calculate the ultimate punching shear strength of the concrete slab, which forms the basis of the current ACI code provision on punching shear design:

$$v_u = \frac{V_u}{b_0 d} = 4.0\sqrt{f_c'}$$

where b_0 is perimeter length of the critical section at $d/2$ from the column face, other variables are same as those in equation (2-20).

2.5 Punching Shear Design

This section examines the punching shear design procedures of some important structural codes of practice. All codes adopt an approach involving a critical section, which is at a certain distance from the column perimeter. The basic rule is that the factored shear stress on the critical section should be less than the nominal shear capacity. Canadian code CSA A23.3-04 and the American Code (ACI 318-05) have similar provisions for punching shear. In both codes, the critical section is 0.5d from the column faces. In other codes such as Eurocode 2 (2004) and CEB-FIB Model Code 90, the positions of the critical section are different. In all codes, shear capacity has contributions from concrete and the shear reinforcement. Both ACI318-05 and CSA A23.3-04 do not account for the effect of flexural reinforcement in calculation of the shear resistance, while the European codes consider the effect.

2.5.1 Punching Shear Design Requirements in CSA A23.3-04

According to the CSA A23.3-04 code, for two way slab-column connections, the factored shear stress v_f on the critical section (the perimeter at a distance $\frac{d}{2}$ from column faces, Figure 2.22) should be no more than the factored shear resistance v_r.

$$v_f \le v_r = v_c + v_s \tag{2-29}$$

where v_c is the factored shear resistance from concrete, v_s is the factored shear resistance form shear reinforcements. Factored shear resistance of the critical section without shear reinforcement is:

$$v_c = \min\left\{\begin{array}{c} 0.38\lambda\phi_c\sqrt{f_c'} = 0.247\sqrt{f_c'} \\ 0.19\lambda\phi_c\sqrt{f_c'}(1+\frac{2}{\beta_c}) = 0.124\sqrt{f_c'}(1+\frac{2}{\beta_c}) \\ \phi_c\lambda\sqrt{f_c'}(0.19+\frac{\alpha_s d}{b_0}) = 0.65\sqrt{f_c'}(0.19+\frac{\alpha_s d}{b_0}) \end{array}\right\} \quad \text{(MPa)} \tag{2-30}$$

Where $\lambda = 1$ for regular concrete, ϕ_c =0.65 is the reduction factor for concrete strength, β_c is the ratio of the long side over short side of the column, b_o is the perimeter length of the critical section. α_s =4, 3, 2 for interior, edge, and corner column, respectively. Equations in (2-30) are equivalent to those in ACI 318-05.

If v_c from equations in (2-30) is less than v_f, shear reinforcements are required. For slabs with shear reinforcements, the shear resistance is also as $v_r = v_c + v_s$, but v_c is calculated as in equation (2-32). For slabs with shear reinforcement, factored shear resistance from shear reinforcement is :

$$v_s = \frac{\phi_s A_{vs} f_{yv}}{b_0 s} \tag{2-31}$$

where $\phi_s = 0.85$ is reduction factor of steel bar. A_{vs} is the section area of the shear reinforcement, f_{yv} is the strength of the shear reinforcement, s is the radial spacing of the shear reinforcement.

For concrete with headed shear reinforcement (shear studs), shear resistance from concrete in the shear reinforced zone is

$$v_c = 0.28\lambda\phi_c\sqrt{f_c'} \tag{2-32a}$$

Maximum shear resistance of section with headed shear reinforcement should satisfy the following equation:

$$v_{r\max} \le 0.75\lambda\phi_c\sqrt{f_c'} \tag{2-33a}$$

For concrete with stirrup shear reinforcement, shear resistance from concrete in the shear reinforced zone is

$$v_c = 0.19\lambda\phi_c\sqrt{f_c'} \tag{2-32b}$$

Maximum shear resistance of section with stirrup shear reinforcement should satisfy the following equation:

$$v_{r\max} \le 0.55\lambda\phi_c\sqrt{f_c'} \tag{2-33b}$$

To calculate the factored shear stress v_f by gravity load and unbalanced moment in the perimeter of the critical section, the following equation is applied:

$$v_f = \frac{V_f}{b_0 d} + \left[\frac{\gamma_v M_f e}{J}\right]_x + \left[\frac{\gamma_v M_f e}{J}\right]_y \tag{2-34}$$

where V_f is the vertical shear force. M_f is the unbalanced moment in x, y direction, which is transferred by slab shear and flexural stresses. γ_v is the fraction of the moment transferred by shear,

$\gamma_v = 1 - \dfrac{1}{1 + \dfrac{2}{3}\sqrt{\dfrac{b_1}{b_2}}}$, b_1 is the width of the critical section side perpendicular to the moment vector, b_2 is the other side length. e is the distance from the centroid of the critical section to the point where shear stress is calculated. J is analogous to polar moment of inertia of the shear critical section around the x, y centrioda1 axes, respectively. In calculations of V_f and M_f, the factors for dead loads and live loads are 1.25 and 1.5 for most load combinations.

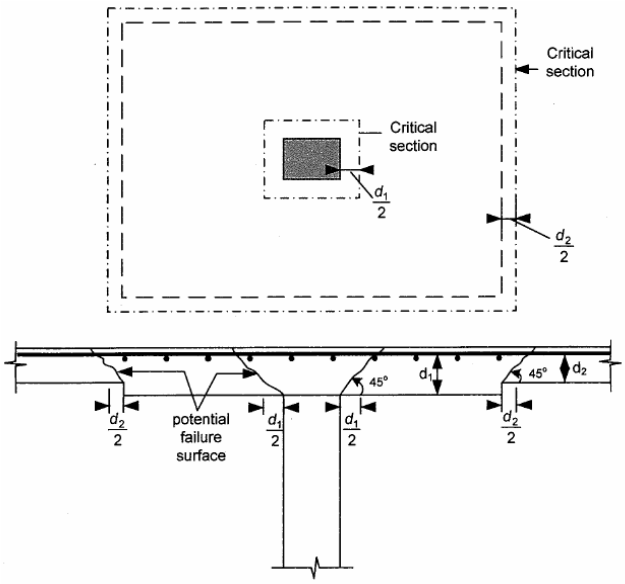

Figure 2.22 Critical sections defined in Canadian code CSA A23.3-04 (Cement Association of Canada, 2006)

2.5.2 Punching Shear Design Requirements in ACI 318-05 (in SI units)

Similar to CSA A23.3-04, ACI 318-05 requires the factored shear stress v_f at the critical section (the perimeter at a distance $\dfrac{d}{2}$ from column faces) should be no more than the product of nominal shear strength v_n times a shear strength reduction factor $\phi = 0.75$:

$$v_f \le \phi v_n \tag{2-35}$$

where $v_n = v_c + v_s$, v_c is the shear resistance from concrete, v_s is the shear resistance from shear reinforcements. To compare with CSA A23.3-94, the strength reduction factor ϕ can be assigned to v_c and v_r , and equation (2-35) can be written as:

$$v_f \le v_r^{'} \tag{2-36}$$

where $v_r^{'} = \phi v_c + \phi v_s = v_c^{'} + v_s^{'}$.

The factored shear resistance of the critical section without shear reinforcement is

$$v_c^{'} = \min\left\{\begin{array}{c} 0.33\phi\sqrt{f_c^{'}} = 0.248\sqrt{f_c^{'}} \\ 0.17\phi\sqrt{f_c^{'}}(1+\frac{2}{\beta_c}) = 0.128\phi\sqrt{f_c^{'}}(1+\frac{2}{\beta_c}) \\ 0.83\phi\sqrt{f_c^{'}}(0.2+\frac{\alpha_s d}{b_0}) = 0.623\sqrt{f_c^{'}}(0.2+\frac{\alpha_s d}{b_0}) \end{array}\right\} \quad \text{(MPa)} \tag{2-37}$$

Where β_c is the ratio of the long side over short side of the column, b_o is the perimeter length of the critical section. α_s =4, 3, 2 for interior, edge, and corner column, respectively.

For slabs with shear reinforcement, shear resistance from shear reinforcement is:

$$v_s^{'} = \frac{\phi\ A_{vs} f_{yv}}{b_0 s} \tag{2-38}$$

where A_{vs} is the section area of the shear reinforcement, f_{yv} is the strength of the shear reinforcement, s is the spacing of the shear reinforcement. Shear resistance $v_c^{'} = 0.17\phi\sqrt{f_c^{'}}$ for concrete with stirrups. Maximum shear resistance of a section with stirrup shear reinforcement shall satisfy the following equation

$$v_{r\max}^{'} \le 0.5\phi\ \sqrt{f_c^{'}} \tag{2-39}$$

When calculating the factored shear stress v_f , the following equation is applied:

$$v_f = \frac{V_f}{b_0 d} + \left[\frac{\gamma_v M_f e}{J}\right]_x + \left[\frac{\gamma_v M_f e}{J}\right]_y \quad (2\text{-}40)$$

where V_f is the vertical shear force, M_f is the unbalanced moment in x, y direction. γ_v is the fraction of the moment M_f transferred by shear, $\gamma_v = 1 - \frac{1}{1 + \frac{2}{3}\sqrt{\frac{b_1}{b_2}}}$, b_1 is the width of the critical section side perpendicular to the moment vector, b_2 is the other side length. e is the distance from the centroid of the critical section to the point where shear stress is calculated. J is the analogous polar moment of inertia of the shear critical section around the x, y centriodal axes, respectively. In calculations of V_f and M_f, the factors for dead loads and live loads are 1.2 and 1.6 for most load combinations.

2.5.3 Eurocode 2 (2004)

The Eurocode 2 (2004) employs a basic control section at a distance $2d$ from the faces of the column or the loaded area. Similarly, the shear stress v_f on the control section should be no more than the shear resistance (v_r).

$$v_f \leq v_r$$

As shown in Figure 2.23, for rectangular columns, the basic control section includes round corners (ACI and CSA code permit right angle corners). The code also requires checks on the column face and on the control section outside the shear reinforcement area.

For interior slab-column connections without shear reinforcements, the shear resistance v_r for the basic control section is calculated as

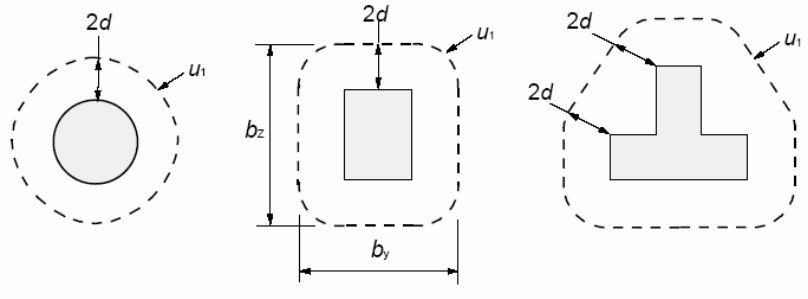

Figure 2.23 Basic control sections defined in Eurocode 2 (2004)

$$v_r = v_c = \frac{0.18}{\gamma_c} k(100\rho f_{ck})^{1/3} \geq v_{\min} \tag{2-41}$$

$k = 1 + (\frac{200}{d})^{0.5} < 2.0$, d in mm

f_{ck} = the characteristic concrete strength, MPa

ρ = flexural reinforcement ratio, $\rho = (\rho_z \rho_y)^{1/2} \leq 0.02$

ρ_z, ρ_y are reinforcing ratios in z, y directions for a slab width equal to column width plus $3d$ each side.

$\gamma_c = 1.5,$ partial factor for persistent and transient concrete.

$v_{\min} = 0.035 k^{3/2} f_{ck}^{1/2}$

The shear stress v_f at the basic control section due to factored external concentric load V_f and unbalanced moment M_f is

$$v_f = \frac{V_f}{u_1 d} \beta \tag{2-42}$$

$\beta = (1 + \frac{\gamma M_f u_1}{V_f W_1})$ for one direction moment, or

$\beta = 1 + 1.8 \sqrt{(\frac{e_y}{b_z})^2 + (\frac{e_z}{b_y})^2}$ for two direction moments

$$W_1 = \int_0^{u_1} |e| dl$$

where u_1 is the length of the basic control section length, γ is the fraction factor of M_f, ($\gamma = 0.6$ for rectangular column), b_y, b_z are the dimensions of the basic control perimeter (Figure 2.23), e_y, e_z are the eccentricities $\frac{M_f}{V_f}$ along y and z axes respectively , (e_y results from a moment from z axis). e is the distance of dl from the moment axis.

If $v_f > v_c$, shear reinforcement is required. The shear resistance strength v_r can be calculated as following:

$$v_r = 0.75 v_c + 1.5(\frac{d}{s_r}) A_{sw} f_{ywd,ef} (\frac{1}{u_1 d}) \sin\alpha \qquad (2\text{-}43)$$

where v_c is calculated as in equation (2-41), s_r is the radial spacing of shear reinforcement, d is the effective depth of the slab, A_{sw} is the section area of all shear reinforcements in one perimeter, $f_{ywd,ef} = 250 + 0.25d \le f_{ywd}$, f_{ywd} is the design yield strength of the shear reinforcements, u_1 is the length of the basic control section length, α is the angle between the shear reinforcement and the slab plane.

At the column face, the shear stress v_f due to V_f and M_f shall be no more than the maximum punching shear resistance $v_{r\max}$ as following.

$$v_{r\max} = 0.5 \nu f_{cd} \qquad (2\text{-}44)$$

$$\nu = 0.6(1 - \frac{f_{ck}}{250}) \qquad (2\text{-}45)$$

$$f_{cd} = f_{ck} / \gamma_c$$

where f_{ck} is the characteristic compressive cylinder strength of concrete at 28 days, $\gamma_c = 1.5$. For interior columns, the shear stress v_f at the column face is

$$v_f = \frac{V_f}{u_0 d} \beta \qquad (2\text{-}46)$$

where u_0 is the length of column periphery (for interior column), β is calculated as in equation (2-42).

2.6 Seismic Requirements for Design of Flat Slab-Column Structures

In addition to the punching shear provisions described in the above Section 2.5, some codes provide special provisions for seismic punching shear requirements.

2.6.1 National Building Code of Canada (NBCC 2005)

NBCC 2005 requires that the primary lateral load resistant system should not be a flat slab-column structure when the building is more than three stories. NBCC (2005) also requires that lateral inter-storey drift ratio should not exceed 1.0% for post-disaster structures, 2.0% for high importance buildings, and 2.5% for other buildings.

2.6.2 Seismic Requirements of CSA 23.3-04

Clause 21.12.3 in the Canadian structural code CSA 23.3-04 requires: for slab column connections subjected to seismic loading, if the shear stress produced by gravity load only is greater than $R_E v_c$, shear reinforcement should be provided. v_c is the shear resistance from concrete (Eq. 2-30) and R_E is calculated using the following formula:

$$R_E = (\frac{0.005}{\delta_i})^{0.85} \leq 1.0 \tag{2-47}$$

where δ_i is the inter-story drift ratio, $\delta_i \leq 0.025$.

When shear reinforcements are required, it is required that the following relation should be satisfied.

$$\frac{V}{V_r} \leq R_E \tag{2-48}$$

where V is the concentric external shear force, V_r is the factored shear force resistance. V_r includes concrete resistance V_c calculated using $0.5 v_c$ and the shear resistance by shear reinforcements.

The code also states that the shear reinforcements shall extend a minimum of $4d$ beyond the face of the column.

2.6.3 ACI 318-05 Seismic Requirements for Slab-column Structures

The American Concrete Institute Code, ACI 318-05 uses the gravity shear ratio VR in Clause 21.11.5

$$VR = \frac{V_{uf}}{\phi v_{nc} b_0 d} \tag{2-51}$$

where

v_{nc} is the nominal shear strength provided by the concrete (stress unit)

V_{uf} the factored shear force due to gravity loading ($U = 1.2D + 1.0L + 0.2S$)

The maximum story drift ratio, DR, when there is no shear reinforcement, is

$$DR = 0.035 - 0.05 * VR \qquad (VR < 0.6)$$

$$DR = 0.005 \qquad (VR \geq 0.6)$$

If DR can not be satisfied, the slab needs shear reinforcement or larger thickness. Minimum shear reinforcement should be

$$v_s = \frac{A_v f_{yv}}{b_0 s} \geq \frac{3.5}{12}\sqrt{f_c'} \qquad \text{(MPa)} \tag{2-53}$$

2.6.4 FEMA 356 Requirements

FEMA 356 Prestandard and Commentary for the Seismic Rehabilitation of Buildings (2000) requires that the structure shall satisfy both global level and member level criteria according to the performance level of the structure. There are three structural performance levels: Immediate Occupancy (IO), Life Safety (LS), and Collapse Prevention (CP). Global level criteria for RC frames are:

IO: allows 1% maximum interstory drift

LS: allows 2% maximum interstory drift

CP: allows 4% maximum interstory drift

Member level criteria are based on plastic rotations for each member. For slab-column connection, limits on plastic rotation angles (radian) by performance level are shown in Table 2.2

Table 2.2 Limit on plastic rotation angles for slab-column connection by performance level

V_g / V_o (Gravity shear ratio)	Continuity Rebar	Plastic Angle Rotation Limit (radian) for "Immediate Occupancy (IO)"	Component (member) Type and Plastic Angle Rotation Limit (radian)			
			Primary		Secondary	
			Life Safety (LS)	Collapse Prevention (CP)	Life Safety (LS)	Collapse Prevention (CP)
0.2	YES	0.01	0.015	0.02	0.03	0.05
0.4	YES	0.0	0.0	0.0	0.03	0.04
0.2	NO	0.01	0.015	0.02	0.015	0.02
0.4	NO	0.0	0.0	0.0	0.0	0.0

2.7 Previous Research Work on Punching Shear at Waterloo

The presented current research is a continuation of the work done at the University of Waterloo since 1996. Therefore the review of this work is provided here. Since 1997, several tests have been done related to punching shear of reinforced concrete slab-column connections. These involved edge and interior slab column connections, with or without openings near columns, with or without shear reinforcements such as shear studs or shear bolts. The previously tested specimens were subjected to vertical and lateral static loads.

El-Salakawy, Polak, and Soliman (1998) tested slab-column connections subjected to high moments. It was found that the shear stress around the column increased due to higher moment-to-shear ratio (Table 2.3). In 1999, El-Salakawy, Polak and Soliman published the test results on reinforced concrete slab-column edge connections with openings (Table 2.3). Research was also carried out on the effect of shear studs on the reinforced concrete slab-column edge connections. El-Salakawy, Polak, and Soliman (2000) found that shear studs can increase stiffness of slab-column edge connections with an opening and also increase the shear strength and ductility of the specimens. Once the opening in the slab is as big as the column dimension, the influence of shear studs was very small.

Shear studs are the type of reinforcement that is embedded into the reinforced concrete specimens before casting. Alternatively, shear bolts can be installed after drilling holes on existing previously

built slab-column connections. In 2003, El-Salakaway et al. published the results of tests on four edge slab-column specimens strengthened by shear bolts. (Table 2.4) The conclusion was that shear bolts, as a new type of retrofitting method, can increase the capacity and ductility of slab-column edge connections, and can change the failure mode from punching shear mode to a favourable flexural mode.

Adetifa and Polak (2005) tested six interior slab column connections strengthened by shear bolts subjected to vertical loading only. (Table 2.5) These specimens were all 1800x1800x120mm reinforced concrete slabs with short column stubs. All the slabs were simply supported on four sides (1500x1500mm) on the bottom. In their test results, compared with the control specimen without shear bolts, the slab-column connection strengthened with four rows of shear bolts had increased ultimate punching shear load by 42.3% and displacement ductility by 229%. They observed that the shear bolts can prevent propagation of shear crack in strengthened slabs and improve the performance of the slabs with openings (Figure 2.24 and Table 2.5).

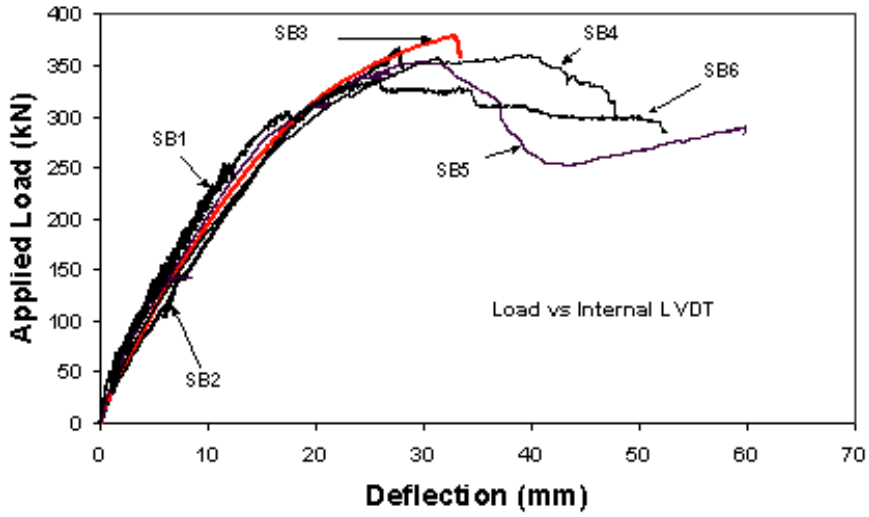

Figure 2.24 Load versus center deflection measured by internal LVDT of the testing frame. (Adetifa and Polak, 2005)

Table 2.3 Edge slab-column connections with or without shear studs (El-Salakaway and Polak et al, 1998, 1999, 2000, 2003)

Specimen	Slab size(mm) (120 thickness)	Shear Bolts/ Shear Studs	Flexural Capacity (Yield Line)		Failure Load (kN)	Failure Moment M_u (kN *m)	Opening Size (mm)	Failure Mechanism	Column dimension/ Position (mm)
			V_{flex} (kN)	M_{flex} kN*m					
XXX	1020x1540	N/A	174.66	52.40	125	37.5	N/A	Punching	250x250 Edge
SF0	1020x1540	N/A	152.65	45.79	110	33.0	150x150	Punching	250x250 Edge
SE0	1020x1540	N/A	159.54	47.86	120	360	150x150	Punching	250x250 Edge
SF1	1020x1540	N/A	174.66	52.40	115	34.5	150x150	Punching	250x250 Edge
SF2	1020x1540	N/A	174.66	52.4	114	34.2	150x150	Punching	250x250 Edge
CF0	1020x1540	N/A	143.27	43.0	87	26.1	250x250	Punching	250x250 Edge
XXX-R	1020x1540	6 row studs	174	52	154	46.2	N/A	Flexural	250x250 Edge
SF0-R	1020x1540	6 row studs	153	46	146	43.8	150x150	Flexural	250x250 Edge
SE0-R	1020x1540	6 row studs	160	48	150	45.0	150x150	Flexural	250x250 Edge
CF0-R	1020x1540	6 row studs	143	43	105	31.5	250x250	Punching	250x250 Edge
HXXXR	1020x1540	6 row studs	94.63	62.46	84.6	55.8	N/A	Punching-Flexural	250x250 Edge
HSF0	1020x1540	6 row studs	82.68	54.57	58.0	38.25	150x150	Punching-Flexural	250x250 Edge
HSE0	1020x1540	N/A	86.40	57.02	64.6	42.64	N/A	Punching	250x250 Edge
HXXX	1020x1540	N/A	94.63	62.46	69.4	45.79	N/A	Punching	250x250 Edge

Table 2.4 Four edge slab-column specimens strengthened with shear bolts (El-Salakaway and Polak et al., 2003)

Specimen	Slab size(mm) (120 thickness)	Shear Bolts/ Shear Studs	Flexural Capacity (Yield Line)		Failure Load (kN)	Failure Moment M_u (kN*m)	Opening Size (mm)	Failure Mechanism	Column dimension/ Position (mm)
			V_{flex} (kN)	M_{flex} kN*m					
SX-1SR	1020x1540	1 row bolts	174.0	52.2	151	45.3	N/A	Punching flexural	250x250 Edge
SX-2SR	1020x1540	3 row bolts	174	52.2	155	46.5	N/A	Flexural	250x250 Edge
SX-2SB	1020x1540	3 row bolts	174	52.2	162	48.6	N/A	Flexural	250x250 Edge
SH-2SR	1020x1540	3 row bolts	153	45.9	141	42.3	150x150	Flexural	250x250 Edge

Specimen	Size (mm)	Shear Bolts/ Studs	Flexural Capacity (Yield Line)		Applied Failure Load (kN)	Ductility mm/mm	Opening Size (mm)	Failure Mechanism	Column Size And Position (mm)
			V_{flex} (kN)	M_{flex} (kN*m)					
SB1	1800x1800	N/A	358	N/A	253	1.04	N/A	Punching	150x150 centered
SB2	1800x1800	2 row bolts	358	N/A	364	2.15	N/A	Punching/ Flexure	150x150 centered
SB3	1800x1800	3 row bolts	358	N/A	372	2.13	N/A	Flexure	150x150 centered
SB4	1800x1800	4 row bolts	358	N/A	360	3.43	N/A	Flexure	150x150 centered
SB5	1800x1800	4 row bolts	358	N/A	353	5.0	150x150 opening 4	Flexure	150x150 centered
SB6	1800x1800	4 row bolts	358	N/A	336	4.08	150x150 opening 2	Flexure	150x150 centered

Table 2.5 Six interior slab-column specimens strengthened with/without shear bolts (adapted from Adetifa and Polak, 2005)

Chapter 3
Experiment Program

3.1 Specimens Design

A total of nine full scale specimens were tested. These specimens can be regarded as part of a prototype structure of which the flat concrete slab spans 3.75m between columns. The slab thickness is 120 mm. Figure 3.1 and Figure 3.2 show the plan view and elevation view of one prototype structure, which is a three-storey flat slab column building. The specimens represent interior slab-column connections which are isolated specimens with dimensions corresponding to the lines of contraflexure under gravity loads.

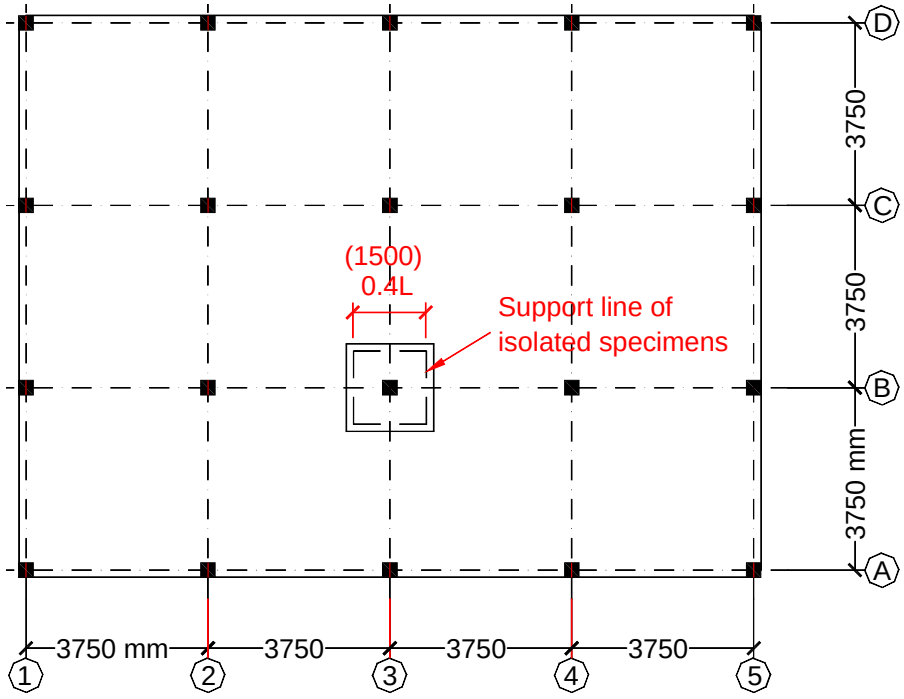

Figure 3.1 Plan view of the prototype structure

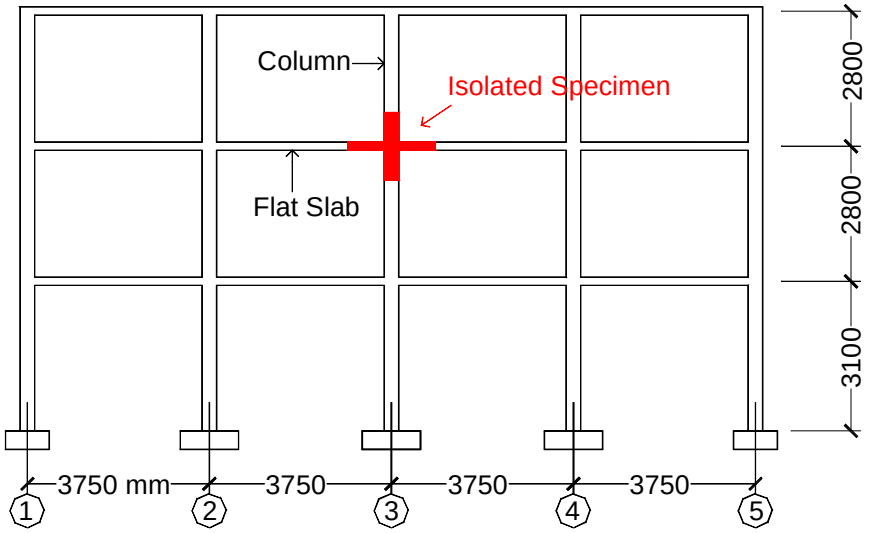

Figure 3.2 Elevation view of the prototype structure

The nine specimens, SW1~SW9, were subjected to a vertical constant load and cyclic reversal lateral displacements. The specimens are divided into two series: Series I (SW1~SW5) and Series II (SW6~SW9). Series I consists of two groups: Group 1 (SW1, SW2, and SW3) and Group 2 (SW4 and SW5). Figure 3.3 shows the five specimens of Series I; Figure 3.4 shows the four specimens in Series II, including the slab names, vertical loads on columns, and the layouts of shear bolts.

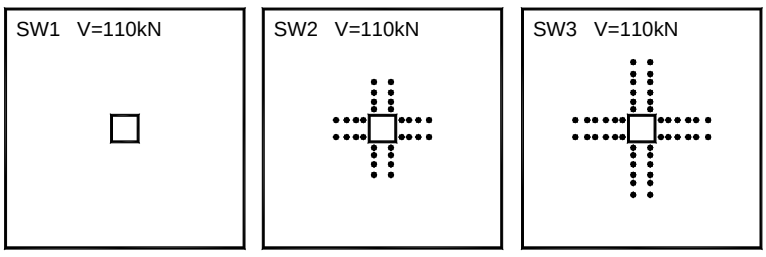

(a)

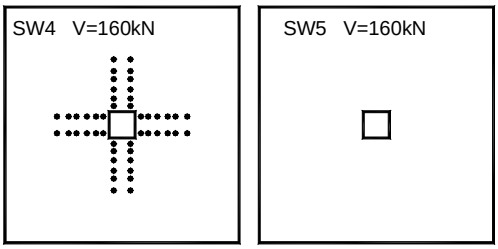

(b)

Figure 3.3 The five specimens (SW1~SW5) of Series I and shear bolt layout

(a) Group 1 (SW1, SW2, SW3); (b) Group 2 (SW4, SW5)

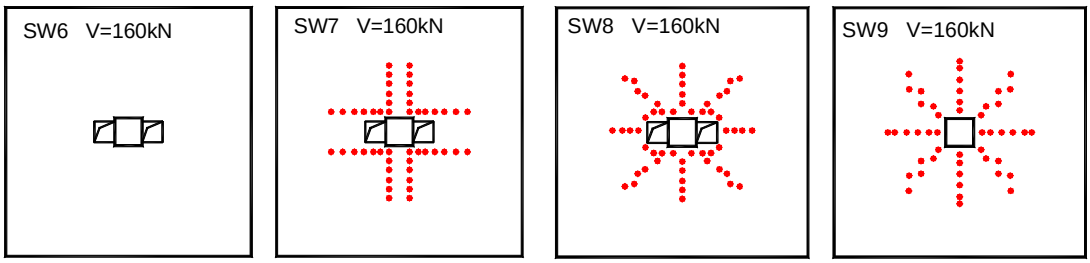

Figure 3.4 The four specimens (SW6~SW9) of Series II and shear bolt layout.

The specimens SW1~SW9 have slab dimensions of 1800mm by 1800mm with top and bottom column stubs (200x200mm) extending out 700mm from the center of the slab (Figure 3.5). In construction practice, the slabs sometimes may require openings near columns. To investigate the seismic behaviour of this type of slab-column connections, three specimens (SW6, SW7, and SW8) are designed to have two 150x150mm openings near the column in the lateral load direction (Figure 3.4 and Figure 3.5). All the specimens are supported on the 1500x1500mm perimeter on the bottom of the slab, with two sides also supported from the top to resist cyclic moments. The “top” of the slab in this project is the slab compression surface under vertical load (Figure 3.5). This is opposite to the situation in a real slab-column system where compression is on the bottom.

The dimensions of the slabs were chosen to represent the locations of contraflexure lines for the case of gravity loads. In case of gravity plus horizontal cycling loads (as in the case of the presented tests), the locations of contraflexure lines normal to horizontal loading direction change depending on the direction of the horizontal loading. Therefore, since in the setup the location of supports remain the same (in-between the actual locations of the lines of contraflexure), thick neoprene pads were provided on top and bottom of the slab to allow rotations. The neoprene pads were about 25mm thick and 50mm wide installed along the supporting lines as shown in Figure 3.5(c) and Figure 3.38.

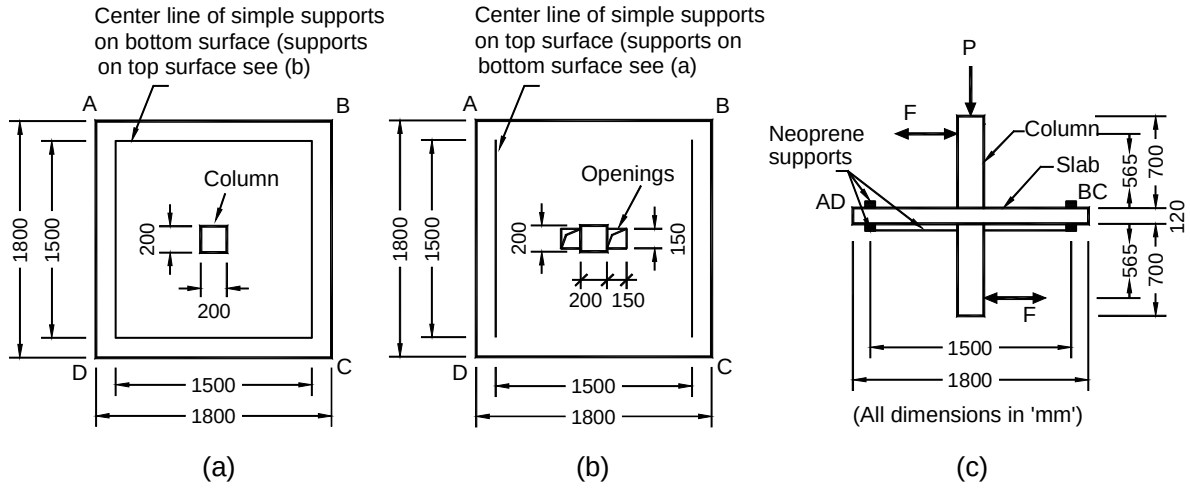

Figure 3.5 Dimensions of the specimens SW1~SW9 (all dimensions in ‘mm’)

(a) Plan view of SW1~SW5 and SW9; (b) Plan view of SW6, SW7 and SW8; (c) Elevation view

3.1.1 Flexural Reinforcement

In the tension surface of the concrete slab, the flexural reinforcement ratio of is 1.3% in the direction of lower bars and 1.1% in the direction of upper bars. The reinforcing ratio on the compression surface of the slab is half of the tension reinforcement. The reinforcement is designed following the results of calculation of Adetifa (2003) assuming a factored vertical distributed load of 18.5kPa to the prototype structures. The specimens’ flexural reinforcement was identical to previous tests in order to allow direct comparisons of results.

The bottom and the top reinforcements are two-way mats. The reinforcement was designed to have the same moment capacities in the two orthogonal directions. The reinforcing ratio of the columns is high and closed ties are used in order to make the column strong enough to transfer shear force and cyclic moments to the slab. Figure 3.6 and Figure 3.7 show the reinforcement of the specimens without or with openings, respectively. The bottom mat, tension surface under vertical load, consists of #10 M @100 in one direction at lower position and #10M@90 in the transverse direction at upper position. Due to this layout, the moment capacities in the two directions are the same. The top mat consists of #10M@200 in two directions. For specimens with openings, the reinforcement in direction 1 (along the lateral force application) is interrupted by the opening. There was no space in the slab to place additional bars along the sides of the opening. However, for direction 2 (normal to lateral loads) the same number of rebars that were cut by the openings are placed beside the opening edges (Fig. 3.7). Figure 3.8 (a) shows the column rebar details. Figure 3.8 (b) shows the positive lateral drifts applied on the top and bottom columns of the specimens. “AD” and “BC” sides of the slab in Figure 3.8(b) can be found in Figure 3.6 and Figure 3.7. These aids in finding the position of the specimens and the loading direction in the testing frame as shown in Figure 3.33.

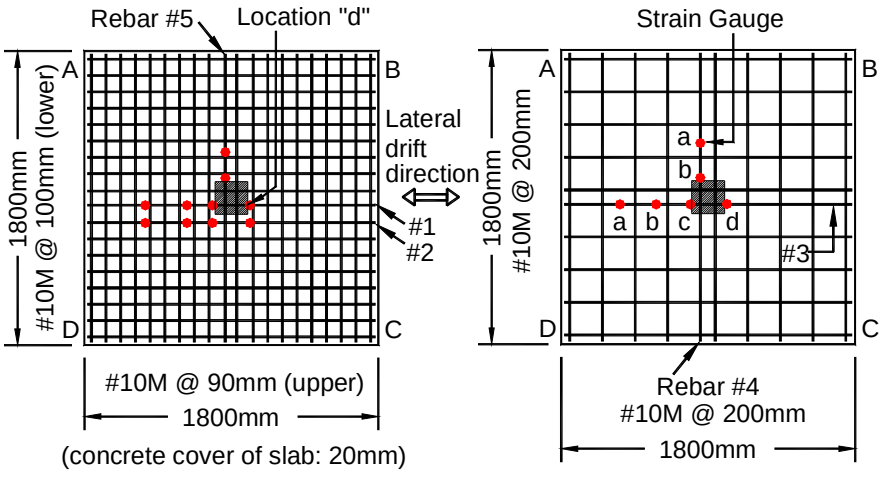

Figure 3.6 Reinforcement detail and strain gauges in specimen SW1~SW5 and SW9

Bottom reinforcement mat; (b) Top reinforcement mat

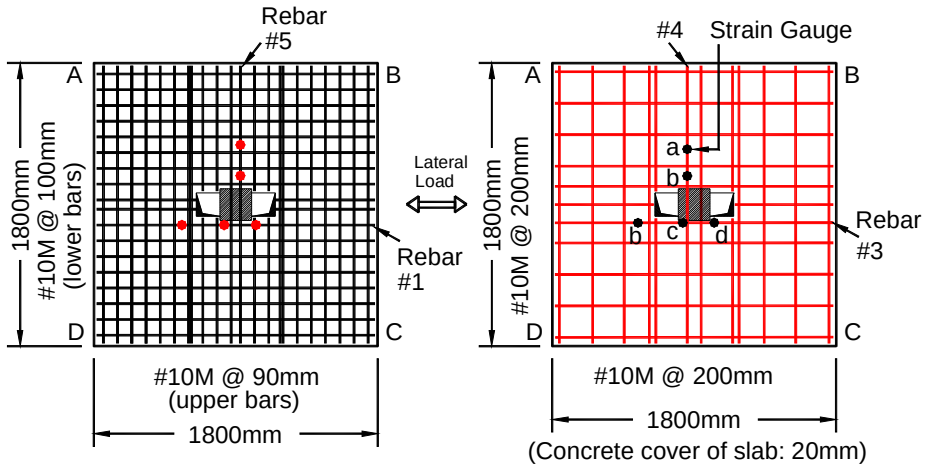

(a) (b)

Figure 3.7 Reinforcement detail and strain gages in Specimen SW6, SW7 and SW8

(a) Bottom reinforcement mat; (b) Top reinforcement mat

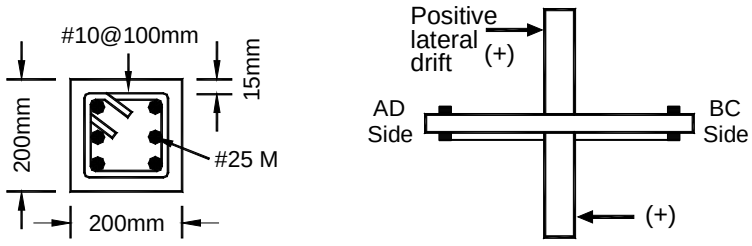

(a) (b)

Figure 3.8 Reinforcement detail of column and lateral load directions

(a) Column section; (b) Positive lateral drift direction

3.1.2 Estimation of the Capacities of the Specimens before Testing

The specimens' design was carried out based on assumed material parameters values. This was done before testing in order to decide on the ultimate punching loads and ultimate slab-column connection moment capacity for each specimen. These estimated loads and moments were used to select the

capacity of the load cells and actuators, to design the experimental setup, and to determine test procedures such as loading rate, constant vertical load, etc. The testing procedures are presented in Section 3.5.

3.1.2.1 Ultimate Punching Loads in Flexural Failure and in Punching Shear Failure

The design of the specimens was done based on the Canadian concrete code CSA A23.3-94. To ensure successful testing, the specimens were designed to fail in punching shear if no moment and no shear reinforcement were present. Flexural capacity of the specimen had to be larger than punching capacity to ensure such a failure. The equation (3-1) (Chapter 2) of full yielding at flexural failure (Rankin and Long, 1987) was used to calculate the ultimate flexural punching load capacity (upper bound) of the slab-column specimen without shear reinforcement and unbalanced moment,

$$P_{flex} = k_{y1} M_b \tag{3-1}$$

where $k_{y1} = 8(\frac{s}{a-c} - 0.172) = 9.7$, $s = 1800$ mm (slab dimension), $c = 200$ mm (column dimension), $a = 1500$ mm (support distance), and M_b = 39kNm, M_b is the nominal flexural moment capacity calculated by CSA A23.4-94 (tension reinforcement only). Therefore P_{flex} = 378.3 kN.

The ultimate punching shear capacity P_{vs} for specimens without shear reinforcement and moment was calculated using Rankin and Long's equation(1987):

$$P_{vs} = 1.66\sqrt{f_c^{'}}(c+d)d(100\rho)^{0.25} \tag{3-2}$$

where $f_c^{'}$ is the concrete compressive strength, c is the length of the column side, d is the effective slab thickness. ρ is the reinforcement ratio. For specimens without openings and shear reinforcement, $c = 200$ mm, $d = 90$ mm, assuming $f_c^{'}$ = 40MPa, then P_{vs} = 290.6 kN.

Using CSA A23.4-94, (the specimens were designed before CSA A23.4-04 is enforced), the estimated nominal punching shear capacity is $P_{vs} = 262kN$ (for $f_c^{'} = 40$ MPa). Specimens SW1~SW3 were tested under the vertical load of 110kN. Specimens SW4 ~ SW9 had a vertical load of 160 kN.

3.1.2.2 Ultimate Moment Capacities of the Specimens

During testing, lateral displacements were applied to the column stubs. The value of the applied moment dependeds on the displacement and the stiffness of the slab-column connections. The displacements increase the cracking, which results in the decrease of the stiffness of the connection. At the same time the punching shear capacity also decrease due to extensive cracking. In order to estimate the behaviour of the slabs, moment capacities of the connections were calculated using yield line analysis and CSA A23.4-94 Provisions.

1) CSA A23.4-94 Provisions

The punching shear formulas of CSA A23.3-94 (without material reduction factors and using unfactored loads) are as follows:

$$v_f = \frac{V_n}{b_0 * d_v} + \frac{\gamma_v M_n e}{J_x} \tag{3-3}$$

$$v_r = v_s + v_c = \frac{nA_{stud} f_y}{s * b_0} + 0.3\sqrt{f_c'} \le 0.8\sqrt{f_c'} \tag{3-4}$$

$$v_r \le v_f \tag{3-5}$$

where V_n is the given vertical load, M_n is the unbalanced moment capacity of the connection. b_0 is the perimeter length of the critical section, d_v is the effective thickness of the slab, s is the bolt spacing in radial direction, n is the number of bolts in each periphery row, A_{stud} is the section area of each bolt. Solving equations (3-1, 3-2, 3-3) results in the value of moment capacity M_n.

$$M_n = \frac{J_x}{\gamma_v e}\left[\frac{nA_{stud} f_y}{s(c_2 + d_v)} + v_c - \frac{V_n}{b_0 d_v}\right] \tag{3-6}$$

$$\text{or} \quad M_n = \frac{J_x}{\gamma_v e}\left[v_{\max} - \frac{V_n}{b_0 d_v}\right] \tag{3-7}$$

where $v_{\max} = 0.8\sqrt{f_c'}$, for slabs with shear reinforcement, $v_c = 0.3\sqrt{f_c'}$.

2) Yield Line Theory to Estimate the Moment Capacity of the Specimens

Using yield line theory, Cao (1993) obtained the formula (3-8) of unbalanced moment capacity of the slab-column connection under vertical load and unbalanced moment.

$$M = 2(1+\pi)(1+k)mc - 0.5cV_f \tag{3-8}$$

where k is the ratio of positive to negative moment flexural capacity per unit width, m is the negative moment per unit width (assuming $m_x = m_y$). c is the column dimension, V_f is the shear force applied to the slab-column connection.

The results of the calculations for the unbalanced moment capacities are listed in Table 3.1. The shear bolt spacing was assumed to be 70mm and the first row of bolts was 50mm far away from the column faces. The maximum calculated moment was 100 kNm which corresponds to lateral loads of 80 kN applied to the specimens. This is less than the capacity of available lateral actuators. Therefore it was decided to used two 50 kip (222kN) load cells for the two horizontal lateral actuators, and 150 kip (667kN) load cell for the vertical actuators.

3.1.2.3. Capacity of Concrete Column

The capacity of the column was examined using the co-relation formula of axial load and moment acting on the column and the material strengths of the column. Top column was subject to both axial compression and moment. Bottom column was subject to moment only. The theoretical maximum capacity point of the column is (P_r, M_r) = (497.6 kN, 93.4 kNm). At the applied axial compression of 110 kN the moment capacity is 81 kNm, and at the applied axial compression of 160 kN the moment capacity is 85 kNm. On the bottom column, since there is no axial load, the moment capacity is about $M_r = 75$ kNm. These moment capacities were adequate for the testing. The columns were designed using 10M diameter stirrups at spacing of 100 mm to ensure adequate shear capacity.

3.2 Properties of Materials used for Specimens

The following subsections address their tested strength. In addition, the strength and elongation of steel shear bolts are also shown. Table 3.2 and Table 3.3 display detailed information of specimens in Series I and Series II, including slab designations, their group number, concrete and rebar batch numbering, bolt rows, dimensions, and vertical load.

Table 3.1 Initial design of moment capacity of the nine slab-column connections before testing

Name of specimen	Assumed material strength			External vertical load (kN)	Row of shear bolts	Moment capacity at critical section d/2 (CSA code) from the column: M_n (kN*m)				Moment capacity at d/2 out of shear bolt M_n (kN*m)	Moment capacity based on Cao's yield line equation M_n (kN*m)	Column size (mm)	Opening size (mm)
	Concrete compr. $f_c^{'}$ (MPa)	Shear bolt yield $f_{yv}^{'}$ (MPa)	Rebar yield f_y (MPa)			No bolts, $v_r = v_c = \min(v_{c1}, v_{c2}, v_{c3})$	No bolts, $v_r = v_c = \max(v_{c1}, v_{c2}, v_{c3})$	With bolts, $v_c + v_s$, $v_c = 0.3\sqrt{f_c^{'}}$	With bolts, $v_r = 0.8\sqrt{f_c^{'}}$				
SW1	40	381	400	110	N/A	36.7	68.6			N/A	86.5	200x200	-
SW2	40	381	400	110	4			88.5	100.5	93.0	86.5	200x200	-
SW3	40	381	400	110	6			88.5	100.5	182.0	86.5	200x200	-
SW4	40	381	400	160	6			76.2	88.2	150.5	81.5	200x200	-
SW5	40	381	400	160	N/A	24.4	56.3			N/A	81.5	200x200	-
SW6	40	381	400	160	N/A	8.7	23.0			N/A	N/A	200x200	150x150 2 openings
SW7	40	381	400	160	6			36.0	37.4	160.7	N/A	200x200	150x150 2 openings
SW8	40	381	400	160	6			36.0	37.4	209.5	N/A	200x200	150x150 2 openings
SW9	40	381	400	160	6			76.2	88.2	194.0	81.5	200x200	

Table 3.2 Details of Specimens of Series I

Series #	Group #	Slab name	Slab dimension (mm)	Column size (mm)	Bolt rows	Vertical constant load (kN)	Concrete batch number	Rebar batch number
Series I	Group 1	SW1	1800x1800x120	200x200x700	0	110	1	1
		SW2	1800x1800x120	200x200x700	4	110		
		SW3	1800x1800x120	200x200x700	6	110		
	Group 2	SW4	1800x1800x120	200x200x700	6	160	2	
		SW5	1800x1800x120	200x200x700	0	160		

Table 3.3 Details of Specimens of Series II

Series #	Slab name	Slab dimension (mm)	Column size (mm)	Number of opening	Size of opening	Bolt rows	Vertical constant load (kN)	Concrete batch number	Rebar batch number
Series II	SW7	1800x1800x120	200x200x700	2	150x150	6 (orth.)	160	2	1
	SW6	1800x1800x120	200x200x700	2	150x150	0	160	3	2
	SW8	1800x1800x120	200x200x700	2	150x150	6 (rad.)	160		
	SW9	1800x1800x120	200x200x700	0	N/A	6 (rad.)	160		

3.2.1 Concrete Compression and Tension Strength

The nine reinforced concrete specimens were cast using ready mixed concrete in three batches. Concrete was provided by Hogg Fuel and Supply Ltd., Ontario. The first batch of concrete was for

specimens SW1, SW2 and SW3; the second batch of concrete went for SW4, SW5, and SW7; SW6, SW8 and SW9 were cast using the third batch of concrete. All the specimens were cured in normal interior temperature (about $22^0 C$). Concrete cylinders (4"diameter x 8"length and 6"diameter x 12 length") were prepared with each casting batch. Some of the 4"diameter x 8"length cylinders were placed in the standard humid room and were tested on the 28^{th} day for compression strength; the others were placed with the slab-column connections in normal interior temperature, and were tested for compression and tension strength at the same time of the slab-column connections testing.

Figure 3.9 Compression test of the concrete cylinder (4"x8")

Table 3.4 shows the average compression strength and average tension strength of each slab-column connection specimen at the testing time; it also shows the 28-day compression strength (cured in humid room) of the cylinders for each batch of concrete. Specimen SW1, SW2, and SW3, cast from the first batch of concrete, had the average standard 28-day compression strength 34.5 MPa and average compression strength from 33.7 to 37.0 MPa at the time of slab testing. In the second cast batch, specimens SW4, SW5, and SW7 had standard 28-day strength of 37MPa and 45.0 to 46.5 MPa compression strength at slab testing. The third cast batch of specimens SW6, SW8, and SW9 reached 52MPa in 28-day standard strength and 51.9 MPa in compression strength at slab testing. Figure 3.9 shows the crushing of a cylinder (4"x8") which was cured in a standard humid room for 28 days. Figure 3.10 shows the splitting (tension) test of 4"x8" concrete cylinders cured in the normal room environment. It can be seen that the color in the cracked surface is lighter than the colour of the third

batch concrete. This may be because the third batch concrete cylinders were tested at a younger age and more plastisizer was added to the concrete to increase the concrete slump.

Table 3.4 Concrete strength of each specimen (4”x8” cylinders)

Test series #	Slab name	Age of slab (from casting to testing, days)	Average compressive strength at slab testing (MPa)	f_c' (MPa) (used in calculations)	Average tensile strength at slab testing (MPa)	Concrete batch number	Average standard (28-day) compression strength (MPa)
Series I	SW1	770	37.0	35	2.86	1	34.5
	SW2	808	34.6	35	2.86		
	SW3	738	33.7	35	2.86		
	SW4	789	46.5	46	3.10	2	37
	SW5	755	45.0	46	3.10		
Series II	SW7	794	46.5	46	3.10		
	SW6	62	51.9	52	3.40	3	52
	SW8	72	51.9	52	3.40		
	SW9	94	51.9	52	3.40		

Figure 3.10 Concrete cylinder tension test

To obtain the compression stress versus strain curves of each batch of concrete, cylinders (6'x12") were tested in the MTS frame (Figure 3.11). The end surfaces of all cylinders were ground to smooth; diameter and length of each cylinder were measured three times in different locations. The load, and external and internal LVDT displacements were recorded throughout the whole testing process. The tests were done by strain control. Table 3.5 shows the compression strength and strain at peak points of each curve. Figure 3.12 shows crushing pattern of the concrete cylinder #6 (6"x12") of the first batch of concrete. Also, Figure 3.13(a), (b) and (c) show three compression stress versus strain curves for the three batches of concrete, respectively.

Figure 3.11 Concrete cylinder (6"x12") compression test

Figure 3.12 Crushing of the concrete cylinder #6 (6”x12”) of the first batch concrete

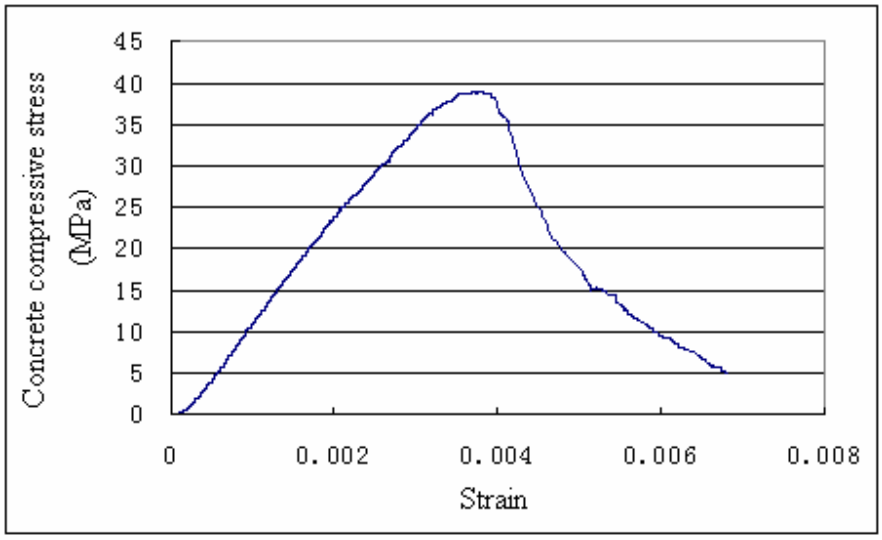

(a)

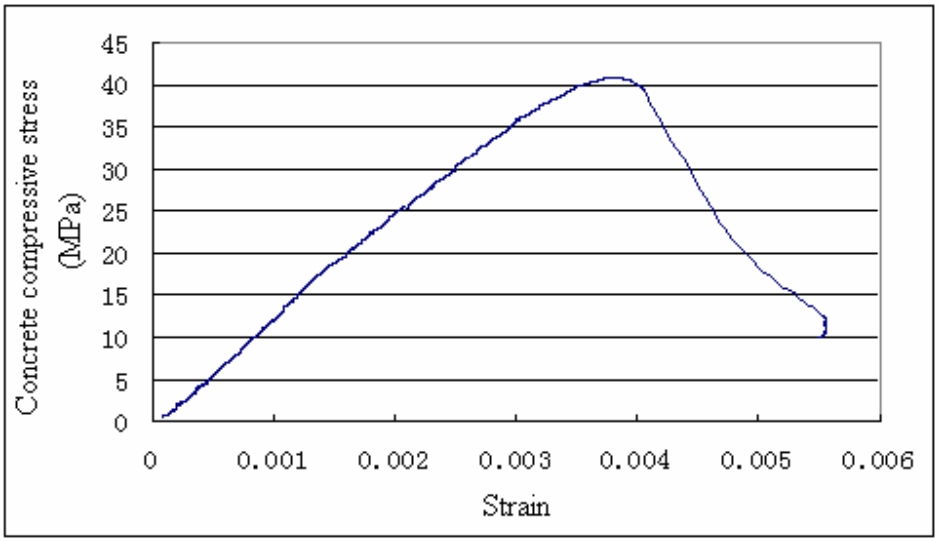

(b)

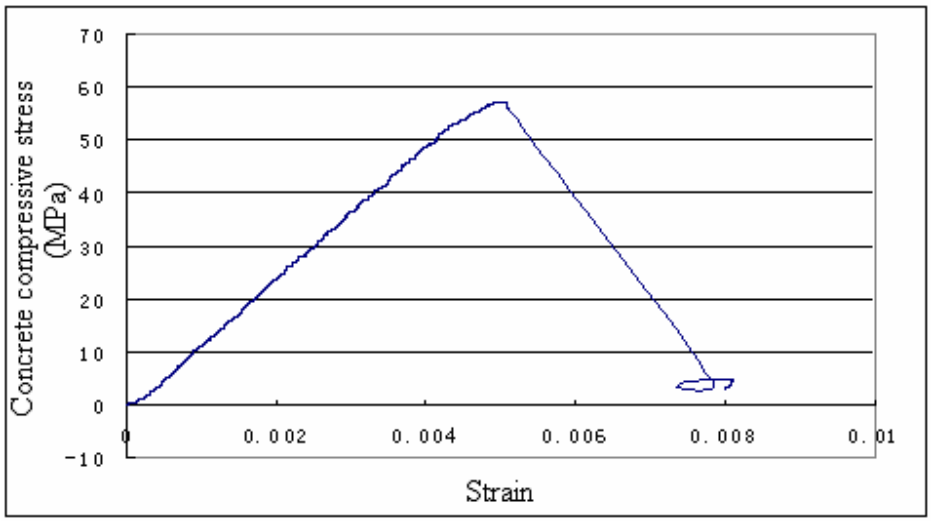

(c)

Figure 3.13 Compression strength versus strain of cylinders of the concrete

(a) cylinder #6 of the 1st batch, (b) cylinder #4 of the 2nd batch, (c) cylinder #2 of the 3rd batch

Table 3.5 Compression strength of concrete cylinders (6”x12”) for the three batches

Cylinder #	First batch of concrete for slabs SW1, SW2, and SW3		Second batch of concrete for slabs SW4, SW5, and SW7		Third batch of concrete for slabs SW6, SW8, and SW9	
	Strain at peak compression stress	Peak compression strength (MPa)	Strain at peak compression stress	Peak compression strength (MPa)	Strain at peak compression stress	Peak compression strength (MPa)
1	0.00391	40.6	0.00394	41.9	0.00471	57.6
2	0.00381	40.7	0.00393	42.0	0.00498	57.2
3	0.00406	41.4	0.00388	40.5	0.00499	58.9
4	0.00380	38.2	0.00381	41.0		
5	0.00399	39.6	0.00389	42.8		
6	0.00354	38.7				
Average	0.00385	39.9	0.00389	41.6	0.00489	57.9

3.2.2 Properties of Steel Reinforcing Bars

The reinforcing bars (M #10 rebar, nominal diameter 11.3mm) of the slabs came from two batches. The first batch of steel rebars was used in specimen SW1, SW2, SW3, SW4, SW5 and SW7. The second batch was used in specimens SW6, SW8, and SW9.

For each batch of steel bars, two types of steel specimens were used to test their strength. One type was the standard round coupons machined from M #10 rebars. The coupons were 1/4” in the center segment and 3/8” at the two anchor ends. A 2” clip strain gauge was used to measure the strain. Figure 3.14 shows the dimensions and picture of the coupons. Figure 3.15 shows the testing of a rebar coupon. The second type of steel specimen was original rebar as rolled. The total length of each

original rebar specimen was 14” long, including 8” gauge length centered and two inches anchor length at each end.

Figure 3.16 shows the original rebar testing and the broken position. It is found that in the original rebar (as rolled) test, the broken locations were all along the roots of ribs of the rebar. Thus the minimum diameters of the rebar were measured for actual tension strength calculation for the rebar. In addition, according to ASTM and CSA code, the rebar strengths were also calculated using nominal section area ($100\,mm^2$).

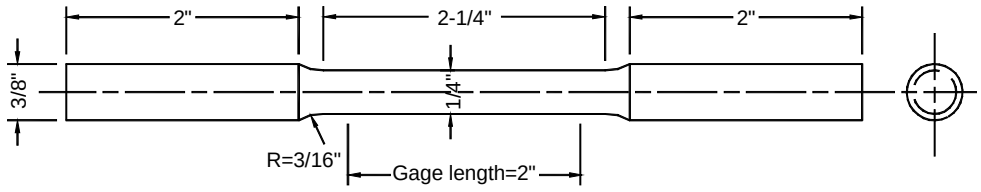

(a)

(b)

Figure 3.14 Standard coupon machined from M #10 rebar (a) Dimensions, (b) Picture

Figure 3.15 Testing of rebar coupon

Figure 3.16 Testing of original rebar

Table 3.6 gives all the original testing data of the rebars. Table 3.7 shows the average values calculated from Table 3.6. Figure 3.17 shows the tension stress versus strain in the original rebar

(rebar-2) of the 1st batch steel. Figure 3.18 shows the tension stress versus strain in the coupon (Coupon-1) of the 1st batch steel. It was decided that, for future calculations and comparisons with code formulas, the yield strength of rebar should be taken as 470 MPa, ultimate strength 650 MPa at 20% elongation.

Table 3.6 Testing results of the steel shear bolts and the two batches steel rebar

Rebar batch number	Original rebar or rebar coupon	Nominal yield strength F_y (MPa)	Nominal tensile strength F_u (MPa)	Elong -ation of 8" length (coupon: of 2")	2" Strain Gauge and the broken position
1	Rebar-1	470	663	12.70%	Broken outside 2"
	Rebar-2	469	661	15.60%	Inside 2"
	Rebar-3	461	655	14.42%	Inside 2"
	Coupon-1	527	755	20.87%	Inside 2"
	Coupon-2	517	745	16.92%	Inside 2"
	Coupon-3	521	755	24.50%	Inside 2"
	Coupon-4	517	751	20.96%	Inside 2"
2	Rebar-4	479	608	15.65%	Broken outside 2"
	Rebar-5	488	613	15.16%	Outside 2"
	Rebar-6	486	610	14.67%	Outside 2"
	Rebar-7	458	575	15.75%	Inside 2"
	Rebar-8	466	576	14.42%	Inside 2"
	Coupon-5	452	623	26.77%	Inside 2"
	Coupon-6	444	616	24.51%	Inside 2"
	Coupon-7	453	617	30.12%	Inside 2"
	Coupon-8	448	614	28.49%	Inside 2"

Table 3.7 Properties of steel reinforcing bars

	Rebar coupon			Original rebar		
Rebar batch number	Average yield strength (MPa)	Average tensile strength (MPa)	Average elong-ation (%)	Average nominal yield strength (MPa)	Average nominal tensile strength (MPa)	Average nominal yield strength used in calculation (MPa)
1	521	751	20.8	467 (562)	670 (807)	470
2	449	617	27.5	477 (555)	596 (695)	470

Note: Nominal strengths were calculated using nominal rebar section area ($100mm^2$); numbers in parenthesis are the strength calculated using average net broken area of rebar section ($83mm^2$) neglecting the ribs.

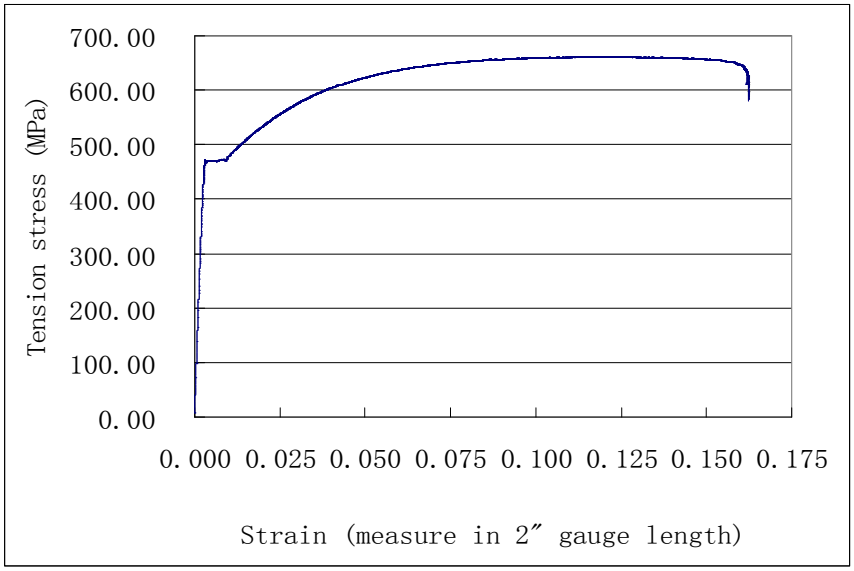

Figure 3.17 Tension stress versus strain in Rebar-2 (first batch rebar)

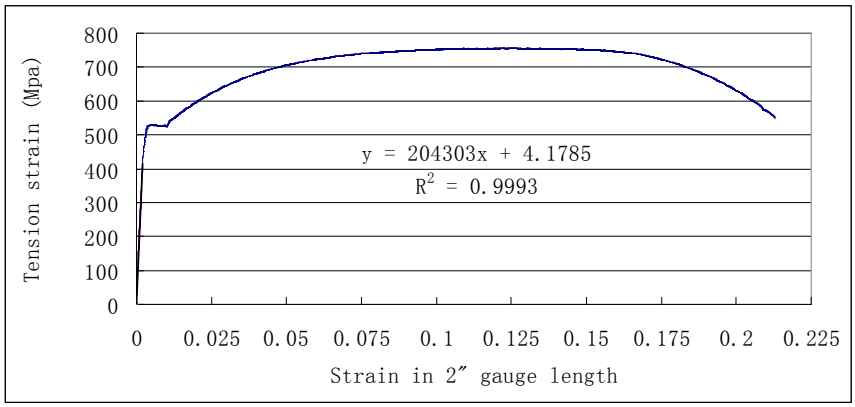

Figure 3.18 Tension stress versus strain in Coupon-1 (first batch rebar)

3.2.3 Properties of Steel Shear Bolts

The shear bolts were also tested using two types of specimens. One type was the standard round coupon machined from shear bolts, shown in Figure 3.19. The second type consisted of the original shear bolts stems.

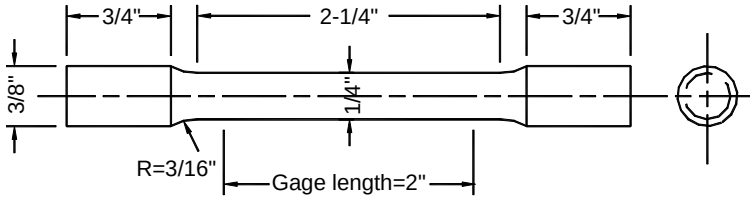

(a)

(b)

Figure 3.19 Standard coupon machined from 3/8” steel shear bolt (a) Dimensions, (b) Picture

Figure 3.20 Testing of the original bolt

Figure 3.20 shows one original shear bolt stem with broken section in the hydraulic grip system. The testing data of original shear bolts and coupons are shown in Table 3.8. The average yield strength, tensile strength, and elongation are in Table 3.9. Again, the nominal strengths from original bolts are smaller than those of coupons. The average nominal yield strength from original bolts was 369 MPa; nominal tensile strength was 494 MPa. From the coupon tests, the average yield strength was 378MPa; tensile strength was 510MPa, and elongation was 11.5%. Figure 3.21 and Figure 3.22 show the tension stress versus strain curves of original shear bolt and coupon. For calculations, the yield strength will be taken as 370 MPa, ultimate tensile strength 500 MPa at 11% elongation.

Table 3.8 Testing data of original shear bolts and coupons

original rebar or rebar coupon	Nominal yield strength F_y (MPa)	Nominal tensile strength F_u (MPa)	Elongation of 2" length	2" Strain Gauge and broken position	Yield strain
coupon-bolt-1	376	520	11.07%	Broken inside 2"	0.0022
coupon-bolt-2	374	500	12.40%	Broken inside 2"	0.00252
coupon-bolt-3	384	510	10.88%	Broken inside 2"	0.0027
bolt-org-1	359	478	20.87%	Broken inside 2"	0.0028
bolt-org-2	378	509	11.02%	Broken inside 2"	0.00216
bolt-org-3		496		Broken inside 2"	

Table 3.9 Properties of steel shear bolts

Original shear bolt		Shear bolt coupon		
Average yield strength (MPa)	Average tensile strength (MPa)	Average yield strength (MPa)	Average tensile strength (MPa)	Average elong-ation (%)
369	494	378	510	11.5

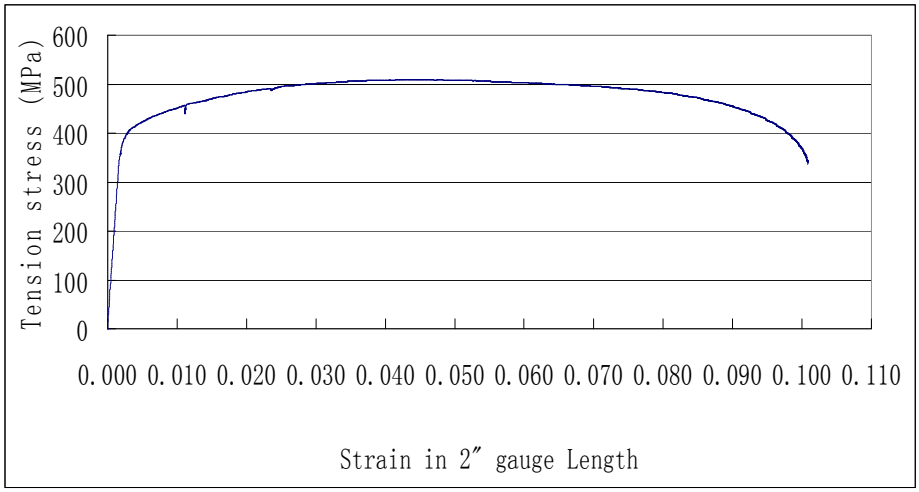

Figure 3.21 Tension stress versus strain of original shear bolts (bolt-org-2)

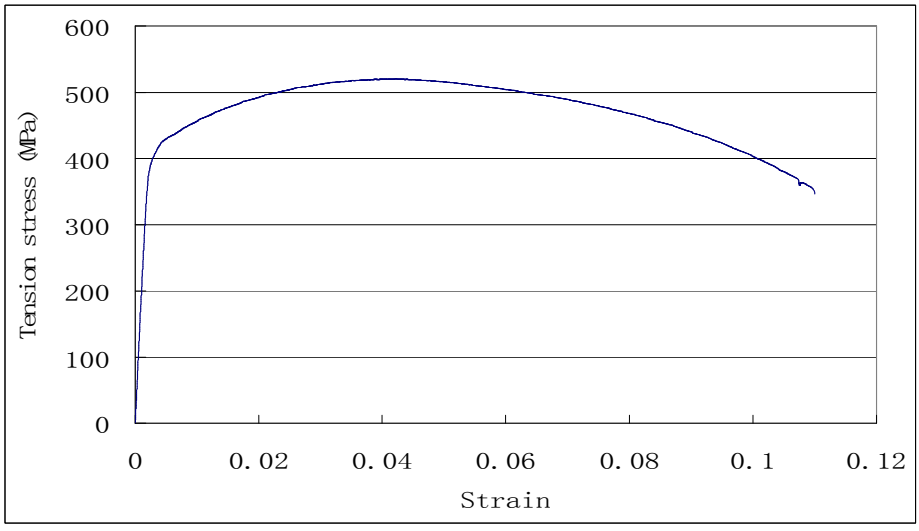

Figure 3.22 Tension stress versus strain of coupon (coupon-bolt-1) shear bolts

3.2.4 Fabrication of the Reinforced Concrete Specimens

The reinforcement cages of each specimen include top mat, bottom mat, and column rebar cages. All the #10M rebars for the slabs had hooks designed at the rebar ends. Figure 3.23 shows the top and bottom rebar mats. Figure 3.24 shows the strain gauges attached onto the rebars. Cages and formwork before casting are show in Figure 3.25 Figure 3.26 shows three specimens just after casting. A picture of specimens stored in the laboratory is shown in Figure 3.27.

Figure 3.23 Rebar cages

Figure 3.24 Strain gauges attached on rebars

Figure 3.25 Rebar cages and formworks before casting of the specimens

Figure 3.26 Specimens just after casting

Figure 3.27 Specimens stored in the laboratory

3.2.5 Shear Reinforcement

Steel shear bolts are installed after drilling holes in the concrete slab of the specimens. The bolts are tightened against the slab by a standard wrench to a torque which causes about 10~15% of yield strain of the bolts.

In series I, four peripheral rows of shear bolts were installed in specimen SW2; six rows of bolts in specimens SW3, SW4. There were no bolts installed in specimens SW1, SW5. Each peripheral row of bolts around the column includes eight bolts (Figure 3.28). Bolt spacing and numbering of bolts with strain gauges in specimen SW2, SW3 and SW4 are shown in Figure 3.28.

In Series II, six peripheral rows of shear bolts were installed in specimen SW7, SW8 and SW9. The shear bolt layout was orthogonal in SW7 and radial in SW8 and SW9 (Figure 3.29). Each peripheral row of bolts around the column includes eight bolts. Specimen SW6 had no bolts.

In Figure 3.28 and Figure 3.29, the numbered shear bolts had strain gauges attached to the center of the bolt stem, along the stem axis. The leads (electricity wires) were connected to the strain gauges and were sent through a small holes drilled in the bolts cap as shown in Figure 3.30. Isolating resin was applied to the strain gauges and the surrounding area on the bolts stem, and black electricity isolating tape was used to wrap the strain gauges. (Figure 3.30)

The spacing between the peripheral rows of shear bolts was not constant, due to interference from flexural bars (Figure 3.28 and 3.29). Radial patterns of shear bolt layout were initially planned for specimen SW8 and SW9. After drilling, the bolt patterns were not perfectly radial. This was also due to the interference of the flexural reinforcing bars. The drilling for shear bolts requires that no flexural bars are cut.

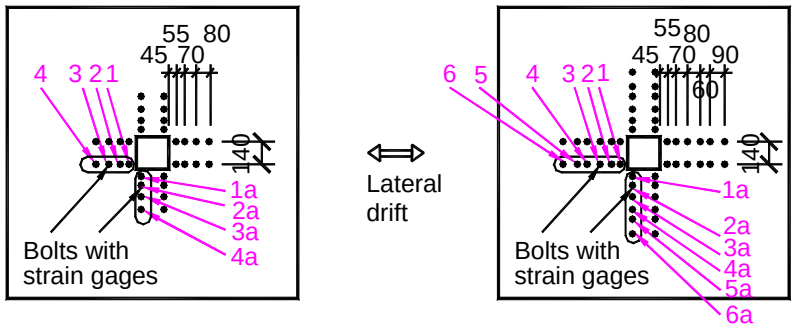

(a) (b)

Figure 3.28 Shear bolt spacing in specimen SW2, SW3, SW4 and numbering of strain gauges on bolts

(a) Specimen SW2 (4-row bolts); (b) Specimen SW3, SW4 (6-row bolts)

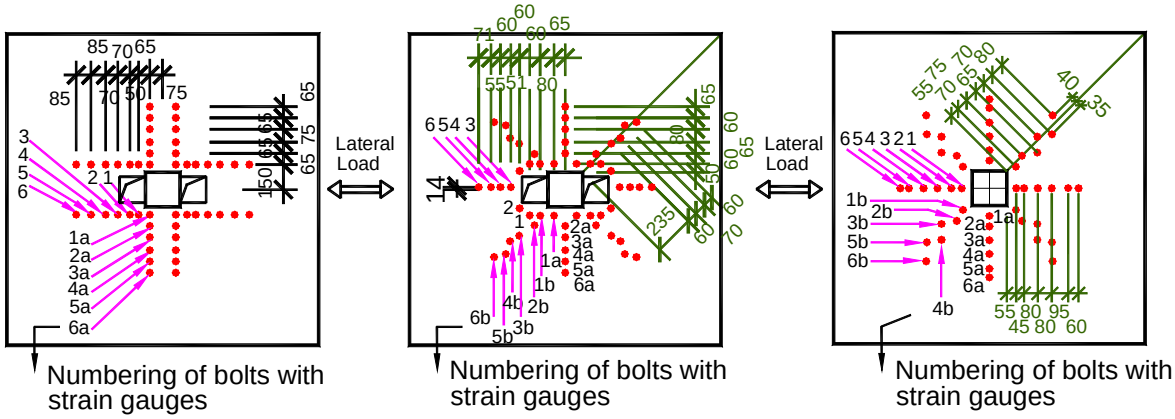

(a) (b) (c)

Figure 3.29 Shear bolt spacing in specimen SW7, SW8, SW9 and numbering of strain gauges on bolts

(a) Specimen SW7(6-row bolts); (b) Specimen SW8(6-row bolts); (c) Specimen SW9(6-row bolts)

Figure 3.30 Shear bolts with strain gauges

3.2.6 Installation of Shear Bolts

A total of 300 holes of 1/2”diameter were drilled through the concrete slabs using Target drilling machine and core drill bits with diamond tips. There was a water hose connected to the core bit to supply water while drilling. During the drilling process, if it was found that the drill bit hit a flexural reinforcing bar in the slab, the drill machine was moved to a different position. The “non-successful holes” were patched using Sikadur 30 plus pool sand (1:1). Figure 3.31 shows the operation of the drilling machine, which was held tight to the concrete slab using a steel angle attached to the machine bottom.

Figure 3.31 Drilling holes in the slab

3.3 Experimental Setup

This section includes three subsections. First, in section 3.3.1, the main components (elements) of the setup are introduced. Second, section 3.3.2 introduces a special steel frame designed and used for lifting and installation of the concrete slab-column specimens. Third, in section 3.3.3, the strength and stiffness of all the members are discussed.

3.3.1 Components of the Experiment Setup

A picture of the experimental setup is shown in Figure 3.32. The names and the numbering of all members of the setup are shown in Figure 3.33 (Elevation A) and Figure 3.34 (Elevation B). The steel setup for the testing includes two main parts: the main frame and the supporting frame.

The main frame consists of four vertical steel columns (①: W310x86), the crosshead (two deep channels, ⑲, MC460x86), and stiffeners for the crosshead. Three hydraulic actuators are installed on the main frame to apply load to the concrete slab-column specimen: two of them are horizontal to apply cyclic lateral drifts (④: 50 kips); the third is a vertical actuator (⑥: 150 kips) to apply the vertical constant load to the column of the specimen.

The ground anchor bolt pattern in the laboratory is shown in Figure 3.35. A short beam (㉑: W310x107, with end plates) connected the two columns (①) at the bottom with four ground anchor bolts holding it in positions.

Figure 3.36 shows the top plan view of the crosshead of the main frame. The 150-kip vertical actuator (⑥) was installed in the middle of the crosshead through a steel plate attached to the bottom of the two deep channels. In order to install the horizontal actuators on each side of the frame, (Figure 3.33), a short beam (⑱: W250x73) with end plates was inserted and bolted between the two columns at the level of the actuator. The height difference between the two horizontal hydraulic actuators was 1250 mm.

The second part of the experimental setup, the specimen supporting frame, is shown in Figure 3.34 and 3.35, and includes a square ring beam (⑭), four supporting columns (⑩), two bottom reaction beams (⑮), two top reaction beams (②), eight vertical reaction rods (⑬), and a base steel panel (⑯) stiffened by paralleled channels (⑰) underneath. This frame was designed to support a concrete slab-column specimen. The concrete slab was supported on its bottom from four sides by the square ring beam. The plane view of the square ring beam is shown in Figure 3.37. To restrain overturning of the specimen due to cyclic lateral loading, two top reaction beams (②) were installed in the direction parallel to Ⓨ1 and Ⓨ2 axes. On each end of this beam, two vertical steel rods (⑬), attached to the bottom beam ⑮, were used to hold the top reaction beam (②) , as shown in Figure 3.32, Figure 3.34, and Figure 3.35.

Figure 3.32 Picture of experimental setup

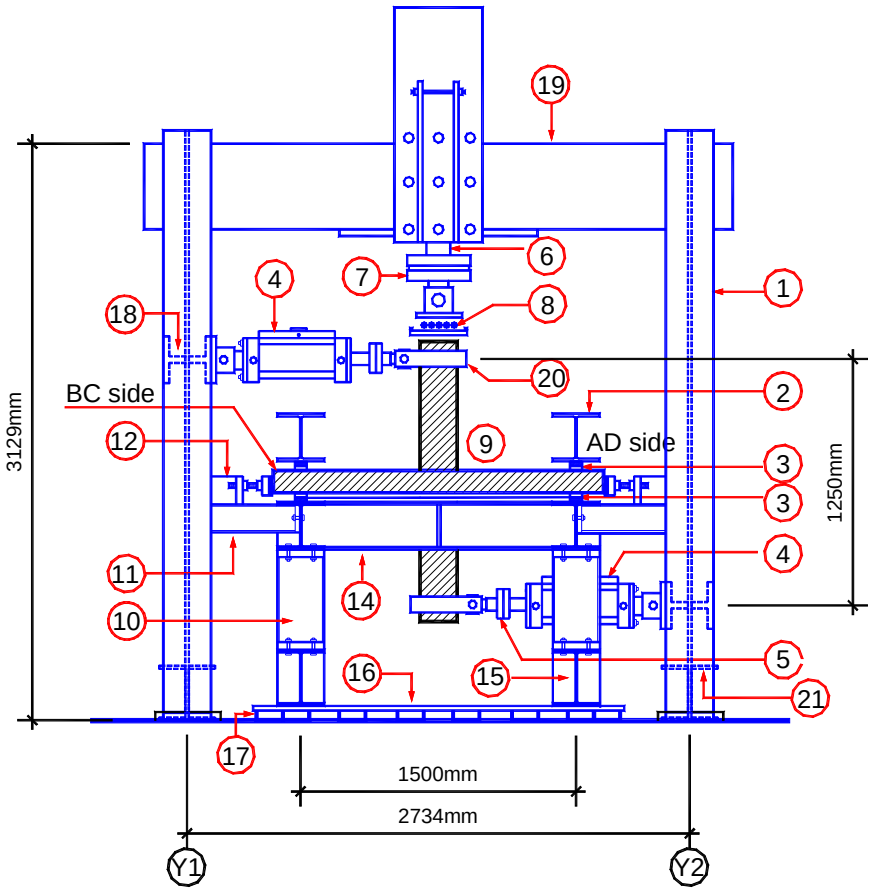

1 Column of steel frame (W310x86)
2 Top reaction beam (W250x89)
3 1"x1" Neoprene pads
4 Horizontal actuator
5 Horizontal load cell (50 kip)
6 Vertical actuator
7 Vertical load cell (150 kip)
8 Steel pan and rollers
9 Concrete slab-column specimen
10 Supporting column (W250x89)
11 Bracing beam (W150x22)
12 Adjustable stopper (W150x22)
13 Reaction steel rods (Ø22mm)
14 Support square ring beam (W250x89)
15 Base reaction beam (W310x73)
16 1" thick steel base panel
17 Steel channels (C150x12)
18 Short beam for actuators (W250x73)
19 Channels of crosshead (MC460x86)
20 Collar system
21 Beam (W310x107, with end plates) connecting the two frame columns at the bottom, achored to the ground by four long bolts

Figure 3.33 Elevation A of the testing setup

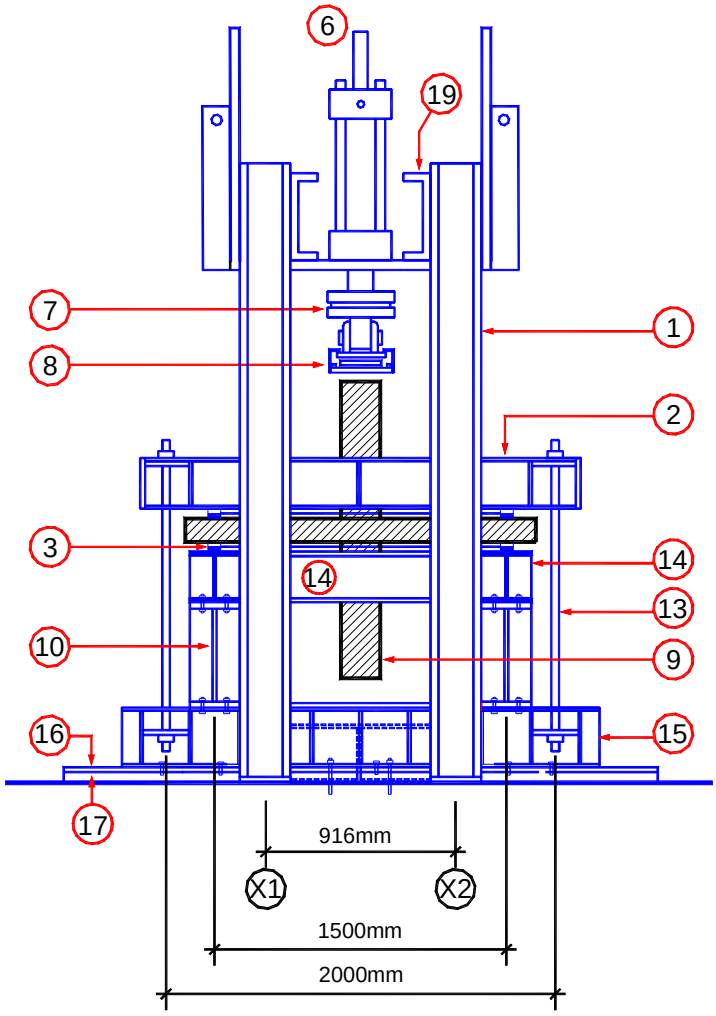

1 Column of steel frame (W310x86)
2 Top reaction beam (W250x89)
3 1"x1" Neoprene pads
6 Vertical actuator
7 Vertical load cell (150 kip)
8 Steel pan and rollers
9 Concrete slab-column specimen
10 Supporting column (W250x89)
13 Reaction steel rods (ø22mm)
14 Support square ring beam (W250x89)
15 Base reaction beam (W310x73)
16 1" thick steel base panel
17 Steel channels (C150x12)
19 Channels of crosshead (MC460x86)

Figure 3.34 Elevation B of the testing setup

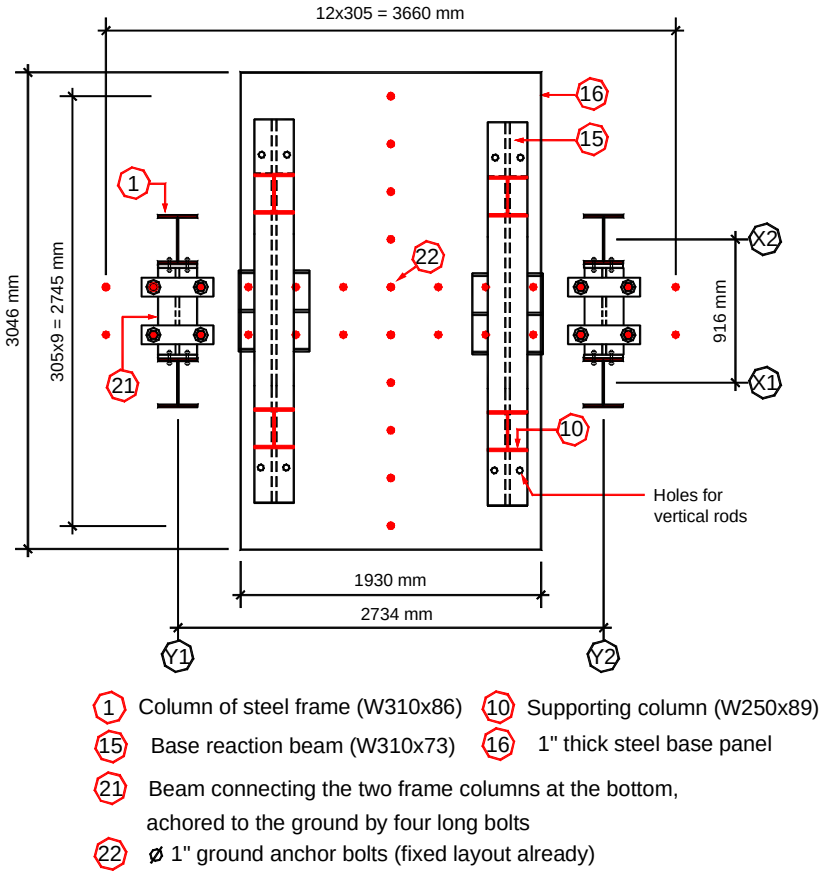

Figure 3.35 Plan view of the main frame near ground level, ground anchor bolts, base panel, and the base reaction beams

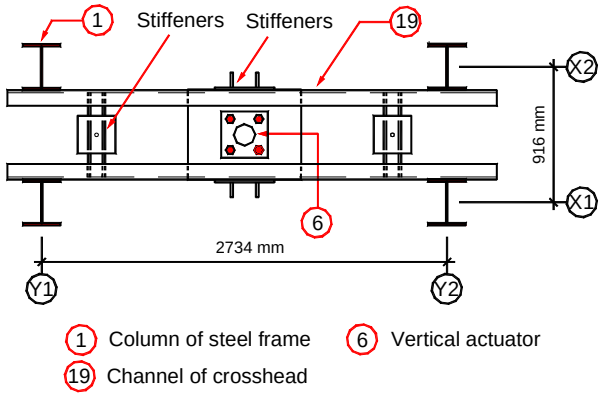

Figure 3.36 Plan view of the main frame at the crosshead level

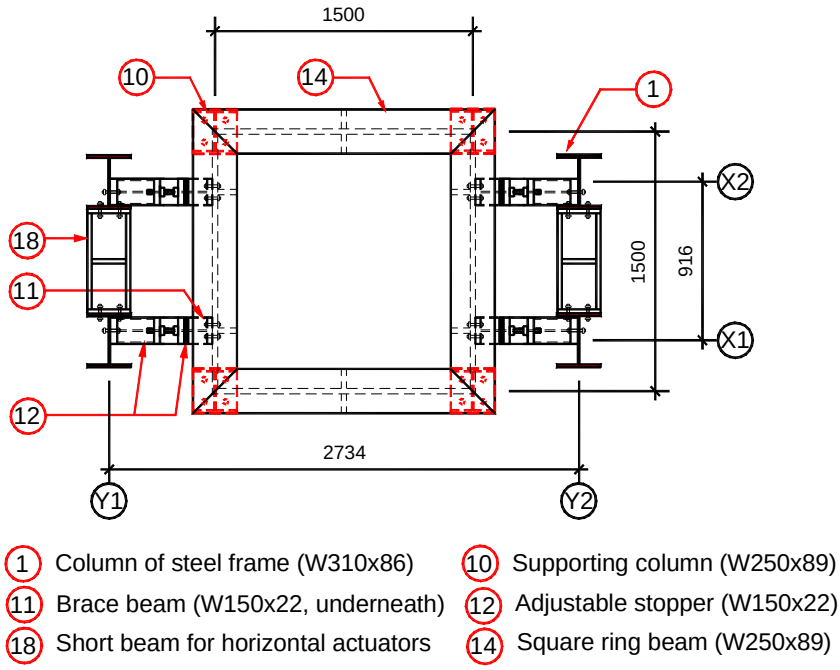

Figure 3.37 Plan view of the square ring beam, bracing beams, and adjustable stoppers

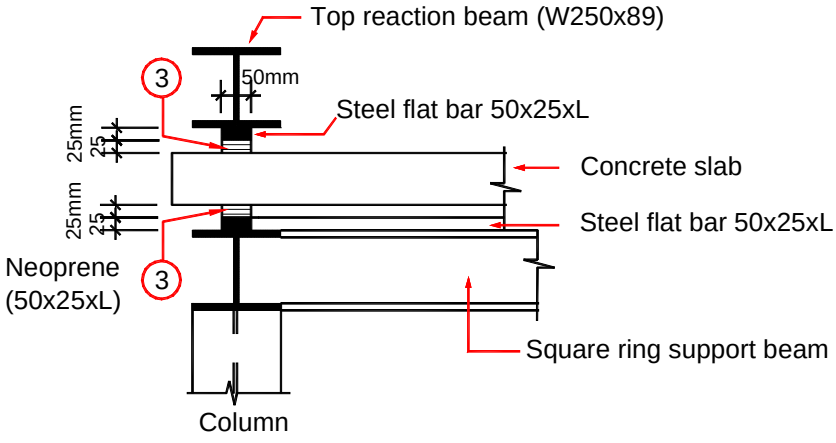

Figure 3.38 Neoprene pads between the concrete slab and the square ring beam or the top reaction beam (L is the support length: L=1550 mm on each side)

Neoprene pads of 25mm thickness were inserted between the concrete slab and the support beams and also between the slab and the top restrain beam along the support lines. Figure 3.38 shows the detail. The reason for using neoprene pads: is to simulate the slab rotation at the contraflexure line of the continuous prototype building due to cyclic moment transfer. The 25 mm thick neoprene flat bars was glued to 25mm thick steel flat bars of the same dimensions with the neoprene. This provided sufficient space for rotation between the concrete slab and the support ring beam or the top reaction beam.

As shown in Figure 3.35, there were no ground anchor bolts directly underneath the eight vertical reaction rods (⑬). Therefore, two base reaction beams (⑮) were designed parallel to Ⓨ1 axis (in Figure 3.34 and 3.35). In the middle of each base beam, four ground anchor bolts held the stiffened bottom flange of the beam. All the ground anchor bolts were of 1" diameter and Grade 8. At each end of the base beam, two vertical reaction rods were fastened as shown in Figure 3.34. Therefore, the base reaction beam acted as a beam cantilevered at its two ends.

The four support columns (⑩ in Figure 3.34 and 3.35) were installed on top of the two base reaction beams (⑮). These columns transferred compression load to the base beams.

Although the strength and the stiffness of the two base beams were designed high enough to sustain the loading during in the experiments, a steel panel (⑯, 2734x2745x25mm) stiffened by steel channels was also provided underneath. This stiffened panel was fastened by all ground anchor bolts that it covered as shown in Figure 3.35. The two base reaction beams were installed on top of the base panel. There were two purposes of using the base panel. First, the bottom flange of each base reaction beam was fastened to the base panel by twelve additional bolts; this made the base beam act together with the base panel to transfer load to more ground anchor bolts. Also, the steel panel provided a base to attach instruments. Some string pots were attached to the steel panel by magnet pieces. The steel racks for displacement transducers for slab bottom surface were also installed on the panel by magnets.

To restrain the lateral sway of the supporting frame, four horizontal bracing beams (⑪: W150x22) installed between the square ring beam and the four columns of the main frame. Figure 3.37 gives the plane view of bracing beam layout and Figure 3.33 provides the elevation view.

In order to restrain any possible excessive horizontal movement of the concrete slab due to horizontal lateral force difference, four adjustable stoppers were installed horizontally on the four main frame columns, at the concrete slab level. Figure 3.33 and Figure 3.37 show the elevation and plan view of these stoppers in the experiment setup. One inch thick neoprene pads were glued to the stoppers to face the concrete slab edges. Figure 3.39 gives the details of a stopper.

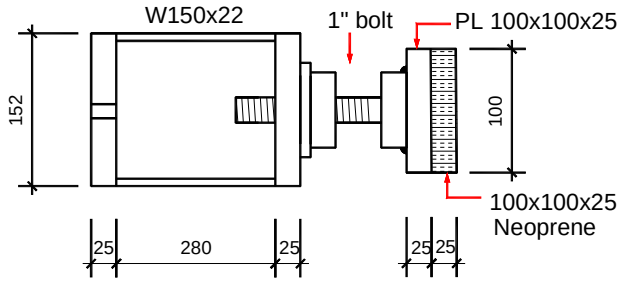

Figure 3.39 Adjustable stopper

The vertical load was first applied by the vertical hydraulic actuator (⑥) which would keep the constant load on top of the upper concrete column. As shown in Figure 3.33 and Figure 3.34, the cylinder (⑥) of the vertical actuator was connected a 150 kip load cell (⑦) and a threaded stud with a pin hole. Through a round steel pin (diameter 49mm), a flat square steel plate was connected to the actuator. The upper and lower concrete columns were also connected to horizontal actuators through steel collars (⑳ in Figure 3.33, detailed in Figure 3.41) to apply horizontal cyclic loading. In order to reduce the friction between the top concrete column and the steel plate, steel rollers were used. A steel pan (⑧) with five steel rollers, shown in Figure 3.40 was inserted between the plate and top surface of the concrete column.

The collar system as shown in Figure 3.41 was a modification from a previous collar system (El-Salakawy, 1998). The previous one was used to apply monotonic horizontal load (the loading was in one direction only). The modified collar system would apply reversed loading. Four threaded rods (3/4”diameter) and five thick steel plates were added to clamp the concrete column.

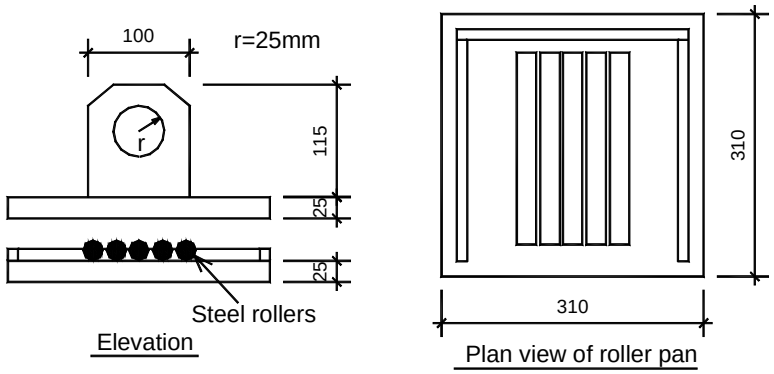

Figure 3.40 Roller on top of the upper concrete column

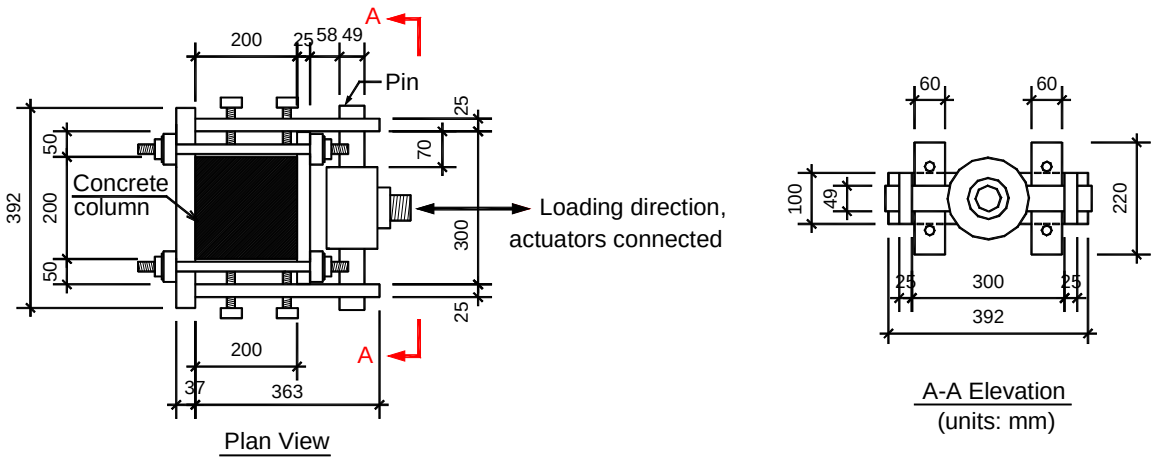

Figure 3.41 Steel collar system connected to horizontal hydraulic actuators

3.3.2 Steel Lifting Frame for Installation of Concrete Slab-Column Specimens

The weight of each reinforced concrete slab-column was about 1000 kg. Four steel coupling nuts were embedded in the four corners of each slab. These were used for four eye bolts for lifting the slab. Due to limitations for space in height and horizontal direction, a special steel lifting frame was fabricated using large steel angles and W-shapes. The drawings of the lifting frame are shown in Figure 3.42.

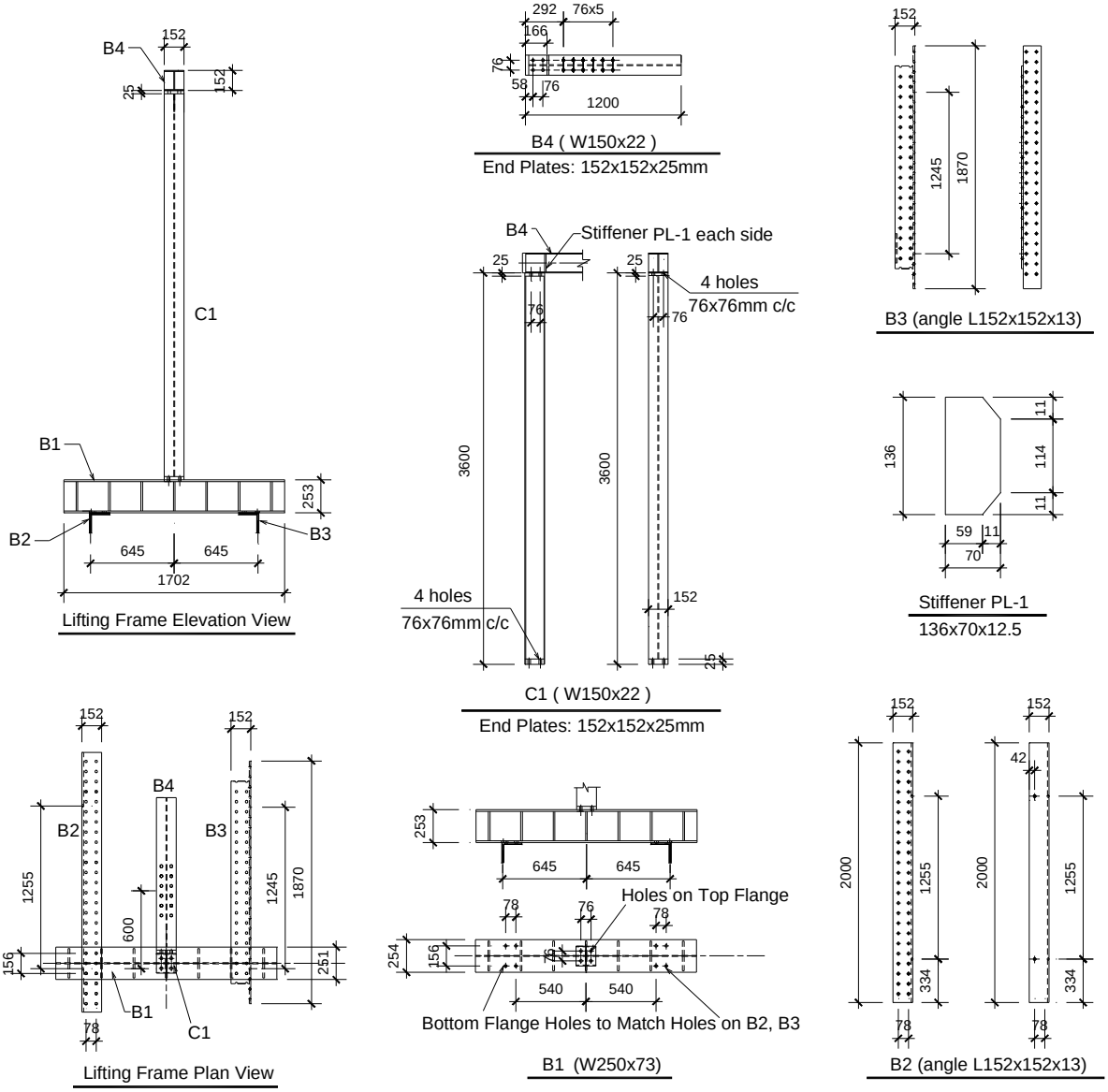

Figure 3.42 Steel frame for specimens lifting and installation

Figure 3.43 Lifting of the concrete specimen

3.3.3 Member Strength and Stiffness of the Steel Experimental Setup

The experimental setup must have enough strength and stiffness to sustain the experimental loading. The main frame was an existing frame used by previous researchers (El-Salakawy ,1998 and Adetifa, 2005). Thus the strength and stiffness of the main frame were assumed sufficient. Similarly, the stiffened base panel was also used by Adetifa (2005). The work on the main frame was to adjust the height of the crosshead and to drill holes in columns to bolt the new bracing beams and the stoppers.

The support frame was a new design, which included the square ring beam, four support columns, two base reaction beams and two top reaction beams, eight vertical reaction rods, four bracing beams, and four stoppers. Before design of all these members, the maximum loads were estimated based on the calculation in section 3.1.2 and Table 3.1 and the previous tests results. The vertical load was kept constant ($V = 160kN$); the maximum horizontal load F on top and bottom column were assumed to be 150kN. Figure 3.44 shows the loads on the concrete slab-column specimen. $Ln = 1.5m$. The height H between the horizontal actuators was assumed 1.47m before design (during installation, H was adjusted to 1.25m). It was assumed that the concrete slab would tilt up on three edges on the bottom surface; only one concrete slab edge (on the right hand side in Figure 3.44) transferred the compression load to the side of the square ring beam. Thus the reaction force R_2 is equal to $(V + F * H / L_n + G)$, where G is the self weight of the concrete specimen and the steel reaction beams on the slab; the reaction force R_1 is equal to $(F * H / L_n)$. Force R_2 was applied on one side of the square ring beam. R_2 was transferred to the support columns. R_1 was used for design of the vertical rods strength and design all the reaction beams. The bracing beams and the stoppers were designed by assuming lateral load F=150kN was applied when one horizontal actuator might accidentally stop working.

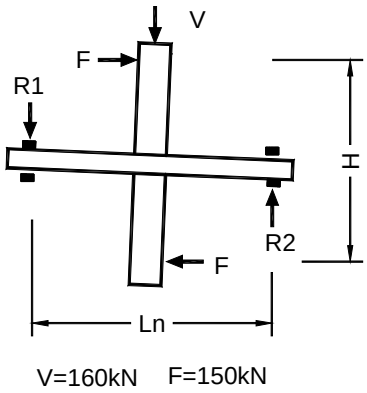

Figure 3.44 Estimated maximum load on the specimen in testing

In addition, each of the three hydraulic actuators was connected to a load cell, connectors, a collar system through threaded studs. These studs, were checked for their tension and compression strength. For the modified collar system, the tension force of the threaded rods and the shear force of the clamping plates were checked.

3.4 Instrumentation

The data acquisition system includes the following: a) three load cells connected to the vertical and the two horizontal hydraulic actuators; b) displacement transducers; c) strain gauges in shear bolts and flexural reinforcements in the concrete slab. The data acquisition system included two data acquisition modules for all the strains, displacements and load cells.

3.4.1 Displacements

The three actuators have their own internal LVDTs to record the cylinder displacements. In addition, external displacement transducers were used. To eliminate the deformation effect of the testing frame, all external displacement transducers were fastened onto a rigid steel rack that was installed independently on the ground. Figure 3.45 shows the elevation including the transducer rack. Figure 3.46 gives the plan view.

On the top and the bottom concrete column ends, string pots (S1 and S2 in Figure 3.45) were attached horizontally to measure the column lateral drifts. On the bottom column ends of the specimen, a string pot (S5) was installed in vertical direction to record the displacement, which is the resultant of vertical and horizontal displacements of that column end. On each side of the concrete slab, perpendicular to the loading direction, a horizontal string pot (S3 or S4) was attached to the center of the slab edge to test the slab movement in the horizontal loading direction.

3.4.2 Crack width

Displacement transducers including LVDTS and DCDTs were installed on both top and bottom slab surfaces in aligned vertical pairs (Figure 3.47**)**. The displacement difference between these pairs gives an estimation of the crack vertical widths inside the slab.

3.4.3 Strains

Strain gauges (5mm-length) were attached at locations “a”, “b”, “c”, and “d” of rebar #1 ~ Rebar #5 in two directions as shown in Figure 3.6 and Figure 3.7.

Shear bolts, at typical locations, had also attached strain gauges in the middle of their bolt stems in longitudinal direction. In specimen SW7, strain gauges were placed on shear bolts in orthogonal lines; in specimens SW8 and SW9, shear bolts in both orthogonal diagonal directions had attached strain

gauges. Layouts and numbering of shear bolts with strain gauges in SW7, SW8 and SW9 are shown in Figure 3.28 and Figure 3.29.

3.4.4 Load Control

The controllers for the vertical 150 kip (667.2 kN) actuator were MTS 442; two 50 kip (222.4 kN) horizontal actuators were controlled by two MTS 406 controllers. The two MTS 406 controllers for the horizontal actuators were connected to a voltage ramp, which could generate voltages corresponding to the designed load path (lateral drift). The two horizontal actuators were controlled by switching the ramp manually.

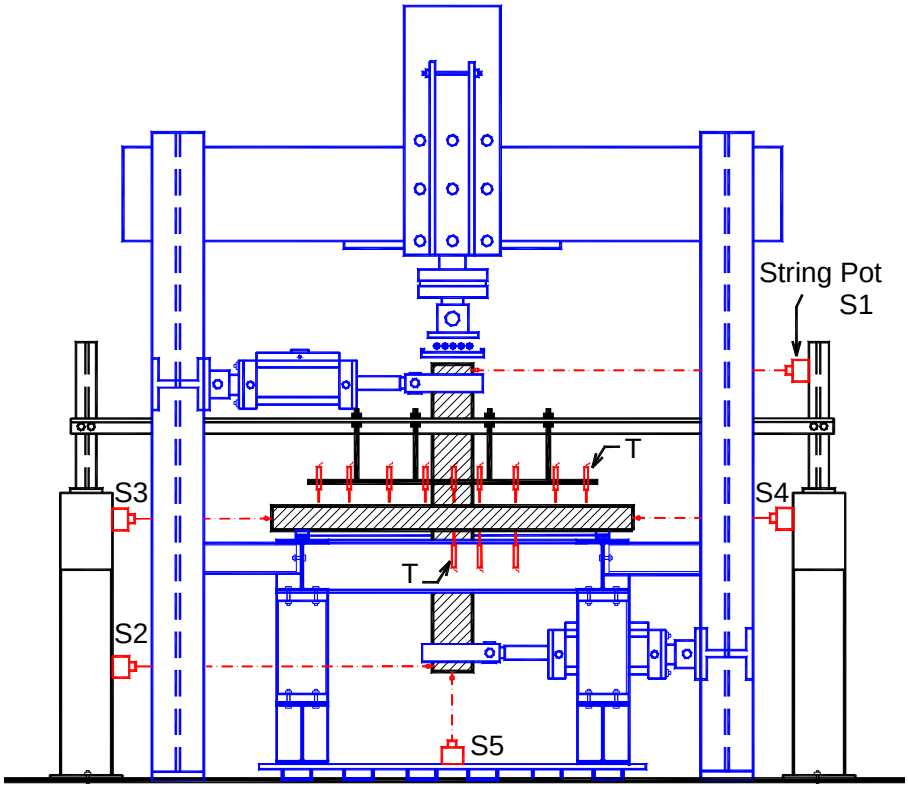

S1-S5: String pots to test displacement

T: Displacement transducers on top and bottom slab surface

Figure 3.45 Displacement transducers on slab and string pots connected to the specimen

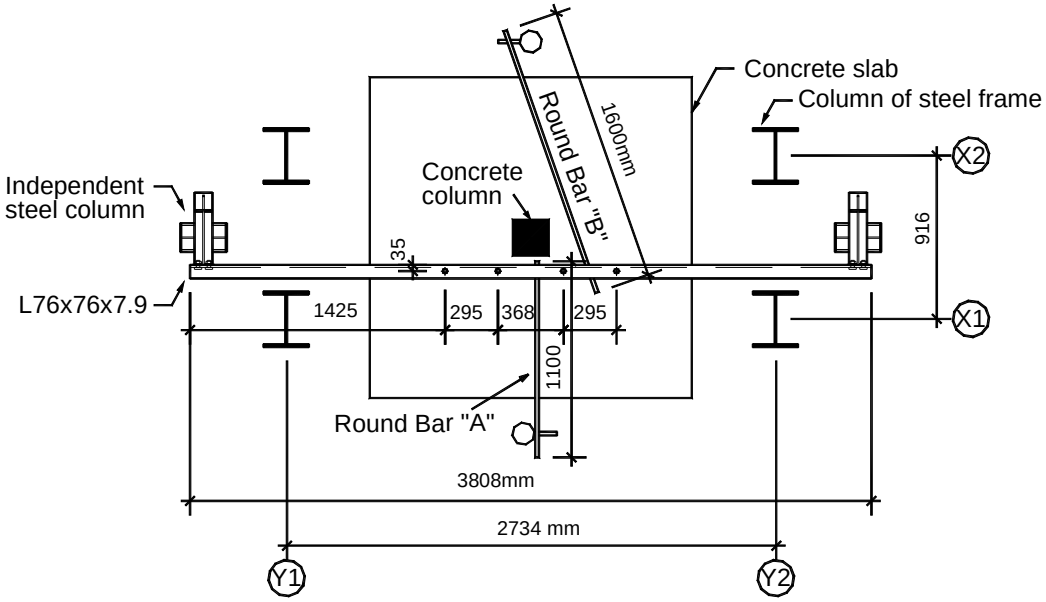

Figure 3.46 Plan view of the independent rack for transducers

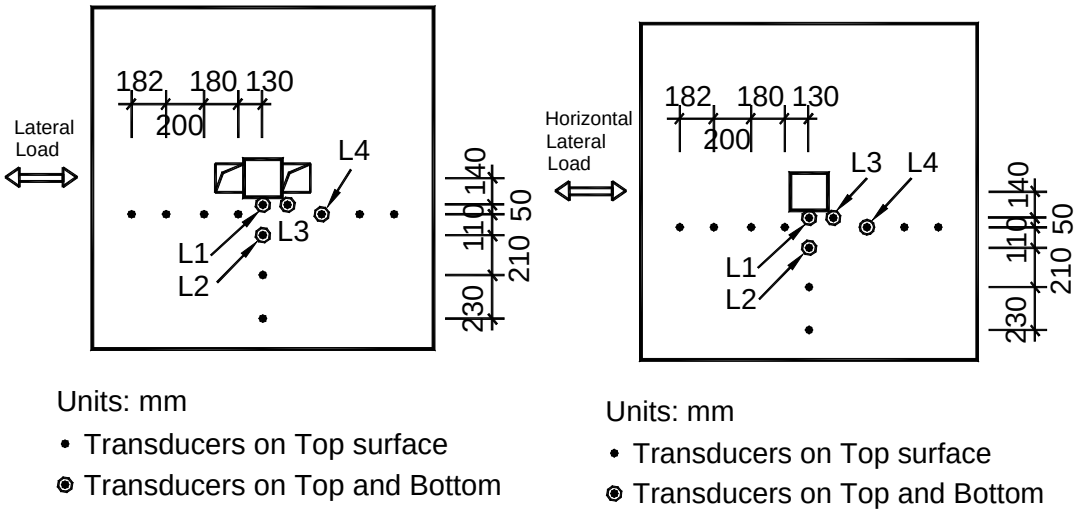

Figure 3.47 Displacement transducers layout on slab

3.5 Testing Procedure

Each specimen was subjected to gravity load from the top vertical actuator, using load control mode, at a loading rate of about 20 kN / minute until the desired load level was attained. The vertical load was then kept constant throughout the test. Specimen SW1, SW2, and SW3 were subjected to 110kN vertical load while SW4~SW9 to 160 kN.

After application of the vertical load, the two horizontal actuators were activated to apply horizontal loading. During this process, the two actuators were controlled in displacement mode. They pushed and pulled the specimen columns simultaneously at the same rate according to a pre-planned cyclic loading path as shown in Figure 3.48. The horizontal loading rate was about 0.6 volt / minute (4.6 mm / minute) before 3% drift ratio and 1.45 volt / minute (11.1 mm / minute) for larger drifts.

The lateral loading cycles were applied from lower to higher drift levels by controlling the horizontal actuators' displacement. At each level, the same drift cycle was repeated three times. After 0.75% drift level, one 0.5% drift cycle was inserted between three-repeated-cycle groups. This small cycle of lower drift is used to evaluate the connection behaviour after larger seismic loading.

The reason for applying three repetitions of each cycle was to show the connection stiffness degradation at each drift level. After 3.0% lateral drift, long and deep cracks formed in the concrete slabs and the intermediate 0.5% drift cycles showed no much change in the behaviour as compared to previous small cycles; therefore the small cycles were stopped after 3.0% drift. The increasing lateral drift cycles were then applied without repetitions to reduce testing time.

The intermediate small drift cycles (0.5%) were applied to show the deformation behaviour, stiffness, and strength of the specimen after higher lateral drifts. It also provides information for possible repair of the structure after large lateral drifts.

Due to unexpected slab movements, and small deformation of the frame during testing, the drifts recorded by external string pots were slightly different from the drifts recorded by internal LVDTs of the actuators. The displacements and drifts reported in this thesis are based on the readings from the external string pots which recorded real displacement of the specimen.

The design of the horizontal loading path followed the main idea of the ACI publication: "Acceptance Criteria for Moment Frames Based on Structural Testing (ACI T1.1-01) and Commentary (T1.1 R-01)." (2001) Although slow, pseudo-dynamic cyclic loading is not fully equivalent to dynamic loading and the loading path cannot represent earthquake loading completely, the result are

representative for the behaviour of slabs in seismic zones. Many similar cyclic testing procedures have been widely used by other researchers and their testing results have been incorporated into structural codes.

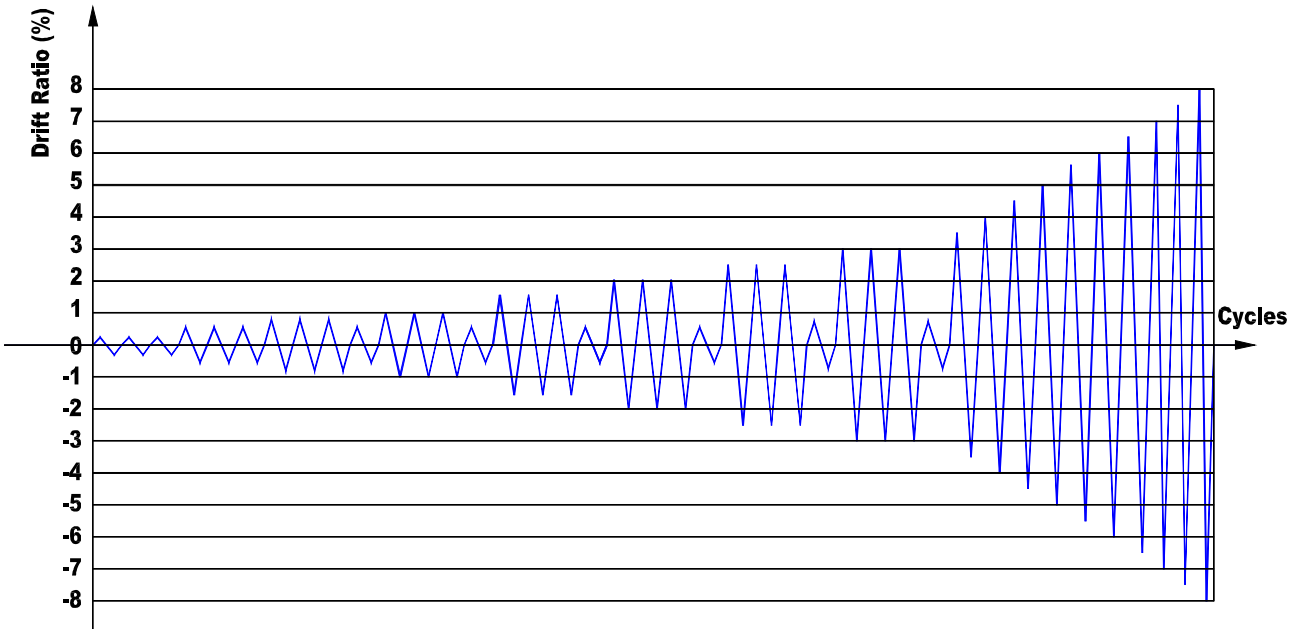

Figure 3.48 Loading path

Chapter 4
Experimental Results and Discussion

4.1 Introduction

This chapter gives the experimental results for Series I and Series II tests. For each series, lateral load versus drift ratio, moment versus lateral drift ratio, backbone curves of horizontal load versus horizontal drift ratio at top column end, peak-to-peak stiffness versus drift ratio, stiffness of small cycles, strains in reinforcements, and crack width are presented.

4.2 Results of Series I

This section introduces the test results of Series I which includes specimens SW1 ~ SW5. Among them, specimens SW1, SW2, and SW3 form Group I; the specimens SW4 and SW5 form Group II.

4.2.1 Lateral Load versus Drift Ratio

For clarity of explanations, it is necessary to specify the positive and negative force directions of the two horizontal hydraulic actuators. It is assumed that when actuators in Figure 3.33 push the concrete column of the specimen the forces are negative; otherwise, the forces are positive. The two horizontal actuators were installed in the experiment setup as shown in Figure 3.33. In the test, side "BC" was on side of Ⓨ1 axis, and side "AD" was on side of Ⓨ2 axis. The horizontal load direction is perpendicular to sides BC and AD. When the top horizontal actuator pushes the top concrete column end from BC side to the AD side, the horizontal load and the drift on the top concrete column are negative. At the same time, for the bottom concrete column, bottom horizontal actuator pushes the bottom concrete column from side AD to the side BC, the horizontal load and the drift on the bottom concrete column are also negative. The sides of "AD" and "BC" of the concrete slab column connections are also specified in Figure 3.6 ~ Figure 3.8, Figure 4.13, and Figure 4.40.

Horizontal lateral load on top column end versus its horizontal lateral drift ratio for specimens SW1, SW2 and SW3 (Group 1) are shown in Figure 4.1**,** and for SW4, SW5 (Group 2) in Figure 4.2. Specimens SW1, SW2 and SW3 (concrete strength: 35MPa) were subjected to vertical load of 110kN on the top column end; SW4 and SW5 (concrete strength: 46MPa) to vertical load of 160kN. As

shown in Table 4.1, it is observed that in Group 1, the peak lateral negative load for SW1 (without shear bolts) was 51.8kN at 2.6% drift ratio, while SW2 (with 4-row bolts) reached 60.4kN at 5.7% drift and SW3 (6-row bolts) reached 61.57kN at 4.3% drift ratio. Comparing with SW1, peak load of specimen SW2 increased 17%, and corresponding drift ratio increased 117%; SW3 showed an increase of 19% in peak load and 61% increase in corresponding drift. For positive peak load, SW2 and SW3 showed 27% and 30% increase, respectively. Also, drift ratio of SW2 and SW3 corresponding to positive peak load increased 109% and 66%, respectively

In Group 2, specimen SW5 (without bolts) had its peak negative lateral load of 52.0kN at 2.7% drift ratio, while SW4 (6-row bolts) reached negative lateral peak load of 74.9kN at 4.5% drift ratio. Specimen SW4 showed 43.9% increase in lateral peak load capacity and 64.2% increase in corresponding lateral drift compared to specimen SW5.

Figure 4.3 shows the five backbone curves of hysteresis curves of lateral load versus lateral drift. These backbone curves were formed by connecting peak points at the first cycle of each same-drift-cycles group. These curves clearly show initiation of punching load failure for SW1 and SW5 (no bolts), the post peak ductility of specimens SW2, SW3 and SW4 (with bolts), and the increase of peak load capacity and the maximum drift ratio of the specimens strengthened with shear bolts.

Specimens SW1 and SW5 without bolts failed abruptly after attaining the peak loads. There was a sudden peripheral crack formed in SW1 and SW5 respectively. Conversely, specimens with bolts (SM2, SM3, and SM4) continued to deform at almost constant lateral load. No sudden peripheral cracks formed and all the cracks were in radial direction. The maximum lateral drift attained by these specimens was 8%. Further testing had to be terminated because the top rollers could not accommodate it.

Table 4.1 Peak load and drift ductility (defined by Pan and Moehle, 1989) of specimen SW1~SW5

Slab name		$\frac{V}{V_0}$	Peak lateral load (kN)		Horizontal drift ratio at peak lateral load (%)		Yield drift ratio (%)		Drift ductility at peak lateral load μ_{peak}		Drift ductility at 95% post peak lateral load $\mu_{0.95}$		Drift ductility at 80% post lateral load $\mu_{0.80}$	
			-	+	-	+	-	+	-	+	-	+	-	+
Group 1	SW1	0.55	-51.79	55.56	-2.65	2.81	-1.55	1.58	-1.71	1.78	2.24	1.81	2.59	1.99
	SW2	0.55	-60.44	70.39	-5.74	5.87	-2.24	2.49	-2.56	2.36	3.05	3.04		
	SW3	0.55	-61.57	72.39	-4.27	-4.67	-1.54	2.08	-2.77	2.25	4.13	3.24		
Group 2	SW4	0.68	-74.89	78.90	-4.50	5.81	-2.09	2.52	-2.15	2.31	3.03	2.72		
	SW5	0.68	-52.04	59.86	-2.74	2.61	-1.41	1.44	-1.94	1.81	2.33	2.2	2.5	2.51

Note: Nominal punching shear capacity of concrete $V_0 = 0.33\sqrt{f_c'}\, b_0 d$ (ACI 318-05, in metric units)

Table 4.2 Drift ductility (using tested first yield drift ratio) of specimen SW1~SW5

Slab name		Tested first yield drift ratio (%)	Drift ductility at peak lateral load μ_{peak}		Drift ductility at 95% post peak lateral load $\mu_{0.95}$		Drift ductility at 80% post peak lateral load $\mu_{0.80}$	
			-	+	-	+	-	+
Group 1	SW1	+1.33	1.99	2.11	2.61	2.15	3.02	2.36
	SW2	-0.91	6.30	6.46	7.51	8.32		
	SW3	-0.68	6.27	6.88	9.35	9.91		
Group 2	SW4	-0.96	4.68	6.06	6.60	7.14		
	SW5	+1.04	2.63	2.51	3.16	3.05	3.39	3.48

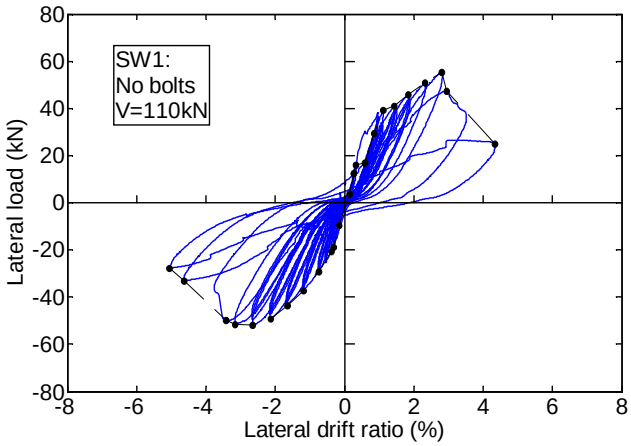

(a)

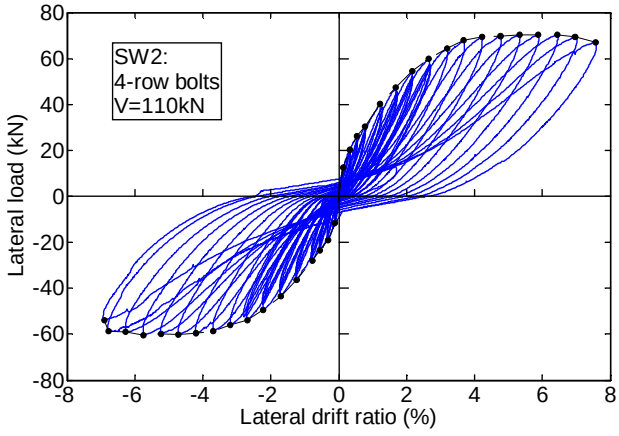

(b)

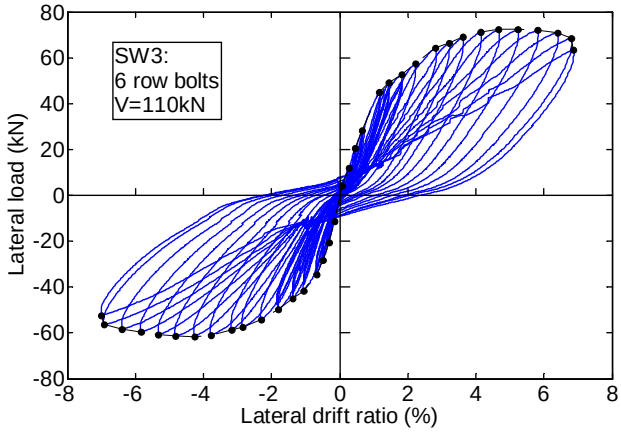

(c)

Figure 4.1 Horizontal load versus horizontal drift ratio at top column end

(a) Specimen SW1, (b) Specimen SW2, (c) Specimen SW3

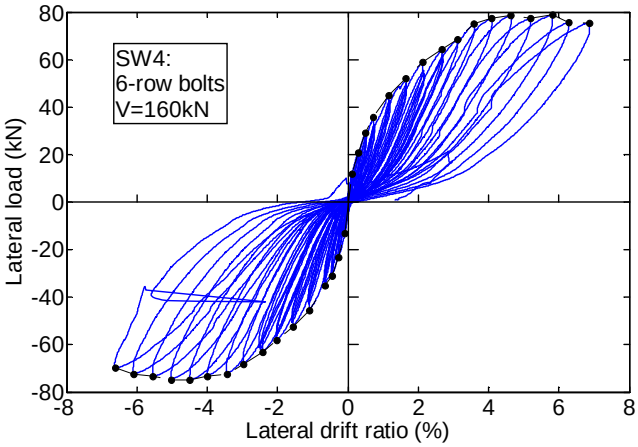

(a)

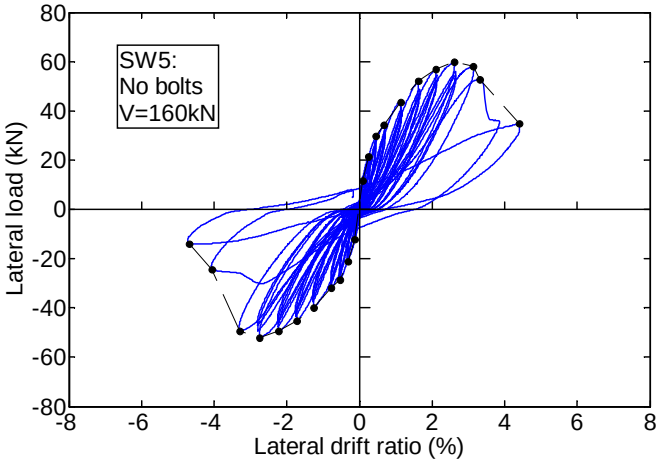

(b)

Figure 4.2 Horizontal load versus horizontal drift ratio at top column end

(a) Specimen SW4, (b) Specimen SW5

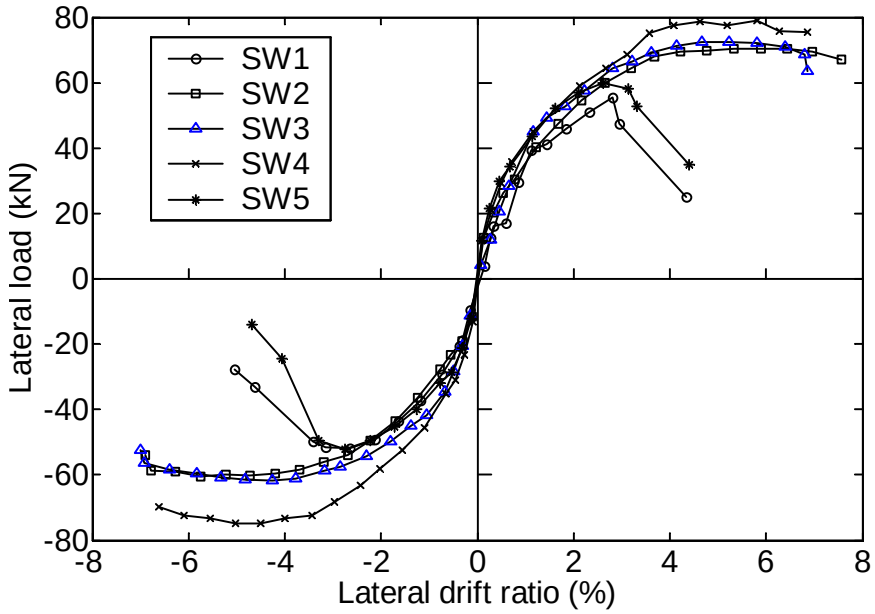

Figure 4.3 Backbone curves of horizontal load versus horizontal drift ratio at top column end.

4.2.2 Moment versus Lateral Drift Ratio

Moment versus drift ratio curves are equivalent to Figures 4.1-4.3. The lever arm for the lateral forces was 1.25m. For completeness, they are presented here. Moment versus lateral drift ratio of specimen SW1-SW3 are shown in Figure 4.4, and for specimens SW4 and SW5 are shown in Figure 4.5. Backbone curves of moment versus lateral drift ratio are shown in Figure 4.6. All observations regarding the behaviour are equivalent to comments from section 4.2.1.

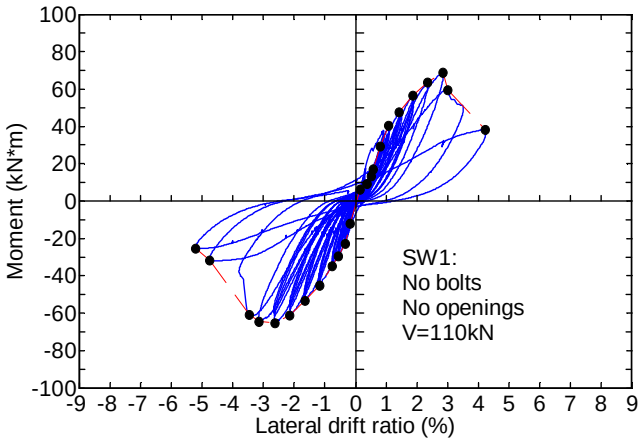

(a)

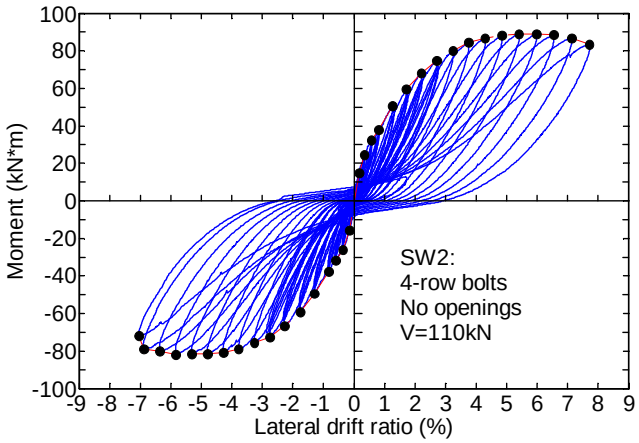

(b)

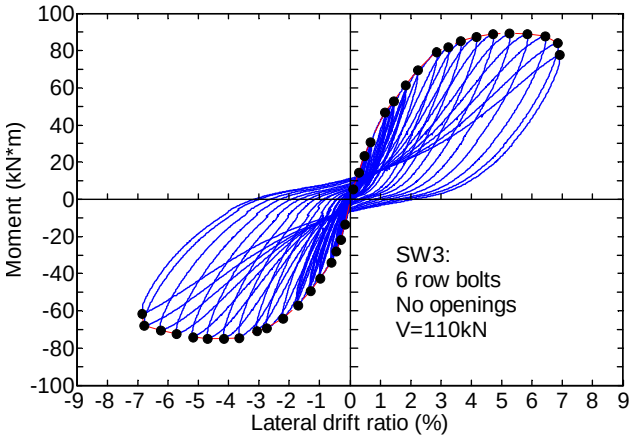

(c)

Figure 4.4 Moment versus lateral drift ratio at top column end

(a) Specimen SW1, (b) Specimen SW2, (c) Specimen SW3

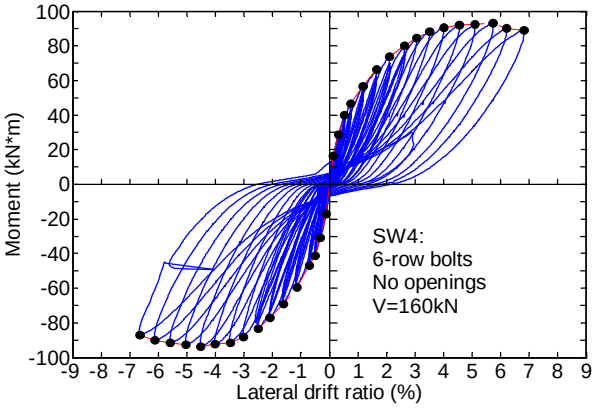

(a)

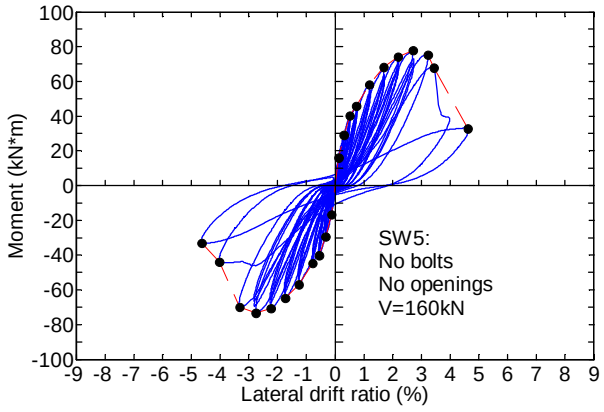

(b)

Figure 4.5 Moment versus horizontal drift ratio at top column end

(a) Specimen SW4, (b) Specimen SW5

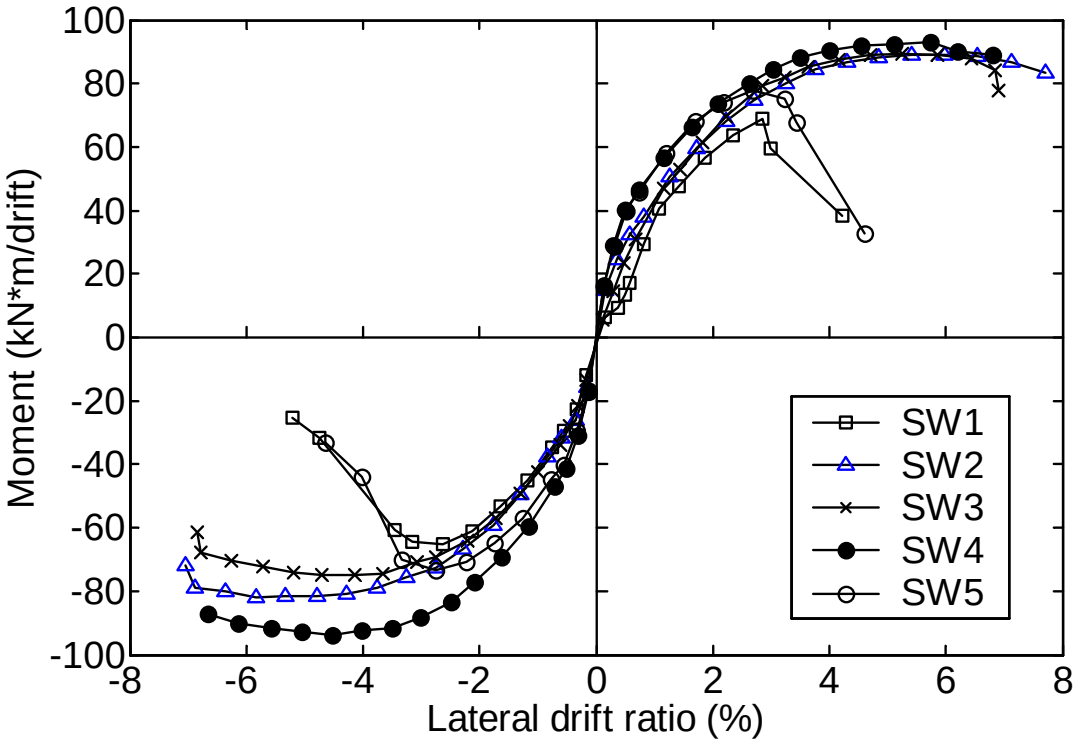

Figure 4.6 Backbone curves of moment versus lateral drift ratio at top column end

4.2.3 Connection Stiffness

Based on the curves of unbalanced moment versus drift ratio, peak-to-peak stiffness of each cycle is calculated (Figure 4.7 and Figure 4.8). Stiffness at the small drift cycles (in between larger drifts) are showed in Figure 4.9.

The connection stiffness decreased rapidly (to 40-50% original stiffness) during the repeated cycles up to 0.75% drift ratio. It should also be noted that the stiffness decreased after each repeated cycle, in every three successive same drift cycles. The stiffness decreased more in the second cycle than it did in the third one. Among each group of three same cycles, the stiffness decrease between the first and second cycles was more than twice the decrease between the second and third cycles. Low drift cycles also showed stiffness degradation.

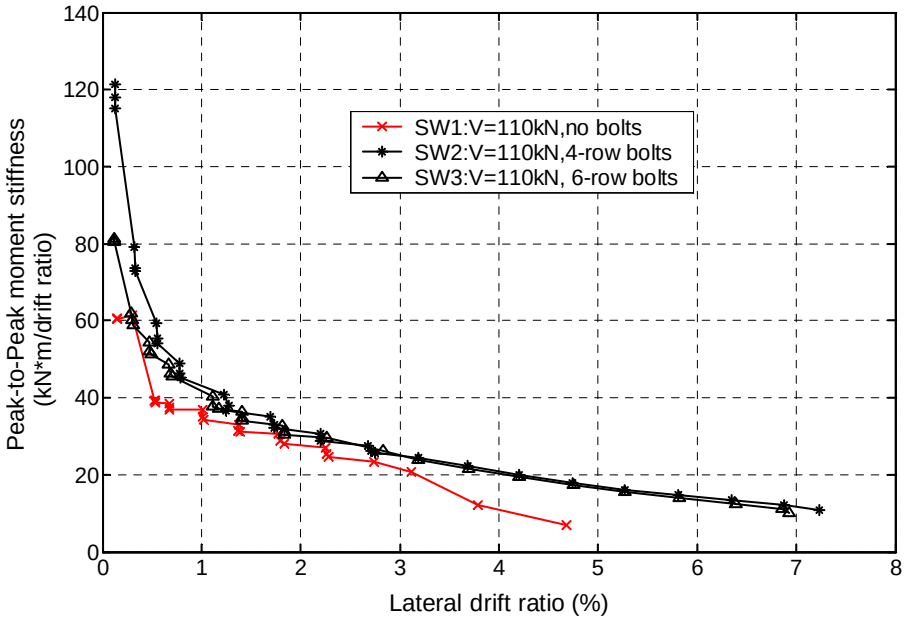

Figure 4.7 Peak-to-peak moment stiffness vs. drift ratio of SW1, SW2 and SW3 (Group I)

Shear bolts had some effect in increasing the connection stiffness, but this effect was not significant, as shown in Figure 4.7 and Figure 4.8. Shear bolts had an effect on the specimen's stiffness at large lateral deformations. Specimen SW1 and SW5, without shear bolts, both showed rapid stiffness decrease at the drift ratio of about 3.0%. At this drift ratio, the specimens failed by punching. However, specimens SW2, SW3, SW4, strengthened with shear bolts, could undergo far more

deformation without abruptly losing stiffness. Shear bolts had little or no effect on stiffness of the deteriorated connections at small deformations (Figure 4.9).

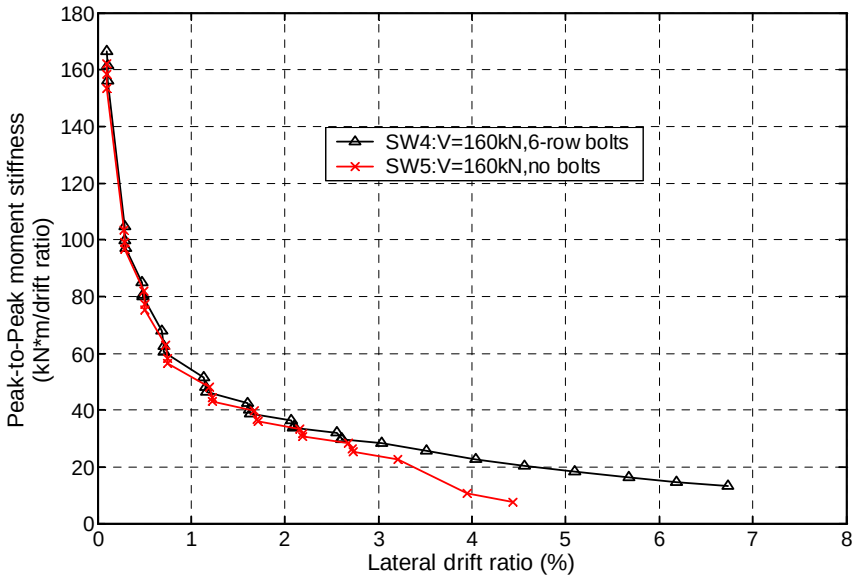

Figure 4.8 Peak-to-peak moment stiffness vs. drift ratio of SW4 and SW5 (Group II)

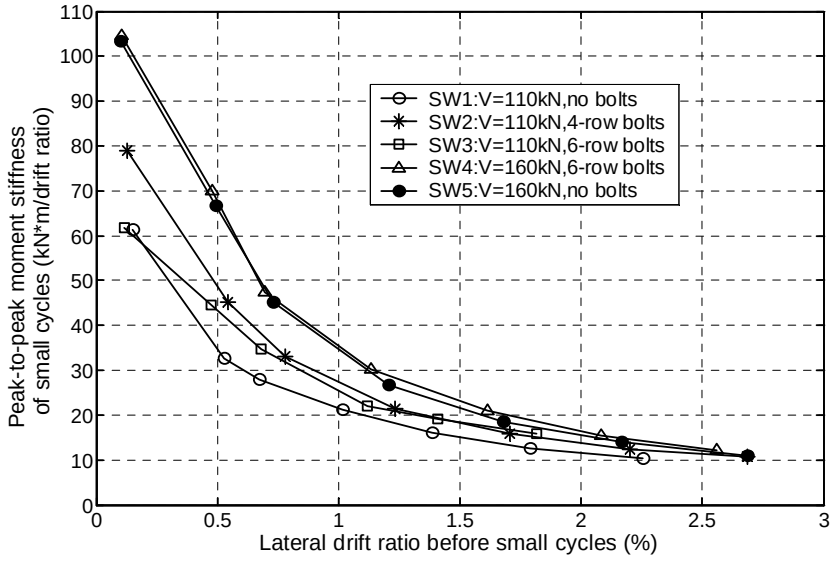

Figure 4.9 Stiffness degradation at small cycles of the five specimens SW1~SW5

4.2.4 Drift Ductility

Ductility is defined by a ratio of $\mu_{\%} = \frac{\delta_{\%}}{\delta_Y}$ where δ_y is the displacement corresponding to flexural yielding of the slab and $\delta_{\%}$ is the displacement corresponding to a certain load (% of the maximum load in the post-peak region). Two methods are used in this thesis to calculate drift ductility of the reinforced concrete slab-column specimens. The difference between the two methods is in the definition of the yield drift ratio.

(1) Method I (Pan and Moehle, 1989)

The method proposed by Pan and Moehle (1989) was adopted to define the drift ductility. It defines points corresponding to $\frac{2}{3}P_{\max}$ and $P_{\max}$ in the backbone curve as shown in Figure 4.10. A line between the origin, the point of $\frac{2}{3}P_{\max}$, and crossing the horizontal line corresponding to $P_{\max}$ defines the assumed yield drift ratio δ_y (or yield displacement). Then ductility at point of peak load and point corresponding to 80% of peak load at decreasing side are calculated as $\mu_{peak} = \frac{\delta_{peak}}{\delta_{yield}}$ and $\mu_{0.8} = \frac{\delta_{0.8}}{\delta_{yield}}$. Similarly, ductility at point corresponding to 95% of peak load at decreasing side is also calculated as $\mu_{0.95} = \frac{\delta_{0.95}}{\delta_{yield}}$.

In Series I of this test program, due to maximum displacement of the roller system, only SW1 and SW5 reached $\delta_{0.8}$. The peak lateral load and ductility at peak load on positive and negative sides of loading cycles were calculated and are shown in Table 4.1. The slabs strengthened with shear bolts reached higher ductility at peak loads. For specimen in Group 1, the ductility at positive peak load of specimen SW1 (without shear bolts) is $\delta^+_{peak} = 1.78$, while SW2 (4-row bolts) reached its δ^+_{peak} of 2.36 (increase of 33%), and SW3 (6-row bolts) reached its δ^+_{peak} of 2.25 (increase of 26%). Similarly, for specimens in Group 2, the ductility at positive peak load of specimen SW5 (without shear bolts) is

$\delta^{+}_{peak} = 1.81$, while SW4 (6-row bolts) reached its δ^{+}_{peak} of 2.31 (increased 27.6%). Drift ductility at peak negative load also showed similar results.

For post peak load ductility $\mu_{0.95}$, comparing to specimen SW1, specimen SW2 and SW3 obtained increase of 36.2% and 84.4% respectively in negative drift direction. In Group II, specimen SW4 obtained 30% increase compared with specimen SW5.

(2) Method II

In this method, the yield drift ratio δ_{yield} is taken from experimental observations as the drift ratio when the flexural rebar first reach yielding. Table 4.2 gives the tested first yield drift ratios of specimens SW1~SW5 and the ductilities defined by Method II. It is found that concrete slabs strengthened with shear bolts attained first flexural rebar yielding earlier than those without shear bolts. The drift ductilities of the specimens with bolts are much larger than those of specimens without bolts. In Group I, specimen SW2 and SW3 achieved 217% and 215% increase in μ^{-}_{peak} respectively comparing with SW1; in Group II, specimen SW4 obtained 78% increase in μ^{-}_{peak} and 141% increase in μ^{+}_{peak} comparing with SW5. As for increase in post peak drift ductility, specimen SW2 and SW3 achieved 188% and 258% increase in $\mu^{-}_{0.95}$, respectively comparing with SW1; specimen SW4 obtained 109% increase in $\mu^{-}_{0.95}$ comparing with SW5. From the trend of backbone curves in Figure 4.3, it can be inferred that increase in $\mu_{0.8}$ would be even larger if it could be reached in the tests.

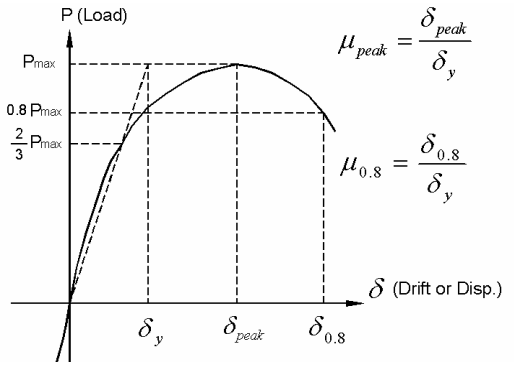

Figure 4.10 Definition of ductility

4.2.5 Strains in Shear Bolts

Strain data were measured for shear bolts, in both lateral loading direction (direction 1) and in transverse direction (direction 2). Shear bolts with strain gauges were numbered as shown in Figure 3.28. An example of the lateral drift ratio versus strain in Bolt #1 of SW2 is shown in Figure 4.11. The backbone (envelope) curves of lateral drift ratio versus bolt strains are shown in Figure 4.12.

Generally, in direction 1, the first two bolts (bolt #1 and bolt #2) close to the column experienced significant strains. The third one (bolt #3) had small strain and the fourth bolt (bolts #4) remained non-active throughout the whole loading history. Bolt #1 and Bolt #2 were activated apparently only after the drift reached at least 1%. This drift corresponds to lateral load of 35~40 kN, which is 50~55% of the maximum lateral load attained by the specimen. In direction 1, only bolt #1 in SW3 yielded.

Bolts in direction 2 experienced larger strains, at the same drift ratios, than their counterparts in direction 1. Strains in bolt # 1a of SW3 and SW4 reached 2.44×10^{-3} and 1.95×10^{-3} respectively, exceeding bolt yield strain ($\varepsilon_y = 1.9\times10^{-3}$). Strain in bolt # 1a of SW2 reached 1.72×10^{-3} which is close to yield strain.

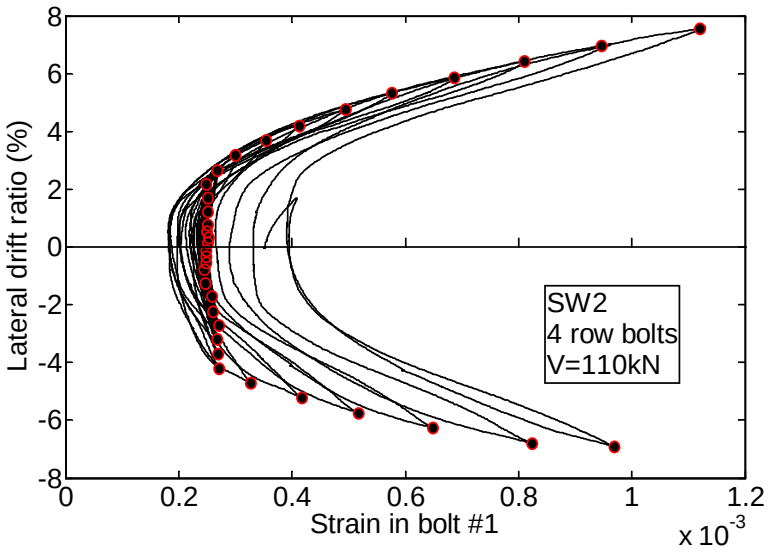

Figure 4.11 Lateral drift ratio versus strain in bolt #1 for specimen SW2

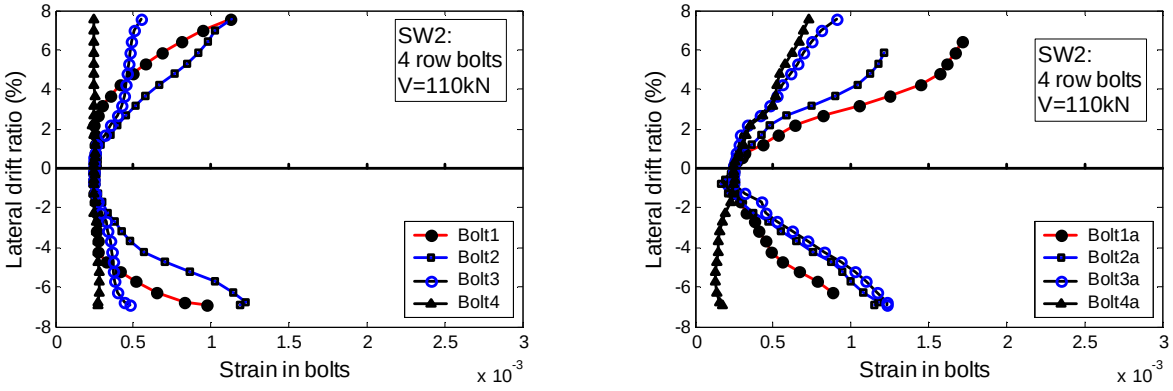

(a)

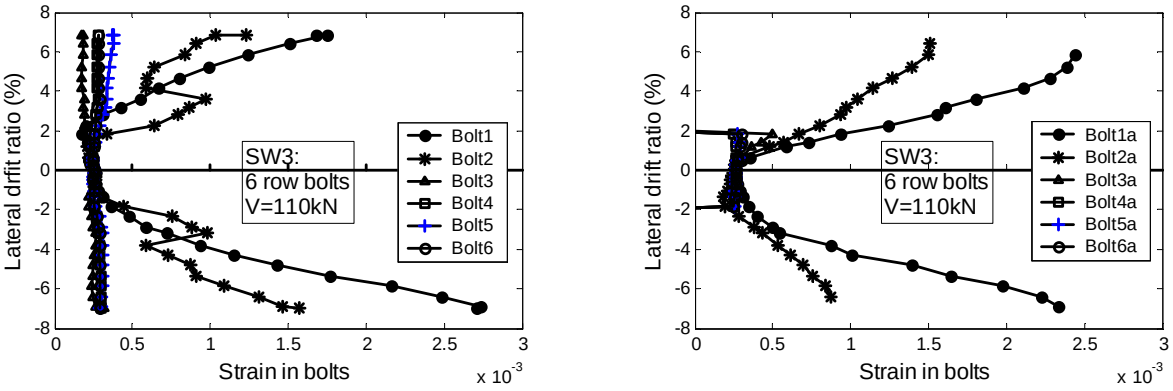

(b)

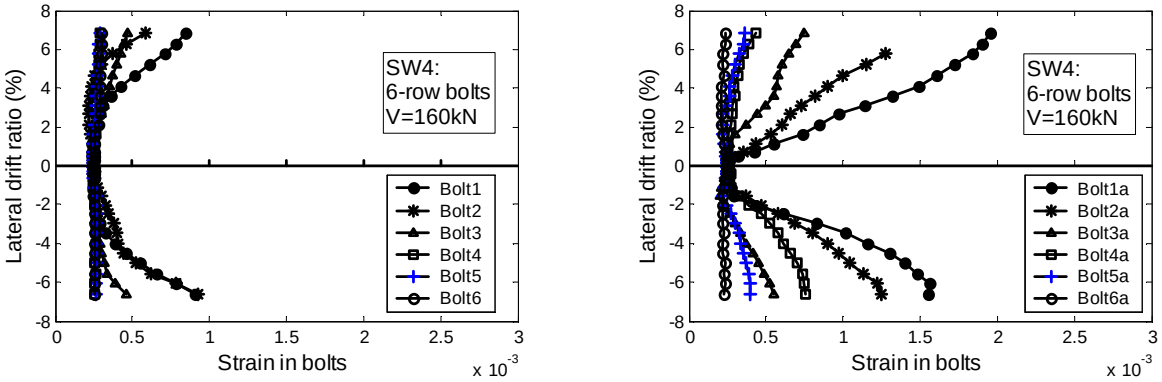

(c)

Figure 4.12 Lateral drift ratio versus strain in each bolt of the three specimens SW2, SW3, and SW4

(a) Specimen SW2; (b) Specimen SW3; (c) Specimen SW4

4.2.6 Flexural Reinforcement Strains

A total of 16 strain gages were attached to reinforcing bars and embedded in the concrete slab. The layout of strain gauges in the reinforcements is shown in Figure 4.13.

Figure 4.14 ~ Figure 4.18 shows lateral drift ratio versus strains at location "d" in rebar #1 in specimen SW1 to SW5, respectively. Rebar #1 passed through the column in specimens SW1 to SW3. Location "d" was 21 mm away from the column edge. In Figure 4.14 to Figure 4.18, the curves on the left side are the lateral drift ratio versus strain throughout the wholes testing process. The graphs on the right side provide extracted response before first rebar yielding. The yield strains were determined using the yield strength of the rebar and the elastic modulus of steel bar ($E_s = 200GPa$). The yield strain of the first batch of rebars (in SW1-SW5, and SW7) was 2.335×10^{-3}; the yield strain of the second batch of rebar (in SW6, SW8, and SW9) was 2.385×10^{-3}. Figure 4.19(a), (b) show the backbones curves together for the five specimens SW1~SW5 (Series I).

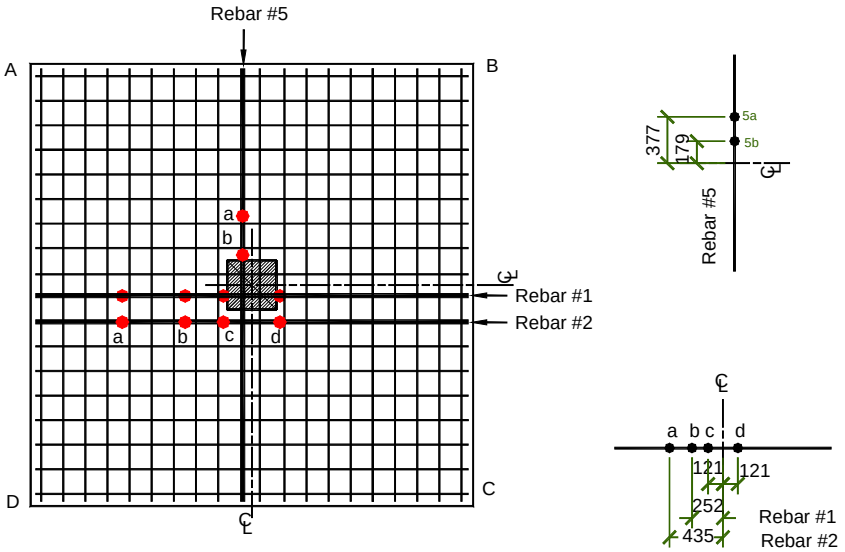

(a)

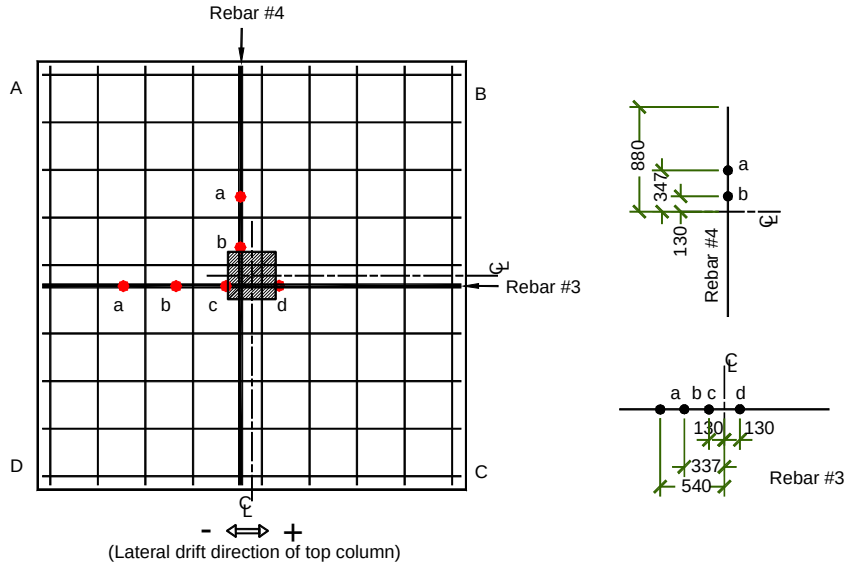

(b)

Figure 4.13 Stain gauge positions on the reinforcement of specimens SW1 ~ SW5 and SW9

(a) Strain gauge locations on bottom reinforcement mat (in test); (b) Strain gauge locations on bottom reinforcement mat (in test)

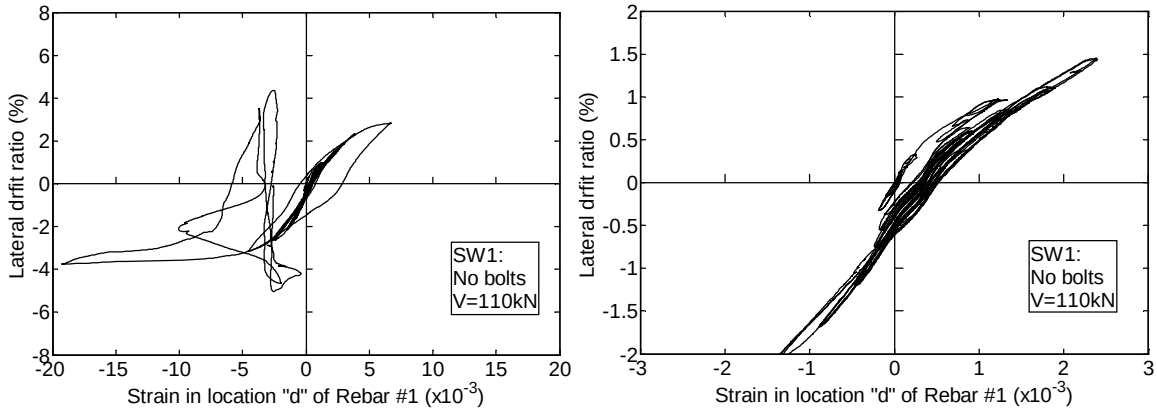

(a) (b)

Figure 4.14 Lateral drift ratio versus strain at location “d” of Rebar #1 in specimen SW1

(a) Response during full testing sequence; (b) Response until first yielding

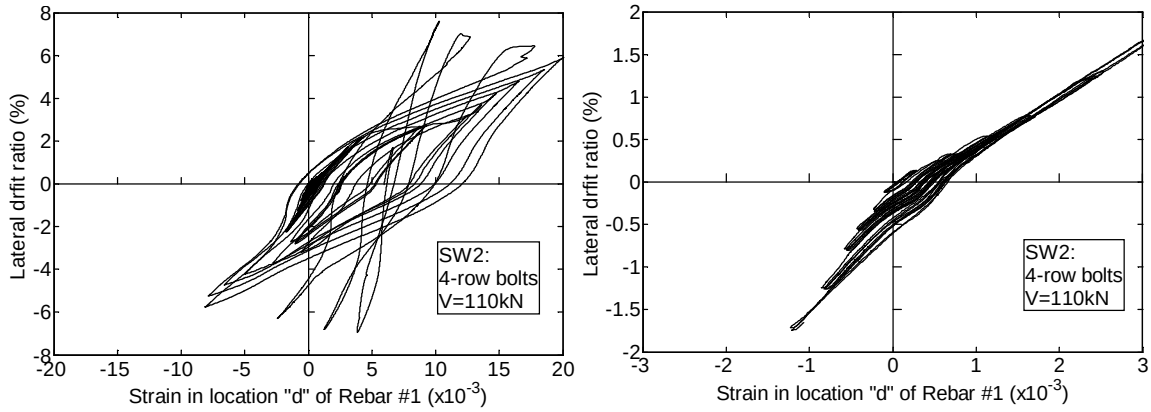

(a) (b)

Figure 4.15 Lateral drift ratio versus strain at location “d” of Rebar #1 in specimen SW2

(a) Response during full testing sequence; (b) Response until first yielding

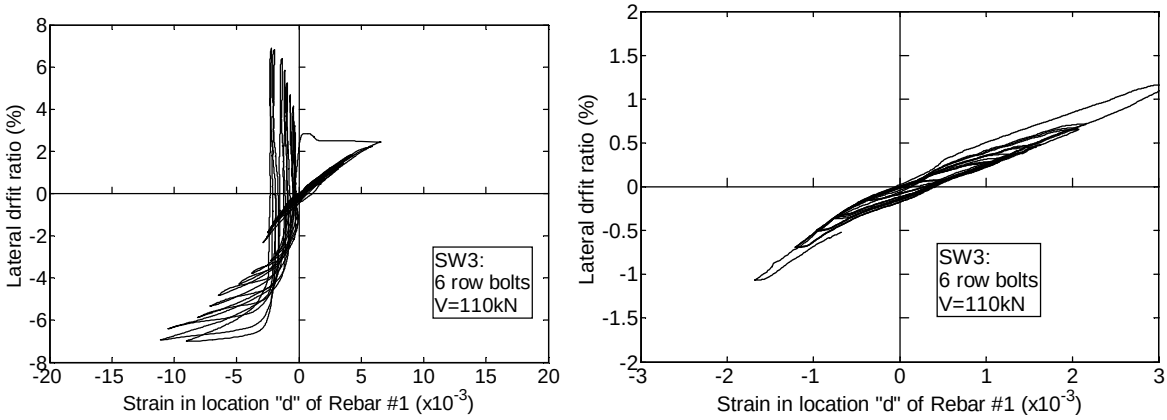

(a) (b)

Figure 4.16 Lateral drift ratio versus strain at location “d” of Rebar #1 in specimen SW3

(a) Response during full testing sequence; (b) Response until first yielding

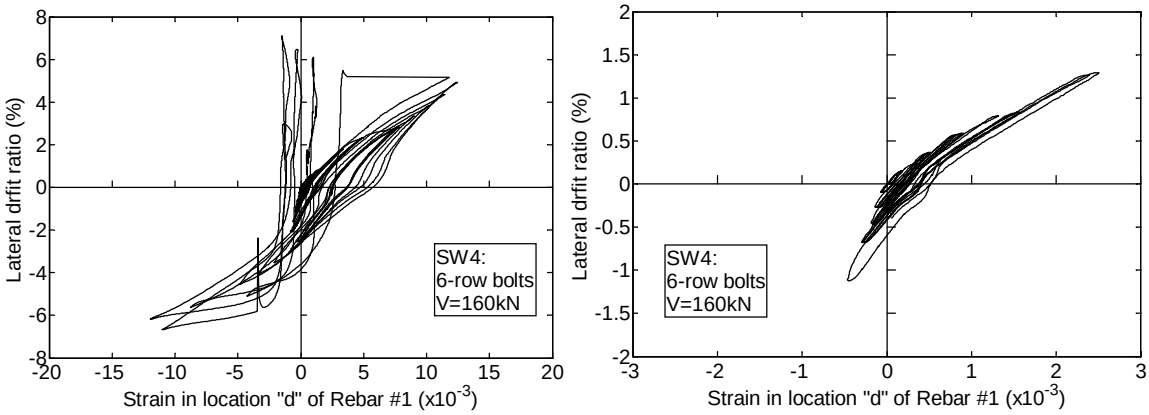

(a) (b)

Figure 4.17 Lateral drift ratio versus strain at location “d” of Rebar #1 in specimen SW4

(a) Response during full testing sequence; (b) Response until first yielding

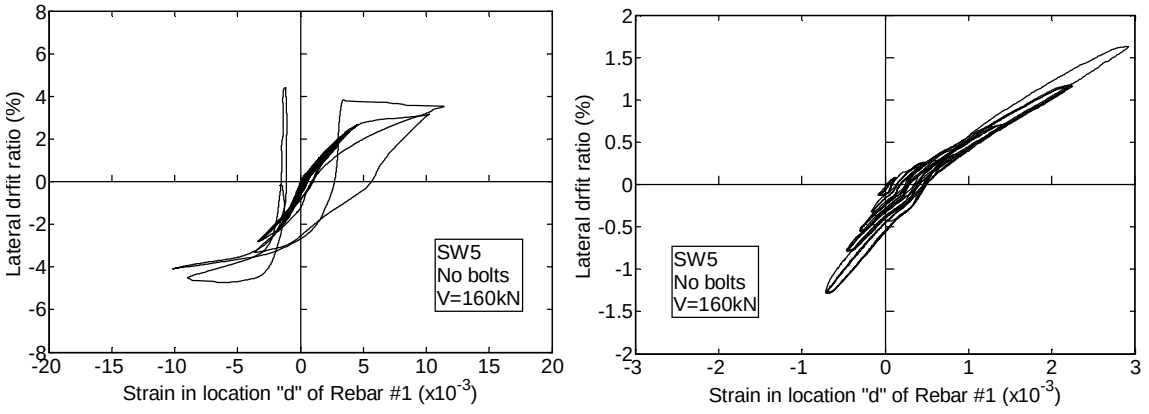

(a) (b)

Figure 4.18 Lateral drift ratio versus steel strain at location “d” of Rebar #1 in each specimen of SW5

(a) Response during full testing sequence; (b) Response until first yielding

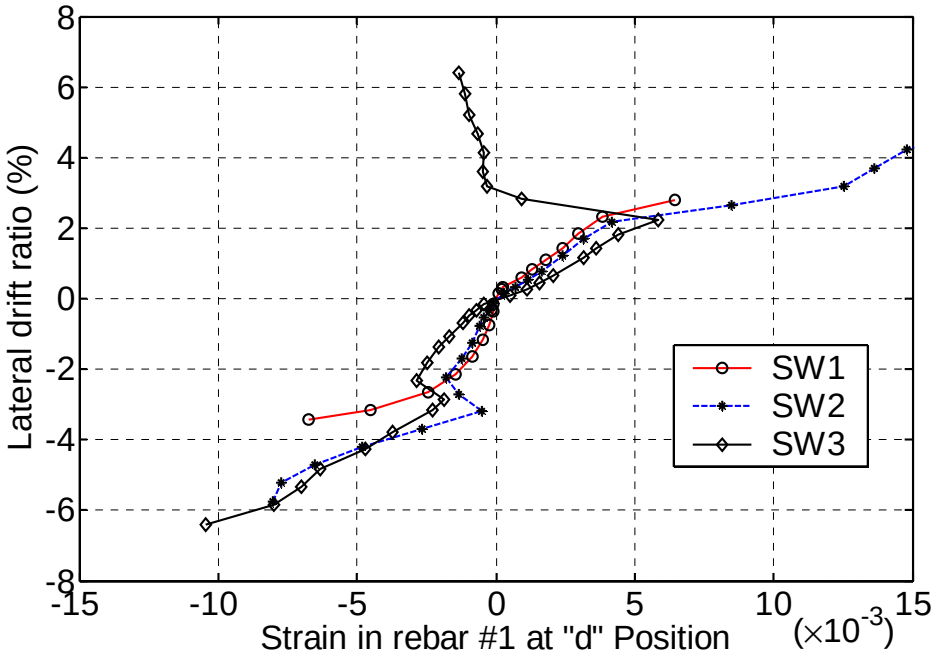

(a)

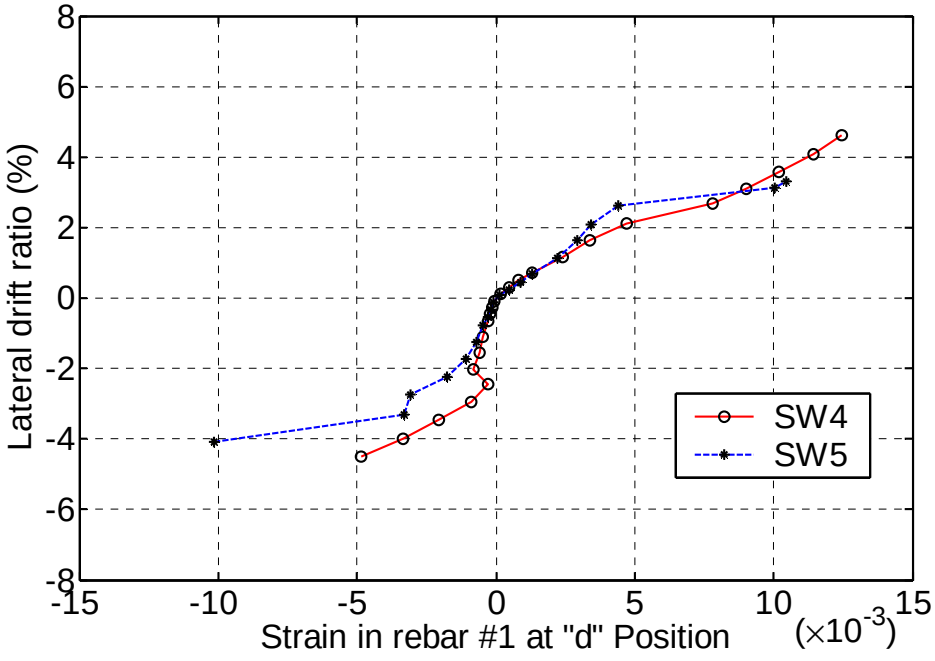

(b)

Figure 4.19 Backbone curves of lateral drift ratio versus steel strain at location “d” of Rebar #1

(a) Group 1: SW1, SW2, and SW3; (b) Group 2: SW4 and SW5

An example of strain variations along the flexural steel bars is shown in Figure 4.20, which shows strains at different locations of different bars at drift ratio -1.2% for all five specimens. The bar numbers are shown in Figure 4.13. The drift ratios and locations at first yielding in the numbered steel bars, for all five specimens, are summarized in Table 4.3 (the positive and negative sign refer to the direction of loading). In the five specimens SW1~SW5, the bottom bar (#1) and the top bar (#3) going through the column in direction 1, yielded first. In specimen SW1 (without bolts), bar #1 yielded at approximately drift ratio +1.33%, and bar #3 yielded at approximately drift ratio -1.54%. However, bar #3 in specimen SW2 (with 4-row bolts) reached first yielding at -0.97% drift ratio; bar #1 in SW3 (with 6-row bolts) reached first yield at -0.7% drift ratio. This suggests that the flexural rebar in concrete slabs with bolts will sustain more loads and deform more than those in slabs without bolts.

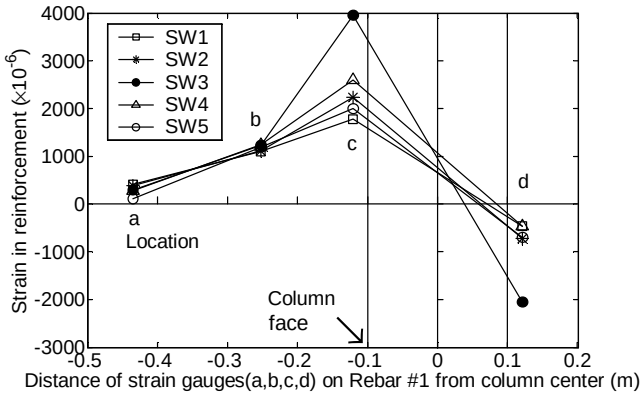

(a)

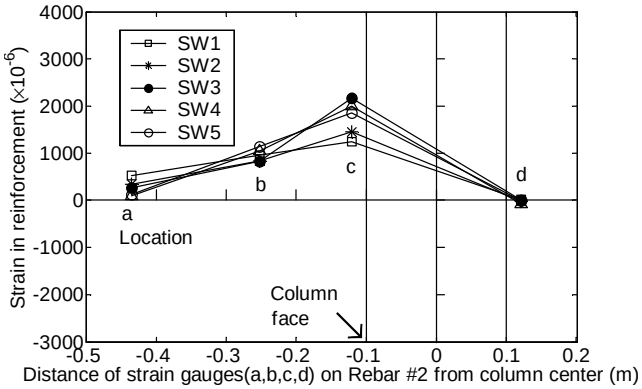

(b)

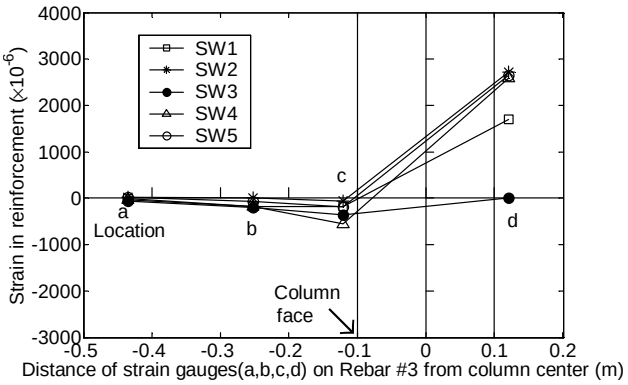

(c)

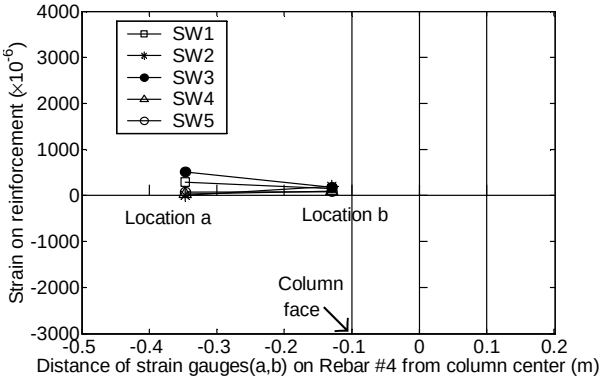

(d)

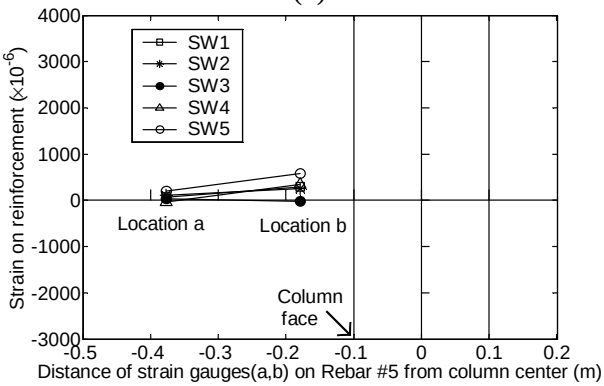

(e)

Figure 4.20 Strains in different locations of each numbered rebar in specimen SW1~SW5 at -1.2% lateral drift ratio

(a) Location “a”, “b”, “c” and “d” of rebar #1; (b) Location “a”, “b”, “c” and “d” of rebar #2; (c) Location “a”, “b”, “c” and “d” of rebar #3; (d) Location “a” and “b” of rebar #4; (e) Location “a” and “b” of rebar #5

Table 4.3 Drift ratios at first yielding of reinforcing bars in the five specimens SW1~SW5

Slab Name	Drift ratio at first yielding				
	Bar #1	Bar #2	Bar #3	Bar #4	Bar #5
SW1	+1.33% at “d”	+1.84% at “d”	-1.54% at “d”	(No yielding)	-3.6% at “b”
SW2	-1.11% at “c”	+1.59% at “d”	-0.91% at “d”	+4.56% at “a”	(No yielding)
SW3	-0.68% at “c”	-1.4% at “c”	+1.73% at “b”	+3.77% at “b”	+4.47% at “a”
SW4	+1.18% at “d”	+1.52% at “d”	-0.96% at “d”	+5.52% at “b”	-6.62% at “b”
SW5	+1.19% at “d”	+1.46% at “d”	+1.04% at “c”	(No yielding)	+3.7% at “b”

Notes: Positive and negative signs correspond to loading directions

Locations of strain gauges are shown in Figure 4.13

Based on the presented results, it is visible that before punching failure of slabs without bolts, shear bolts do not influence the strains in flexural reinforcements. This is consistent with the results related to connection stiffness, which also did not depend on the presence of shear reinforcing elements.

4.2.7 Vertical Crack Width

As shown in Figure 3.47, in locations “L1”, “L2”, “L3”, and “L4”, the displacement transducers (LVDTs) were set on both top and bottom surfaces. The displacement difference was used as an estimation of opening width (vertical) of inclined crack through slab thickness. Figures 4.21 through Figure 4.25 show all the crack widths in position “L1, L2, L3, L4” of each slab under cyclic horizontal loading. It can be observed that for specimen SW1 and SW5 (no bolts), there was an abrupt crack width increase at lateral drift +3.0%. The two specimens had reached their peak load just before. The specimens SW2, SW3 and SW4, strengthened with shear bolts, lasted many more cycles without sudden crack expansion. The crack width in location “L1” at 1.5%, 2.0%, and 3.0% drifts are summarized in Table 4.4.

Table 4.4 Crack width at 1.5%, 2.0% and 3.0% drift ratio for specimen SW1~SW5

Slab name	Crack width (mm)		
	at +1.5% drift ratio	at +2.0% drift ratio	at +3.0% drift ratio
SW1	0.18 (at -1.5% drift ratio)	0.32 (at -2.0% drift ratio)	0.70 (at -3.0% drift ratio)
SW2	0.21	0.33	0.74
SW3	0.26	0.44	0.71
SW4	0.11	0.26	0.58
SW5	0.13	0.29	1.26

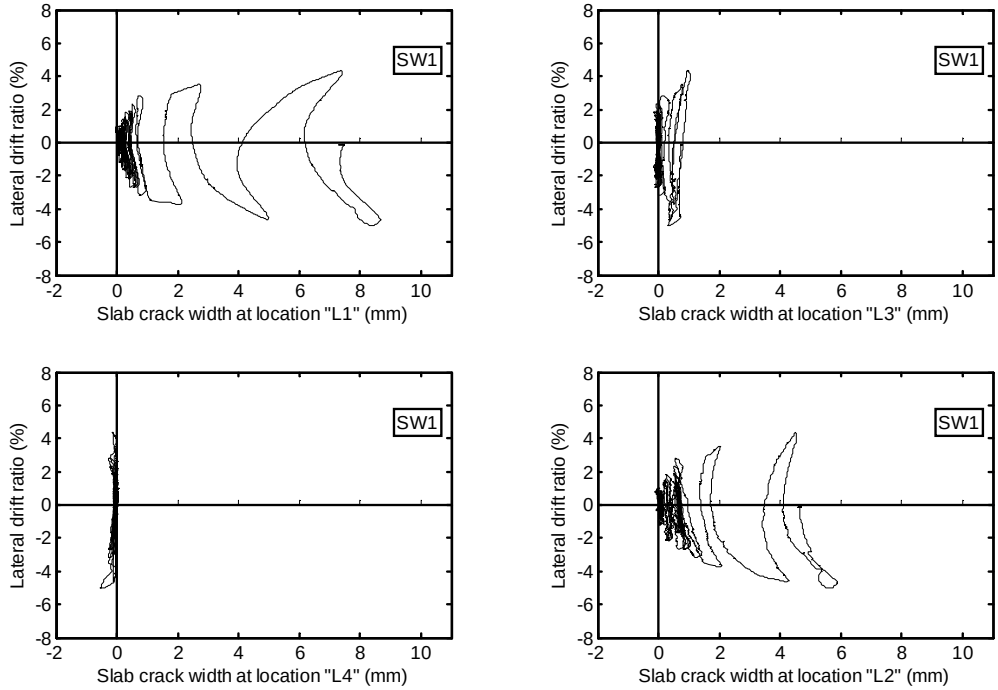

Figure 4.21 Crack width at locations “L1”, “L2”, “L3”, and “L4” in the slab of SW1

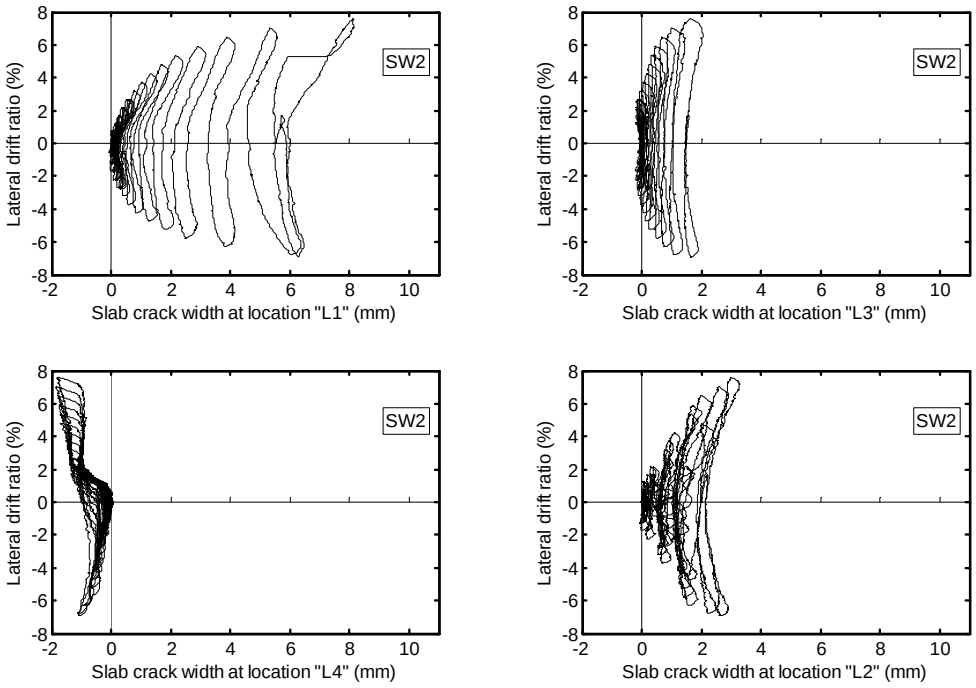

Figure 4.22 Crack width at locations “L1”, “L2”, “L3”, and “L4” in the slab of SW2

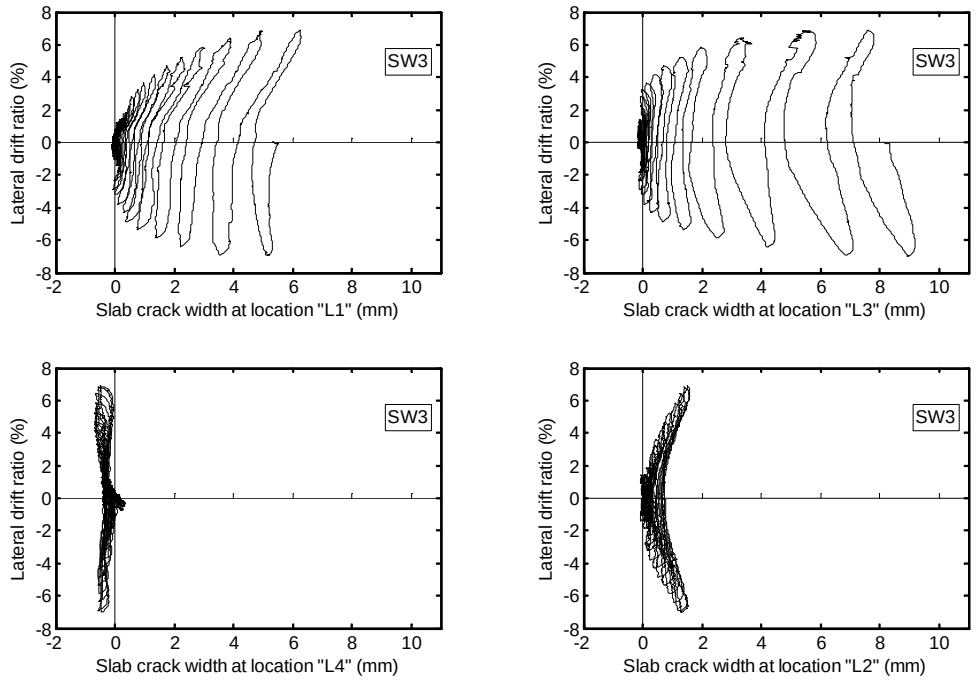

Figure 4.23 Crack width at locations “L1”, “L2”, “L3”, and “L4” in the slab of SW3

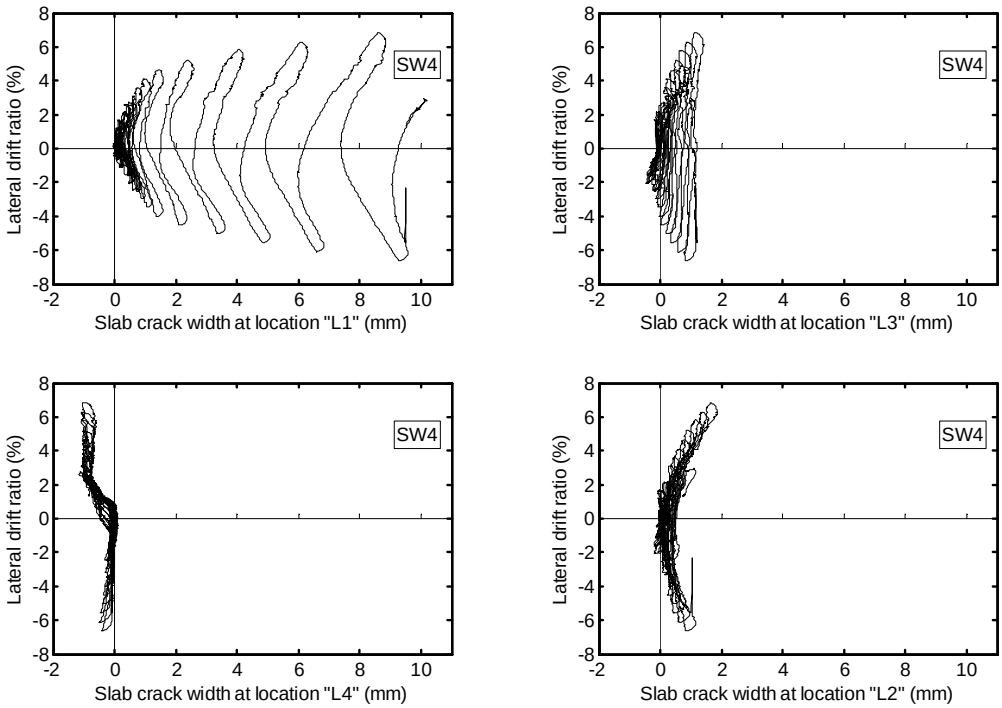

Figure 4.24 Crack width at locations “L1”, “L2”, “L3”, and “L4” in the slab of SW4

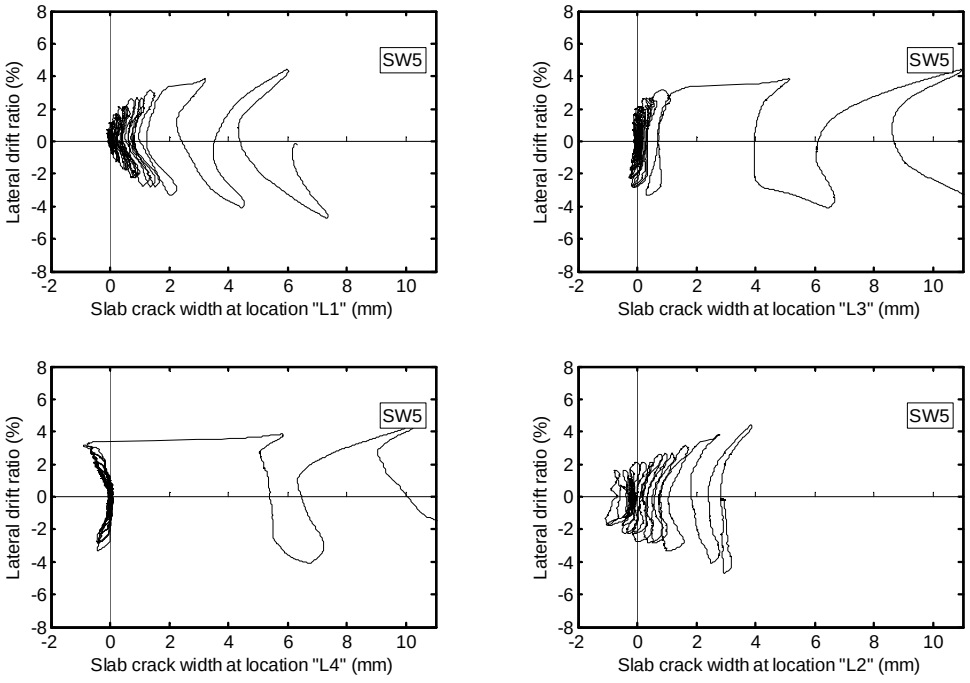

Figure 4.25 Crack width at locations “L1”, “L2”, “L3”, and “L4” in the slab of SW5

Crack measurements show that, before punching, all slabs experienced similar initial cracks (Table 4.4). The cracks increased rapidly after punching of the specimens without bolts. The largest cracks were experienced at location “L1”.

4.2.8 Cracking and Failure Modes of the Specimens

Cracks on slab surfaces started from corners of the column on the tension side, first on the bottom slab surface (which was subjected to tension from gravity load) and then on top surface. First crack on top of the slab was usually observed at about 0.6~0.75% drift ratio. On bottom surfaces, cracks first propagated toward the four slab edges and corners, while on slab top surface, initial cracks developed from column corner to the direction perpendicular to the lateral loading direction. The final crack patterns of top and bottom slab surfaces for all five specimens are shown in Figure 4.26. Column inclined crack were first observed at about 4.0~4.5% drift ratios for slabs with shear bolts. For the specimens SW1 and SW5 (without bolts), there were no inclined crack observed in column (the slabs failed at small drifts). From the crack pattern and the hysteresis curves, it can be found that SW1 and SW5 failed by punching shear mode; the other three slabs (SW2, SW3 and SW4) were subjected to flexural failure mode. The three slabs attained the peak lateral load during testing, which decreased only slightly (by 10%) in the post peak behaviour.

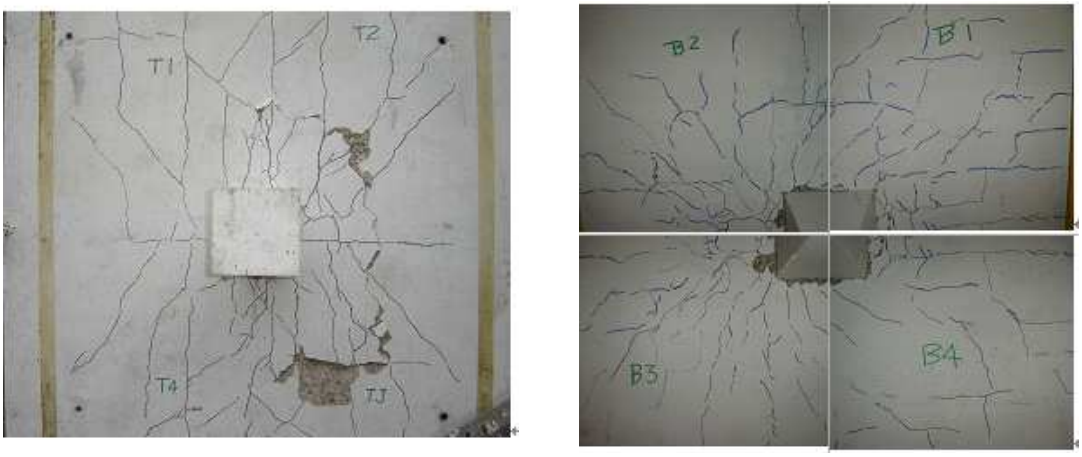

SW1 top surface SW1 bottom surface

(a)

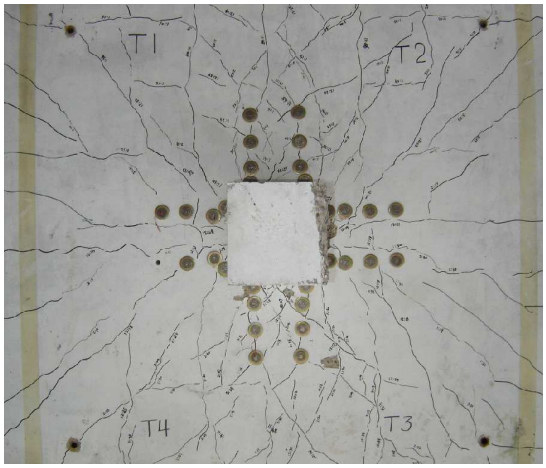

SW2 top surface

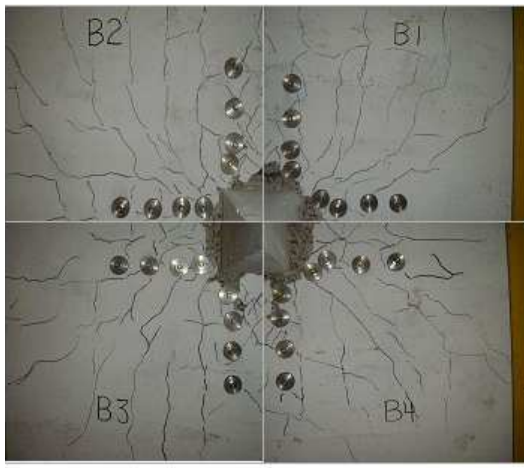

SW2 bottom surface

(b)

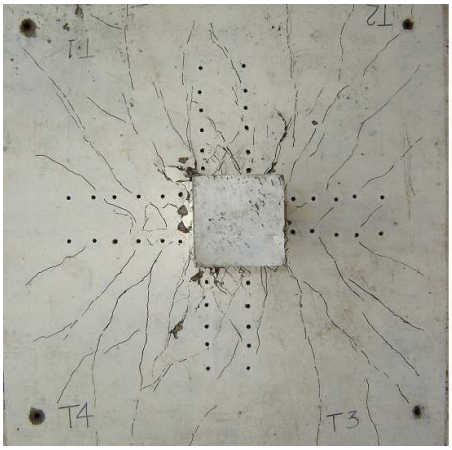

SW3 top surface

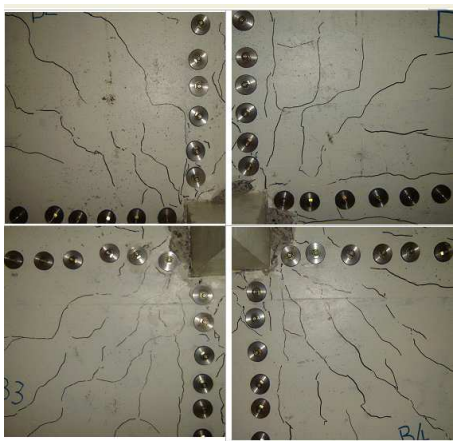

SW3 bottom surface

(c)

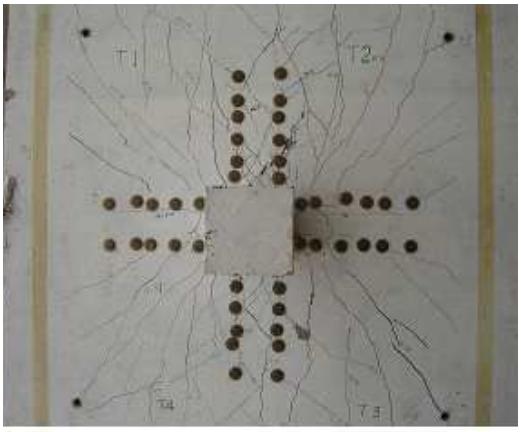

SW4 top surface

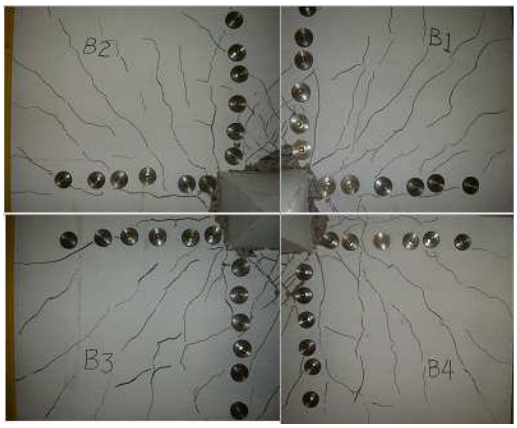

SW4 bottom surface

(d)

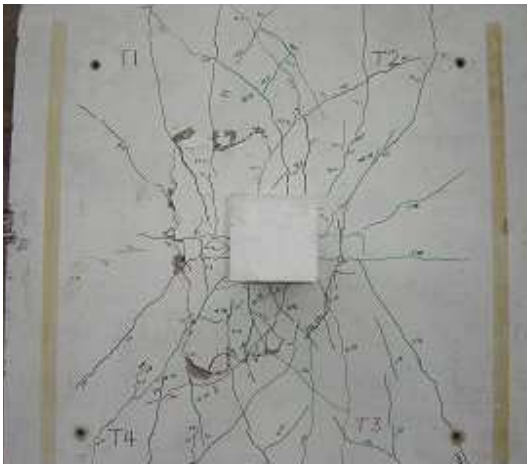

SW5 top surface

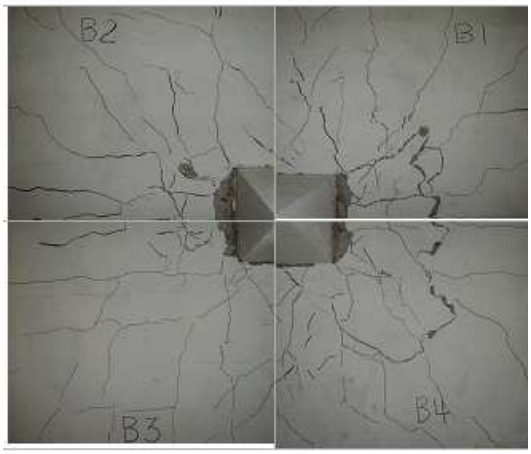

SW5 bottom surface

(e)

Figure 4.26 Final crack pattern on top and bottom surface of each specimen

(a) SW1, (b) SW2, (c) SW3, (d) SW4, and (e) SW5

4.3 Results of Series II

This section introduces the test results of Series II which includes specimens SW6 ~ SW9. Specimens SW6, SW7, and SW8 had openings next to the column. Specimen SW6 had no shear reinforcements.

Specimen SW7 had an orthogonal pattern of six peripheral rows of bolts. Specimens SW8 and SW9 had a radial layout of steel shear bolts (6-row). Whenever appropriate, comparisons are made with specimens from Series I. In Series I, three specimens had orthogonal pattern of shear bolts: specimen SW2 had 4-row shear bolts; specimen SW3 and SW4 had 6-row shear bolts.

4.3.1 Connection Moment versus Lateral Drift Ratio

Connection moment is calculated from the moments of the top and bottom lateral forces multiplied by the distance between them. The distance between the two horizontal hydraulic actuators was 1.25m. The lateral drift ratio was calculated from the lateral displacement measured by the external string pot divided by the distance between slab-column center and the string pot. Since top and bottom lateral drift ratios are slightly different, the average drift ratio is used herein. Figures 4.27 (a) to (d) show the curves of moment versus lateral drift ratio for specimen SW6 to SW9 respectively.

In each curve, the peak points were marked and linked by a dashed line (backbone curve). The four backbone curves are plotted together in Figure 4.28, from which it is observed that, among the three specimens with the same openings, SW6 (no bolts) had the minimum moment capacity, 52.28 kNm, at negative peak point, while SW7 (orthogonal bolt pattern) reached 56.59 kNm (8.2% increase) and SW8 (radial bolt pattern) reached 63.58 kNm (21.6% increase). Corresponding drifts at the negative peak points are: -1.31% (SW6), -2.88% (SW7, 120% increase) and -2.77% (SW8, 111.5% increase)

Table 4.5 shows the moments at negative and positive peak points, the yield drift ratio, and drift ductility at peak points and 80% of peak moment in post peak region. As expected, the specimen SW9, without openings but strengthened with radial pattern of shear bolts, showed highest moment capacity and ductility. Compared with specimen SW8 (with two openings and also strengthened with radial pattern of shear bolts), SW9's moment capacity was 76-80% larger; its lateral drift ratio at peak moment was 145-211% larger; drift ductility at 80% peak load (post peak) increased by 44-55%.

Table 4.5 Peak moment and drift ductility (defined by Pan and Moehle, 1989) of specimen SW6~SW9

Slab name	$\frac{V}{V_0}$	Peak moment (kN*m)		Peak lateral drift ratio at peak moment (%)		Yield drift ratio (%)		Drift ductility at peak moment μ_{peak}		Drift ductility at 95% post peak moment $\mu_{0.95}$		Drift ductility at 80% post peak moment $\mu_{0.8}$	
		-	+	-	+	-	+	-	+	-	+	-	+
SW6	0.74	-52.28	54.38	-1.31	1.71	-0.82	0.80	1.60	2.16	2.04	2.39	2.56	3.0
SW7	0.79	-56.59	58.52	-2.88	2.90	-1.05	1.14	2.75	2.56	3.05	3.17	4.0	4.03
SW8	0.74	-63.58	64.45	-2.77	2.74	-1.15	1.17	2.40	2.35	2.59	2.54	3.15	3.21
SW9	0.66	-92.23	97.70	-4.08	4.19	-1.71	1.68	2.38	2.50	2.98	3.30	3.98	4.31

Note: Nominal punching shear capacity of concrete $V_0 = 0.33\sqrt{f_c'}b_0 d$ (ACI 318-05, in metric units); the perimeter length b_0 of critical section of each specimen (SW6, SW7, and SW8) with openings excluded the opening effected length

Table 4.6 Drift ductility (using tested first yield rebar strain) of specimen SW6~SW9

Slab name	Tested first yield drift ratio (%)	Drift ductility at peak moment μ_{peak}		Drift ductility at 95% post peak moment $\mu_{0.95}$		Drift ductility at 80% post peak moment $\mu_{0.8}$	
		-	+	-	+	-	+
SW6	+1.07	1.23	1.61	1.56	1.79	1.96	2.24
SW7	+2.24	1.29	1.30	1.43	1.61	1.88	2.05
SW8	+2.85	0.97	0.96	1.05	1.04	1.27	1.32
SW9	1.01	4.03	4.16	5.05	5.49	6.74	7.17

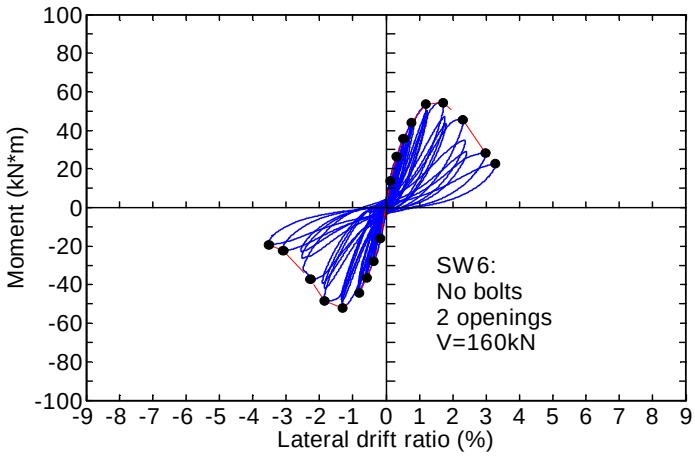
Moment (kN*m)
Lateral drift ratio (%)
SW6:
No bolts
2 openings
V=160kN

(a)

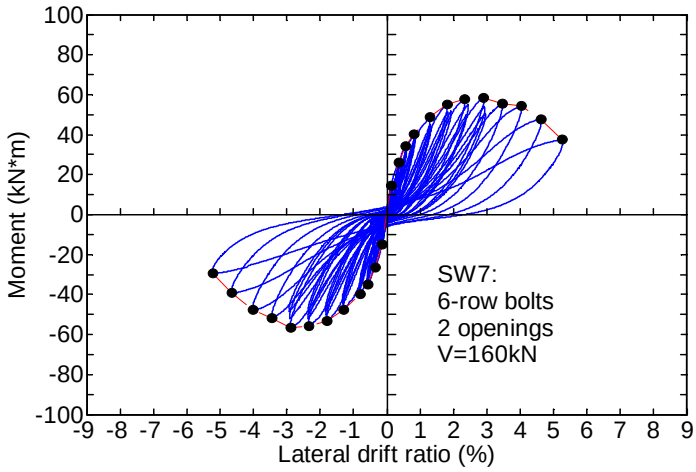
Moment (kN*m)
Lateral drift ratio (%)
SW7:
6-row bolts
2 openings
V=160kN

(b)

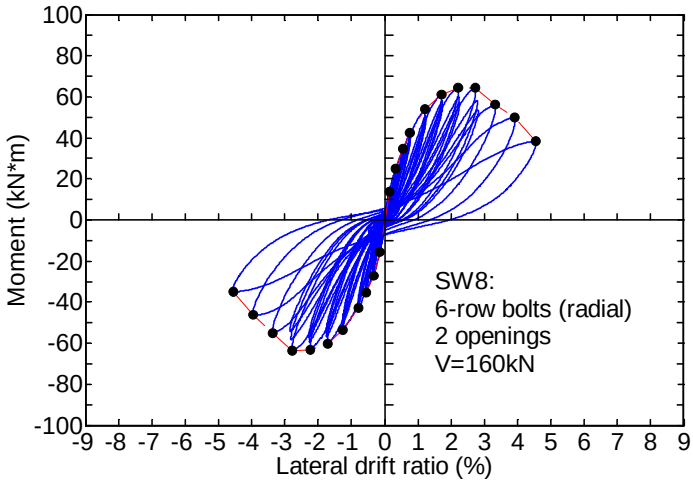

(c)

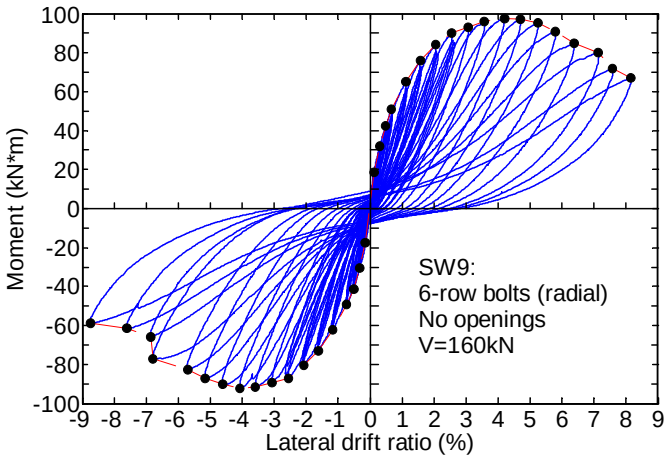

(d)

Figure 4.27 Moment versus lateral drift ratio of specimen SW6~SW9.

(a) Specimen SW6; (b) Specimen SW7; (c) Specimen SW8; (d) Specimen SW9

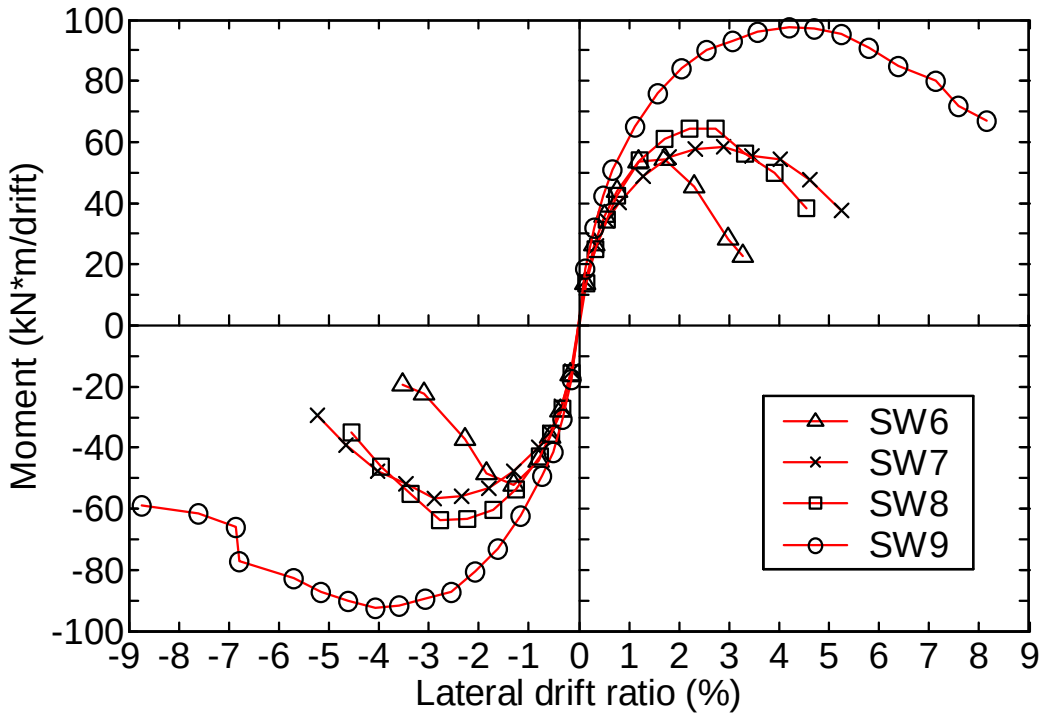

Figure 4.28 Backbone curves of moment versus lateral drift ratio for SW6~SW9.

4.3.2 Drift Ductility

Drift ductility is defined in section 4.2.4, by Method I (Pan and Moehle, 1989) and Method II (using tested first yield rebar strain). For Series II, the peak lateral moment and ductility (Method I) at peak points on positive and negative sides of loading cycles are calculated and shown in Tables 4.5. Ductilities defined by Method II are shown in Table 4.6**.** For the three slabs with openings, SW6, SW7, and SW8 in Table 4.5, it is observed that the slabs strengthened with steel bolts (SW7 and SW8) show higher ductility defined by Method I than specimen SW6 (no bolts). However, if the ductility is defined by Method II, given in Table 4.6, the strengthened slabs (SW7 and SW8) show even lower ductility than SW6; this is because the rebar strain recorded for SW6 is not very reasonable as shown in Figure 4.41. From Figure 4.28, it can be easily determined that specimens SW7 and SW8 obtained apparent higher drift ductilities than specimens SW6. In the following sections, ductilities are also compared between slabs with and without opening, with or without bolts, and with orthogonal bolt

layout or radial bolt layout. Generally, slab strengthened with shear bolts had higher ductility at peak loads and at failure.

4.3.3 Effect of Openings on Connection Moment Capacity and Ductility

To find the effect of openings on connection moment capacity and ductility, several comparisons are made as presented in this section. It should be noted that for specimens with openings, the reinforcement in direction 1 (along the lateral force application) was interrupted by the opening. There was no space in the slab to place additional bars along the sides of the opening. However, for direction 2 (normal to lateral loads) the same number of rebars that were cut by the openings weree placed beside the opening edges (Fig. 3.7):

(1) Specimen SW5 (no bolts, no openings) and SW6 (no bolts, two openings)

Their moment and drifts are shown in Figure 4.29 and Table 4.7. It is found that the two openings in SW6 result in peak moment decrease of 28% (-) or 30% (+) and lateral drift ratio at peak point decrease of 52% (-) or 37% (+). From Table 4.7, the ductility of SW5 and SW6, defined by method I (Pan and Moehle, 1989), showed no much difference. However, the ductility of specimen SW5 defined using tested first yield strain in rebar, is much larger than ductility of SW6 (Table 4.8). For example, $\mu_{0.8}{}^{+}$ is 3.48 for SW5 (no opening), and 2.24 for SW6 (with two openings).

(2) Specimen SW4 (6-row orthogonal bolts, no openings) and SW7 (6-row orthogonal bolts, two openings)

As shown in Figure 4.30 and Table 4.11**,** similar to case (1), the two openings lead to a decrease of 40% (-) or 37% (+) in peak moment, a decrease of 36% (-) or 49% (+) in lateral drift at peak. The drift ductility of SW4 and SW7 is close if they are defined by Method I (Pan and Moehle, 1989). However, in Table 4.12, their ductilities (defined using tested first yield drift ratio) are different. Specimen SW4 (no opening, 6-row orthogonal bolts) obtained $\mu_{0.95}^{+}$=7.14, and SW7 (two openings, orthogonal bolts) obtained $\mu_{0.95}^{+}$=1.61 only.

(3) Specimen SW8 (6-row radial bolts, two openings) and SW9 (6-row radial bolts, no openings)

As shown in Figure 4.31 and Table 4.9, compared with SW9, the peak moment of SW8 decreased 31% and 34%; lateral drift ratio at peak moment decreased 32% and 35%; drift ratio at yield

decreased 30% and 33%. Ductility (defined by method I) at 0.8 Peak load decreased 21% and 26%, but from Table 4.10, the ductility (method II) of SW9 reached 7.17 at $\mu_{0.8}^{+}$, while SW8 only reached 1.32 at $\mu_{0.8}^{+}$.

Table 4.7 Comparison of peak moment and drift ductility between SW5 and SW6

Slab name	$\frac{V}{V_0}$	Peak moment (kN*m)		Peak lateral drift ratio at peak moment (%)		Yield drift ratio (%)		Drift ductility at peak moment μ_{peak}		Drift ductility at 95% peak moment $\mu_{0.95}$		Drift ductility at 80% peak moment $\mu_{0.80}$	
		-	+	-	+	-	+	-	+	-	+	-	+
SW5	0.68	-73.28	77.95	-2.75	2.70	-1.41	1.44	1.96	1.87	2.38	2.41	2.58	2.51
SW6	0.74	-52.28	54.38	-1.31	1.71	-0.82	0.80	1.60	2.16	2.04	2.39	2.56	3.0

Table 4.8 Comparison of drift ductility (using tested first yield drift ratio) between SW5 and SW6

Slab name	Tested first yield drift ratio (%)	Drift ductility at peak moment μ_{peak}		Drift ductility at 95% post peak moment $\mu_{0.95}$		Drift ductility at 80% post peak moment $\mu_{0.80}$	
		-	+	-	+	-	+
SW5	+1.04	2.63	2.51	3.16	3.05	3.39	3.48
SW6	+1.07	1.23	1.61	1.56	1.79	1.96	2.24

Table 4.9 Comparison of peak moment and drift ductility between SW7 and SW8 (effect of openings and shear bolts layout patterns)

Slab name	$\frac{V}{V_0}$	Peak moment (kN*m)		Peak lateral drift ratio at peak moment (%)		Yield drift ratio (%)		Drift ductility at peak moment μ_{peak}		Drift ductility at 95% post peak moment $\mu_{0.95}$		Drift ductility at 80% post peak moment $\mu_{0.8}$	
		-	+	-	+	-	+	-	+	-	+	-	+
SW9	0.66	-92.23	97.70	-4.08	4.19	-1.71	1.68	2.38	2.50	2.98	3.30	3. 98	4. 31
SW8	0.74	-63.58	64.45	-2.77	2.74	-1.15	1.17	2.40	2.35	2.59	2.54	3. 15	3. 21

Table 4.10 Comparison of drift ductility (using tested drift ratio) between SW8 and SW9

Slab name	Tested first yield drift ratio (%)	Drift ductility at peak moment μ_{peak}		Drift ductility at 95% post peak moment $\mu_{0.95}$		Drift ductility at 80% post peak moment $\mu_{0.80}$	
		-	+	-	+	-	+
SW9	1.01	4.03	4.16	5.05	5.49	6.74	7.17
SW8	+2.85	0.97	0.96	1.05	1.04	1.27	1.32

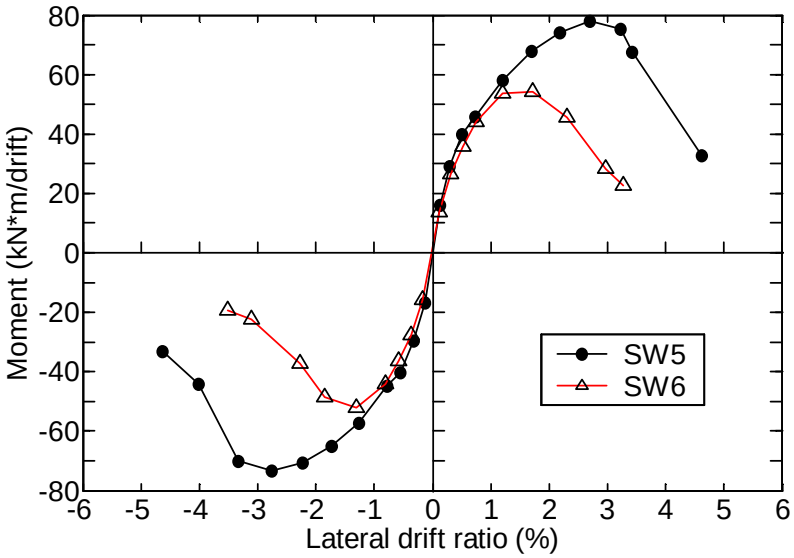

Figure 4.29 Backbone curves of moment versus lateral drift ratio between specimen SW5 and SW6

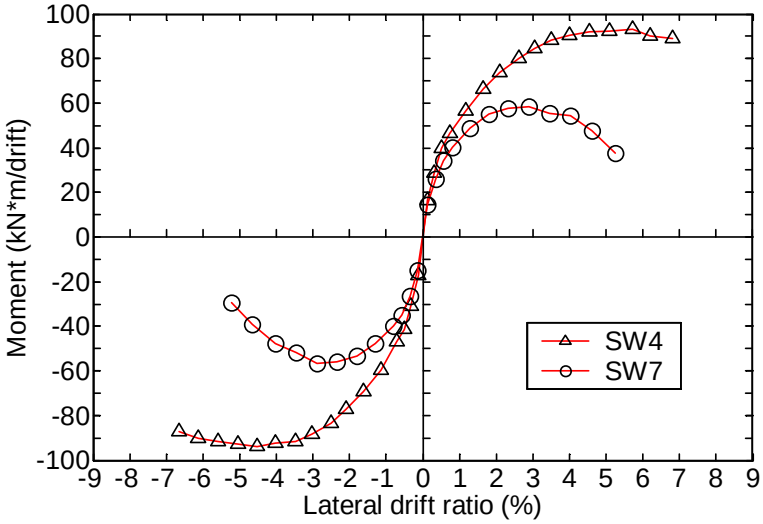

Figure 4.30 Backbone curves of moment versus lateral drift ratio between specimen SW4 and SW7

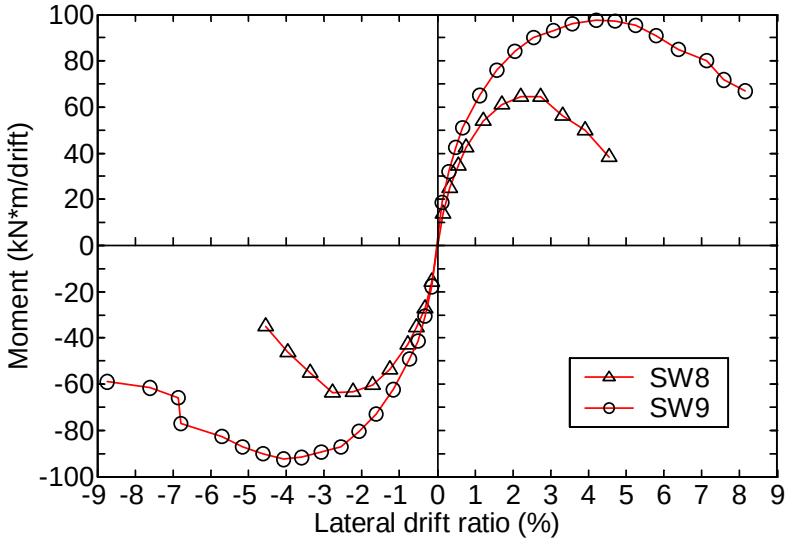

(c)

Figure 4.31 Comparison of backbone curves of moment versus lateral drift ratio between specimen SW8 and SW9

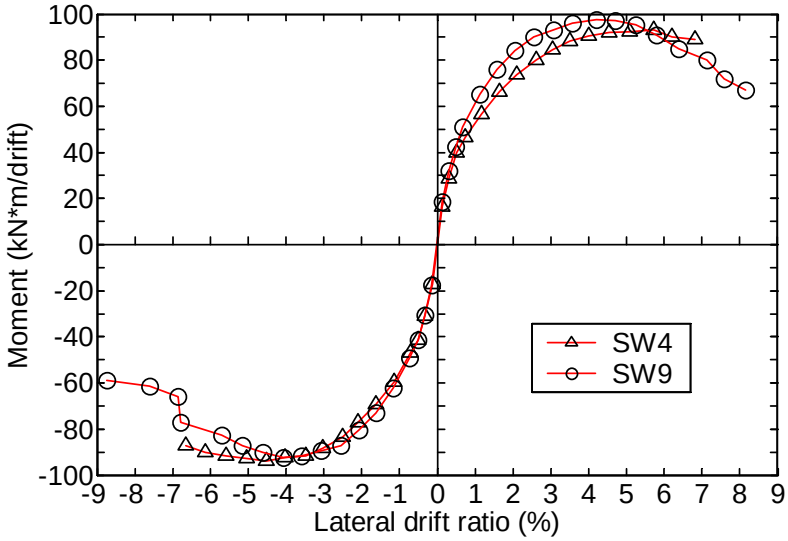

Figure 4.32 Backbone curves of moment versus lateral drift ratio for SW4 and SW9

Table 4.11 Comparison of peak moment and drift ductility between SW4 and SW7, SW4 and SW9 (effect of openings and shear bolts layout patterns)

Slab name	$\frac{V}{V_0}$	Peak moment (kN*m)		Peak lateral drift ratio at peak moment (%)		Yield drift ratio (%)		Drift ductility at peak moment μ_{peak}		Drift ductility at 95% peak moment $\mu_{0.95}$		Drift ductility at 80% peak moment $\mu_{0.80}$	
		-	+	-	+	-	+	-	+	-	+	-	+
SW4	0.68	-93.68	93.15	-4.52	5.72	-1.95	2.14	2.32	2.68	3.26	3.18		
SW7	0.79	-56.59	58.52	-2.88	2.90	-1.05	1.14	2.75	2.56	3.05	3.17	4.0	4.03
SW9	0.66	-92.23	97.70	-4.08	4.19	-1.71	1.68	2.38	2.50	2.98	3.30	3.98	4.31

Table 4.12 Comparison of drift ductility (using tested first yield drift ratio) in SW4, SW7, and SW9

Slab name	Tested first yield drift ratio (%)	Drift ductility at peak moment μ_{peak}		Drift ductility at 95% post peak moment $\mu_{0.95}$		Drift ductility at 80% post peak moment $\mu_{0.80}$	
		-	+	-	+	-	+
SW4	-0.96	4.68	6.06	6.60	7.14		
SW7	+2.24	1.29	1.30	1.43	1.61	1.88	2.05
SW9	1.01	4.03	4.16	5.05	5.49	6.74	7.17

4.3.4 Effect of Shear Bolt layout Pattern on Connection Moment Capacity and Ductility

Shear bolts were installed orthogonally in SW7 and SW4 and in radial pattern in SW8 and SW9. They are compared as follows:

(1) Specimen SW4 (6-row orthogonal bolts, no openings) and SW9 (6-row radial bolts, no openings)

From Figure 4.32 and Table 4.11, it is found that, compared with SW4, specimen SW9 had a 2% decrease in negative peak moment and 5% increase in positive peak point, a decrease of 10% and 27% in lateral drifts at peak points, a 3% increase in ductility (Pan and Moehle, 1989) at negative peak moment and a 6.7% ductility (method I) decrease at positive peak points. The overall behaviour of both specimens was almost identical. However, comparing ductilities defined by method II (using tested first yield rebar strain), specimen SW4 (orthogonal bolt pattern) has better ductile behaviour than specimen SW9 (radial bolt pattern). For example, from Table 4.12, $\mu^{+}_{0.95}$ is 7.14 for SW4 and 5.49 for SW9.

(2) Specimen SW7 (6-row orthogonal bolts, two openings) and SW8 (6-row radial bolts, two openings). From Figure 4.28 and Table 4.13, it is observed that SW8 had an increase of 10% and 12% in peak moments but 4% and 6% decrease in lateral drifts at peak points, 8% and 13% ductility (Method I, Pan and Moehle, 1989) decrease at peak points and 20% and 21% ductility (Method I) decrease at 0.8 peak load (post peak). Comparison of ductilities defined using Method II shows also specimen SW7 has better ductile behaviour. For example, in Table 4.14, $\mu^{+}_{0.80}$ is 2.05 for SW7 but only 1.32 for SW8 (36% less).

4.3.5 Connection Stiffness

Based on curves of moment versus drift ratio, peak-to-peak stiffness of each cycle was calculated for every specimen. Figure 4.33 shows the peak-peak stiffness versus lateral drift ratio of SW6, SW7 and SW8. Figure 4.34 shows the peak-peak stiffness of specimen SW5 and SW9. Stiffness at small drift cycles (0.5% drift) are displayed in Figure 4.35. In general, the connection stiffness decreased quickly during the repeated cycles until 0.75% drift ratio. The stiffness decreased after each repeated moment cycle; in every three successive same drift cycles, the stiffness dropped about 1.5 times more in the second cycle than it did in the third one. Small cycles also showed a decreasing trend in stiffness.

Table 4.13 Comparison of peak moment and drift ductility between SW7 and SW8 (effect of openings and shear bolts layout patterns)

Slab name	$\frac{V}{V_0}$	Peak moment (kN*m)		Peak lateral drift ratio at peak moment (%)		Yield drift ratio (%)		Drift ductility at peak moment μ_{peak}		Drift ductility at 95% post peak moment $\mu_{0.95}$		Drift ductility at 80% post peak moment $\mu_{0.8}$	
		-	+	-	+	-	+	-	+	-	+	-	+
SW7	0.79	-56.59	58.52	-2.88	2.90	-1.05	1.14	2.75	2.56	3.05	3.17	4.0	4.03
SW8	0.74	-63.58	64.45	-2.77	2.74	-1.15	1.17	2.40	2.35	2.59	2.54	3.15	3.21

Table 4.14 Comparison of drift ductility (using tested drift ratio) in SW7 and SW8

Slab name	Tested first yield drift ratio (%)	Drift ductility at peak moment μ_{peak}		Drift ductility at 95% post peak moment $\mu_{0.95}$		Drift ductility at 80% post peak moment $\mu_{0.80}$	
		-	+	-	+	-	+
SW7	+2.24	1.29	1.30	1.43	1.61	1.88	2.05
SW8	+2.85	0.97	0.96	1.05	1.04	1.27	1.32

Comparing stiffness of the three specimens with openings, SW6, SW7 and SW8, we can find that specimen SW6 (without shear bolts) had stiffness very similar to SW7 and SW8 but showed more rapid stiffness decrease after 1.2% drift ratio. By comparison between SW5 and SW9, it is found the stiffness of SW5 (without shear bolts) decrease quickly after drift ratio 2.5% when it failed in punching. Generally, shear bolts had little influence on the stiffness of the connections before punching failures occurred in specimens without shear bolts.

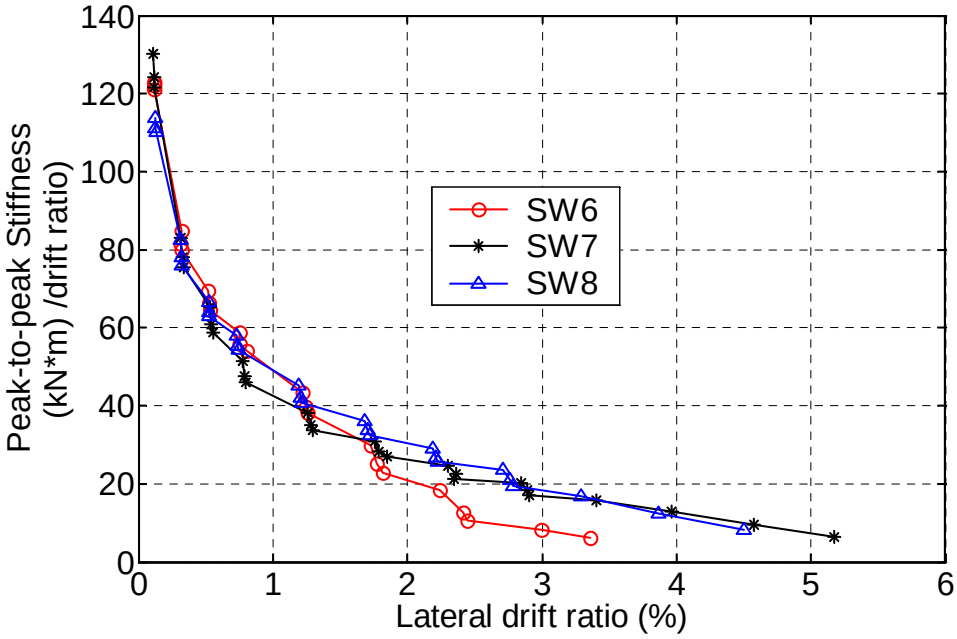

Figure 4.33 Moment peak-to-peak stiffness versus drift ratio of specimen SW6, SW7, SW8

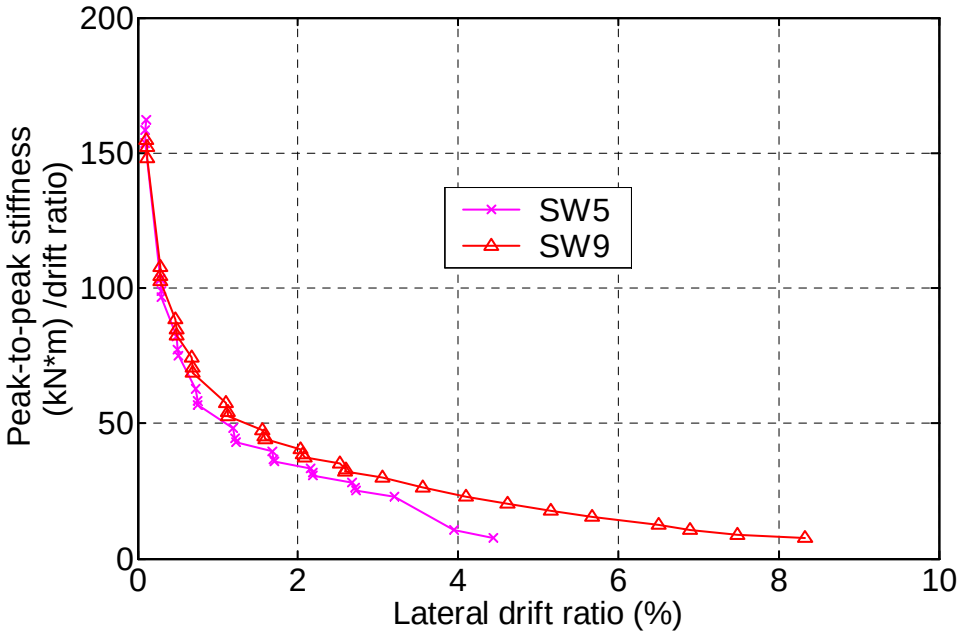

Figure 4.34 Moment peak-to-peak stiffness versus drift ratio of specimen SW5 and SW9

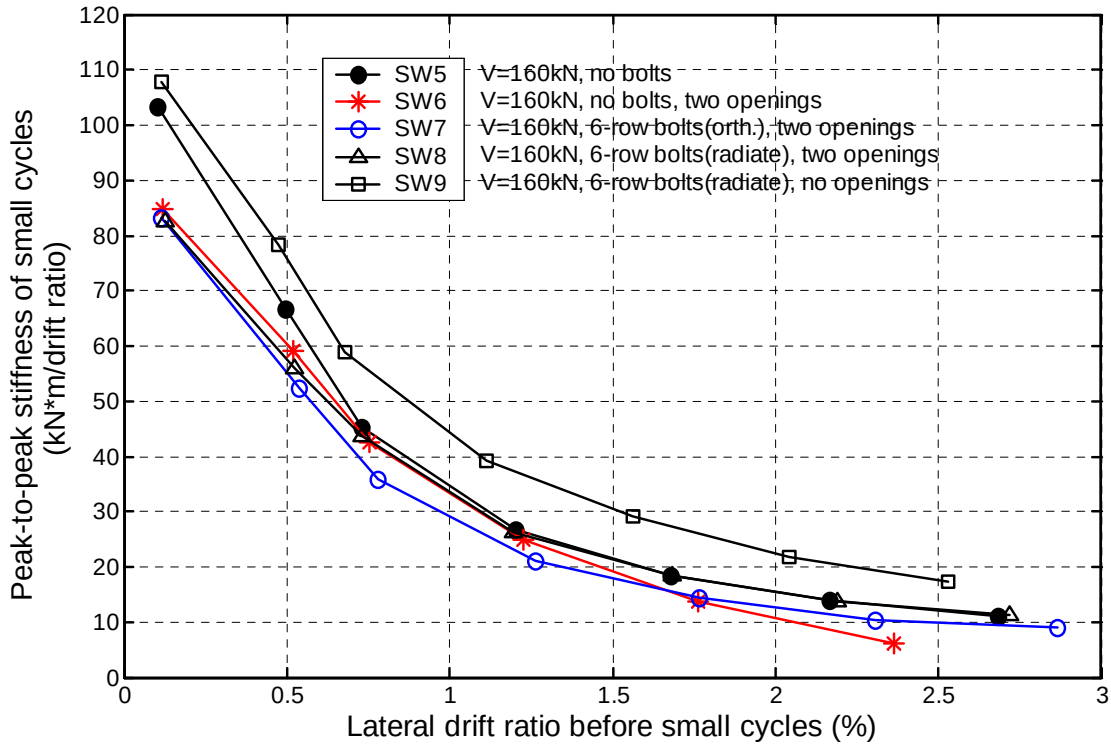

Figure 4.35 Peak-to-peak stiffness of small drift cycles of SW5 ~ SW9

4.3.6 Strains in Shear Bolts

For slab SW7, a total of twelve strain data were measured on six bolts along and transverse to the loading direction. For slab SW8 strengthened with 6-row radial bolts, strains were measured on bolts: six in lateral loading direction, six in direction perpendicular to lateral load, and six in diagonal direction. Bolts with strains gages are numbered as in Figure 3.29. Strains in Bolts #1a of slab SW7 versus lateral drift direction are shown in Figure 4.36. Figure 4.37 to Figure 4.39 show the backbone curves of lateral drift ratio versus strain on bolts for specimen SW7, SW8, and SW9. These figures demonstrate that shear bolts in the transverse direction show higher tension strains than those in the lateral loading direction. In the lateral loading direction, the 4th and 5th row shear bolts, far from the column face, had very small tension strains. Only the 1st row shear bolts in the direction transverse to the lateral loading direction yielded at very large drift ratios.

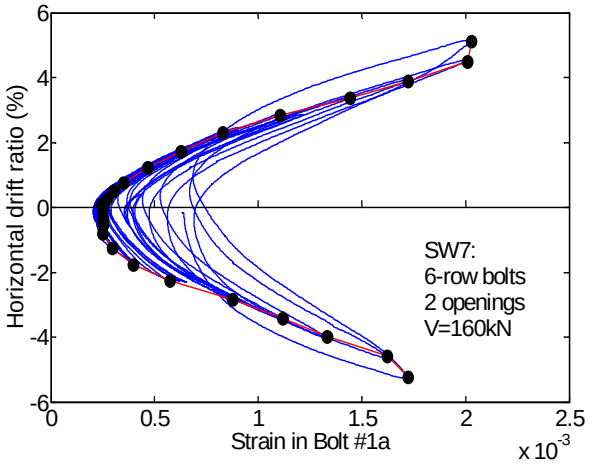

Figure 4.36 Figure 15–Horizontal load versus strain in bolt #1a of SW7.

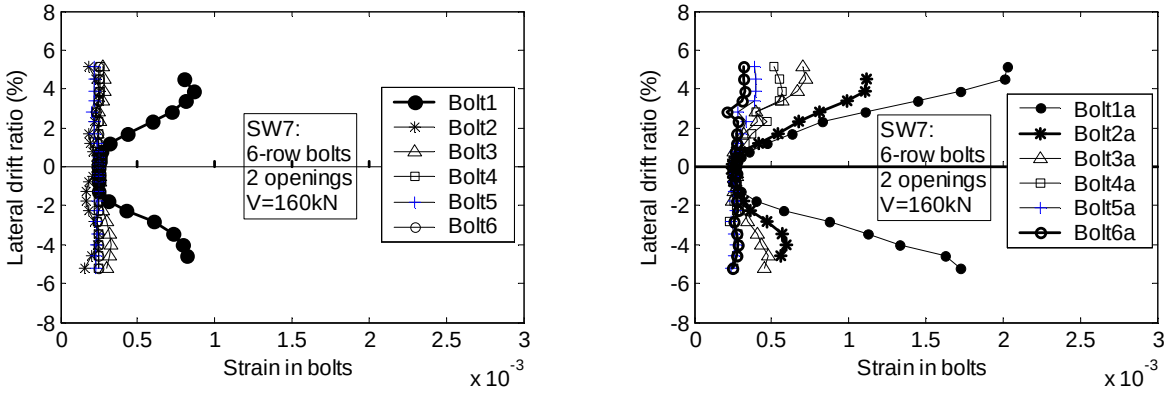

Figure 4.37 Backbone curves of lateral drift ratio versus strain in each bolt of specimens SW7

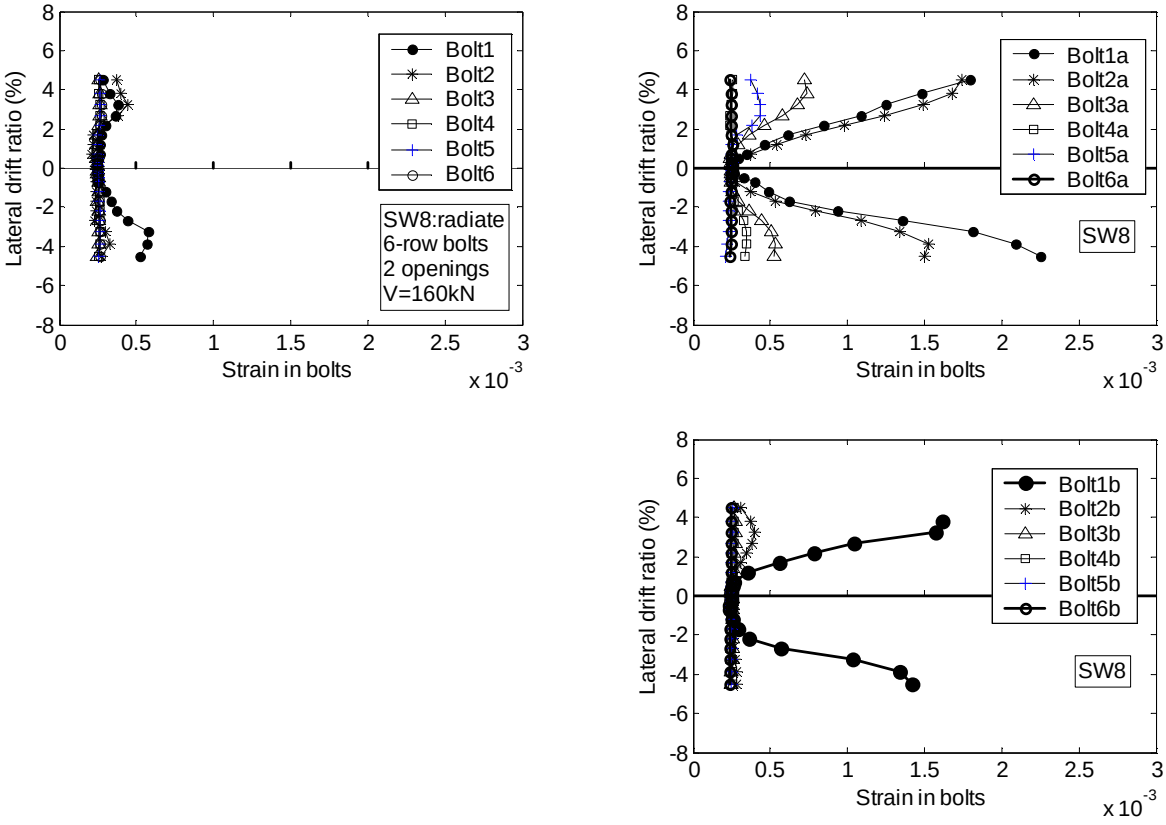

Figure 4.38 Backbone curves of lateral drift ratio versus strain in each bolt of specimens SW8

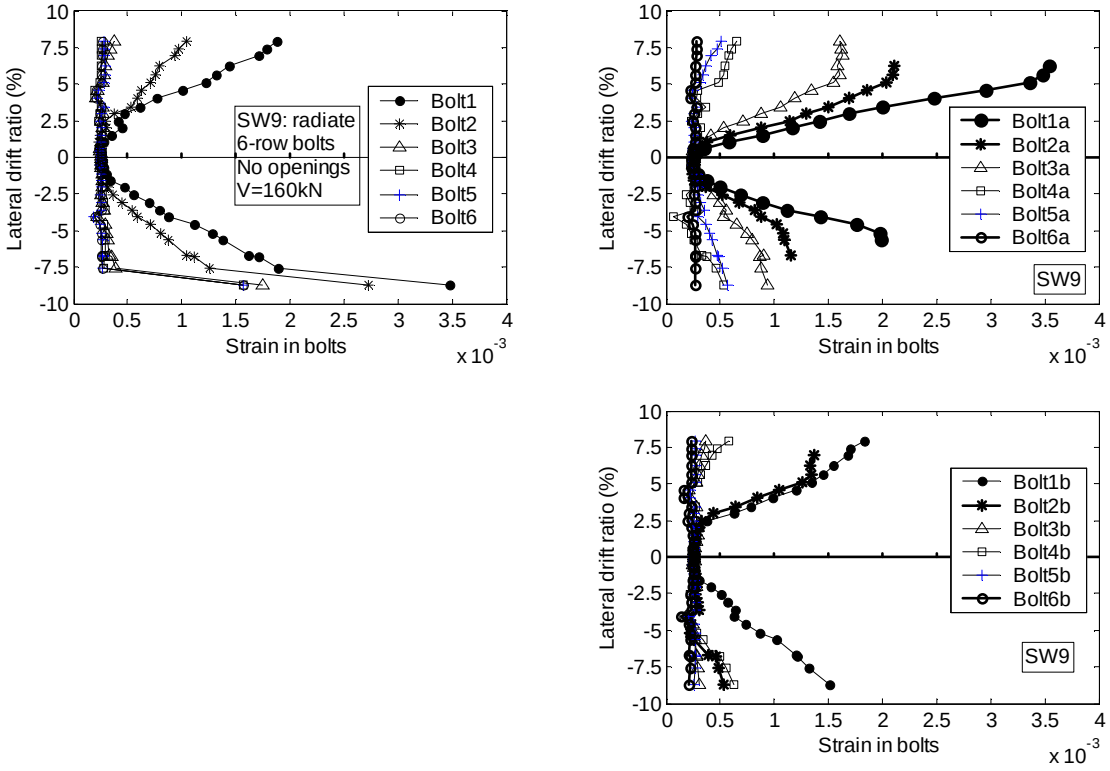

Figure 4.39 Backbone curves of lateral drift ratio versus strain in each bolt of specimens SW9

4.3.7 Strains in Flexural Reinforcements

A number of strain gages were attached to flexural rebar and embedded in concrete in each slab. The numbering and locations of them are shown in Figure 4.40. For each specimen, strains are shown in Figure 4.41 to Figure 4.44 for specified locations on rebars close to the column. Strain gauge readings at different locations in each rebar are drawn in Figure 4.45 for drift ratio of 1.15%. It can be seen that only rebar in SW5, going through the column in the direction of lateral loading, has yielded at drift ratio of -1.15%.

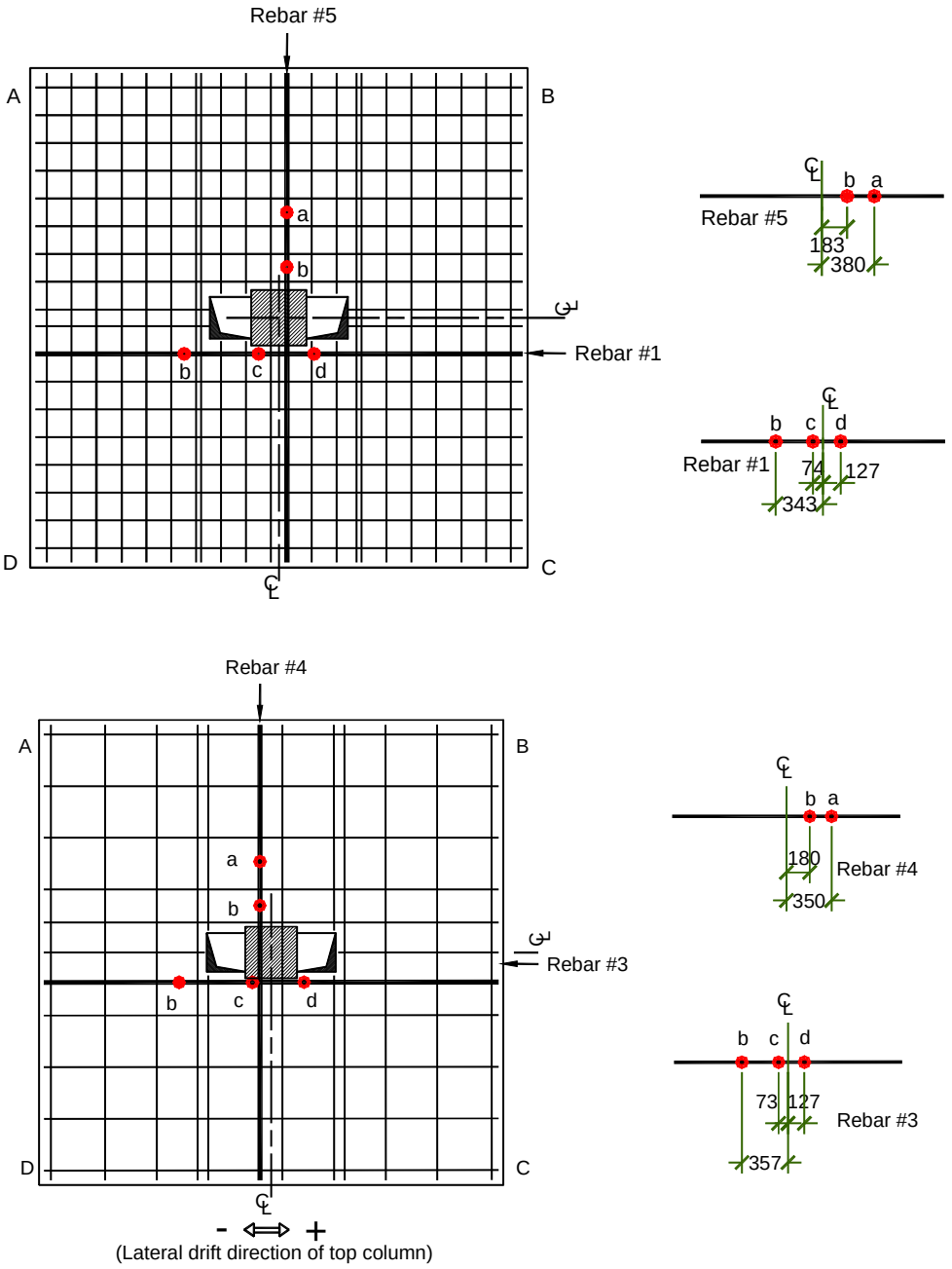

Figure 4.40 Strain gauges layout in specimens SW6, SW7, and SW8

(a) Strain gauge locations on bottom reinforcement mat; (b) Strain gauge locations on top reinforcement mat

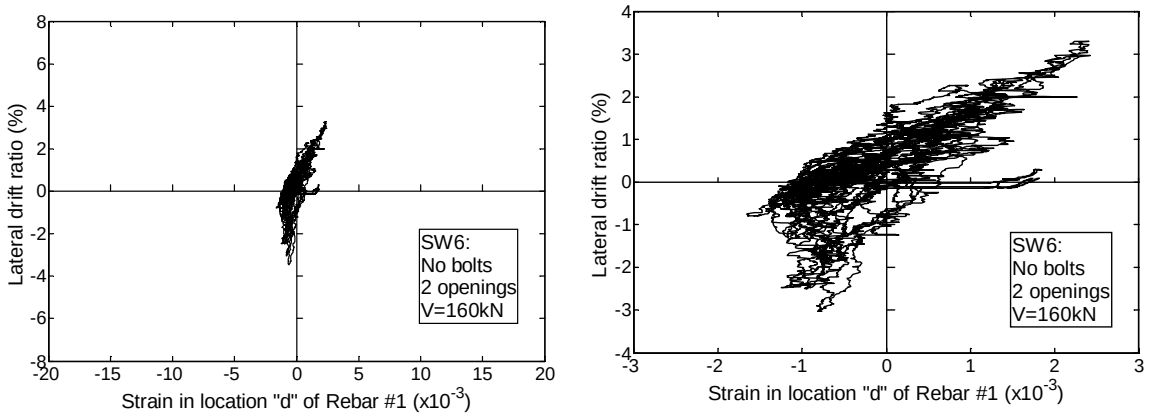

(a) (b)

Figure 4.41 Lateral drift ratio versus strain at location “d” of Rebar #1 in specimen SW6

(a) Response during the full testing sequence, (b) Response until yielding

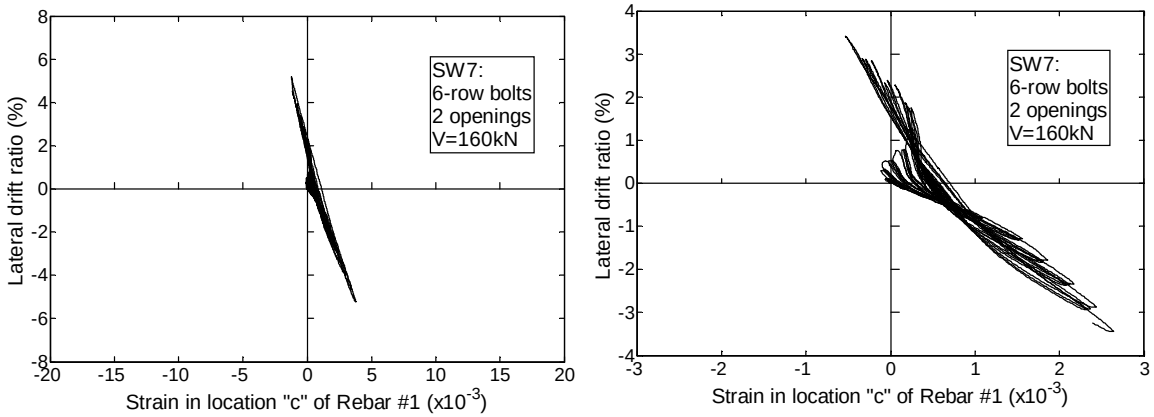

(a) (b)

Figure 4.42 Lateral drift ratio versus strain at location “c” of Rebar #1 in specimen SW7

(a) Response during the full testing sequence, (b) Response until yielding

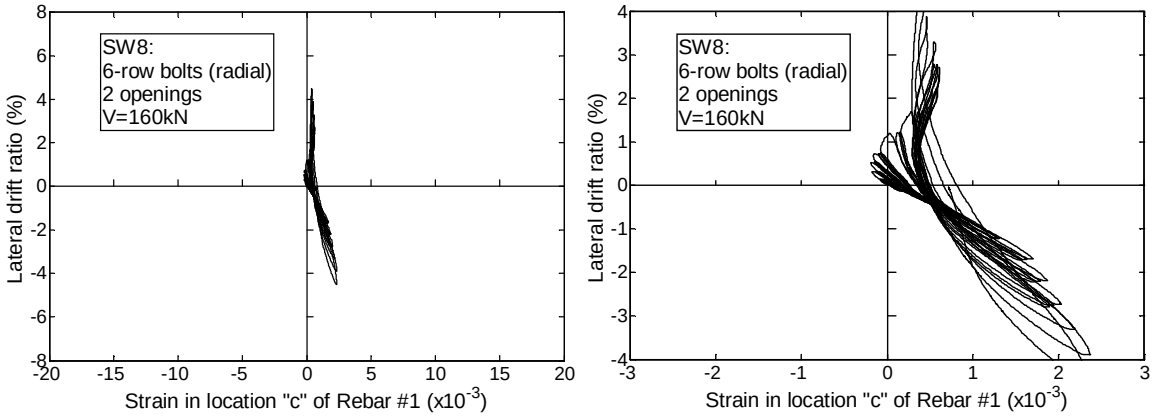

(a) (b)

Figure 4.43 Lateral drift ratio versus strain at location “c” of Rebar #1 in specimen SW8

(a) Response during the full testing sequence, (b) Response until yielding

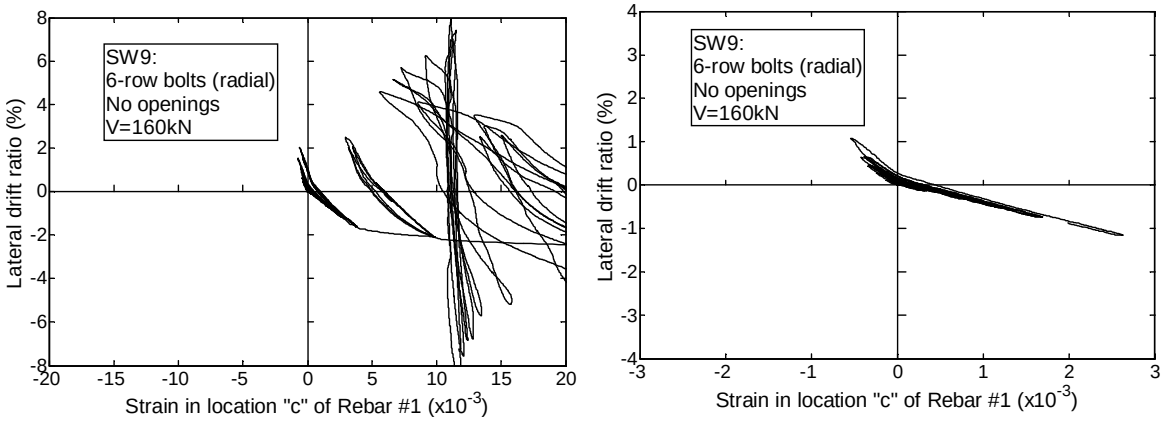

(a) (b)

Figure 4.44 Lateral drift ratio versus strain at location “c” of Rebar #1 in specimen SW9

(a) Response during the full testing sequence, (b) Response until yielding

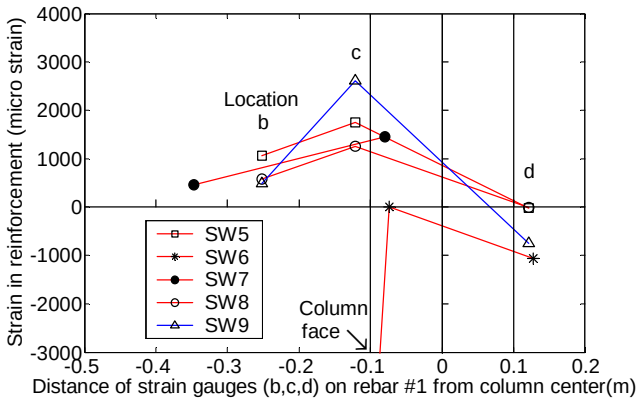
Strain in reinforcement (micro strain)
Distance of strain gauges (b,c,d) on rebar #1 from column center(m)
Location
b
c
d
SW5
SW6
SW7
SW8
SW9
Column
face

(a)

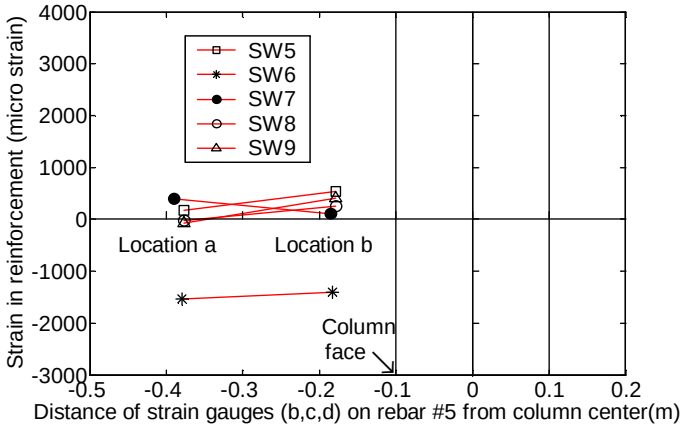
Strain in reinforcement (micro strain)
Distance of strain gauges (b,c,d) on rebar #5 from column center(m)
SW5
SW6
SW7
SW8
SW9
Location a
Location b
Column
face

(b)

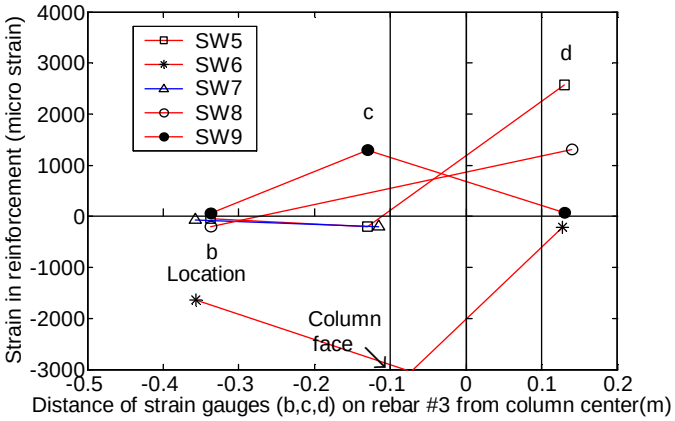
Strain in reinforcement (micro strain)
Distance of strain gauges (b,c,d) on rebar #3 from column center(m)
SW5
SW6
SW7
SW8
SW9
d
c
b
Location
Column
face

(c)

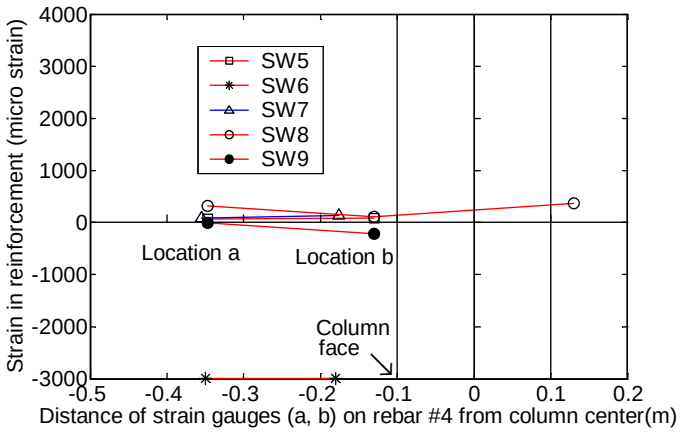

(d)

Figure 4.45 Strains in different locations of each numbered rebar in specimen SW5~SW9 at -1.15% lateral drift ratio

(a) Strain in location “b”, “c” and “d” of rebar #1; (b) Strain in location “a”, “b” on rebar #5; (c) Strain in location “b”, “c”, and “d” on rebar #3; (d) Strain in location “a” and “b” on rebar #4

4.3.8 Estimation of Vertical Crack Width

As shown in Figure 3.47, in location L1, L2, L3, and L4, displacement transducers were placed on both top and bottom surfaces of the slabs. The displacement differences are used as estimates of slab opening width through slab thickness. Figure 4.46 – Figure 4.49 show all the crack widths in position “L1”, “L2”, “L3”, and “L4” of each slab under cyclic horizontal loading. If the crack width is negative in the figures, it is either due to errors in testing or rupture of concrete slab underneath the transducers. Table 4.15 shows crack width of specimen SW6, SW7, SW8, and SW9 at lateral drift of 1.5%, 2.0%, and 3.0%. From the crack figures, it can be found that crack width in the slab is wider in L1 (close to column side) and L3 (close to the column corners) than those in L2 and L4. For slabs with openings, the crack widths at 3% drift are large because they all reached peak load before 3% drift ratio. The specimens without bolts (SW6) had wider crack width than those strengthened with shear bolts (SW7, SW8) after 2% drift. Specimen SW9 (without openings) had smaller crack width at 3% drift than SW6~SW8 because it had not reached its peak load yet.

Table 4.15 Crack width at 1.5%, 2.0% and 3.0% drift ratio for specimen SW6~SW9

Slab name	Crack width (mm)		
	at +1.5% drift ratio	at +2.0% drift ratio	at +3.0% drift ratio
SW6	0.52	1.61	4.76
SW7	0.65	1.01	2.00
SW8	-0.09	0.09	1.01
SW9	0.11	0.16	0.46

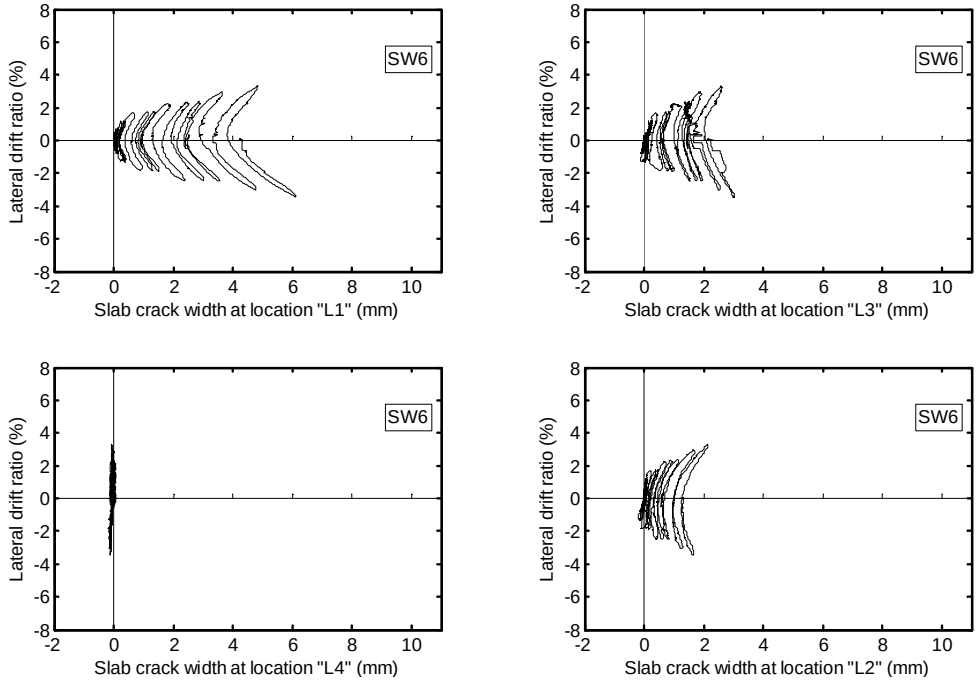

Figure 4.46 Crack width at locations “L1”, “L2”, “L3”, and “L4” in the slab of SW6

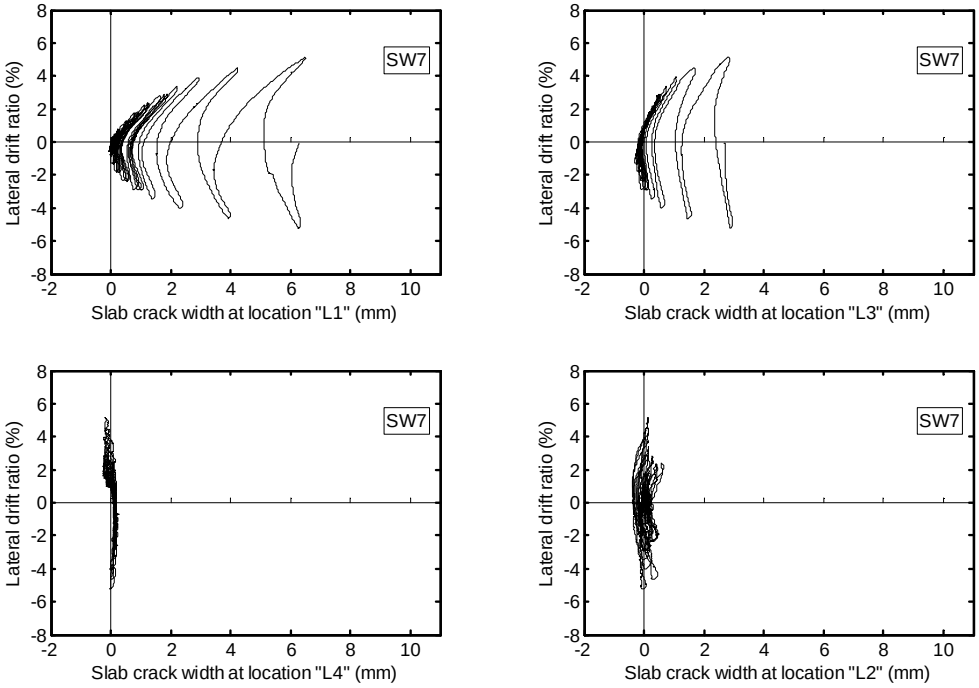

Figure 4.47 Crack width at locations “L1”, “L2”, “L3”, and “L4” in the slab of SW7

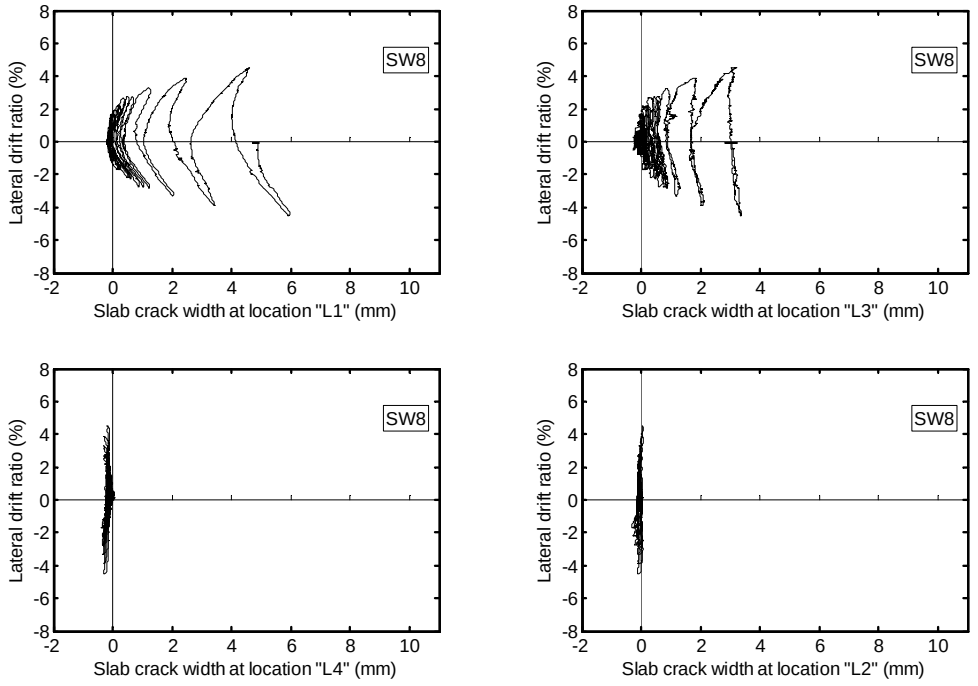

Figure 4.48 Crack width at locations “L1”, “L2”, “L3”, and “L4” in the slab of SW8

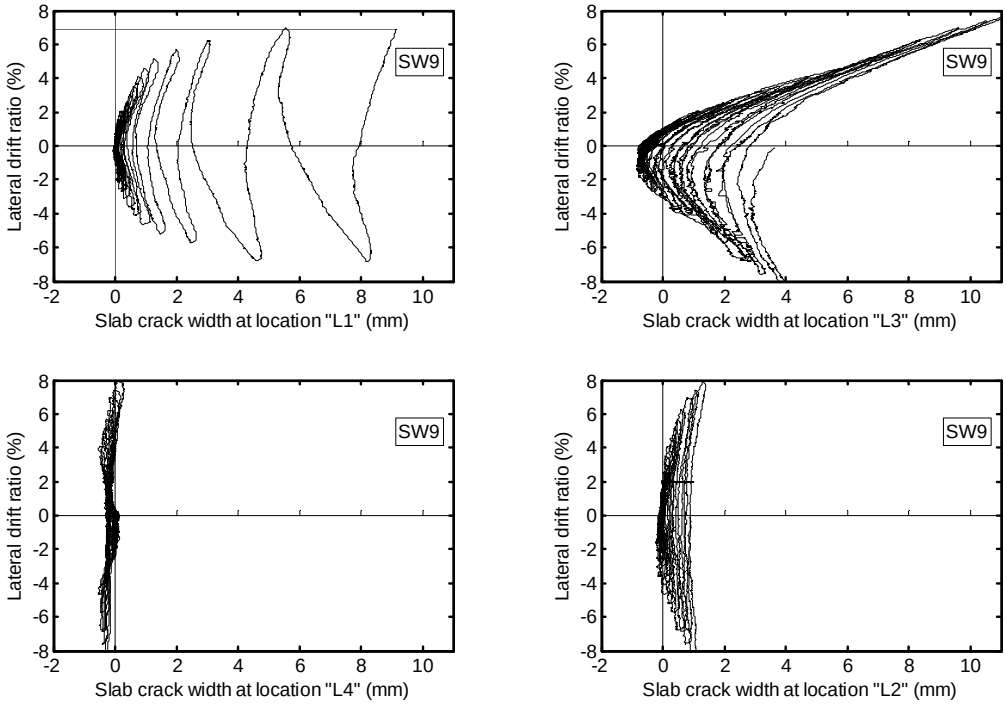

Figure 4.49 Crack width at locations “L1”, “L2”, “L3”, and “L4” in the slab of SW9

4.3.9 Cracking and Failure Mode of the Specimens

Cracks on slabs started from the corners of columns on the tension side, first at the bottom slab surface and then on top surface. First crack usually was observed at about 0.6~0.75% drift ratio. On bottom surface, cracks first propagated toward the slab edge and corners, while on slab top surface, initial cracks developed from column corner to the direction perpendicular to the lateral loading direction. The final crack patterns of top and bottom slab surfaces for all specimens are shown in Figure 4.50. From the crack pattern and the hysterosis curves, it can be found that SW5 and SW6 failed by punching shear mode; the other two, SW7 and SW8 were subjected to flexural failure mode.

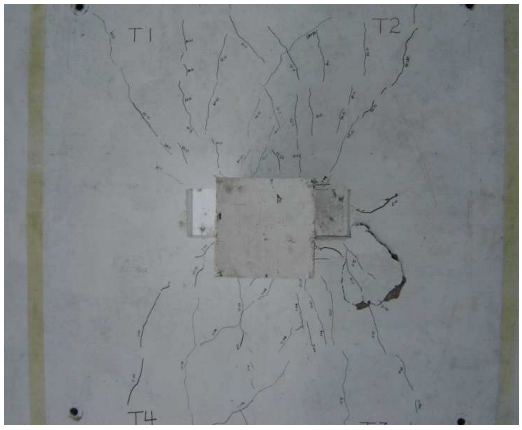

SW 6 top view

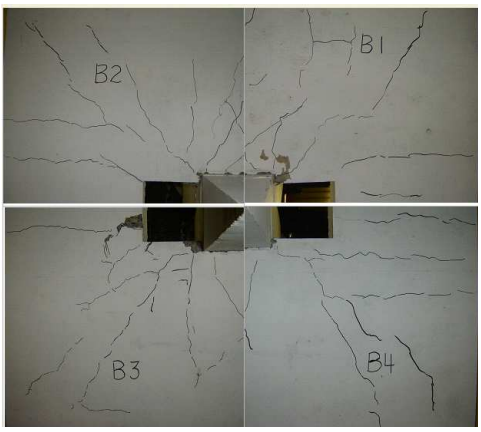

SW 6 bottom view

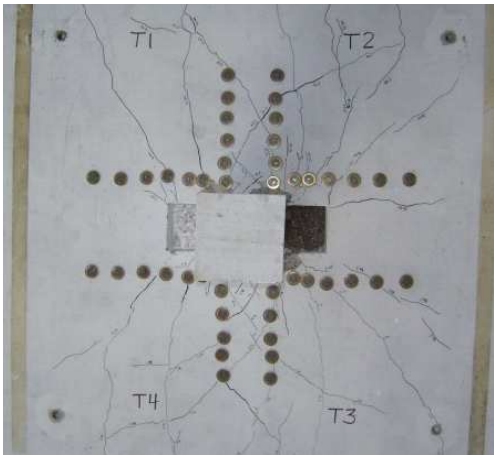

SW7 top view

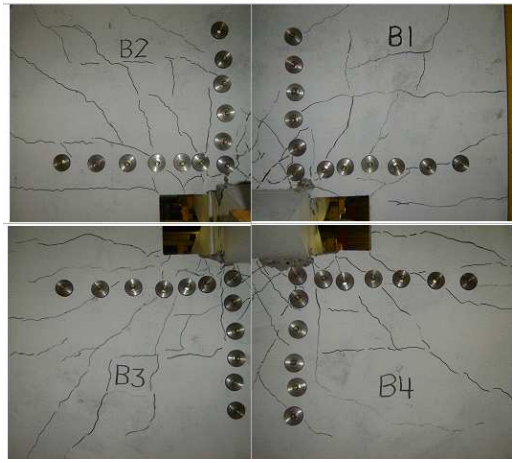

SW7 bottom view

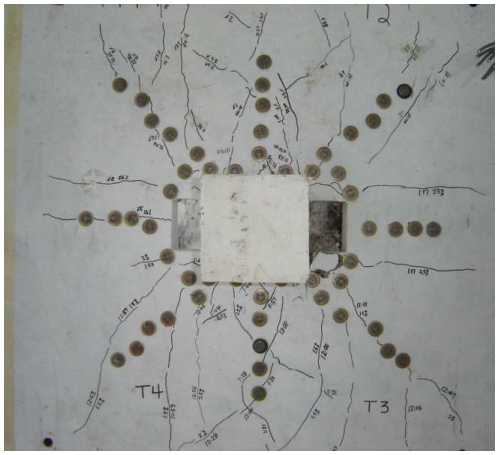

SW8 top view

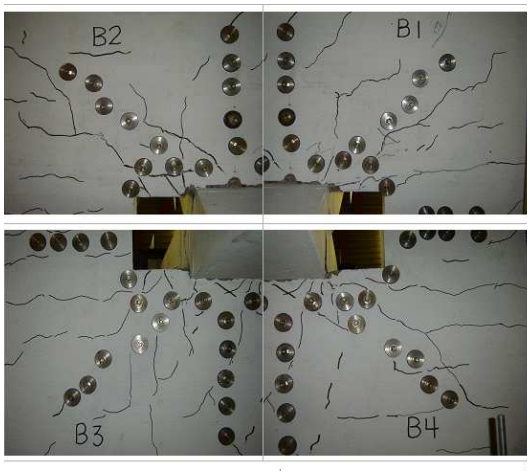

SW8 bottom view

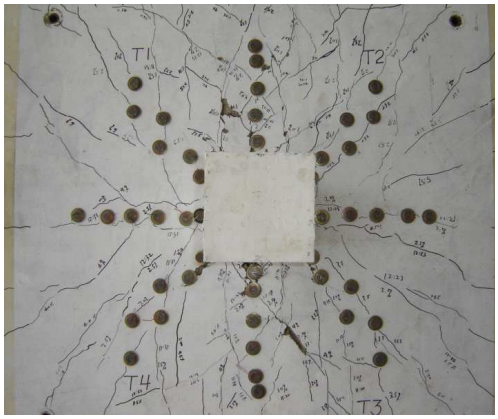

SW9 top view

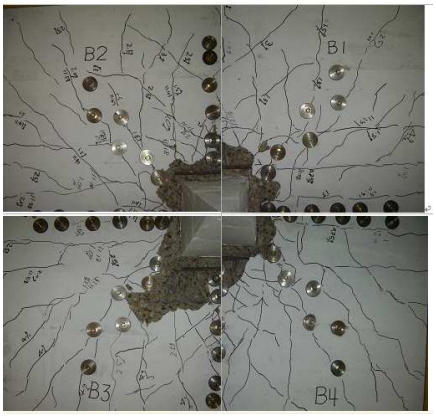

SW9 bottom view

Figure 4.50 Crack pattern (final) of top and bottom surfaces of specimen SW6~SW9

4.4 Comparison of Testing Results with the Building Codes of ACI318-05, CSA A23.3-04 and Eurocode 2 (2004)

The nominal moment capacity for each specimen was calculated using the applied gravity load and the material strengths. The design formulae of building codes, ACI318-05, CSA A23.3-04, and Eurocode 2(2004) were used. The calculated nominal moment and the peak moment measured in the test for each specimen are compared in Table 4.16.

As introduced in Section 2.5, the American code ACI318-05 provides formulae for punching shear design of two-way slab under gravity load and unbalanced connection moment. The shear stress on the critical section due to external moment and vertical load can be calculated by equation (2-34). In this research, the moment was applied in one direction (along x direction) only, thus equation (2-34) can be written into following equation (4-1). The design shear strength v_r is calculated by equation (4-2).

$$v_f = \frac{V_f}{b_0 d} + \frac{\gamma_v M_f e}{J_x} \tag{4-1}$$

$$v_r = \frac{\phi}{b_0 d}(V_s + V_c) \tag{4-2}$$

$$v_r \le v_f \tag{4-3}$$

where V_f is the factored vertical load, V_c , V_s are nominal resistance forces from concrete and shear reinforcement respectively, M_f is the factored unbalanced moment of the connection, b_0 is the perimeter length of the critical section, d is the effective thickness of the slab, $\gamma_v = 0.4$, J_x is the analogy of polar moment of inertia about the moment axis. ϕ is the strength reduction factor ($\phi = 0.75$ for shear). Solving equations (4-1), (4-2), (4-3) results in the value of a factored moment M_f:

$$M_f = \frac{J_x}{\gamma_v e}\left[\frac{\phi}{b_0 d}(V_s + V_c) - \frac{V_f}{b_0 d}\right] \tag{4-4}$$

For comparison with the test, resistance factor ϕ, is taken as unity, and V_f is replaced by the vertical constant load V in the experiments $(V = 110kN, or 160kN)$, then the nominal unbalanced moment M can be computed as in equation (4-5), which can be compared with the experimental results.

$$M = \frac{J_x}{\gamma_v e}\left[\frac{1}{b_0 d}(V_s + V_c) - \frac{V}{b_0 d}\right] \tag{4-5}$$

ACI318-05 has no special provisions for headed shear studs or shear bolts. It provides provisions for shear reinforcements of in the form of stirrups (wires and bars) and shear head (steel shapes). For a

slab with stirrups (wires and bars), the nominal shear resistance force V_c from concrete is $V_c = 0.17 b_0 d \sqrt{f_c^{'}}$ (metric), and shear resistance V_s from the shear reinforcements is $V_s = \frac{A_{vs} f_{yv} d}{s}$, where A_{vs} is the section area of all shear reinforcements around one peripherial section, f_{yv} is the yield strength of the shear reinforcement (taken as MPa), s is the radial spacing of shear reinforcements. The sum of shear force from both concrete and shear reinforcements $(V_s + V_c)$ must be no more than $0.5 b_0 d \sqrt{f_c^{'}}$. Since there are openings in SW6, SW7 and SW8, the sectional area of critical section is reduced due to the openings.

Canadian code CSA A23.3-04 adopts similar equations to those of ACI318-5 for punching shear design. It has equivalent provisions for slabs with stirrups: nominal shear force V_c from concrete is $V_c = 0.19 b_0 d \sqrt{f_c^{'}}$ and nominal shear resistance V_s from the stirrups is $V_s = \frac{A_{vs} f_{yv} d}{s}$; the total of these two nominal forces must be no more than $0.55 b_0 d \sqrt{f_c^{'}}$. The difference in the factors in ACI and CSA codes comes from the difference in the safety factors in the two codes.

CSA A23.3-04 provides particular clauses for design of headed shear studs, in which the nominal shear force V_c from concrete is $V_c = 0.28 b_0 d \sqrt{f_c^{'}}$, and the sum of the nominal shear forces from concrete and shear reinforcements shall be no more than $0.75 b_0 d \sqrt{f_c^{'}}$. These values are larger than those for stirrups.

Moreover, according to Clause 21.12.3 in CSA A23.3-04, for slabs with headed shear reinforcements under seismic loading, the factored gravity shear stress v_g shall satisfy the following formula (4-6).

$$v_g = \frac{V_f}{b_0 d} \le R_E \left[0.5(0.28 \lambda \phi_c \sqrt{f_c^{'}}) + \frac{\phi_s A_{vs} f_{yv}}{b_0 s} \right] \qquad (4\text{-}6)$$

For this research, $\frac{A_{vs} f_{yv}}{b_0 s}$ is given for each specimen. Setting the material reducing factors ϕ_c, ϕ_s to unity, the nominal allowed maximum gravity load V_{a1} can be calculated as

$$V_{a1} \le R_E \left[0.5(0.28\sqrt{f_c^{'}}) + \frac{A_{vs} f_{yv}}{b_0 s} \right] b_0 d \tag{4-7}$$

where R_E is defined in equation (2-47), A_{vs} is the area of shear reinforcements, f_{yv} is the yield strength of the shear reinforcement, s is the radial spacing, b_0 is the critical section length, d is the effective slab thickness.

Clause 21.12.3 of CSA A23.3-04 also specifies the allowable maximum gravity load for seismic slabs without shear reinforcements.

$$v_g = \frac{V_f}{b_0 d} \le R_E v_c \tag{4-8}$$

where v_c is defined in equations in (2-30). From equation (4-8), the allowable maximum gravity load for a seismic slab without shear reinforcement is

$$V_{a2} = (b_0 d) R_E (0.38\sqrt{f_c^{'}}) \tag{4-9}$$

According to Eurocode2 (2004), Clause 6.4.3 (3) and 6.4.5 (1), design moment M_f can be calculated by equating the shear resistance v_r of equation (2-43) and the shear stress v_f in equation (2-42) due to external load V_f and unbalanced moment M_f.

$$M_f = \left[0.75 v_c + 1.5(\frac{d}{s_r}) A_{sw} f_{ywdef} (\frac{1}{u_1 d}) \sin\alpha - \frac{V_f}{u_1 d} \right] \frac{W_1 d}{\gamma} \tag{4-10}$$

$$v_c = \frac{0.18}{\gamma_c} (1 + \sqrt{\frac{200}{d}}) (100 f_{ck} \sqrt{\rho_x \rho_y})^{1/3} \tag{4-11}$$

$$f_{ywdef} = 250 + 0.25d \le f_{ywd} \tag{4-12}$$

where d is the effective depth of slab, s_r is the radial spacing of shear reinforcements, A_{sw} is the cross section area of shear reinforcements of each periphery row, u_1 is the length of the basic control

section, $\gamma = 0.6$ for square column, $W_1 = \int_0^{u_1} |e| dl$, e is the distance of dl to the moment axis, α is the angle between the reinforcement and the slab plane, $\gamma_c = 1.5$ for persistent concrete, f_{ck} is the characteristic cylinder compressive strength (28-day), ρ_x, ρ_y are the flexural reinforcing ratios of the slab in two orthogonal directions, f_{ywd} is the design yield strength of the shear reinforcement.

To obtain the nominal moment M from equation (4-10) ~ (4-12), let the partial factor for concrete be $\gamma_c = 1.0$; use the following relation between $f_c^{'}$ and f_{ck} proposed by Reineck (1999) (Gardner, 2005); and replace V_f by vertical constant load V applied in the tests.

$$f_{ck} = f_c^{'} - 1.60 \quad \text{(MPa)} \tag{4-13}$$

Thus, there is following equation (4-14) for the nominal moment, in which all parameters are specified as for equation (4-10).

$$M = \left[0.75 v_c + 1.5 (\frac{d}{s_r}) A_{sw} f_{ywdef} (\frac{1}{u_1 d}) \sin\alpha - \frac{V}{u_1 d} \right] \frac{W_1 d}{\gamma} \tag{4-14}$$

$$v_c = \frac{0.18}{1} (1 + \sqrt{\frac{200}{d}}) \left[100 (f_c^{'} - 1.6) \sqrt{\rho_x \rho_y} \right]^{1/3} \tag{4-15}$$

All the calculated and measured moments for the specimens were shown in Table 4.9. The maximum allowable gravity loads are also presented for seismic slabs with or without shear reinforcements. For slabs strengthened with shear bolts, ACI318-05 provisions give smaller nominal values than the CSA A23.3-04, since ACI318-05 provisions used above were mainly for stirrups and wires. The Eurocode 2(2004) gives too large nominal results, even larger than the measured peak moments, which is not reasonable. CSA A23.3-04 is the best to predict the nominal moment capacity, but for slabs with openings or with shear reinforcements, the predicted values are smaller than the tested peak moments.

Table 4.16 Measured peak moments and the predicted nominal moments using codes of ACI318-05, Eurocode 2(2004) and CSA A23.3-04

Specimen name	Measured peak moment (kN*m)	Nominal moment predicted by ACI318-05 (kN*m)	Nominal moment predicted by Eurocode2 (2004) (kN*m)	Nominal moment predicted by CSA A23.3-04 (kN*m)	Gravity load V applied in the tests (kN)	Gravity load ratio $\frac{V}{V_0}$	Nominal Max. allowed gravity load V_{a1} by CSA for seismic slabs with shear bolts (kN)	Nominal Max. allowed gravity load V_{a2} by CSA for seismic slabs without shear bolts (kN)
SW1	68.7	22.2	31.7	29.6	110	0.55	N/A	70.9
SW2	88.9	47.5	112.3	82.6	110	0.55	110.6	70.9
SW3	89.3	47.5	108.2	79.4	110	0.55	107	70.9
SW4	93.2	45.2	99.5	74.6	160	0.68	112.8	80.4
SW5	77.9	16.4	21.8	24.9	160	0.68	N/A	80.4
SW6	52. 3	7.0	-4.0	11.1	160	0.74	N/A	76.4
SW7	56. 6	18.0	54.4	35.1	160	0.79	109.4	71.1
SW8	63. 6	20.9	56.5	37.2	160	0.74	112.6	76.4
SW9	92. 2	51.5	98.3	75.3	160	0.66	111.6	86.4

Note: 1. Gravity load ratios $\frac{V}{V_0}$ were calculated using $V_0 = 0.33 b_0 d \sqrt{f_c'}$ (ACI 318-05, in Metric units). 2. Nominal Maximum allowed gravity load V_{a1} and V_{a2} were calculated assuming allowed lateral drift ratio $\delta_i = 2\%$ in CSA A23.3-04 Clause 21.12.3.

This variation among different codes in calculation of nominal moment is mainly caused by the following reasons:

(1) The material strength reduction factors in different codes are different; in each code, these factors are calibrated with their corresponding load factors and load combination factors. In Table 4.16, the nominal moment capacities are calculated neglecting the material and strength reduction factors only.

(2) The code predictions, for slabs without shear bolts, cover a wide range of slab thicknesses. However, test results vary with specimen thickness. According to Bazant and Cao (1987) and Choi et al. (2007), punching shear strength decreases as slab thicknesses increase. Therefore, the predicted

nominal moments using codes, for the specimens SW1, SW5, and SW6 (without shear bolts), are much lower than maximum moments measured.

Chapter 5
Design of Steel Shear Bolts and Concrete Slab with Shear Bolts

This chapter consists of three parts. First, in Section 5.1, the design of steel shear bolts is introduced, which includes the determination of bolt head thickness, head area and bolt stem diameter. Second, section 5.2 gives suggestions on how to design retrofit of flat concrete slabs using shear bolts. This section analyzes slab shear resistance and provides guidance regarding the layout of the shear bolts. Third, suggestions are given for construction methods during retrofit using shear bolts.

5.1 Design of Steel Shear Bolts

A steel shear bolt consists of a bolt stem, a head at one end, and a washer and nut at the other end. The washer and the head must be designed for adequate thickness and area. The work involves design of the head thickness, the head area, and their relation to the bolt stem strength. The size of the stem is determined based on slab strength considerations. The general procedure to determine the shear bolts for concrete retrofitting is: (1) to determine the shear bolts layout and bolt head area according to the slab thickness, concrete strength, and steel strength of the bolts; (2) to determine bolt stem diameter and heat thickness.

5.1.1 Thickness of the Bolt Head

The bolt head thickness was analyzed using the elastic thin plate theory and the finite element method. It can be determined using bolt stem diameter and the hole diameter. These are explained in two following subsections.

5.1.1.1 Determination of Bolt Head Thickness using Elastic Thin Plate Theory

The bolt head and the bolt stem can be considered as an axisymmetric elastic body. The bolt head is assumed to be a circular thin plate. The round stem applies an evenly distributed circular load at the center of the head. The head diameter is $2R_0$. The diameter of the bolt stem is $2r_0$, and the drilled hole in the concrete slab for the bolts has a diameter of $2R$. The load from the bolts stem is q which is equal to the yield stress. The head is assumed to be simply supported on the concrete slab surface.

The bolt and bolt head are shown in Figure 5.1. The internal force conventions for an axisymmetric slice element are shown in Figure 5.2.

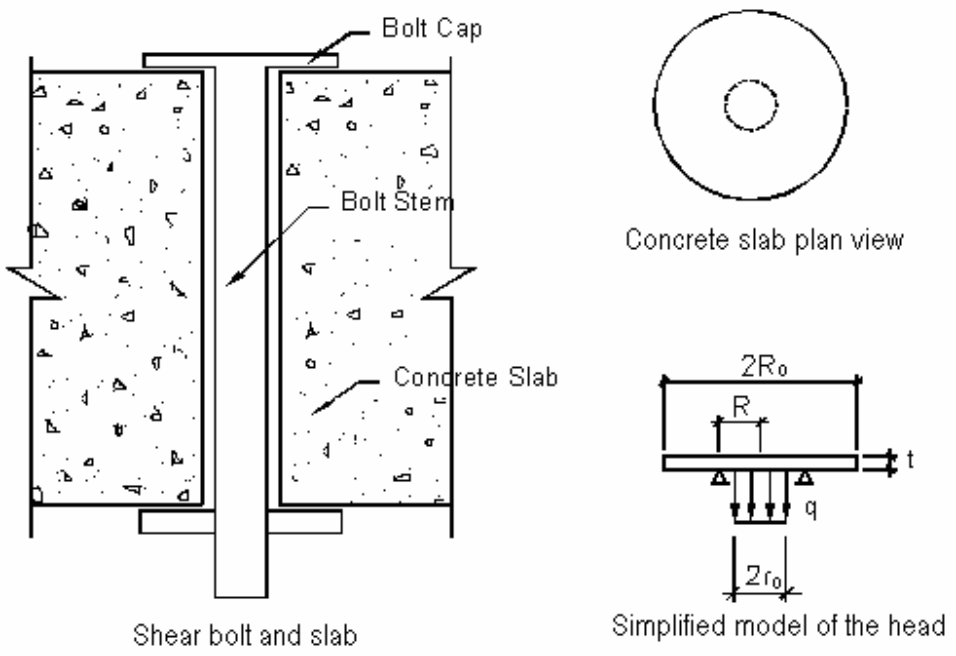

Figure 5.1 Shear bolt and bolt head

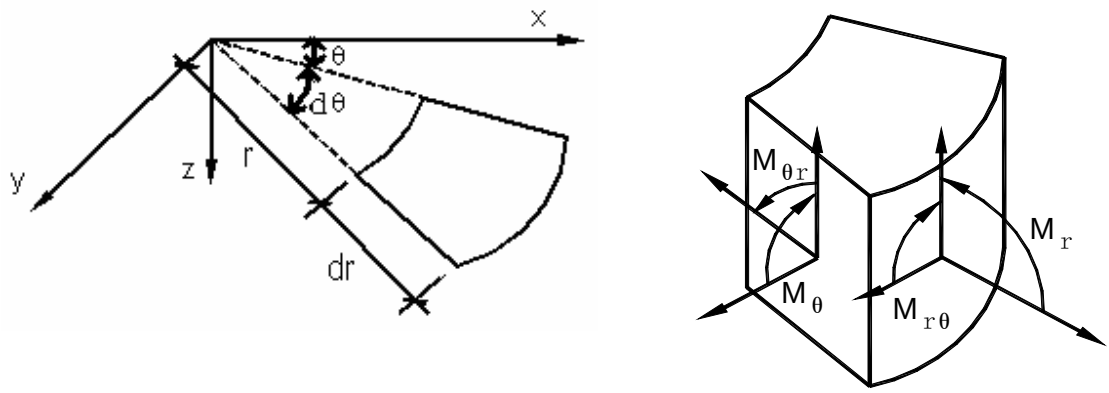

Figure 5.2 Axisymmetric element and its internal forces

Using elastic thin plate theory, one can obtain the internal force equations as following.

$$\begin{aligned} M_r &= (M_x)_{\theta=0} \\ &= -D(\frac{\partial^2 w}{\partial x^2} + \mu \frac{\partial^2 w}{\partial y^2})_{\theta=0} \\ &= -D[\frac{\partial^2 w}{\partial r^2} + \mu(\frac{1}{r}\frac{\partial w}{\partial r} + \frac{1}{r^2}\frac{\partial^2 w}{\partial \theta^2})] \end{aligned} \tag{5-1}$$

$$\begin{aligned} M_\theta = (M_y)_{\theta=0} &= -D(\frac{\partial^2 w}{\partial y^2} + \mu \frac{\partial^2 w}{\partial x^2})_{\theta=0} \\ &= -D\left[(\frac{1}{r}\frac{\partial w}{\partial r} + \frac{1}{r^2}\frac{\partial^2 w}{\partial \theta^2}) + \mu \frac{\partial^2 w}{\partial x^2}\right] \end{aligned} \tag{5-2}$$

$$M_{r\theta} = M_{\theta r} = (M_{xy})_{\theta=0} = -D(1-\mu)(\frac{\partial^2 w}{\partial x \partial y})_{\theta=0} \tag{5-3}$$

$$= -D(1-\mu)(\frac{1}{r}\frac{\partial^2 w}{\partial r \partial \theta} - \frac{1}{r^2}\frac{\partial\ w}{\partial \theta})$$

Since q is symmetric around z axis, deformation plane of the circular plate is also symmetric about z axis, w is only the function of r, not θ, therefore

$$M_{r\theta} = M_{\theta r} = (M_{xy})_{\theta=0} = 0 \tag{5-4}$$

$$Q_r = (Q_x)_{\theta=0} = -D(\frac{\partial}{\partial x}\nabla^2 w)_{\theta=0} = -D\frac{\partial}{\partial r}\nabla^2 w \tag{5-5}$$

$$Q_\theta = (Q_y)_{\theta=0} = -D(\frac{\partial}{\partial y}\nabla^2 w)_{\theta=0} = -D\frac{1}{r}\frac{\partial}{\partial \theta}\nabla^2 w \tag{5-6}$$

$$\nabla^2 w = \frac{\partial^2 w}{\partial r^2} + \frac{1}{r}\frac{\partial w}{\partial r} + \frac{1}{r^2}\frac{\partial^2 w}{\partial \theta^2}$$

The stresses in the plate are

$$\sigma_r = \frac{12 M_r}{t^3} z \tag{5-7}$$

$$\sigma_\theta = \frac{12M_\theta}{t^3} z \tag{5-8}$$

$$\tau_{r\theta} = \tau_{\theta r} = \frac{12M_{r\theta}}{t^3} z = 0 \tag{5-9}$$

$$\tau_{rz} = \frac{6Q_r}{t^3}(\frac{t^2}{4} - z^2) \tag{5-10}$$

$$\tau_{\theta z} = \frac{6Q_\theta}{t^3}(\frac{t^2}{4} - z^2) \tag{5-11}$$

$$\sigma_z = -2q(\frac{1}{2} - \frac{z}{t})^2(1 + \frac{z}{t}) \tag{5-12}$$

The maximum stresses are

$$(\sigma_r)_{z=\frac{t}{2}} = -(\sigma_r)_{z=-\frac{t}{2}} = 6\frac{M_r}{t^2} \tag{5-13}$$

$$(\sigma_\theta)_{z=\frac{t}{2}} = -(\sigma_\theta)_{z=-\frac{t}{2}} = 6\frac{M_\theta}{t^2} \tag{5-14}$$

$$\tau_{r\theta} = \tau_{\theta r} = 0 \tag{5-15}$$

$$(\tau_{rz})_{z=0} = \frac{3Q_r}{2t} \tag{5-16}$$

$$(\tau_{\theta z})_{z=0} = \frac{3Q_\theta}{2t} \tag{5-17}$$

$$(\sigma_z)_{z=-\frac{t}{2}} = -q \tag{5-18}$$

At the bottom point of the plate, since $\tau_{rz} = 0, \tau_{\theta z} = 0, \sigma_z = 0$, σ_r and σ_θ become the principal stresses. According to Von Mises Criterion, we have

$$\sigma_{ys} = \sqrt{\sigma_1^2 + \sigma_2^2 - \sigma_1\sigma_2} = \sqrt{\sigma_r^{\,2} + \sigma_\theta^2 - \sigma_r\sigma_\theta} \tag{5-19}$$

where σ_{ys} is the yield stress of the steel. Substituting $(\sigma_r)_{z=\frac{t}{2}}, (\sigma_\theta)_{z=\frac{t}{2}}$ (Equation 5-13, 5-14) into the equation 5-19, we get

$$\frac{36M_r^{\,2}}{t^4} + \frac{36M_\theta^{\,2}}{t^4} - \frac{36M_rM_\theta}{t^4} = \sigma_{ys}^2 \tag{5-20}$$

By rearranging this equation, we obtain:

$$t = \sqrt[4]{\frac{36}{\sigma_{ys}^2}(M_r^2 + M_\theta^2 - M_r M_\theta)} \tag{5-21}$$

The bolt head is connected to the bolt stem. Therefore only stresses in the plate around the stem are of interest. Based on the equations from W.D. Pilkey's Handbook (Page 1010), equations of the internal forces of the circular plate under centered circular distributed load q are:

$$M_r = \frac{1}{16}qR^2(3+\nu)(1-\alpha^2) - \frac{1}{16}qR^2\left[(3+\nu-\frac{1-\nu}{\alpha^2}\beta^4)(1-\alpha^2) + 4(1+\nu)\beta^2\ln\alpha\right] \tag{5-22}$$

$$M_\theta = \frac{1}{16}qR^2\left[3+\nu-(1+3\nu)\alpha^2\right] - \frac{1}{16}qR^2\left[\begin{array}{l}(1+3\nu+\frac{1-\nu}{\alpha^2}\beta^4)(1-\alpha^2) + 4(1+\nu)\beta^2\ln\alpha \\ +2(1-\nu)(1-\beta^2)^2\end{array}\right] \tag{5-23}$$

$$Q_r = \frac{1}{2}qr_0(\alpha - \frac{\beta^2}{\alpha}) - \frac{1}{2}qR\alpha \tag{5-24}$$

where R is the radius of the circular head plate (radius of the hole drilled in the concrete slab since the head is assumed to be simply supported at the edge), r_0 is the radius of the loading area on the head (circular bolt stem area attached to the head), $\alpha = \frac{r}{R}$, $\beta = \frac{r_0}{R}$.

Figure 5.3 shows bolt head thickness versus net hole clearance and ratio r_0 / R for 3/8" (9.5mm) diameter bolts which were used in this program. Figure 5.4 shows bolt head thickness versus net hole clearance and ratio r_0 / R for 1/2" (12.7mm) diameter bolts which were used previously for edge connection. Figure 5.5 gives the head thickness at the bolt stem edge versus hole radius for three type of bolts: diameter 4.76mm, 6.35mm, 7.94mm bolts. Figure 5.6 shows the combined graph of normalized coordinates. The x axis is the normalized by the distance from the bolt edge to the hole edge: $\frac{x}{R(1-\beta)}$, and y axis is the ratio of head thickness over the bolt stem diameter: $\frac{t}{r_0}$. The relation curves are drawn for different β values. Figure 5.6 can be used for steel shear bolt design. The maximum thickness at the stem, for x = 0 should be 0.9 to $1.2r_0$ for typical drilled holes. The thickness can be reduced with the distance from the stem.

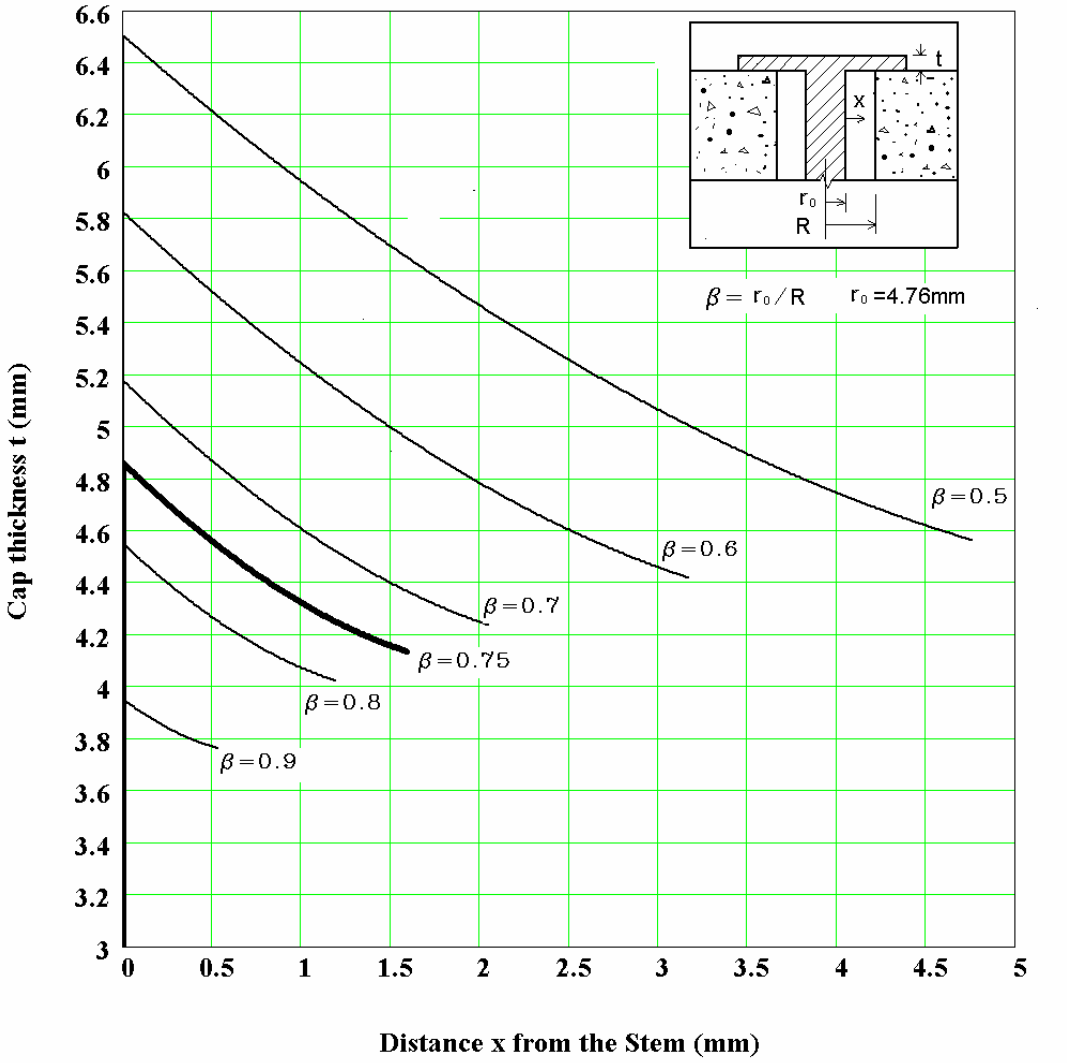

Figure 5.3 Bolt head thickness versus net hole clearance and ratio r_0 / R for 3/8" diameter bolts

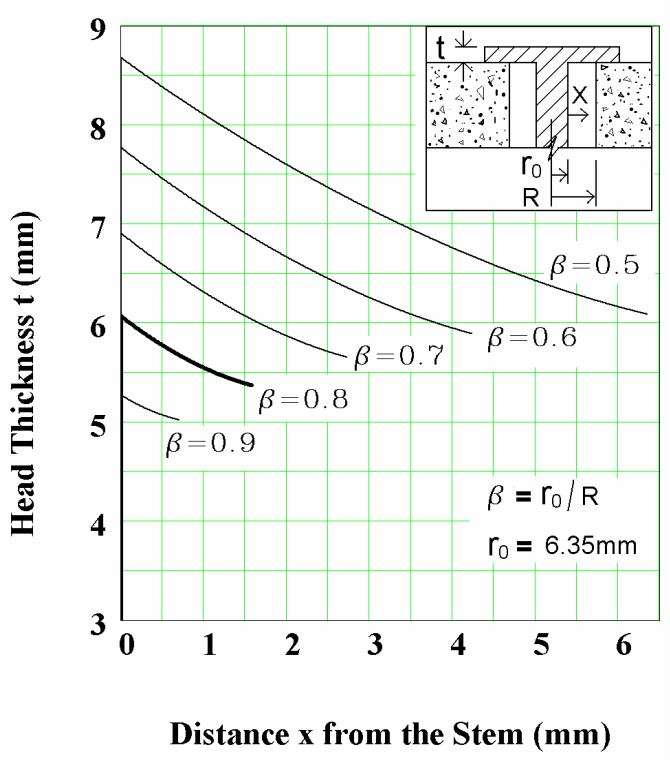

Figure 5.4 Bolt head thickness versus net hole clearance and ratio r_0 / R for 1/2” diameter bolts

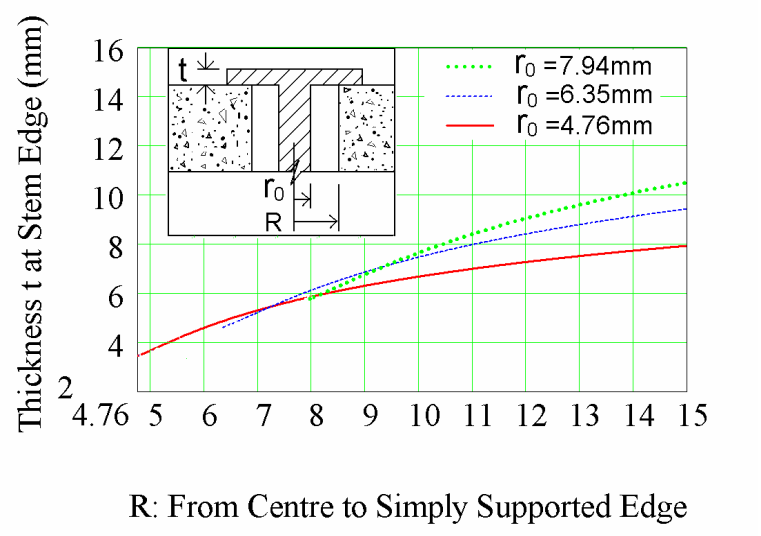

Figure 5.5 Head thickness at the bolt stem edge versus hole radius

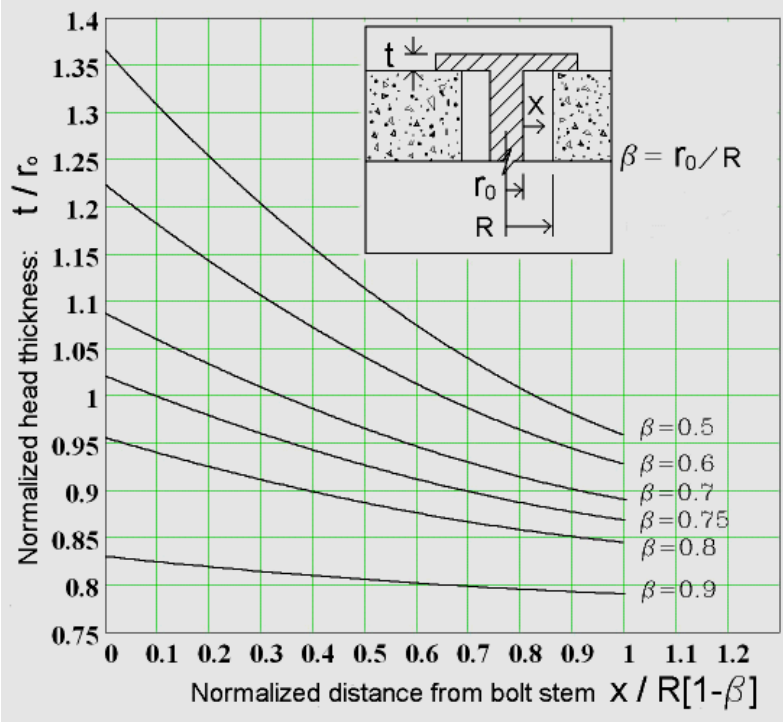

Figure 5.6 Normalized bolt head thickness versus normalized distance from bolt stem (for all stem diameters)

5.1.1.2 Determination of Bolt Head Thickness using Finite Element Method

In order to check the results according to thick plate theory, eight-node isoparametric finite element (Figure.5.7) was used to analyze the bolt head for the bolt of 3/8" diameter (2R=9.5mm). The hole diameter ($2r_0$) is 6.75mm and $\beta = \frac{r_0}{R} = 0.67$. This element is based on the Mindlin thick plate assumptions: 1) The plate deflection is small; 2) The line perpendicular to the mid plane before deformation remains straight but not necessary normal to the mid plane after deformation; 3) The stress perpendicular to the mid plane can be neglected (Figure.5.7). The displacements w , θ_x, θ_y are expressed as

$$\begin{Bmatrix} w \\ \theta_x \\ \theta_y \end{Bmatrix} = \begin{Bmatrix} w \\ \dfrac{\partial w}{\partial x} + \phi_x \\ \dfrac{\partial w}{\partial y} + \phi_y \end{Bmatrix} \tag{5-25}$$

where ϕ_x, ϕ_y denote the average shear deformation.

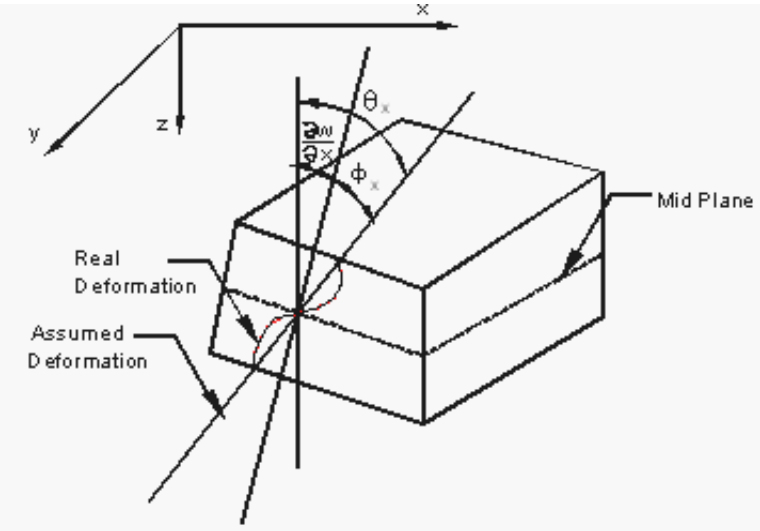

Figure 5.7 Mid-thick plate section deformation

The shape functions of this type element are

$$\begin{aligned} N_1(\xi,\eta) &= -\frac{1}{4}(1-\xi)(1-\eta)(1+\xi+\eta) \\ N_2(\xi,\eta) &= \frac{1}{2}(1-\xi^2)(1-\eta) \\ N_3(\xi,\eta) &= \frac{1}{4}(1+\xi)(1-\eta)(-1+\xi-\eta) \\ N_4(\xi,\eta) &= \frac{1}{2}(1-\eta^2)(1+\xi) \end{aligned} \tag{5-26}$$

$$N_5(\xi,\eta)=\frac{1}{4}(1+\xi)(1+\eta)(-1+\xi+\eta)$$

$$N_6(\xi,\eta)=\frac{1}{2}(1-\xi^2)(1+\eta)$$

$$N_7(\xi,\eta)=\frac{1}{4}(1-\xi)(1+\eta)(-1-\xi+\eta)$$

$$N_8(\xi,\eta)=\frac{1}{2}(1-\xi\ )(1-\eta^2)$$

To analyze one quarter of the steel bolt head (evenly distributed thickness), eight-node isoparametric plate element (Figure 5.8) is used.

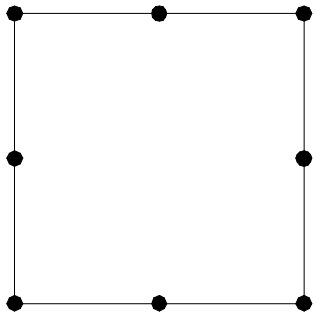

Figure 5.8 Eight-node isoparametric plate element

The geometric coordinates are expressed as:

$$\begin{bmatrix} x \\ y \end{bmatrix}=\sum_{i=1}^{8} N_i \begin{bmatrix} x_i \\ y_i \end{bmatrix} \tag{5-27}$$

The quadrant is discretized into eleven elements as shown in Figure 5.9. ABE area represents a quadrant of the bolt stem; BE is the edge of the bolt, and CF is corresponding to the edge of the drilled hole in the concrete slab. CDGF area is supported by the concrete slab surface. In the FE model, the vertical displacement on the hole edge CF are restrained. The calculated four Gauss point internal forces of element ② and ④ are as follows.

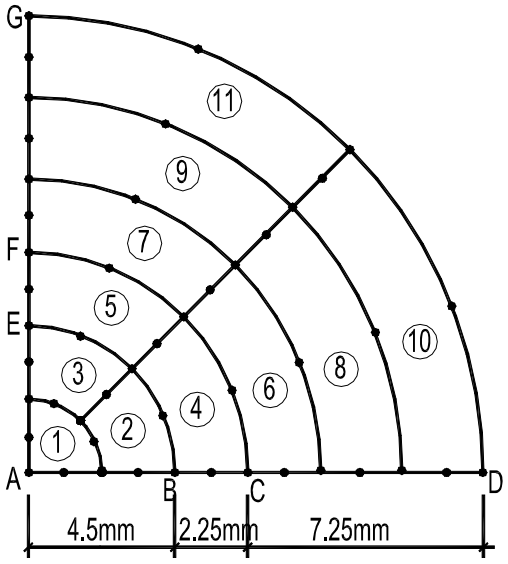

Figure 5.9 Finite element mesh for a quadrant

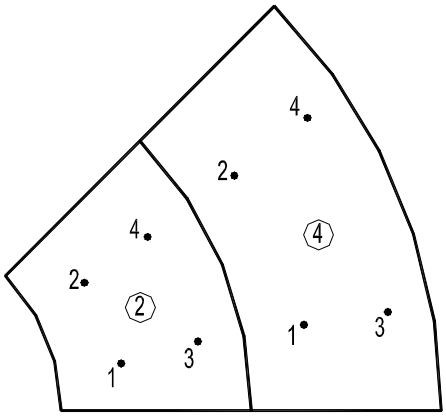

Figure 5.10 Gauss point numbering of element 2 and 4

G.P.	X-COORD.	Y-COORD.	X-MOMENT	Y-MOMENT	XY-MOMENT	XZ-S.FORCE	YZ-S.FORCE
ELEMENT NO.=	2						
1	2.6867	.4605	.27516E+04	.29921E+04	-.42194E+02	-.53757E+03	-.71433E+02
2	2.2206	1.5679	.28417E+04	.29186E+04	-.11877E+03	-.43696E+03	-.32884E+03
3	3.9661	.6788	**.20123E+04**	**.25556E+04**	-.87766E+02	-.79146E+03	-.14415E+03
4	3.2833	2.3195	.21997E+04	.23721E+04	-.27282E+03	-.66269E+03	-.45596E+03

```
 ELEMENT NO.=    4
1    4.9029     .8388  .11612E+04  .50288E+03  .10775E+03 -.80238E+03 -.13408E+03
2    4.0603    2.8688  .93977E+03  .72450E+03  .32949E+03 -.66202E+03 -.47296E+03
3    6.1830    1.0579  .17840E+03  .27164E+03 -.16046E+02 -.63595E+03 -.10511E+03
4    5.1204    3.6178  .20885E+03  .24092E+03 -.46271E+02 -.52457E+03 -.37644E+03
```

The moments at stem edge BE are calculated assuming that the average of the two adjacent elements represent the actual moments:

$$M_r = (2012.3 + 1161.2)/2 = 1586.75 N*mm$$

$$M_\theta = (2555.6 + 502.88)/2 = 1529.24 N*mm$$

Using Von Mises Criterion (Equation 5.19) and Equation 5-21, the required thickness is t = 5.03 mm. This thickness corresponds well with the thickness calculated using thin plate theory which is in this case equal to 5.2mm (Figure 5.3).

5.1.2 Determination of Bolt Head Area

The CSA A23.3-04 requires that the head area of the headed shear stud shall be at least ten times the stud stem area. This is not suitable for the shear bolts. Since the headed studs are embedded in the concrete slab, part of the force in the stud stem may come from bond between the stem and the concrete. Also, there is no space (hole) between concrete and the stem.

The main consideration for the bolt head area is to check the bearing resistance of the concrete under the bolt head. In the Canadian structural code CSA A23.3-04, Clause 10.8.1 specifies that the factored bearing resistance of the concrete can be taken as $0.85\phi_c f_c' A_1$, and when the supporting surface is wider than the loaded area, the resistance can be multiplied by a magnifying factor of up to 2, where ϕ_c is the material strength reducing factor for concrete, f_c' is the concrete compressive strength, and A_1 is the loaded area. Thus, maximum nominal concrete resistance of $1.70 f_c' A_1$ was used in this calculation. Assuming the bolt stem yields at failure and equating the yield load F_{bolt} and the bearing resistance F_n, the following equation can be obtained.

$$F_{bolt} = F_n \tag{5-28}$$

$$F_{bolt} = f_{yv} \pi r_0^2 \tag{5-29}$$

$$F_n = 1.7\phi_c f_c^{'}\pi(R_0^2 - R^2) = 1.7\phi_c f_c^{'}\pi(R_0^2 - \frac{r_0^2}{\beta^2}) \quad (5\text{-}30)$$

The bolt head area A_c is πR_0^2 and the stem section area A_b is πr_0^2. R_0 and r_0 are the radii of the head and bolt stem section respectively. R is the hole diameter. f_{yv} is the yield strength of the bolts.

$\beta = \frac{r_0}{R}$. From equations (5-28) ~ (5-30), the ratio of $\frac{A_c}{A_b}$ $(= \frac{R_0^2}{r_0^2})$ was derived.

$$\frac{A_c}{A_b} = \frac{f_{yv}}{1.70\phi_c f_c^{'}} + \frac{1}{\beta^2} \quad (5\text{-}31)$$

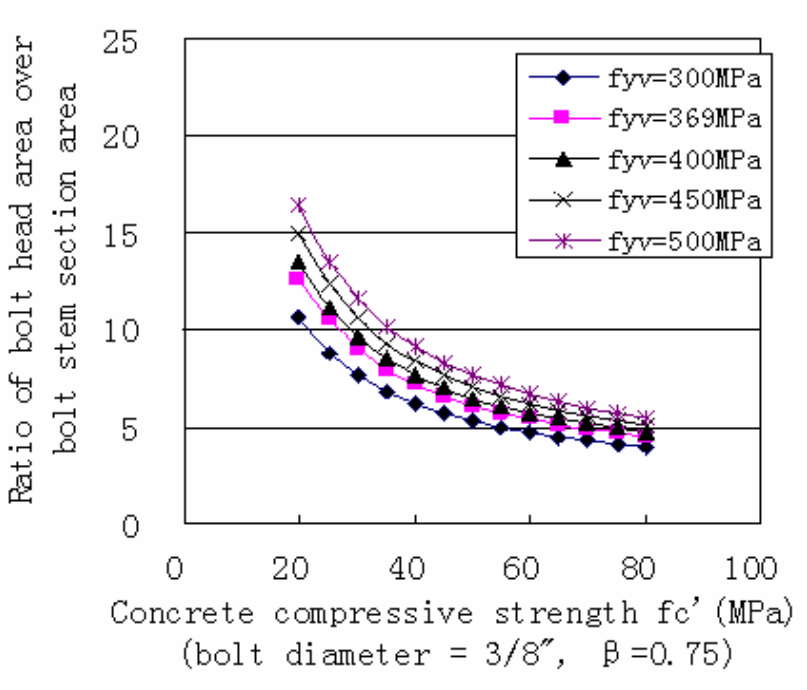

(a)

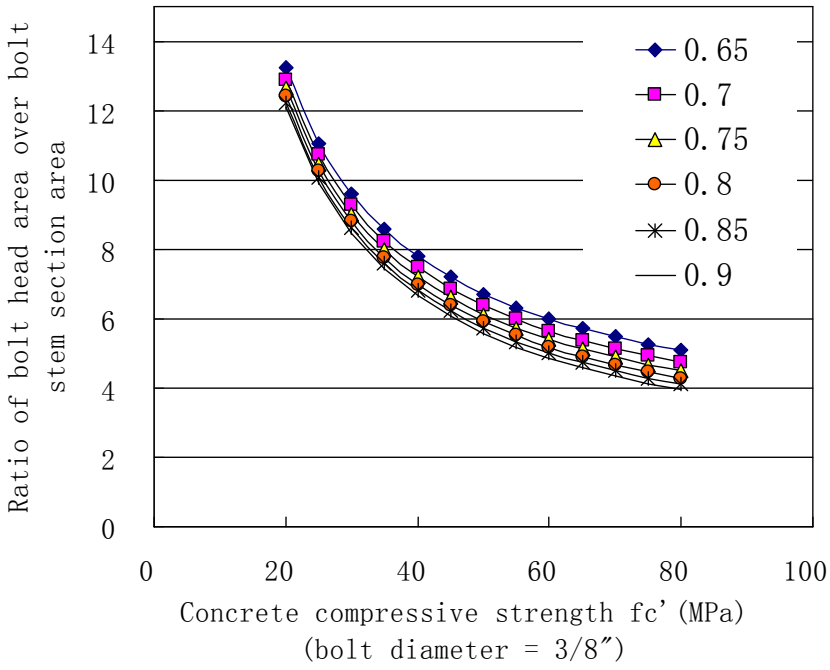

(b)

Figure 5.11 Ratio of bolt head area over bolt stem section area versus concrete compressive strength

(a) $\frac{A_c}{A_b}$ versus $f_c^{'}$ (f_{yv} varies, $\beta = 0.75$); (b) $\frac{A_c}{A_b}$ versus $f_c^{'}$ (β varies, $f_{yv} = 370MPa$)

In Equation 5-31, the ratio of the bolt head area over the bolt stem area is related to three parameters: the ratio (β) of bolt stem radius r_0 over the radius of the hole, the yield strength of the bolts f_{yv}, and the concrete strength $f_c^{'}$. Figure 5.11a gives the ratio of bolt head area over bolt stem section area for a 3/8" (9.5mm) diameter bolt. The ratio varies with the concrete strength and the steel bolt yield strength. For low strength concrete, the ratio is higher. Steel bolts with higher yield strength need bigger head areas. The effect of bolt diameter is very small. For conservative design, the bolt head area should be 16 times the bolt stem section area for bolts of maximum 500 MPa yield strength. Figure 5.11b shows the ratio of bolt head area over bolt stem section area for a 3/8" diameter bolt

with different ratio of β. For the same shear bolt stem and concrete strength, when β increase, the bolt head area will decrease.

5.1.3 Stresses in a Concrete Slab Caused by a Shear Bolt

Linear finite element analysis was carried out for calculation of the concrete stress distribution under the shear bolts. It was done to determine the influence of the confining stress from the head on concrete underneath the head.

Assume the head and the washer of each shear bolt are applying uniform pressure on top and bottom surfaces of the concrete slab (Figure 5.12 a). The resultant of the pressure on concrete is assumed to be equal to the yield force in the bolt stem. Pressure $q = 19.7$ MPa produced by yield force was used herein (Figure 5.12 b). Since the bolt heads are small compared with the slab area, the stresses caused by bolt heads were only affecting a small vicinity zone. The stresses in the slab from the effect of bolts are also symmetric about the slab mid-surface. Therefore, the stresses caused by each bolt in the concrete slab can be calculated using axisymmetric analysis.

Let the longitudinal axis of the bolt stem be the axis of symmetry, and a vertical slab section ABCD is isolated as show in Figure 5.13. Since the slab is symmetric in geometry and loading about the slab mid plane, the length of ABCD is 240mm (which is twice the slab thickness) and its height is 60 mm. The bottom side AD is restrained in y direction only. (The displacement of the mid plane of the concrete slab remains zero under equal pressure from bottom and top surface). The other boundaries are free.

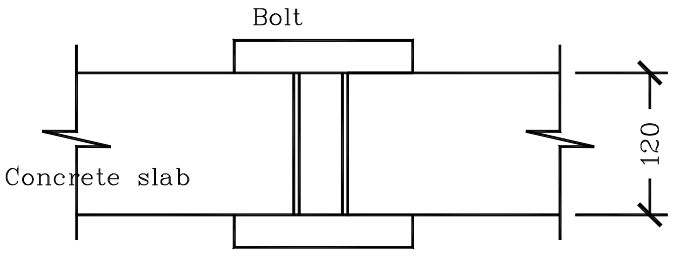

(a) Bolt and slab

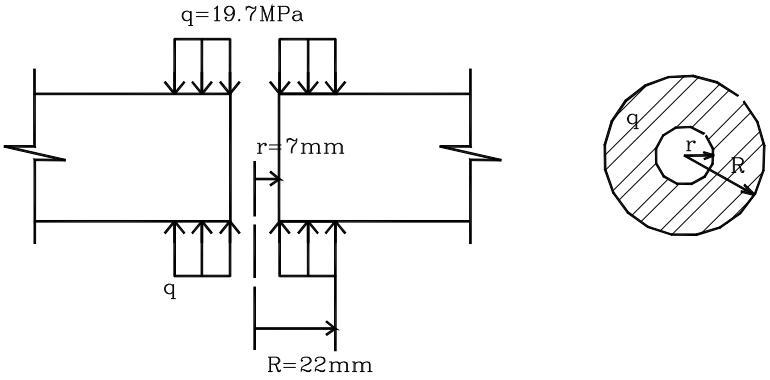

(b) Pressure on the slab by bolt head

Figure 5.12 Pressure on concrete slab surfaces by bolts head and washer

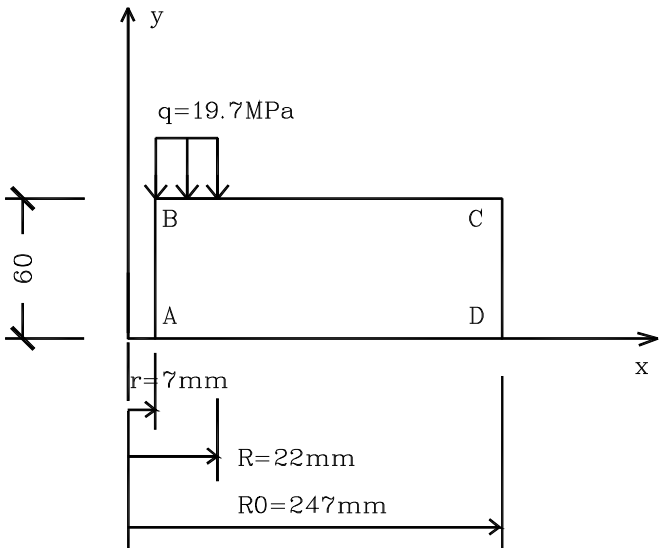

Figure 5.13 Axisymmetric analysis of the concrete slab around the bolts hole

From the results, it is found that the locations beyond $r = 150$ mm from the bolt hole center are affected by very small stresses (close to zero). Therefore it is assumed that the affected distance is 150mm (1.25h). Figure 5.14 shows stress $\sigma_x, \sigma_y, \sigma_z, \tau_{xy}$ distribution along top line BC of the section. Figure 5.15 shows stress $\sigma_x, \sigma_y, \sigma_z, \tau_{xy}$ distribution along bottom line AD of the section.

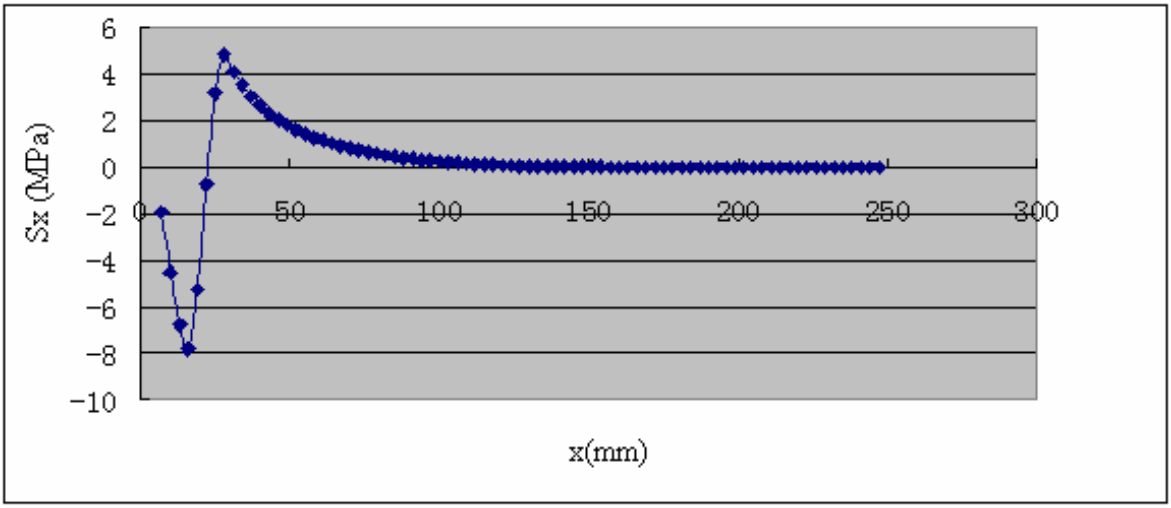

(a) Stress σ_x, (Sx) distribution along top line BC

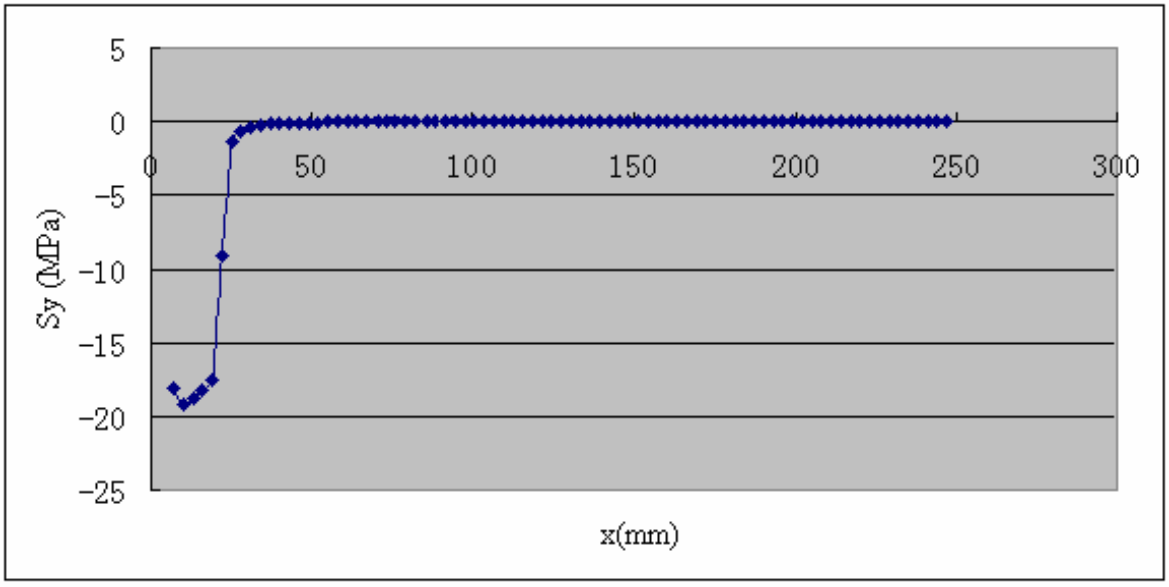

(b) Stress σ_y, (Sy) distribution along top line BC

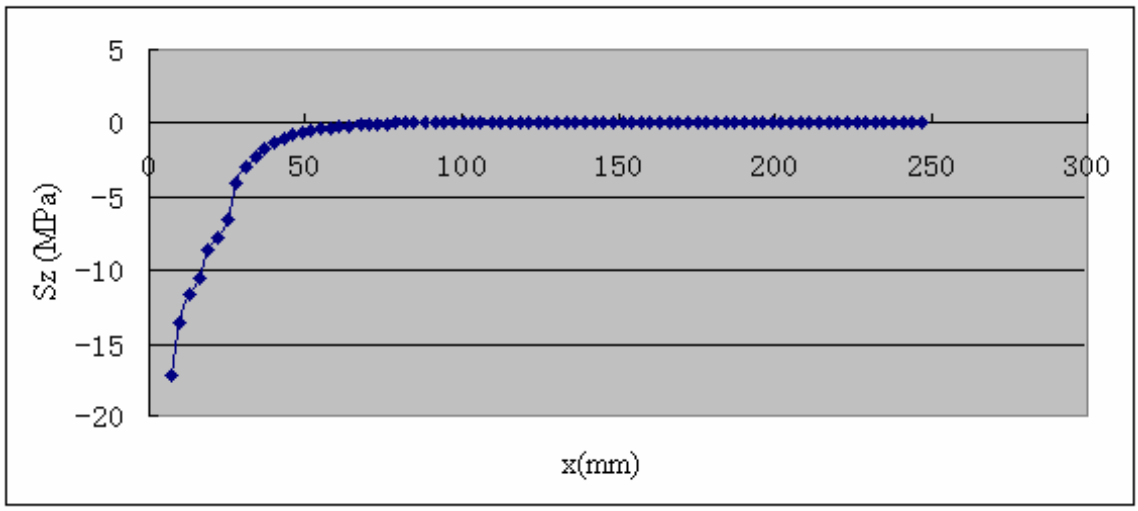

(c) Stress σ_z , (Sz) distribution along top line BC

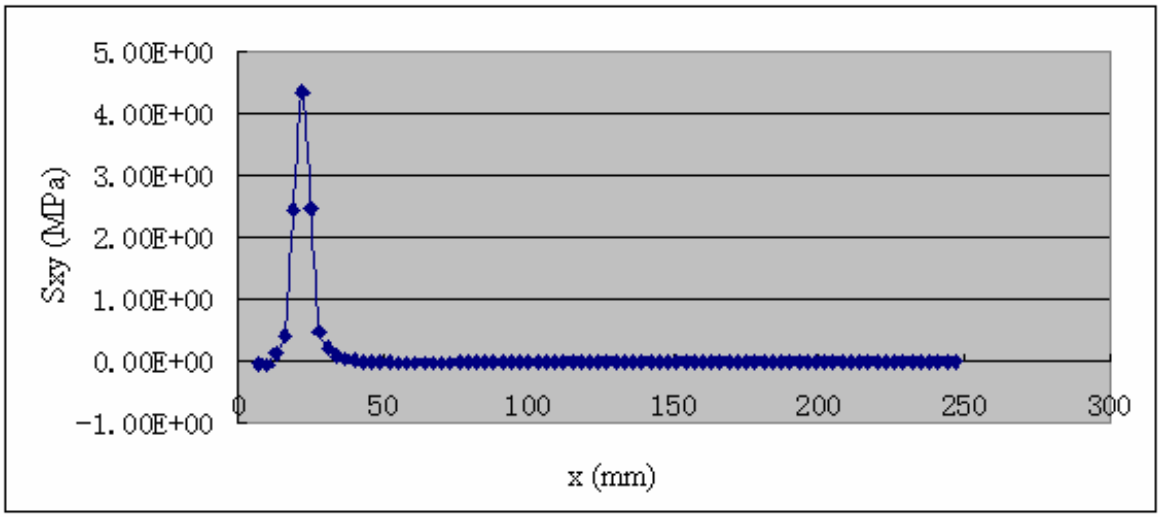

(d) Stress τ_{xy} distribution along top line BC

Figure 5.14 Stress distribution along the top line BC

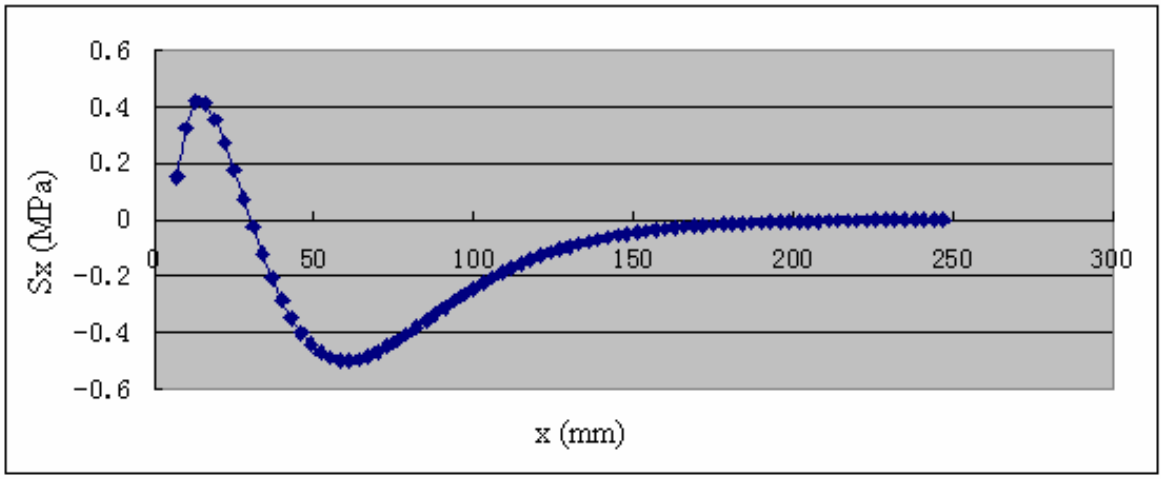

(a) Stress σ_x, (Sx) distribution along bottom line AD

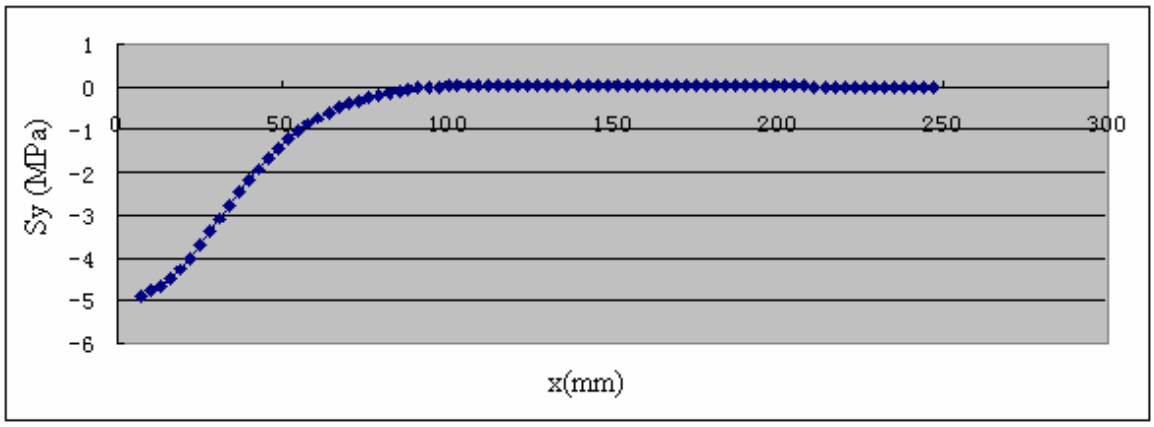

(b) Stress σ_y, (Sy) distribution along bottom line AD

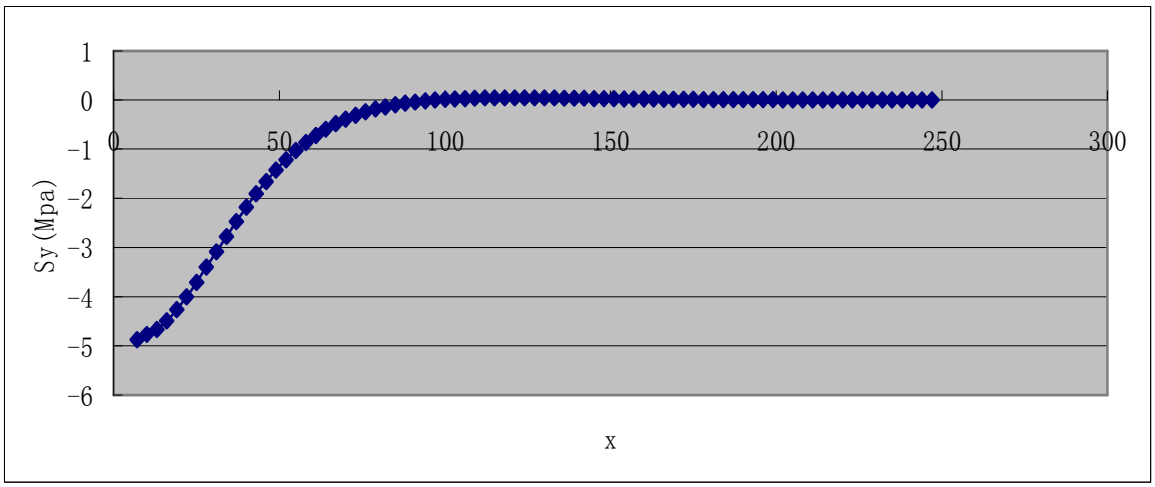

(c) Stress σ_z, (Sz) distribution along bottom line AD

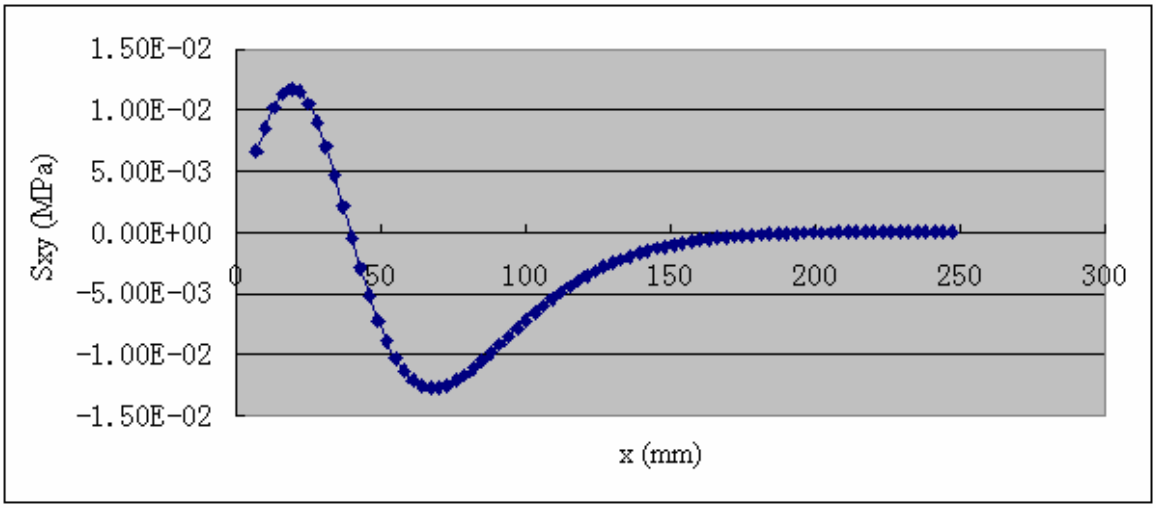

(d) Stress τ_{xy}, (Sxy) distribution along bottom line AD

Figure 5.15 Stress distribution along the top line AD

5.2 Design of Steel Shear Bolts for Concrete Flat Slab Strengthening

This section describes the design of the flat concrete slab strengthened with steel shear bolts, including the strength of the concrete slab and layout of the shear bolts in the slab.

5.2.1 Strength of the Retrofitted Slab

The punching shear strength of the slab strengthened with shear bolts can be calculated using similar equations and provisions of CSA A23.3-04 for headed shear studs. However, the critical section area is reduced due to drilled holes along the perimeter of the critical section. Thus the effective critical section perimeter length $b_0^{'}$ is equal to ($b_0 - n * d_0$), where b_0 is the critical section ($d/2$ from column perimeter) length. n is the number of holes drilled along critical section perimeter. d_0 is the diameter of the drilled holes.

In design, the shear bolt tension capacity (along bolt stem) can be taken as the smaller of the following three cases:

(1) The yielding force (F_t) of the bolt stem at the root of thread grooves,

$$F_t = f_{yv} * A_n \tag{5-32}$$

where f_{yv} is the yield (tension) strength of the shear bolts, A_n is the section area of the bolt stem excluding threads.

(2) The yield shear force (F_{s1}) by threads on the bolt stem.

(3) The yield shear force (F_{s2}) by threads on the nut.

Case (2) and case (3) can be considered together. According to Barrett's "Fastener Design Manual" (1990), the pullout load P of the bolt against the nut can be calculated using the following equation:

$$P = \frac{\pi d_m L f_v}{3} \tag{5-33}$$

where d_m is the pitch diameter of the threads, L is the length of thread engagement, f_v is the smaller shear strength (stress) of the two materials of the bolt and nut.

Consequently, the punching shear strength v_r (stress) of the retrofitted slab is

$$v_r = v_c + v_s \tag{5-34}$$

where v_c is the factored shear resistance from concrete, v_s is the factored shear resistance from shear reinforcements.

$$v_s = \frac{\phi_s n F_b}{b_0' s} \tag{5-35}$$

where $\phi_s = 0.85$ is reduction factor of steel strength. n is the number of shear bolts in a periphery row parallel to column perimeter. F_b is the smaller result of equation (5-32) and (5-33). s is the radial spacing of the shear reinforcement. b_0' is the effective critical section perimeter length. Shear resistance from concrete in the shear reinforced zone is:

$$v_c = 0.28\lambda\phi_c\sqrt{f_c'}$$

Maximum shear resistance of section with shear reinforcement should satisfy the following equation:

$$v_{r\max} \le 0.75\lambda\phi_c\sqrt{f_c'}$$

Seismic requirements of the concrete slabs strengthened with shear bolts can follow CSA 23.3-04 (Clause 21.12.3), i.e. equation (2-47) and (2-51) in Chapter 2, but effective critical section and shear strength of bolt threads are necessary to be used.

5.2.2 Shear Bolt Layout in the Flat Concrete Slab

Shear bolts layout requires determination of a radial pattern or an orthogonal pattern in the concrete slab. This section compares the two patterns and discusses the number of bolt rows and spacing between the bolts in radial and tangential direction. Radial direction is defined as away from the column (S_0, S_1 in Figure 5.16). Tangential direction is along the perimeters of shear bolts and parallel to the column sides (S_2 in Figure 5.16).

5.2.2.1 Comparison of Radial and Orthogonal Layout Patterns of Shear Bolts

As described in section 4.3.2, for slab without openings, the slab (SW9) strengthened with radial bolts layout pattern showed close capacity and ductility to that of the slab (SW4) with orthogonal bolt pattern. For slab with openings, the slab (SW8) with radial bolts showed some moment capacity

increase, however, SW8 had higher concrete strength (50MPa) than SW7 (40MPa). Moreover, SW8 showed some decrease in ductility. Therefore, for the flat slab column structure, if the lateral loading direction is parallel to the two main orthogonal directions, just as the case in the experiments, the orthogonal bolt layout would be preferable. However, in real situations lateral load comes from an arbitrary direction and possibly a more uniform bolt distribution around the column might be preferable. For strengthening method, it is recommended here to combine the two patterns, i.e. the orthogonal pattern plus an extra line of bolts in radial direction in each quadrant. Due to interference from the flexural reinforcement in the concrete slab, the radial bolts may not form a straight line. A simple rule can be followed that the shear bolts pattern should be symmetric about the two main axes of the column.

5.2.2.2 Bolt Spacing in Radial Direction

Let's assume the shear bolts are orthogonally installed as shown in Figure 5.16. To decide the bolts spacing S_0 and S_1, the factor considered here is the punching shear crack inside the slab. According to the observations, the angles of punching shear cracks in the slab without shear reinforcements range from 25~35 degree. Also, Regan (1974) pointed out that "the critical shear cracks, at a connection without shear reinforcement, extend from heads at about d/4 to d/2 from the column faces, to tails situated where the cracks intersect the main tensile steel at distances of 2d or more from the column" (Figure 5.17) The shear reinforcement should be placed across the crack in the middle of the slab. For specimens strengthened with shear bolts, the spacing S_1 need special considerations, which are explained later in this section.

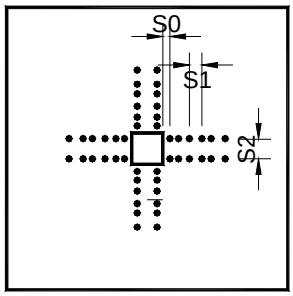

Figure 5.16 Spacing S_0, S_1 and S_2 of shear bolts

(S_0, S_1 - radial direction spacing; S_2 - tangential direction spacing)

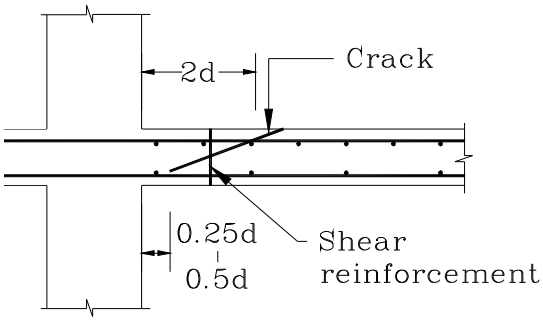

Figure 5.17 Punching shear cracks in the concrete slab without shear reinforcement

For slabs with shear reinforcements, the shear cracks in the zone with shear reinforcement have steeper inclined angle (θ_1) than that of cracks in the non-shear reinforced zones (θ_2). Dilger and Ghali (1980) found that in the concrete slab with headed shear studs, angle θ_1 can be about 40 – 50 degree, while angle θ_2 is usually around 20– 30 degrees (Figure 5.18).

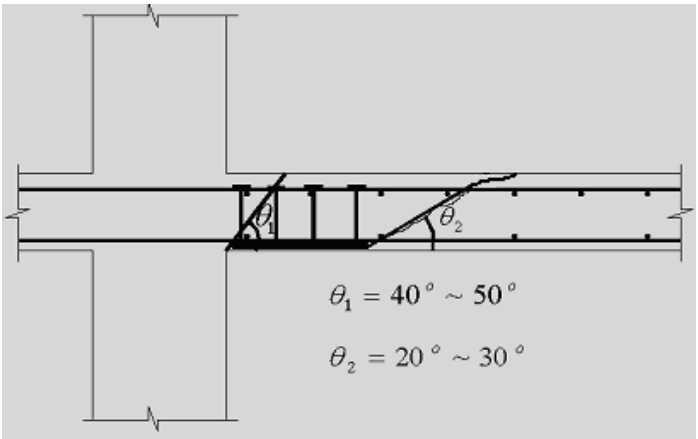

Figure 5.18 Shear rack angles in slab zones with or without shear studs

The tests done in this research showed similar crack angles to those mentioned above. The three specimens without shear bolts, SW1, SW5, and SW6, were subjected to sudden punching shear

failure. The distances between the column center and the crack tails were measured, which are shown in Figure 5.19(a), (b) and (c). The heads of all shear cracks were assumed at the column faces. Therefore, the crack angles can be estimated using the slab thickness and the distances of the crack tails to the column faces. For example, for SW1 (Figure 5.19(a)), the tail distances to column faces are 313mm, 310mm, 350mm, and 470mm. The slab thickness is 120mm. Thus the corresponding angles are 21^o, 21.1^o, 18.9^o, and 14.3^o. The largest angle for SW5 (Figure 5.19(b)) is 25^o; the largest angle for SW6 is 33.2^o. SW6 is the specimen with openings as shown in Figure 5.19(c). In reality, these angles are likely to be slightly larger than the above calculations suggest due to spalling of the concrete cover which likely made the presented length measurements larger.

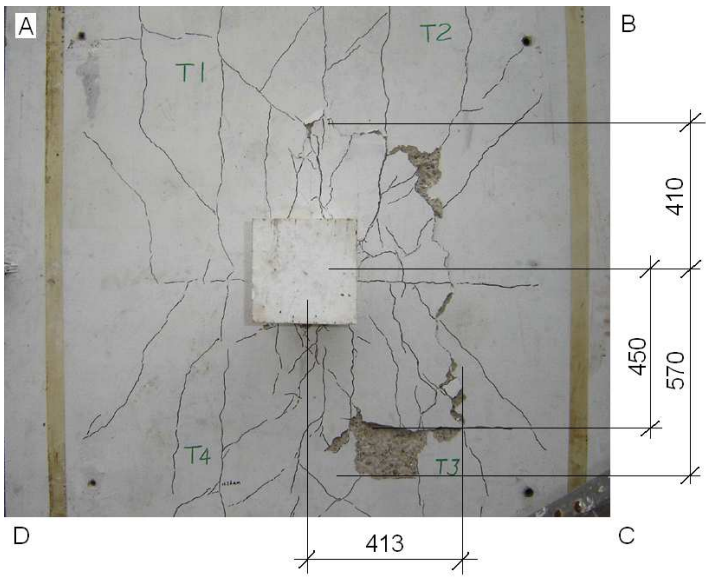

(a) SW1

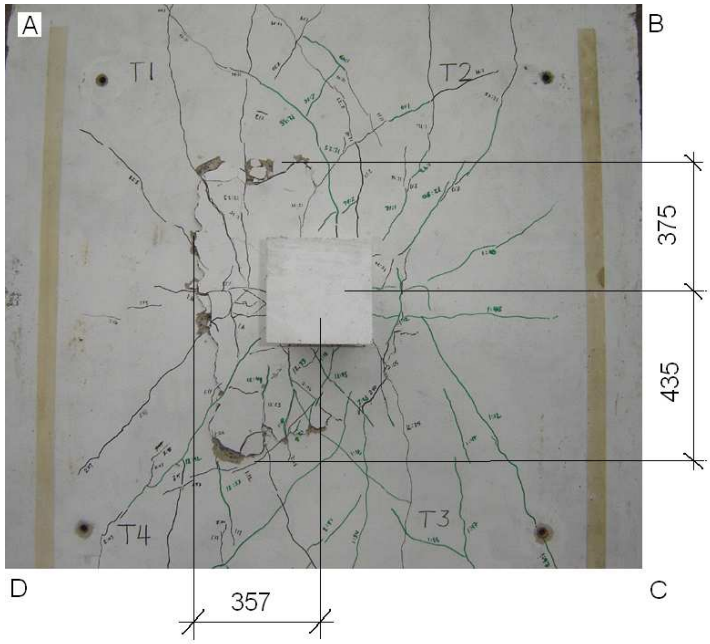

(b) SW5

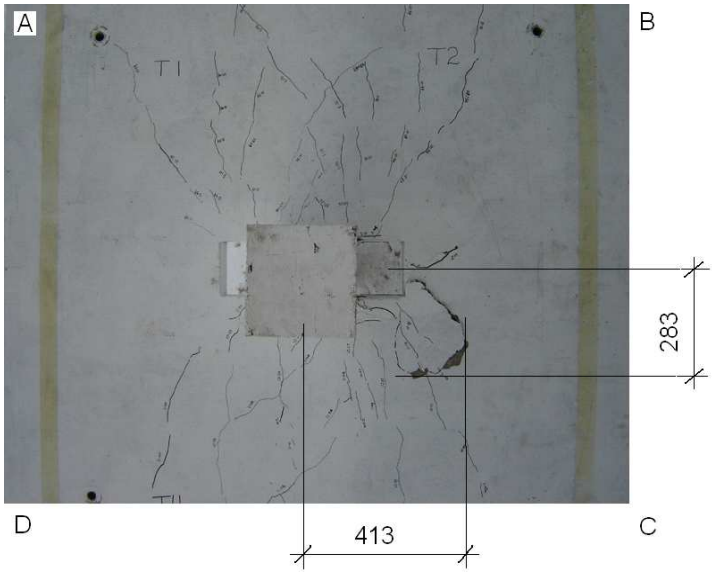

(c) SW6

Figure 5.19 Distance of punching shear crack tail to the column center

The slabs with openings provide an opportunity to observe the crack angles on the opening edges. The three slabs with openings were SW6 (without shear bolts), SW7 and SW8 (with shear bolts). Figure 5.20 shows the cracks of SW6 at the opening face parallel to the lateral load direction. It is found the main cracks are at angles of about 31 degree, which corresponds well with the angle estimated from surface measurements. In Figure 5.21, the slab (SW8) was strengthened with shear bolts around the openings and in the radial layout. The angles of the main inclined cracks are about 45 – 50 degree. In Figure 5.22, the slab (SW7), strengthened by shear bolts but in orthogonal pattern, has crack angles smaller than 45^0. The reason can be the fact that the shear bolts were not as close to the openings as in SW8. It also shows that the crack angle in shear reinforced slabs varies from $20-50^o$, depending on the location of the bolts.

All these main shear cracks started from the column faces. Therefore, the distance between the first shear bolts and the column face, S_0, should cross the inclined crack. Therefore, assuming bolts cross the crack in the middle:

For $\theta_1 = 40^o$, S_0 = 0.5*d/(tan 40^o) = 0.59 d.

For $\theta_1 = 50^o$, S_0 = 0.5*d/(tan 50^o) = 0.42d.

Considering the beneficial effect (confinement) of the bolt head it can be recommended that $S_0 = 0.45d \sim 0.55d$ from the column face. This also covers the fact that the drilling of the holes requires certain distance from the column which is at least 45mm.

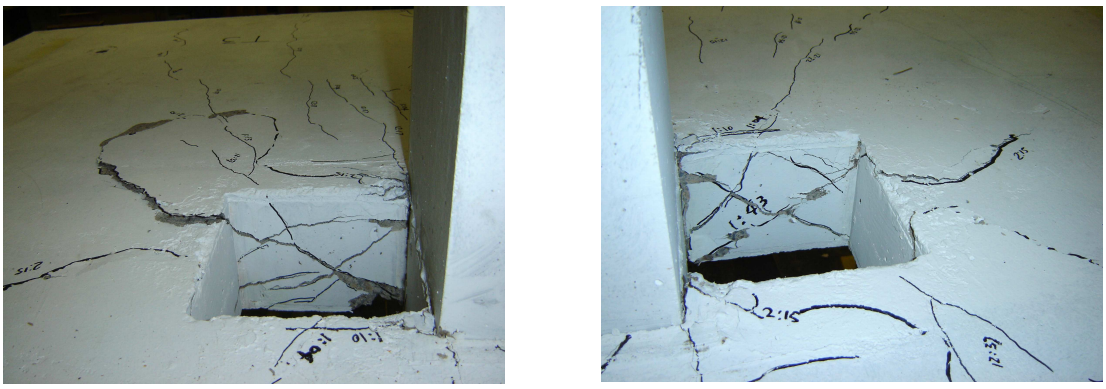

(a) (b)

Figure 5.20 Shear cracks in the opening edges of the slab (SW6) without shear bolts

(a)

(b)

Figure 5.21 Shear cracks in the opening edges of the slab (SW8) with shear bolts of radial layout

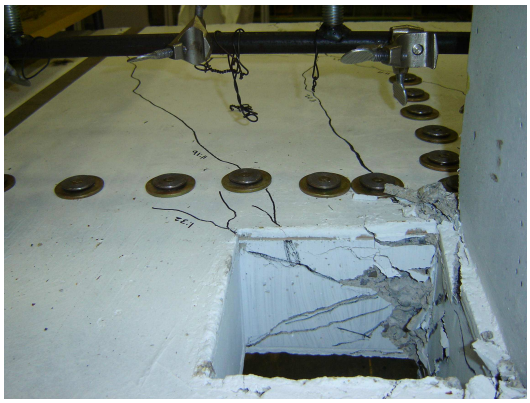

(a)

(b)

Figure 5.22 Shear cracks in the opening edges of the slab (SW7) with shear bolts of orthogonal layout

Two approaches were used to theoretically determine the spacing S_1 between shear bolt rows.

(1) Crack Angle Approach

Figure 5.23 shows the section of the concrete slab strengthened with shear bolts. The crack angle is θ_1. The crack is assumed going across from the bolt edge from the bottom to the top flexural rebar on the adjacent bolt outer edge. Based on observation, the crack angle θ_1 was assumed to be from 40^o to 50^o. The relation is:

$$\tan\theta_1 = d / x \tag{5-36}$$

where d is the effective depth of the flexural reinforcement, d = h-c-b. x is the spacing between the two adjacent bolt outer stem edges, x = $S_1 + b_1$, b_1 is the diameter of the shear bolts.

Table 5.1 shows the ratio of S_1/d for slabs of thickness from 120mm to 900mm and of 40^o crack angles. It is found S_1/d is between 1.08 and 1.17. Table 5.2 gives the ratio of S_1/d for crack angle 50^o for slabs of thickness from 120mm to 900mm. It shows the ratio S_1/d is between 0.73 and 0.82.

Considering that steeper cracks are likely to form under heavy vertical loads, it is recommended that:

For normal loads ($v_f \le 0.56\lambda\phi_c\sqrt{f_c'}$), $S_1 \le 1.0d$;

For heavy loads ($v_f > 0.56\lambda\phi_c\sqrt{f_c'}$), $S_1 \le 0.75d$

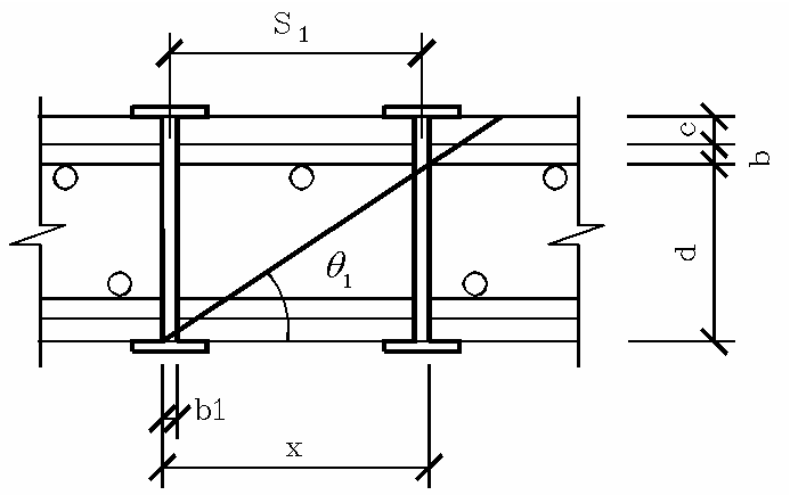

Figure 5.23 Crack angle θ_1 in the slab strengthened with shear bolts

Table 5.1 Spacing s_1 when $\theta_1 = 40^o$ using crack angle method

Slab thickness h (mm)	Assumed rebar diameter b (mm)	Assumed shear bolt diameter b_1 (mm)	Concrete cover c (mm)	Assumed effective depth d (mm) d=h-c-b	Angle θ_1 (degree)	x /d= $1/(\tan\theta_1)$	$S_1 = x - b_1$	S_1 /d
120.00	11.30	9.50	20.00	88.70	40	1.19	96.21	**1.08**
150.00	11.30	9.50	20.00	118.70	40	1.19	131.96	**1.11**
200.00	16.00	9.50	20.00	164.00	40	1.19	185.95	**1.13**
250.00	16.00	12.50	20.00	214.00	40	1.19	242.54	**1.13**
300.00	19.50	12.50	20.00	260.50	40	1.19	297.95	**1.14**
350.00	19.50	12.50	20.00	310.50	40	1.19	357.54	**1.15**
400.00	25.00	15.00	25.00	350.00	40	1.19	402.11	**1.15**
450.00	25.00	15.00	25.00	400.00	40	1.19	461.70	**1.15**
500.00	25.00	15.00	25.00	450.00	40	1.19	521.29	**1.16**
900.00	25.00	20.00	25.00	850.00	40	1.19	992.99	**1.17**

Table 5.2 Spacing s_1 when $\theta_1 = 50^o$ using crack angle method

Slab thickness h (mm)	Rebar diameter b (mm)	Shear bolt diameter b_1 (mm)	Concrete cover c (mm)	Effective depth d (mm) d=h-c-b	Angle θ_1 (degree)	x /d $=1/(\tan\theta_1)$	$S_1 = x - b_1$	S_1/d
120.00	11.30	9.50	20.00	88.70	50	0.84	64.93	**0.73**
150.00	11.30	9.50	20.00	118.70	50	0.84	90.10	**0.76**

200.00	16.00	9.50	20.00	164.00	50	0.84	128.11	**0.78**
250.00	16.00	12.50	20.00	214.00	50	0.84	167.07	**0.78**
300.00	19.50	12.50	20.00	260.50	50	0.84	206.09	**0.79**
350.00	19.50	12.50	20.00	310.50	50	0.84	248.04	**0.80**
400.00	25.00	15.00	25.00	350.00	50	0.84	278.68	**0.80**
450.00	25.00	15.00	25.00	400.00	50	0.84	320.64	**0.80**
500.00	25.00	15.00	25.00	450.00	50	0.84	362.59	**0.81**
900.00	25.00	20.00	25.00	850.00	50	0.84	693.23	**0.82**

(2) Comparison with Shear Studs Requirements

The Canadian concrete code CSA A23.3-04 includes design provisions for headed shear studs. In Clause 13.3.8.6, it specifies the maximum bolt row spacing S_1 to be 0.75d or 0.5d, depending on the level of factored shear stress v_f at the critical section. If $v_f \le 0.56\lambda\phi_c\sqrt{f_c'}$, maximum S_1 can be 0.75d, otherwise, S_1<0.5d. Figure 5.25 shows the concrete slab section with headed shear studs. Note the heads of the studs are at the level of the outer flexural reinforcing bars. Also, t is the head thickness, h_s is the net length of the bolt stem. R_s is the radius of the shear stud head ($R_s = R_0$). Therefore the radial spacing S_1 (0.75d or 0.5d) for shear studs is known, which can be used to determine the radial shear bolt spacing S_1 in Figure 5.24.

Assuming that the compressive stresses under the head follow 45^0 angle, for both stud and bolt, the comparison can be made between the two types of reinforcing elements. Bolts are longer than studs; they cover whole thickness of the slab. Bolts also, generally have larger diameter heads. In the following derivations, the bolt and stud head dimensions are assumed equal. This provides conservative results.

Figure 5.24 shows the assumed compressive stress distribution in the slab concrete due to the shear bolt heads. Note the bolt heads are on the slab surfaces. R_0 is the radius of the bolt head, h is the concrete slab thickness, S_1 is the bolt spacing, and Δ is the overlap length. r_0 is the radius of the shear bolt stem section.

Assuming the angle of principal compressive stress is 45 degree, the following relation for overlap length Δ in concrete slab with shear bolts can be developed as (Figure 5.24):

$$\Delta = h - (S_1 - 2R_0) \tag{5-37}$$

where h is the slab thickness, S_1 is the radial bolt spacing to be determined, R_0 is the radius of the bolt head. Assume $S_1 = \alpha h$ in calculation, where $\alpha = \frac{S_1}{h}$ for slab with shear bolts.

For the shear studs case in concrete slab (Figure 5.25), the radial spacing S_1 is known as 0.75d or 0.5d, thus the overlap length Δ in the concrete slab with shear studs is obtained as:

When $v_f \le 0.56\lambda\phi_c\sqrt{f_c'}$, $S_1 = 0.75d$,

$$\Delta = h_s - (0.75d - 2R_0) \tag{5-38}$$

When $v_f > 0.56\lambda\phi_c\sqrt{f_c'}$, $S_1 = 0.5d$,

$$\Delta = h_s - (0.5d - 2R_0) \tag{5-39}$$

where $h_s = h - 2c - 2t$, h is the slab thickness, c is the concrete cover, t is the shear stud head thickness.

To obtain the radial spacing S_1 of shear bolts in Figure 5.24, we can equal the right sides of Equation 5-37 and Equation 5-38 ($v_f \le 0.56\lambda\phi_c\sqrt{f_c'}$), and equal Equation 5-37 and Equation 5-39 ($v_f > 0.56\lambda\phi_c\sqrt{f_c'}$).

Using these equations, the ratio of $\psi = \frac{S_1}{d}$ (where S_1 is the radial spacing shear bolts) can be calculated for slabs of different thicknesses and corresponding rebar and bolt dimensions. Table 5.3 gives Coefficients $\psi = \frac{S_1}{d}$ for various slab (interior weather) thickness when $v_f \le 0.56\lambda\phi_c\sqrt{f_c'}$, Table 5.4 is similar to Table 5.3 but for slabs in exterior weather. The minimum ratio of $\psi = \frac{S_1}{d}$ is 0.84.

Table 5.5 and Table 5.6 are for the case when $v_f > 0.56\lambda\phi_c\sqrt{f_c'}$, in which the minimum ratio of $\psi = \frac{S_1}{d}$ is 0.59.

Comparing the two methods above, it is reasonable to suggest that the maximum shear bolt radial spacing S_1 be:

1). For $v_f \le 0.56\lambda\phi_c\sqrt{f_c'}$

0.75d for slab thickness above 200 mm and

1.0d for slab thickness of 200mm or less and

2). For $v_f > 0.56\lambda\phi_c\sqrt{f_c'}$

0.75d for slab thickness of 200mm or less and

0.60d for slab thickness above 200mm and

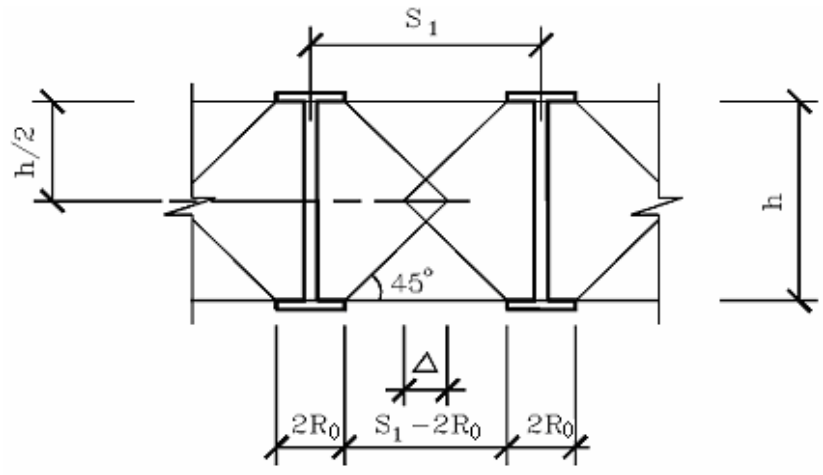

Figure 5.24 Assumed pressure in the slab concrete by the shear bolt heads

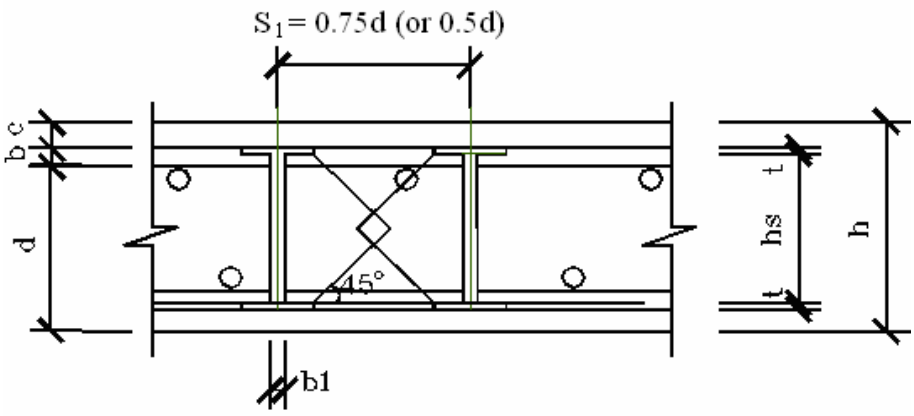

Figure 5.25 Spacing S_1=0.75d (or 0.5d) for Headed shear studs by CSA A23.3-04

Table 5.3 Coefficients $\psi = \frac{S_1}{d}$ for various slab (interior weather) thickness, $v_f \le 0.56\lambda\phi_c\sqrt{f_c'}$

Slab thickness h (mm)	Assumed rebar diameter b (mm)	Concrete cover for interior weather c (mm)	Bolt / stud head thickness t (mm)	Effective depth d (mm) d=h-c-b	Net stem length of studs h_s (mm) h_s =h-2c-2t	d/h	h_s/h	(h_s - 0.75d)/h	$\alpha = \frac{S_1}{h}$	$\psi = \frac{S_1}{d}$
120.00	11.30	20.00	3.00	88.70	74.00	0.74	0.62	0.06	0.94	**1.27**
150.00	11.30	20.00	3.00	118.70	104.00	0.79	0.69	0.10	0.90	**1.14**
200.00	16.00	20.00	4.00	164.00	152.00	0.82	0.76	0.15	0.86	**1.04**
250.00	16.00	20.00	4.00	214.00	202.00	0.86	0.81	0.17	0.83	**0.97**
300.00	19.50	20.00	5.00	260.50	250.00	0.87	0.83	0.18	0.82	**0.94**
350.00	19.50	20.00	5.00	310.50	300.00	0.89	0.86	0.19	0.81	**0.91**
400.00	25.00	25.00	5.00	350.00	340.00	0.88	0.85	0.19	0.81	**0.92**
450.00	25.00	25.00	6.00	400.00	388.00	0.89	0.86	0.20	0.80	**0.91**
500.00	25.00	25.00	6.00	450.00	438.00	0.90	0.88	0.20	0.80	**0.89**
900.00	25.00	25.00	13.00	850.00	824.00	0.94	0.92	0.21	0.79	**0.84**

Table 5.4 Coefficients $\psi = \frac{S_1}{d}$ for various slab (exterior weather) thickness, $v_f \leq 0.56\lambda\phi_c\sqrt{f_c'}$

Slab thickness h (mm)	Assumed rebar diameter b (mm)	Concrete cover for exterior weather c (mm)	Bolt / stud head thickness t (mm)	Effective depth d (mm) d=h-c-b	Net stem length of studs h_s (mm) h_s =h-2c-2t	d/h	h_s /h	(h_s - 0.75d)/h	$\alpha = \frac{S_1}{h}$	$\psi = \frac{S_1}{d}$
120.00	11.30	30.00	3.00	78.70	54.00	0.66	0.45	-0.04	1.04	**1.59**
150.00	11.30	30.00	3.00	108.70	84.00	0.72	0.56	0.02	0.98	**1.36**
200.00	16.00	30.00	4.00	154.00	132.00	0.77	0.66	0.08	0.92	**1.19**
250.00	16.00	30.00	4.00	204.00	182.00	0.82	0.73	0.12	0.88	**1.08**
300.00	19.50	30.00	5.00	250.50	230.00	0.84	0.77	0.14	0.86	**1.03**
350.00	19.50	30.00	5.00	300.50	280.00	0.86	0.80	0.16	0.84	**0.98**
400.00	25.00	37.50	5.00	337.50	315.00	0.84	0.79	0.15	0.85	**1.00**
450.00	25.00	37.50	6.00	387.50	363.00	0.86	0.81	0.16	0.84	**0.97**
500.00	25.00	37.50	6.00	437.50	413.00	0.88	0.83	0.17	0.83	**0.95**
900.00	25.00	37.50	13.00	837.50	799.00	0.93	0.89	0.19	0.81	**0.87**

Table 5.5 Coefficients $\psi = \frac{S_1}{d}$ for various slab (interior weather) thickness, $v_f > 0.56\lambda\phi_c\sqrt{f_c'}$

Slab thickness h (mm)	Assumed rebar diameter b (mm)	Concrete cover for interior weather c (mm)	Bolt / stud head thickness t (mm)	Effective depth d (mm) d=h-c-b	Net stem length of studs h_s (mm) h_s =h-2c-2t	d/h	h_s /h	(h_s - 0.50d)/h	$\alpha = \frac{S_1}{h}$	$\psi = \frac{S_1}{d}$
120.00	11.30	20.00	3.00	88.70	74.00	0.74	0.62	0.25	0.75	**1.02**
150.00	11.30	20.00	3.00	118.70	104.00	0.79	0.69	0.30	0.70	**0.89**

200.00	16.00	20.00	4.00	164.00	152.00	0.82	0.76	0.35	0.65	**0.79**
250.00	16.00	20.00	4.00	214.00	202.00	0.86	0.81	0.38	0.62	**0.72**
300.00	19.50	20.00	5.00	260.50	250.00	0.87	0.83	0.40	0.60	**0.69**
350.00	19.50	20.00	5.00	310.50	300.00	0.89	0.86	0.41	0.59	**0.66**
400.00	25.00	25.00	5.00	350.00	340.00	0.88	0.85	0.41	0.59	**0.67**
450.00	25.00	25.00	6.00	400.00	388.00	0.89	0.86	0.42	0.58	**0.66**
500.00	25.00	25.00	6.00	450.00	438.00	0.90	0.88	0.43	0.57	**0.64**
900.00	25.00	25.00	13.00	850.00	824.00	0.94	0.92	0.44	0.56	**0.59**

Table 5.6 Coefficients $\psi = \frac{S_1}{d}$ for various slab (exterior weather) thickness, $v_f > 0.56\lambda\phi_c\sqrt{f_c'}$

Slab thickness h (mm)	Assumed rebar diameter b (mm)	Concrete cover for exterior weather c (mm)	Bolt /stud head thickness t (mm)	Effective depth d (mm) d=h-c-b	Net stem length of studs h_s (mm) h_s =h-2c-2t	d/h	h_s /h	(h_s - 0.50d)/h	$\alpha = \frac{S_1}{h}$	$\psi = \frac{S_1}{d}$
120.00	11.30	30.00	3.00	78.70	54.00	0.66	0.45	0.12	0.88	**1.34**
150.00	11.30	30.00	3.00	108.70	84.00	0.72	0.56	0.20	0.80	**1.11**
200.00	16.00	30.00	4.00	154.00	132.00	0.77	0.66	0.28	0.73	**0.94**
250.00	16.00	30.00	4.00	204.00	182.00	0.82	0.73	0.32	0.68	**0.83**
300.00	19.50	30.00	5.00	250.50	230.00	0.84	0.77	0.35	0.65	**0.78**
350.00	19.50	30.00	5.00	300.50	280.00	0.86	0.80	0.37	0.63	**0.73**
400.00	25.00	37.50	5.00	337.50	315.00	0.84	0.79	0.37	0.63	**0.75**
450.00	25.00	37.50	6.00	387.50	363.00	0.86	0.81	0.38	0.62	**0.72**
500.00	25.00	37.50	6.00	437.50	413.00	0.88	0.83	0.39	0.61	**0.70**
900.00	25.00	37.50	13.00	837.50	799.00	0.93	0.89	0.42	0.58	**0.62**

5.2.2.3 Bolt Spacing in Tangential Direction

The bolt spacing in tangential direction must follow the rules:

(1) The bolt layout shall be symmetric about the x, y axis of the slab column connection (Figure 5.26). Since the existing rebar mats in the concrete slab sometimes do not permit the drilled holes be strictly symmetric (Figure 5.26 b), the bolts should be arranged in concentric rows and be as close to x' and y axes as possible.

(2) Maximum spacing in tangential direction S_2 shall greater than d but less than $2d$ (slab effective thickness) for first row of bolts.

(3) The amount of shear bolts in each quadrant should be the same.

(4) The outmost row of shear bolts shall be placed at a distance not greater than $0.5d$ within the perimeter at which no shear bolts are required.

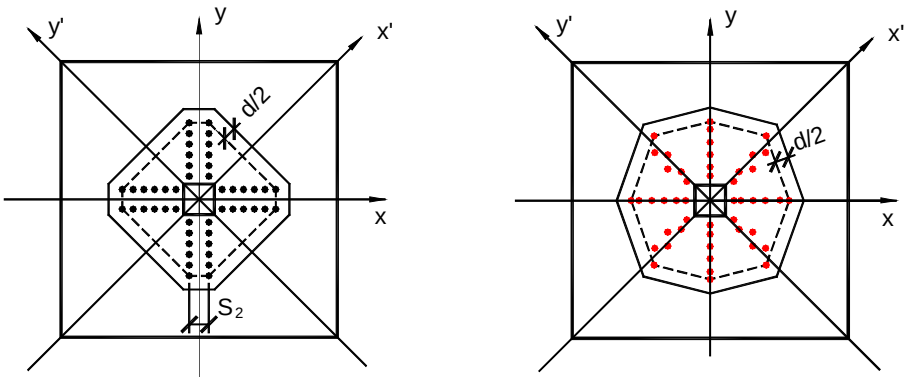

(a) (b)

Figure 5.26 Symmetric layout of shear bolts

(a) Orthogonal bolt layout; (b) Radial bolt layout

5.3 Construction Requirements

The retrofit procedure should start with defining the location of the holes to be drilled. To avoid drilling through the slab flexural rebar, it is very important to read the design drawings and construction records of the concrete slabs. The location of the rebar must be determined first. NDT method can also be used to locate the rebars. Then the drilling locations must be marked.

If the drill bit hits the rebar, drilling should be stopped. The neighboring location should be used instead. The unsuccessful holes should be patched using high strength expoxy cement, such as Sikadur 30 components.

Before drilling, it is important to check the capacity of the slabs with the holes. Two options are possible for installation sequence:

Shore the flat slab on the bottom, remove the live and removable gravity load on the floor. The shoring has two advantages: prevent slab punching shear failure and protect the bottom concrete cover from ripping off by the drill bit. Drill all holes and install the shear bolts.

Drill one (or a few) hole at a time. Install the bolts before proceeding to drill another set of holes. This method ensures that drilling of the holes does not excessively weaken the slab. All live and removable gravity loads should also be removed from the slabs before retrofitting.

Fire and corrosion protection of bolts need further investigation. However, some recommendations can be offered. After installation of all shear bolts, the heads of the bolts shall be covered by concrete paste, to isolate the bolt from corrosion. Alternatively, epoxy or paint can be applied on the shear bolts and nuts before installation.

Chapter 6
Conclusions and Recommendations

This chapter presents the conclusions from the research described in this thesis and recommendations for further research. The conclusions based on the experimental results are presented first, followed by the theoretical investigations on design of slabs with shear bolts.

Based on the experimental research on the flat slab-column connections strengthened with steel shear bolts, it is concluded that steel shear bolts are an effective method for retrofitting slabs in seismic zones. Proper application of shear bolts to existing reinforced concrete slabs will result in a change of the failure mode from brittle punching to ductile flexural. Slabs strengthened with shear bolts showed higher ductility, larger peak load at larger drift ratio, and the capability of undergoing more large drift cycles than slabs without such shear bolts.

Openings in the concrete slabs decrease the punching shear capacity and ductility rapidly, especially under lateral displacement loading. Shear bolts are effective in strengthening slabs with openings; strengthened slabs experienced ductile failures and were able to undergo large deformations.

Experimental results show that there is no significant difference between the effectiveness of radial and orthogonal layouts of shear bolts (with the same amount of shear bolts). The slabs behaved very similarly regardless of the shear reinforcing layout. But the slab strengthened with orthogonal bolt pattern showed slightly higher ductility (defined by Method II). In addition, from the practical point of view retrofitting in radial pattern can be difficult due to interference from flexural reinforcement.

Design of shear bolts was done based on the elastic solution and finite element analysis. Strength of shear bolts retrofitted slabs was estimated using same equations as for other shear reinforcing elements (CSA A23.3 -04). The analysis for spacing of the peripheral row of shear bolts indicates that their spacing can be slightly increased as compared to the spacing of shear studs.

6.1 Experimental Series I

Based on the results of the first series of experiments (specimens SW1 – SW5), the following detailed conclusions are drawn:

1. Shear bolts are effective in increasing peak lateral load capacity of slab-column connections. For the tested specimens, for four rows of bolts an increase of 17%~27% was observed, while for specimens with six rows of shear bolts the peak load increase was 19~44%).
2. Drift ratio at peak load of the slab-column connection can be significantly increased by installation of shear bolts. The increase of drift ratio at peak loads was raging from 66% up to 123%.
3. By using shear bolts, the drift ductility of the slab-column connection at peak load point and post peak can be substantially increased (26% - 84% increase in ductility defined by Method I, 78% - 258% increase in ductility defined by Method II).
4. The specimen with shear bolts can undergo more lateral drift cycles at large deformation, showing a significant increase in energy dissipation capacity.
5. Larger ratio of $\frac{V}{V_0}$ (vertical load over nominal punching shear capacity) leads to less energy dissipation capability of the flat slab column connection.
6. Shear bolts can change failure mode of the flat slab column connections. Slabs properly retrofitted with shear bolts will exhibit desirable flexural failure while slabs without shear bolts can be subjected to abrupt punching shear failure.
7. Shear bolts are installed through the slab in the close vicinity of the column face. For bolts farther away from the column, at a distance between the bolt and column face exceeding about four times the slabs effective thickness, d, the effect of shear bolts is small. This was shown in the strain readings on the instrumented bolts.
8. Strains on the bolts normal to the applied lateral displacements were generally larger than the strain in the direction of loading.
9. Strains on the bolts were small. Only few bolts yielded at very large drifts.
10. Vertical crack width remained in the range of approximately 1 mm until the punching shear failure.

6.2 Experimental Series II

Based on the results of second series of experiment for specimens (SW6 – SW9), the following detailed conclusions are obtained:

11. The two openings in the slab, next to the column and located along the direction of the applied lateral displacement resulted in 30% decrease in lateral load peak capacity and lateral drift ratio

decrease of approximately 45% for the two slabs without shear bolts (SW5 and SW6). It should be noted however, that the openings, in this case, did cut the flexural reinforcement placed along the moment application at the location of the openings.

12. Similarly, for slabs with same shear bolts (SW4, SW7, and SW8), the two openings in SW7 and SW8 resulted in a decrease of approximately 40% in peak moment, and 45% in lateral drift at peak loads.
13. The radial pattern of bolts lead to 2-5% decrease in peak load and a corresponding 10-27% decrease in lateral drift at peak loads, for specimens without openings (SW4 and SW9). These differences in peak loads and drift between radial and orthogonal patterns of bolts are very small and warrant a conclusion that bolt pattern does not influence the response of the slab to earthquake loads. Possible reason for the slight decrease in loads and displacements is the fact that in this test configuration, loads were applied exactly along the column sides. Thus the orthogonal layout of bolts would be a little more effective for this particular loading direction. In real earthquake situation, the lateral loads would be applied in an arbitrary direction with respect to the column sides; the radial pattern could prove, in fact, to be slightly more effective then.
14. For slab with openings, radial pattern bolts lead to an increase of 10 – 12% in peak moments but 4 – 6% decrease in lateral drifts at peak loads (SW7 and SW8). Based on these results it is concluded that the bolts layout also did not have any significant influence on the behaviour of slabs with openings.
15. The ductilities (defined by Method I) for the specimens with radial and orthogonal bolt layout were very similar, for both: slabs with and without openings. However, the specimen strengthened with orthogonal bolt showed higher ductility (defined by Method II).
16. The strengthened slab-column connections with two openings (SW7 and SW8) did not reach the peak lateral load as high as that of the unstrengthened slab without openings (SW5). However, shear bolts increased the drift ratios corresponding to peak loads. The shear bolts also enables the ductile post-peak behaviour of these two slabs with openings allowing large post peak drift ratios without brittle failure.
17. Specimen with openings strengthened by radial bolt layout showed higher peak lateral load but same drift ratio increase than specimen with openings strengthened by orthogonal bolt layout.

6.3 Shear Bolt Design and Analysis

The design of shear bolts included primarily determination of bolt head area and thickness, which are related to the size of bolts stem and the slab's concrete strength. The following detailed conclusions and recommendations are offered:

18. Thickness of a shear bolt head is related to the bolts stem cross sectional area, its yield strength, and the size of the drilled holes. The larger the clearance between the bolt stem and the hole edge, the thicker the head must be. Their relation is given in normalized curves for designing in Figure 5.6.
19. For practical reasons, clearance between the bolt stem and the slabs' drilled hole shall not exceed 2mm (to reduce the bolt head thickness).
20. The ratio of the bolt head area to the stem section area is related to the slab concrete strength and bolt steel yield strength. The larger the ratio of bolt yield strength to slab concrete compressive strength, the higher the ratio of bolt head area over bolt stem area. For low concrete strength, $f_c^{'} = 20MPa$, the head diameter needs to be sixteen times bolt stem sectional area. Thus, it is recommended that the head (or washer) area shall be 15 to 20 times the bolt stem sectional area.
21. The linear finite element analysis shows that, for the specimens in this research, each bolt has stress effect in the slab in a maximum range of 1.25d from the bolt center.
22. To determine the required amount of shear bolts for a concrete slab, the code (CSA A23.3-04) design equations for steel contribution from shear reinforcements can be followed. The radial spacing s of shear bolts can be specified as follows: (For notations see Chapter 5, section 5.2)

a). 1.0d for slab thickness of 200mm or less and $v_f \le 0.56\lambda\phi_c\sqrt{f_c^{'}}$

b). 0.75d for slab thickness above 200 mm and $v_f \le 0.56\lambda\phi_c\sqrt{f_c^{'}}$

c). 0.75d for slab thickness of 200mm or less and $v_f > 0.56\lambda\phi_c\sqrt{f_c^{'}}$

d). 0.60d for slab thickness above 200mm and $v_f > 0.56\lambda\phi_c\sqrt{f_c^{'}}$

23. Both layouts: orthogonal and radial are acceptable. The best option is to have shear bolt layout symmetric with respect to two orthogonal x and y axes. If perfect symmetry is not possible (due to problems with drilling holes not interfering with flexural reinforcements) then at least the

requirement of same amount of shear reinforcing elements in each quadrant of the slab defined by x-y axes should be maintained.

24. Before drilling holes in the concrete slab, it is important to remove the live gravity load on the floor. Installation of shear bolts can be done gradually by drilling few holes only and installing shear bolts in them before proceeding to drill more holes (and install bolts in them).
25. Protection of shear bolts from corrosion and fire is also important. Polymeric resins or cement grout can be used to fill the drilled holes. Typical fire protection for steel element should be used.

6.4 Recommendations for Future Research

In the presented test programs, the lateral loading direction was kept constant; along the column sides. In order to fully understand the influence of the shear bolt layout on the behaviour of retrofitted slabs, the loading should be applied along both orthogonal axes of the column, which would effectively result in the lateral loading applied at arbitrary direction with respect to the axes defined by the column sides.

More research could also be done on the effects of openings on the behaviour of slabs with shear reinforcements. Openings located on different sides of the column and at a distance from the column could be researched by testing appropriate specimens.

Work should also be done on the effect of shear bolts on corrosion of flexural steel and the method to protect the reinforcements from corrosion. Polymeric resins should possibly be injected in the drilled holes for that purpose.

Experimental programs are expensive and time consuming and, therefore, can only provide limited amount of data and information about various parameters influencing slab behaviour. Therefore future research should include nonlinear finite element modeling of the behaviour of these slabs. Properly calibrated 3-dimensional finite element analysis can be a powerful tool in drawing conclusions regarding slabs' and reinforcements' behaviour and can lead to the development of future design code formulations. The presented experimental programs will be excellent sources for calibrating such finite element formulations.

.

Appendix A
Abbreviations and Notations

ACI American Concrete Institute

ASCE American Society of Civil Engineers

CEB Comite Euro-international du Beton

CSA Canadian Standard Association

A_{vs} Section area of the shear reinforcement

A_{st}^{T} Section area of flexural reinforcements that is close enough to the column to participate as a shear strut

A_{bar} Area of a single reinforcing bar

A_{sw} Section area of shear reinforcements of each periphery row

b Perimeter length of the critical section

b_1 Width of the critical section side perpendicular to the moment vector

b_2 Width of the critical section side parallel to the moment vector

b_0 Perimeter length of the critical section at $d/2$ from the column face

b_{bot} Bottom edge length of the facet

b_{top} Top edge length of the facet

c_x, c_y Column dimensions

d Effective thickness of a slab

D Dowel force in the reinforcement intersecting with the conical shear crack

DR Maximum story drift ratio

d' Cover of reinforcing mat measuring from center of the mat to the near slab surface

d_b Diameter of the rebar

e Distance from the centroid of the critical section to the point where shear stress is calculated

f_c Uniaxial concrete strength

$f_c^{'}$ Concrete compressive strength

f_{ck} Characteristic cylinder compressive strength (28-day), MPa

f_y Yield strength of the reinforcement

f_{ywd} Design yield strength of the shear reinforcement

f_{yv} Strength of the shear reinforcement

f_t Tensile strength of concrete

h Slab thickness

h_s Net length of the bolt stem

$h_{s,eff}$ Average effective length of the stud

J Analogous to polar moment of inertia of the shear critical section around the x, y centrioda1 axes, respectively

k Correlation coefficient determined from experiment data

M_f Factored unbalanced moment in x, y direction, which is transferred by slab shear and flexural stresses

M_{neg} Flexural capacity of the strip

n Number of shear studs

P Punching shear load on the connection (the applied load at the slab periphery or at the column)

$P_{\max}$ Maximum lateral load

R Radius of drilled hole in the concrete slab for the bolts

R_0 Shear bolt head radius

κR_1 Force component in the tangential direction of reinforcement cutting across the shear crack

R_2 Force in radial direction of the reinforcement cutting across the shear crack

R_3 Force of shear reinforcement (not included in this model)

R_4 Tangential resultant of concrete compression stress at the bottom of the section

r_0 Radius of the bolt stem

S_0 Space between the column face and the first bolt row

S_1 Radial direction bolt spacing

S_2 Tangential direction spacing

s Radial spacing of the shear reinforcement

s_{eff} Effective tributary width of reinforcing bar

T Tension force in the flexural reinforcements

T_v Tension force in each shear stud

t Bolt / stud head thickness

u_1 Length of the basic control section

V Concentric external shear force

$V_0^{'}$ Fictitious reference value of shear

V_0 Nominal shear capacity of slab in the absence of moment transfer

V_f Factored vertical shear force

V_n Nominal punching shear strength (vertical punching shear force of the column)

V_{flex} Vertical punching shear force at the calculated ultimate flexural capacity of the slab

V_u Direct shear force at peak lateral load

$V_{sf,simple}$ Nominal shear force resisted by the connection as given by shear friction

V_r Factored shear force resistance

V_{uf} Factored shear force due to gravity loading

VR Gravity shear ratio

W_I Energy dissipated at the failure surface

W_P Work done by the punching load P

x_{bot} Distance between column face and the bottom of the failure facet

y Vertical height of the conical shell from the slab bottom surface

α Incline angle of the imaginary compression concrete conical shell, in Figure 2.12

α_s 4, 3, 2 for interior, edge, and corner column, respectively

β_c Ratio of the long side over short side of the column

θ Angle of the failure facet

θ_1 Angle of shear cracks in the zone with shear reinforcement

θ_2 Angle of cracks in the non-shear reinforced zones

ϕ_c Reduction factor for concrete strength, ϕ_c =0.65

ϕ_s Reduction factor of steel bar, $\phi_s = 0.85$

ϕ Shear strength reduction factor in ACI 318-05, $\phi = 0.75$

φ Friction angle of concrete

$\Delta\varphi$ Slice angle of the rigid section,

σ Normal stress on that plane

γ_c Partial factor for concrete

γ_v Fraction of the moment transferred by shear

$\mu_{\%}$ Ductility defined by a ratio, $\mu_{\%} = \dfrac{\delta_{\%}}{\delta_Y}$

δ_y Displacement corresponding to flexural yielding of the slab and

$\delta_{\%}$ Displacement corresponding to a certain load (% of the maximum load in the post-peak region)

v Shear stress on a concrete failure surface

v_r Factored shear resistance

v_f Factored shear stress

v_c Factored shear resistance from concrete

v_s Factored shear resistance form shear reinforcements

v_n Nominal shear strength

v_{nc} Nominal shear strength provided by the concrete

w Calculated from the maximum force gradient in the reinforcement perpendicular to the radial strip

ρ Effective reinforcing ratio (tension reinforcement on the slab top) within the radial strip

ρ_x, ρ_y Flexural reinforcing ratios of the slab in two orthogonal directions

References

ACI-ASCE Committee 326 (1962), "Shear and Diagonal Torsion, Chapter 8 - Slabs and Footings", Journal of the American Concrete Institute, Proceedings, V. 59, No. 3, Mar. 1962, pp. 353-396.

ACI-ASCE Committee 352, (1988) "Recommendations for Design of RC Slab-Column Connections in Monolithic Reinforced Concrete Structures," *ACI Structural Journal,* Vol. 85, No.6, November-December, pp. 675-696.

ACI-ASCE Committee 421 (1999), Shear Reinforcement for Slabs (ACI 421.1 R-99), American Concrete Institute, Farminton Hills, Michigan.

ACI Committee 318, Building Code Requirements for Structural Concrete (ACI 318-05), American Concrete Institute, Farminton Hills, Michigan, 2005.

ACI Innovation Task Group 1 and Collaborators, "Acceptance Criteria for Moment Frames Based on Structural Testing (ACI T1.1-01) and Commentary (T1.1R-01)," American Concrete Institute, Farmington Hills, Mich., 2001, 17 pp.

Adetifa, B., (2003) "A New Punching Shear Strengthening Technique for Reinforced concrete Slabs at Interior Slab-Column Connections," M.A.Sc Thesis, University of Waterloo, Waterloo, Ontario, Canada.

Adetifa, B., Polak, M.A., (2005), "Retrofit of Interior Slab Column Connections for Punching using Shear Bolts", *ACI Structural Journal,* March April.

Alexander, S.D.B., Simmonds, S.H., (1987) "Ultimate Strength of Slab-Column Connections," *ACI Structural Journal,* Vol. 84, No. 3, May-June, pp. 255-261.

Alexander, S.D.B., Simmonds, S.H., (1992) "Bond Model for Concentric Punching Shear," *ACI Structural Journal,* Vol. 89, No. 3, May-June, pp. 325-334.

Anderson, J. C., (1989) "Dynamics Response of Building", *The Seismic Design Handbook,* edited by Farzad Naeim, Van Nostrand Reinhold.

Barrett, R. T., (1990) "Fastener Design Manual," NASA Reference Publication 1228, National Aeronautics and Space Administration, Office of Management, Scientific and Technical Information Division

Bazant, Z. P., and Cao, Z., "Size effect in Punching Shear Failure of slabs," ACI Structural Journal, V.84, No.1, Jan.-Feb. 1987, pp. 44-53.

Bertero, V., (1994), Foreword, *International Handbook of Earthquake Engineering (Codes, Programs, and Examples)*, edit by Mario Paz, Chapman & Hall Inc.

Brastrup, M.W., Nielsen, M.P., Jensen, B.C., Bach, F., (1976) "Axisymmetric Punching of Plain and Reinforced Concrete," Structural Research Laboratory, Technical University of Demark.

Broms, C. E., (1990) "Punching of Flat Plates-A Question of Concrete Properties in Biaxial Compression and Size Effect," *ACI Structural Journal*, Vol. 87, No.3, May-June, pp. 292-304.

Bu, W., Polak, M.A., "Seismic Retrofit of RC Slab-Column Connections using Shear Bolts" ACI Structural Journal, 30 pp. submitted

Bu, W., Polak, M.A., (September, 2007), "Punching Shear Retrofit of Reinforced Concrete, Flat Slabs Subjected to Static and Reversed Cyclic Loads," International Association for Bridge and Structural Engineering (IABSE) Conference, Weimar , 8 pages

Building and Fire Research Laboratory of NIST (USA), (2003) *Building and Fire Research at NBS/NIST 1975-2000,* National Institute of Standards and Technology Building Science Series 179, 339 pages, CODEN: NBSSES, December.

Carino, N. J., Woodward, K.A., Leyendecker, E.V., Fattal, S.G., (1983) "A Review of the Skyline Plaza Collapse," *Concrete International*, Vol. 5, No. 7, July, pp. 35-42.

Cao, H., (1993) "Seismic Design of Slab-Column Connections," M. A. Sc. Thesis, University of Calgary, Alberta, Canada.

CEB-FIP MC 90 (1993), Design of Concrete Structures, CEB-FIB-Mode -Code 1990, Thomas, Telford.

Choi, K. K., Taha, M. M. R., Sherif, A. G., (2007) "Simplified Punching Shear Design Method for Slab-Column Connections Using Fuzzy learning," *ACI Structural Journal*, Vol. 104, No.4, July-August, pp. 438-447.

Criswell, M.E., Hawkins, N.M., (1974) "Shear Strength of Slab: Basic Principle and Their Relation to Current Methods of Analysis," *Shear in Reinforced Concrete (Volume 2),* ACI Publication SP-42, pp. 641-676.

Cope, R. J., Clark, L. A., (1984) "Concrete Slabs Analysis and Design", Elsevier Applied Science Publishers Ltd., ISBN 0-85334-254-7.

CSA Technical Committee on Reinforced Concrete Design, *A23.3-94 Design of Concrete Structures*, Canadian Standard Association, Rexdale, Ontario, 1994, 199 pp.

CSA Technical Committee on Reinforced Concrete Design, *A23.3-04 Design of Concrete Structures*, Canadian Standard Association, Rexdale, Ontario, 2004.

Dechka,D.C., (2001) "Response of Shear-Stud-Reinforced Continuous Slab-Column Frames to Seismic Loads," Ph.D. Dissertation, University of Calgary, Alberta, Canada

Derecho, A. T., (1989) "Seismic Design of Reinforced Concrete Structures", *The Seismic Design Handbook*, edited by Farzad Naeim, Van Nostrand Reinhold.

Dilger, W.H., (2000) "Flat Slab-Column Connections," *Progress in Structural Engineering and Materials*, John Wiley & Sons, Ltd., Volume 2, Issue 3, pp. 386-399.

Dilger, W.H., Ghali, A., (1981) "Shear Reinforcement for Concrete Slabs," *Journal of the Structural Division, Proceedings of the ASCE*, Vol. 107, No. ST12, December.

Ebead, U., Marzouk, H., (2002) "Strengthening of Two-Way Slabs Subjected to Moment and Cyclic Loading," *ACI Structural Journal*, Vol. 99, No.4, July-August, pp. 435-444.

Elstner, R.D., Hognestad, E., (1956) "Shearing Strength of Reinforced Concrete Slabs," *ACI Structural Journal*, Vol. 53, No.1, July 1956, pp. 29-58.

El-Salakawy, E.F., Polak, M.A., Soudiki, K.A., (2003) "New Shear Strengthening Technique for Concrete Slab-Column Connections," *ACI Structural Journal*, Vol. 100, No.3, pp. 297-304.

El-Salakawy, E.F., Polak, M.A., Soliman, M.H. (1998) "Slab-Column Edge Connections Subjected to High Moments," *Canadian Journal of Civil Engineering*, Vol. 25, pp. 526-538.

El-Salakawy, E.F., Polak, M.A., Soliman, M.H. (1999) "Reinforced Concrete Slab-Column Edge Connections with Openings," *ACI Structural Journal*, Vol. 96, No.1, pp. 79-87.

El-Salakawy, E.F., Polak, M.A., Soliman, M.H. (2000) "Reinforced Concrete Slab-Column Edge Connections with Shear Studs," *Canadian Journal of Civil Engineering*, Vol. 27, pp. 338-348.

El-Salakawy, E.F., Polak, M.A., Soudiki, K.A., (2003) "New Shear Strengthening Technique for Concrete Slab-Column Connections," *ACI Structural Journal*, Vol. 100, No.3, pp. 297-304.

EL-Salakawy, E. F., (1998) "Shear Behaviour of Reinforced Concrete Flat Slab-Column Edge Connections with Openings," Ph.D. Thesis, University of Waterloo, Waterloo, Ontario, Canada.

Emam, M., Marzouk, H., Hilal, M.S., (1997) "Seismic Response of Slab-Column Connections Constructed with High-Strength Concrete," *ACI Structural Journal*, Vol. 94, No.2, pp. 197-205.

Eurocode 2: Design of Concrete Structures - Part 1-1: General Rules and Roles for Buildings, BS EN 1992-1-1, 2004, British Standard, CEN

Feld, J., Carper, K. L., (1997), Construction Failure, 2nd Edition, John Wiley & Sons, Inc., ISBN 0-471-57477-5, 512 pp.

FEMA 356 – Prestandard and Commentary for the Seismic Rehabilitation of Buildings, ASCE and FEMA, November, 2000, USA.

Fib - fédération internationale du béton, The International Federation for Structural Concrete, *Punching of structural concrete slabs*, fib Bulletin No. 12, 2001, 314 pp.

Ghali, A., Sargious, M. A., Huizer, a., (1974) "Vertical Prestressing of Flat Plates Around Columns," *Shear in Reinforced Concrete (Volume 2)*, ACI Publication SP-42, pp. 905-920.

Hawkins, N.M.,(1974) "Shear Strength of Slabs With Shear Reinforcement," *Shear in Reinforced Concrete (Volume 2)*, ACI Publication SP-42, pp. 785-815.

Hawkins, N. M., Corley, W. G., (1974a) "Moment Transfer to Columns in Slabs with Shearhead Reinforcement," *Shear in Reinforced Concrete (Volume 2)*, ACI Publication SP-42, pp. 847-879.

Hawkins, N. M., Criswell, M.E., Roll, F., (1974b) "Shear Strength of Slabs Without Shear Reinforcement," *Shear in Reinforced Concrete (Volume 2)*, ACI Publication SP-42, pp. 677-720.

Hawkins, N. M., Mitchell, D., Hanna, S. N., (1975) "The Effect of Shear Reinforcement on the Reversed Cyclic Loading Behaviour of Flat Plate Structures," *Canadian Journal of Civil Engineering*, Vol. 2, pp. 572-582.

Islam, S., Park, R., (1976) "Tests on Slab-Column Connections with Shear and Unbalanced Flexure," *Journal of Structural Division*, Proceedings of the ASCE, Vol. 102, No. ST3, pp. 549-568.

King, S., Delatte, N. J., (2004) "Collapse of 2000 Commonwealth Avenue: Punching Shear Case Study," *Journal of Performance of Constructed Facilities*, Vol. 18, No.1, Feb. 1, pp. 54-61.

Kinnunen, S., (1963) “Punching of Concrete Slabs with Two-Way Reinforcement with Special Reference to Dowel Effect and Deviation of Reinforcement from Polar Symmetry,” Transactions, No.198, Royal Institute of Technology, Stockholm, Sweden.

Kinnunen, S., Nylander, H., (1960) “Punching of Concrete Slabs without Shear Reinforcement,” Transactions, No.158, Royal Institute of Technology, Stockholm, Sweden.

Loov, R.E. (1978), “Design of Precast Connections,” Presentation at a seminar organized by Compa International Pte. Ltd., Singapore, 1978, 8 pp.

MacGregor, J. G., Bartlett, F. M., (2000) Reinforced Concrete Mechanics and Design, 1st Edition, Prentice Hall Canada Inc., Scarborough, Ontario.

Megally, S., Ghali, A., (2000a) “Punching Shear Design of Earthquake-Resistant Slab-Column Connections,” *ACI Structural Journal*, Vol. 97, No.5, pp. 720-730.

Megally, S., Ghali, A., (2000b) “Seismic Behaviour of Edge Slab-Column Connections with Stud Shear Reinforcement,” *ACI Structural Journal*, Vol. 97, No.1 pp. 53-60.

Megally, S., Ghali, A., (2000) “Seismic Behaviour of Slab-Column Connections,” *Canadian Journal of Civil Engineering*, .Vol. 27, pp. 84-100.

Moehle, J. P. (1996) “Seismic Design Considerations for Flat-Plate Construction,” *Mete A. Sozen Symposium: A Tribute from his Students*, ACI Publication SP-162, pp.1-33.

Moehle, J.P., (2000) "State of Research on Seismic Retrofit of Concrete Building Structures in the US," US-Japan Symposium and Workshop on Seismic Retrofit of Concrete Structures - State of Research and Practice, September.

Moehle, J. P., Diebold, J. W., (1985) “lateral Load Response of Flat-Plate Frame,” *Journal of Structural Division*, Proceedings of the ASCE, Vol. 111, No. 10, pp. 2149-2164.

Moe, J., (1961) “Shearing Strength of Reinforced Concrete Slabs and Footings Under Concentrated Loads,” *Development Department Bulletin D47*, Portland Cement Association, Skokie, Apr. 1961, 130 pp.

Mo, Y.L., (1994)Dynamic Behaviour of concrete Structures, Elsevier Science B. V.

National Building Code of Canada 2005, Canadian Commission on Building and Fire Codes, National Research Council, Ottawa

Pan, A. D., Moehle, J. P., (1989) “Lateral Displacement Ductility of Reinforced Concrete Flat Plates,” *ACI Structural Journal*, Vol. 86, No. 3, pp. 250-258.

Pan, A. D., Moehle, J. P., (1992) “An Experimental Study of Slab-Column Connections,” *ACI Structural Journal*, Vol. 89, No.6 pp. 626-638.

Park, R., Paulay, T., (1975) Reinforced Concrete Structures, John Wiley & Sons, Inc.

Paulay, T., Priestley, M. J. N., (1992) Seismic Design of Reinforced Concrete and Masonry Buildings, John Wiley & Sons, Inc.

PILKLEY W. D., (2005), "Formulas for Stress, Strain, and Structural Matrices, Second Edition", John Wiley & Sons, Inc., Hoboken, New Jersey, USA.

Polak, M.A., Bu, W., (2006), "Application and Design of Shear Bolts for Retrofit of Concrete Slabs", IABSE Conference, Budapest, 8 pp.

Polak, M.A., (2005), "Ductility of Reinforced Concrete Flat Slab-Column Connections", Computer-Aided Civil and Infrastructure Engineering, 35 pages, accepted.

Polak, M.A., Adetifa, B., (2004), "Strength and Ductility of Slab-Column Interior Connections Strengthened with Shear Bolts, Canadian Society of Civil Engineering Conference, Saskatoon, 9 pages.

Polak, M.A., El-Salakawy, E., (2002), "Punching Shear Strengthening of Existing Slabs", fib International Congress in Osaka, Japan, 8 pp.

Rankin, G.I.B., and Long, A.E., (1987) "Predicting the Punching Strength of Conventional Slab-Column Specimens," Proceedings of Institution of Civil Engineers, Part 1, 82, April.

Regan, P. E., (1974) "Design for Punching Shear," *The Structural Engineer*, June, 1974, No.6, Volume 52, pp. 197-207

Robertson, I. N., and Durrani, A. J. (1992) "Gravity Load Effect on Seismic Behaviour of Interior Slab-Column Connections," *ACI Structural Journal*, Vol. 89, No.1, pp. 37-45.

Roll, F., Zaidi, S.T.H., Sabnis, G., Chuang, K., (1971) "Shear Resistance of Perforated Reinforced Concrete Slabs," *Cracking, Deflection, and Ultimate Load of Concrete Slab Systems*, Publication SP-30, American Concrete Institute, Michigan.

Rosenblueth, E., Meli, R., (1986) "The 1985 earthquake: causes and effects in Mexico City," *Concrete International*, May.

Sabol, T. A., (1994) "Flat Slab Failure in Ductile Concrete Frame Building," *1994 Northridge Earthquake*, Case Study 1.13, pp. 167-187.

Shehata, I. A.E.M., Regan, P. E. (1989) "Punching in R.C. Slabs," *Journal of Structural Engineering*, ASCE, Vol. 115, No. 7, pp. 1726-1740.

Simmonds, S.H., Alexander, S.D.B., (1987) "Truss Model for Edge Column-Slab Connections," *ACI Structural Journal*, pp. 296-303.

Stark, A., Binici, B., Bayrak, O., (2005) “Seismic Upgrade of Reinforced Concrete Slab-Column Connections Using Carbon Fiber-Reinforced Polymers,” *ACI Structural Journal*, Vol. 102, No.2, March-April, pp. 324-333.

Talbot, A.N. (1913), “Reinforced Concrete Wall Footings and Column Footings”, Engineering Experiment Station, University of Illinois, Urbana, Illinois, USA, Bulletin No. 67, Mar. 1913, 114pp.

Wallace, J.W., Kang, T.H.K, Changsoon RHA, “Seismic Performance of Flat plate Systems,” *4th US-Japan Workshop on PBD for RC Buildings (Proceedings),* http:// www.seas.ucla.edu/~tkang/.

Wakabayashi, M., (1986) Design of Earthquake-Resistant Buildings, R.R. Donnelley & Sons Company.

Wey, E. H., Durrani, A., (1992) “Seismic of Interior Slab-Column Connections with Shear Capitals,” *ACI Structural Journal*, Vol. 89, No.6, pp. 682-691.

Yitzhaki, D., (1966) “Punching shear Strength of Reinforced Concrete Slabs,” *Proceedings of ACI*, Vol.63, May, pp. 527-542.